Joining metal matrix composites and related alloys

Lindsay, Neil J.

Award date:
1993

Awarding institution:
University of Bath

JOINING METAL MATRIX COMPOSITES AND RELATED ALLOYS

Submitted by Neil J. Lindsay for the degree of Ph.D.

University of Bath, 1992

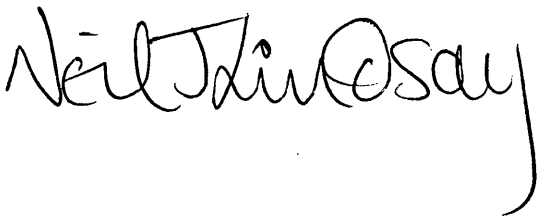

ProQuest LLC
789 East Eisenhower Parkway
P.O. Box 1346
Ann Arbor, MI 48106-1346

List of Contents:

1. ACKNOWLEDGEMENTS

I would like to thank my two supervisors, Prof. Vic Scott at the University of Bath and Mr. Richard Trumper at the Defence Research Agency, Holton Heath for the contributions, time and effort they have made to this project.

Additionally, I would like to thank Mr J. Manson & Mr T. Nowell at DRA Holton Heath and to Mr T. Bennett for his help with photographic printing and developing.

Support was made available by SERC and MOD.

2. SUMMARY

The feasibility of joining fibre reinforced aluminium alloys was investigated using adhesive and diffusion bonding techniques.

Initial studies were carried out on three aluminium matrix alloys, commercially pure aluminium, a medium strength casting alloy A357 and a high strength casting alloy ARE415. The effect of adhesive bonding pretreatment using a mixed acid etch (FPL) on the matrix alloys revealed a large variation in response. Commercially pure aluminium, showed a uniform scalloped topography when etched, and, after adhesive bonding, showed an improvement in single-lap shear strength. The grain boundaries and eutectic phases in A357 and ARE415 were vigorously attacked by the FPL etch. Adhesive bond tests performed on these materials tended to induce some peel forces. Reductions in bond strengths were observed with ARE 415, this alloy was sensitive to heat treatment since lower strength samples were more prone to bending. Furthermore, the etch topography on ARE415 and A357 gave rise to air entrapment when a thixotropic epoxy adhesive was used; this outgassed during adhesive cure and lowered single-lap shear strength.

A method was developed to measure oxide film thickness to characterise the oxidising effect of the FPL solution. The technique was based upon electron-probe microanalysis (EPMA) and involved a comparison of characteristic oxygen x-rays produced from FPL etched specimens and an alumina standard under identical operating conditions.

High temperature diffusion bonding studies were carried out on matrix alloys. The work involved the design and construction of a hot press and employed controlled conditions of time, temperature and deformation strain. Copper and silver foils were investigated as an aid to bonding and joint strengths were assessed by single-lap shear testing. Microstructural analysis at the bond-lines showed the presence of either continuous, banded intermetallics or eutectic phases of liquid origin, depending on bonding temperature.

Adhesive bonding experiments were carried out on carbon-reinforced A357 specimens. The FPL etch resulted in more severe attack of the composite especially in the matrix regions surrounding the fibres. When adhesively bonded joints were tested they were found to fail within the composite and this was attributed to defects introduced during manufacture of the composite. Similar results were obtained when using the diffusion bonding technique, again due to the poor properties of the composite.

Thus it is concluded that the quality of the metal matrix composites require significant improvement before any systematic work can be carried out on the prospects of joining them and such joining methods can be applied successfully.

3. REVIEW OF LITERATURE

3.1 EARLY WORK ON METAL MATRIX COMPOSITES

The benefits and advantages of metal matrix composites compared with rival structural materials are widely reported. The incorporation of a ceramic reinforcement into a metal matrix can generally give rise to enhanced characteristics such as specific strength and modulus. This increase in specific properties has resulted in a very large perceived market and has been responsible for a significant research drive, particularly over the past two decades.

Much of the basic research into composite science was conducted in the 1950's and 1960's using polymer matrices. Advances in organic chemistry led to the production of high performance resin systems which evolved a gradual increase in desired properties such as temperature resistance and durability. The manufacture of higher quality, stronger fibres progressed in parallel with resin development and techniques were devised to produce more complex fibre arrangements. The application of weaving and braiding methods from the textile industry finally enabled the manufacture of fibre preforms that conferred highly specific reinforcement, and hence controllable anisotropy, in the composite material.

Notwithstanding the increasing quality of resin matrix systems, polymer composites are, to this day, limited in their use by temperature considerations. Technological advances, particularly in engine and aerospace technology, have driven operating temperatures upwards to levels well beyond those of conventional polymer composites. Increasing demands on performance, especially in aerospace, are now challenging the suitability of traditional structural materials such as steels and even aluminium alloys. In many cases, materials are required that exhibit either enhanced strength, equivalent strength but with lower weight, or strength-at-temperature.

In addition to these considerations, applications have developed that do not require global reinforcement but, instead, demand locally enhanced properties within a component. Wear resistance in a bearing without the need for a bush-insert is just one example.

The general response to these technical demands has been to reinforce a metal matrix, in much the same way as a polymer matrix. The most tangible benefit from this is to increase the temperature capability of the material. Structural components for hot-zones in aircraft engines were some of the first projected applications for metal matrix composites.

The number of combinations of metal matrix to reinforcement is bewildering. Any metal can be used and the reinforcement can be fibres, whiskers or particles, metallic or non-metallic. In practice, only a certain number of combinations are practicable, mainly due to cost or compatibility.

Metal matrix composites have yet to achieve widespread use and this may be explained in two ways. Firstly, high quality fibres are very expensive to produce. This makes the metal matrix composite a high value-added product suitable mainly for military applications where cost is a secondary factor. Typically, fibres may lie in the £100-£5000/kg bracket. Secondly, problems are still encountered during processing. These problems may involve a number of considerations such as wetting, fibre break-up and chemical reactivity of the components.

In order to make the production of metal matrix composites easier many techniques have evolved. In some cases the technique is merely a variant based on existing metallurgical methods. In other cases the fabrication method has been developed with a specific product or component in mind. An example of this is the structural tube design used in the Space Shuttle programme. The most significant fabrication methods are described in the following sections.

3.2 MANUFACTURE OF METAL MATRIX COMPOSITES

Many references exist relating to manufacturing methods for metal matrix composites; often the papers describe newly patented, processes that are highly specific. Exact details are not necessary for every different method so some of the following information has been categorised and ordered along the lines of some of the many reviews found in press[1,2,3].

3.2.1 Solid Phase Fabrication Techniques

a) Diffusion Bonding

This method was one of the earliest used to fabricate net shape metal matrix composite components and is discussed in more detail in later sections.

b) Isostatic Pressing

This is a particular form of pressing which can be performed either hot or cold. Tape preforms may be laid up and diffusion bonded by using isostatic pressing.

Cold isostatic pressing is often used to consolidate powder-based composites and is characterised by good uniformity of density. This is mainly due to the uniform pressure distribution occurring during pressing. A major advantage of isostatic pressing is that components with re-entrant angles can be consolidated, unlike conventional rigid die techniques.

Isostatic pressing may be performed "wet" or "dry". The former technique uses a liquid to set up the isostatic conditions and the powder is contained within a flexible bag. This technique can be relatively slow. Faster cycle times are possible for the "dry" isostatic technique, which uses a completely sealed bag that needs to be removed on completion.

This technique was used with tape preforms wound onto mandrel to produce the space shuttle struts mentioned in section 3.6.4 a).

c) Explosive Welding

This is a highly specialised technique used to make sheet material which originated in the Soviet Union (ex). The nature of the process allows large areas to be bonded in one cycle. The method was originally used to clad metals with a different alloy and some success has apparently been achieved in cladding cylinders with a circumferentially wrapped reinforcement.

d) Other Mechanical Techniques

There are a number of solid state techniques available for metal matrix composite production other than those described previously. The first is a combination of diffusion bonding and mechanical working and is generally known as roll diffusion bonding, this method is of interest to the production engineer as it may allow the manufacture of continuous metal matrix composite strip that is wider than that made by other methods. Consolidation of the strip is characterised and achieved by higher flow stresses than conventional pressing. This leads to reduced production times but can lead to extensive fibre breakup.

Tanikawa has researched the production of preformed sheets made by plasma spraying metal onto drums wound with the fibres[4]. Matrix metal was regulated to produce a $40\%_{vol}$ composite. The sheets were then cut from the drums, stacked to the correct thickness, heated in air and then hot rolled until consolidation was complete. According to the authors it was possible to make a metal matrix composite without breaking the fibre preform arrangement. Temperature was important and some fibre surface degradation was noted for samples manufactured at 913K (640°C). Mechanical testing showed a reduction of properties which were attributed to oxidation of the fibre/matrix interface (processing was all performed in air).

Thermomechanical processing of metal matrix composites is a generic description of many mechanical techniques that are carried out at elevated temperatures. A large variety of cheap or expensive reinforcements can be included in a metal matrix in this way, these may include: sand, mica, graphite, SiC, zircon, anthracite and glass (particles or micro-balloons).

Work has been published concerning the mechanical processing of particulate reinforced metal matrix composites[5]. The paper reviewed reinforcement systems that were comprised of particles, usually greater than 20μm. The benefits accruing from thermomechanical working were based not only on conventional alloy modifications such as work hardening and grain refinement, but also on other considerations such as improved matrix/particle bonding and reinforcement alignment. The effects obtained are varied, for example extruding an aluminium powder alloy mixed with a glass reinforcement increased strength by up to 4 times compared to the unworked composite. The glass particles tended to become fibrized, adding to the directional enhancements noted in this system, the glass fragments also limited tool wear by acting as die lubricants during extrusion. In a similar fashion, aluminium alloys reinforced with graphite showed particle elongation after extrusion, probably due to mechanically induced slip along the basal planes of the graphite during extrusion. Most of these alloy/particle combinations were formulated for wear applications where inherent strength may not always be of prime importance. The choice of particle reinforcement may also be economically driven, simple wear components may not need expensive synthetic ceramic reinforcements.

Rapid solidification has also been employed to manufacture metal matrix composites. This method is often used to produce alloys with enhanced properties such as elongation and yield strength. The extremely complex equipment required for this method means that only laboratory scale quantities have only been made to date[6]. In this paper two related techniques were used to manufacture metal matrix composites. In the first, SiC particles were added to a semi-solid matrix slurry in a similar manner to compocasting.

The alloy was then remelted and promptly rapidly solidified by melt spinning. The spun ribbon was chopped into flakes, compacted and then extruded at 450°C.

The second technique required that the matrix alloy was melt spun on its own. The resulting ribbon was then chopped into flakes and then milled into smaller particles. These were then combined with the particulate reinforcement and mechanically mixed. Compaction, heating and extrusion then followed in the same way as for the other method. The method did not produce successful metal matrix composites as there was practically no bond between the matrix and the reinforcement. Also extrusion pressures for the second technique were higher with extrusion speeds being lower than for the first method. Successful metal matrix composites were produced using the first method described but only with 3μm SiC particles. If larger diameter particles of SiC (20μm) were used instead, the reinforcement tended to fracture before the matrix.

Mechanical alloying has also been applied to the manufacture of these composites[7]. The benefits gained by this method usually involve the incorporation of elements that are difficult to include by conventional casting. Also very uniform, refined microstructures may be developed. Composites were made by attritor milling of metal powders and SiC particles. Alloying was 50-75% complete after 12 hours of milling after which the mixture was degassed and compacted at 600°C. Alloying progress was monitored by using x-ray diffraction of powder samples. The main reason for making composites by this route was to incorporate hard ceramic particles for wear applications. Mechanical alloying was chosen as it was considered to allow total control over alloy composition and good dispersion of ceramic particles could be achieved. The published conclusions are rather light but there was a 4-fold reduction in wear damage by the inclusion of only $5\%_{vol}$ SiC in the composite.

3.2.2 Liquid Phase Fabrication Techniques

a) Rheocasting and Compocasting

This method is one of the most popular of the liquid phase techniques, probably because the method is very well established in the foundry industry. The basis of the rheocasting technique is the vigorous agitation of a semi-solid metal slurry. The metal slurry behaves in a thixotropic manner, i.e displays low viscosities even with solid contents as high as $60\%_{vol}$. As a result of this agitation, the cast metal has significantly shorter interdendritic spacings. In point of fact, ideal specimens are actually non-dendritic due to the enormous shearing imparted by the mixer blades onto the slurry; in simple terms the dendrite arms are knocked off, producing a more spheroidal type of microstructure when solidified.

The variation of rheocasting that involves the inclusion of either particulate or whisker reinforcement is known as compocasting. The partially solid nature of the matrix alloy stops the reinforcement from either settling out or agglomerating. Continued exposure to the molten metal enables wetting of the reinforcement which improves final properties. In the simplest case the slurry containing the reinforcement is simply poured into a mould or die to produce the final product.

The volume fraction of reinforcement is dependant on the spacing of the matrix spheroids. This is, in turn, dictated by the quantity of alloying elements. Up to $60\%_{vol}$ of particles have been successfully incorporated into an aluminium matrix. However, the highest volume fraction composites are very difficult to cast and complementary techniques need to be used to consolidate a successful casting. These additional measures may include superheating if necessary, followed by squeeze casting, injection casting or rolling and extrusion.

Quigley et al.[8] described a compocasting process using an Al-4%Mg alloy. The alloy was melted and degassed with nitrogen and then transferred to the compocasting apparatus. After slurry shearing and the inclusion of discontinuous Al_2O_3 fibres the ingot

was allowed to solidify. Wetting of the fibres was confirmed by the presence of a $MgAl_2O_4$ spinel, indicating a chemical reaction between the fibres and the melt. The authors actually thought that the spinel was important as it produced a strong fibre/matrix bond. Researchers are sometimes ambivalent over this opinion as an interfacial phase may actually reduce composite strength due to its brittle nature. The orientation of the $23\%_{vol}$ fibres in this composite was essentially random, so a secondary processing method was devised that enabled some realignment to take place. This involved re-melting and squeezing in a die (presumably with the consequential risks of more fibre/matrix degradation). Final mechanical testing showed increases in various properties such as tensile strength and modulus.

Karandikar et al. have published a paper examining compocasting aluminium matrix composites with DuPont's FP-Al_2O_3 fibres[9]. The physical state of the matrix during various stages of manufacture was seen as important to the final properties of the composite. In other words, the matrix was either allowed to solidify, was kept mushy, or was fully liquid through the various stages of fibre addition, stirring and casting. Final composite consolidation was carried out by squeeze casting. This reduced any porosity trapped during compocasting, especially in the semi-solid state. It was also stated that the squeeze casting broke down the dendritic structure of the composite. This exact problem was eliminated by the higher shear stirring in the previous reference, although heavy shear may be disadvantageous by causing fibre damage before casting.

A non-uniform reinforcement distribution resulted when Al_2O_3 fibres were stirred into a fully liquid melt. This happened because there were no solid metal particles present to divide and space out the fibres. Mechanical testing showed an increase in modulus but no significant increase in tensile strength. This was connected to the fact that the failure strain of the composite was slightly lower than that of the fibres alone. The fibre clustering mentioned above was put forward as the cause of this reduced failure strain.

b) Pressure-Aided Infiltration

Mortensen's group at MIT produced a rig suitable for the pressure infiltration of packed particulate preforms. The arrangement involved a tube into which was placed the reinforcement. A slug of magnesium was placed on top of this and the whole arrangement was evacuated and heated so that the metal melted. The whole array was left to soak at temperature for 30 minutes, in which time the melt penetrated the preform. The chamber was finally pressurised with, presumably, an inert gas to complete the consolidation process. Pressure was maintained during solidification which took roughly 20 minutes. Exact experimental details are rather vague but this is probably because the system has been patented by MIT. The microstructures produced using this method are rather impressive, little or no porosity is observable and composites with up to $48\%_{vol}$ particles were manufactured. Some interfacial reaction was reported with the production of Mg_2Si, predicted as the reaction product of molten magnesium and the SiC particles. When smaller diameter particles were used (and hence the specific area increased) the quantity of this second phase increased, supporting the idea that the Mg_2Si is indeed an interfacial reaction product.

Turbine blades have also been manufactured by a similar route. Fibre preforms of tungsten and thoria wires/fibres were incorporated in a mould with a polymeric binder. This binder was subsequently burned off by the molten superalloy, which was forced through the preforms with inert argon gas[10].

c) Squeeze Casting

Squeeze casting differs from pressure infiltration in a very simple way. The previous technique relied on the pressure of a gas to drive the molten alloy through the preform, squeeze casting drives the infiltration forward by direct contact with a mechanical ram. The liquid metal is pressed into a fibre preform, contained in a die, hopefully producing a finished net-shape component. The pressures involved are higher than those used for ordinary pressure casting, for example, several orders of magnitude difference may exist.

With these kind of pressures care needs to be taken not to crush a fibre preform and thus induce catastrophic fibre breakup, in addition care needs to be taken to stop a preform from being squeezed so tight that the molten metal cannot penetrate. This is a common problem that is manifested by "dry" areas in the composite that are totally non-infiltrated.

Squeeze casting has however become a very popular method for producing metal composites. The attraction of this technique is that simple modifications to laboratory equipment can lead to a perfectly workable system. Hydraulic presses and hammers are all suitable candidates for conversion. Almost any combination of matrix and reinforcement is possible, in addition to this the method allows quick cycle times if controlled correctly.

The benefits of squeeze casting were recognised quickly by the Japanese who patented the process and up to the present day have the largest-volume application of metal matrix composite technology in the world. The component chosen by the Toyota Corporation was an automotive piston crown, this component required selective reinforcement for wear and thermal shock considerations. Production of the individually reinforced piston components now runs into millions each year, all of which are produced by squeeze casting. The Toaz Corporation in the USA are also producing reinforced piston crowns. These are for heavy diesel motors and generators and involve selective reinforcement of the piston combustion bowl[11].

Research into squeeze-cast metal matrix composites has been carried out for some years now at Surrey University. Bader, Clyne et al. have described work concerning aluminium alloys reinforced with Saffil fibres (short Al_2O_3 fibres manufactured by ICI Ltd)[12]. Quick cycle times were demonstrated in the paper, complete infiltration took only 2-3 seconds. Solidification followed and specimens were removed with the aid of a tapered dovetail machined into the punch of the casting machine. Mechanical tests showed that room temperature stiffness could be enhanced by as much as 30% for specimens with $24\%_{vol}$ reinforcement. Examination of fractured specimens showed little evidence of fibre pullout, hence it was deduced that a good fibre/matrix bond was produced. The

tensile strength of the composites was only modestly improved at room temperatures, however, strengths at higher temperatures were promising, being higher than for conventional alloys alone. This would seem to fulfil some of the perceived benefits of metal matrix composites in elevated temperature environments.

A Japanese research group has used a common casting flaw as a method for producing metal matrix composites[13]. In conventional sand casting, especially if carried out under pressure, some penetration of a sand mould occurs by the molten metal. The research team have used this phenomena as the basis for producing inexpensive composites of alloys reinforced with particle materials. Columnar bars of compacted particulates were placed in a heated die. Molten metal was then poured onto the compact and compressed. The effect of particulate pre-heat temperature and casting pressure were investigated. Various metals were also used, such as tin, lead and zinc. The degree of infiltration was determined by simply slicing along the length of the powder compact bar and examining the exposed cross-section.

Three applications were suggested as a result of the studies. Firstly, simple metal/particle composites could be manufactured for applications such as wear resistant bearings. Distribution of particles could be ensured by mixing with powder particles of the same composition as the alloy melt. Secondly, metal/intermetallic composites were manufactured by infiltrating metal particle compacts with another metal, e.g copper particles in a zinc matrix. Finally permeable structures were obtained by infiltrating a salt-grain compact with a molten metal followed by aqueous dissolution of the salt after cooling. These three products demonstrate the extreme versatility of squeeze casting as a method for manufacturing metal matrix composites.

d) Vacuum Infiltration

Fibres or alloys may exhibit high reactivities when heated in air or other gases. Under these circumstances it may be beneficial to heat the preforms and alloys under vacuum and then proceed with the infiltration also under vacuum. In addition to this, the surface

activity of fibres or preforms may in fact be higher in a vacuum, increasing the chances of good wetting.

An example of this type of technique is described by Aghajanian et al[14]. The arrangement was extremely simple, a preform was placed in a sintered alumina tray in a vacuum furnace with a block of solid Al-Mg alloy sitting above. The furnace was then evacuated, heated and then back-filled with an oxygen-free, nitrogen-containing gas (once again no details as the process was patented). A slight positive gas pressure enabled the atmosphere to be maintained. In this environment the alloy melted and spontaneously wet the preform, producing a completely consolidated composite. In the conclusions it was stated that this process could only work if the atmosphere contained nitrogen and the alloy contained magnesium. The additional presence of copper in the alloy retarded infiltration whilst silicon increased the effective infiltration.

Liquid Metal Infiltration (LMI) is the trade name for a technique that has been developed within the Defence Research Agency (DRA) at Holton Heath, Poole. The process involves a pressure vessel containing an inert crucible surrounded by radiant heaters. A variety of dies are placed above the crucible, these dies are connected to the pressure vessel by a ceramic riser tube which dips below the surface of the molten alloy charge. In simple terms, the pressure vessel is evacuated and the metal charge is melted, the die is also evacuated by a series of valves connected to the pumping apparatus. When the charge has melted a low pressure is applied to the inside of the evacuated pressure vessel. This induces the alloy charge to travel up the riser tube and into the die. The process has many benefits, the technique is performed *in vacuo* thereby reducing the risk of melt contamination and gas entrapment; also the pressures applied are quite low and therefore do not induce damage in the fibre preforms. It is now the subject of a number of patents and is being continuously evolved within the DRA. Composite specimens for this project were manufactured in this way.

e) Directional Solidification

This was, and still is, an elegant method of producing metal matrix composites. The process requires the controlled cooling of a eutectic composition alloy in such a way that fibrous, directional microstructures are formed *in situ*. The structure of these lamellae is strongly dependant on cooling conditions and alloy composition, the volume fraction of the reinforcing structure is obviously fixed by the position of the eutectic point.

In practice, the method is carried out in a manner similar to that used to directionally solidify superalloy and single crystal turbine blades. A chilled stage nucleates solidification, the stage is then gradually lowered from the hot zone inducing solidification in the direction of travel. Speeds may be of the order of centimetres per hour. An example of a composite manufactured in this way is nickel reinforced with TaC.

f) Spraying Techniques

An early example of a spraying technique was developed by Alcan Research Laboratories at Banbury[15]. An existing technique known as Osprey was modified so that ceramic particles could be incorporated into the jet of molten metal sprayed at a substrate. This method became known as spray co-deposition and is now the subject of a number of patent applications. The technique involves a crucible of molten alloy which has a nozzle arrangement at the bottom of the container. Pressure is applied to the melt and the resulting jet of molten metal is gas atomised. A stream of ceramic particles is incorporated into this jet which lands and is solidified on a rotating dish. The rotating dish is gradually lowered as the deposit grows, thus providing a type of continuous casting. The ingot, which can be up to 15' long is then mechanically worked in the same way as an unreinforced alloy. Alcan developed the technique to produce low volume fraction composites whose increase in mechanical properties could enable them to be substituted for conventional alloy structural components on a one-to-one basis.

Flame spraying has also been used to produce metal matrix composites[16]. Aluminium alloy matrix material was melted in a stream of C_2H_2/O_2 and short Al_2O_3 whiskers were then injected into a flame nozzle using N_2 gas. It was possible to produce a composite with approximately $13\%_{vol}$ reinforcement. Unfortunately, the composite exhibited high porosity and had to be extensively forged to reduce this and hence produce a fully consolidated material.

3.3 REINFORCEMENTS FOR METAL MATRIX COMPOSITES

3.3.1 Discontinuous

a) Particulate

Particulate reinforcements have been used in a number of production methods, such as spray co-deposition and compocasting. Various materials are used, mainly based on non-metallic compounds. Candidates can be found in standard particulate abrasive media, e.g Al_2O_3 and SiC[17] and a mixture of SiO_2/Al_2O_3[18]. In addition ThO_2 and mica[19] have also been used.

b) Short Fibre

Short fibre composites can include two types of reinforcement. The first is true, short fibres such as ICI's Saffil Al_2O_3 fibre. This fibre is often slurry cast into cake-like preforms especially for squeeze casting operations, as in the Toyota piston crown.

Secondly there are the whisker reinforcements. The difference between these two categories can be a fine one but is usually based on a difference in fibre diameter. Whiskers are generally short fibres having a diameter less than 1μm. SiC whiskers have been used in squeeze casting Al-Mg-Si alloys[20]. The abrasive nature of SiC can present problems in secondary processing of composites, for example in machining and finishing. To counter this effect, softer potassium titanate ($K_2O.6TiO_2$) whiskers have

been incorporated into aluminium matrices[21]. This whisker system was also much less expensive than SiC and also did not react so greatly with the metal matrix.

3.3.2 Continuous

A continuous type of reinforcement is needed in order to obtain optimum properties in a specific direction. Most manufacturers have therefore attempted to produce a continuous fibre, in some cases merely extending the length of existing discontinuous fibres, e.g ICI's Safimax fibres and their relationship with the Saffil family of short fibres.

Other examples of continuous fibres and their manufacturers are[22]:

Boron (monofilament)	Avco, Inc.,
SiC [Nicalon](yarn)	Nippon Carbon.,
Carbon [Celion G50](yarn)	Celanese Corp.,
SiTiCO [Tyranno](yarn)	Ube Industries, Jpn.,
$SiO_2/B_2O_3/Al_2O_3$ [Nextel]	3M Corp.,
Al_2O_3 [FP Alumina]	DuPont Corp.,

Methods for producing carbon fibres from polymeric precursors have been described by Balasubramanian[23]. These type of fibres have been used to manufacture composite material for this project and have been described in more detail in section 5.1.2 b).

DuPont's FP Alumina fibres have been incorporated into both aluminium and magnesium matrices[24], whilst continuous boron fibres coated with SiC have been incorporated into an Al-Zn-Mg matrix at Bath University[25].

3.3.3 Interfacial Considerations

The importance of the interfacial regions between the fibre reinforcement and the matrix has long been recognised as crucial to the production of high strength metal matrix composites.

Early studies of Al/Al_2O_3 composites showed that no readily identifiable compound formed at the fibre/matrix interface[26]. In some samples, where the matrix contained small amounts of magnesium, there was some evidence for the formation of a very thin magnesium-rich layer on the fibre surface. This may have been formed by the diffusion of magnesium atoms into vacancy sites on the fibre surface.

More reactive systems exist, such as carbon-reinforced aluminium. An interfacial carbide often forms with the formula Al_4C_3. This has been recorded by Chernyshova et al[27].

More reactive matrices have also been examined with carbon reinforcements[28]. Incorporating carbon into a Mg-Al-Si alloy matrix actually produced more intermetallics of $Mg_{17}Al_{12}$ than magnesium carbides. However these aluminides segregated at the fibre/matrix interface. Carbide needles were formed at and grew perpendicular to the fibre/matrix interface. These were aluminium carbides and were formed due to the presence of aluminium in the alloy formulation.

More complex phases may form in other systems. For example Al_2CuMg, $CuAl_2$ and the $MgAl_2O_4$ spinel has been shown to form in an Al-Cu-Mg matrix reinforced with Saffil fibres[29]. These phases are mostly brittle and may seriously degrade the performance of the composite. In such cases fibre surfaces may be altered or treated to prevent the formation of these compounds.

In many cases, a metal coating may be applied to the surface of a ceramic fibre to promote wetting by the matrix metal. Examples of this method are given by Abraham[30]. In the first of these references an aluminium coating was applied to alumina fibres by vacuum evaporation. The aluminium film adhered to the alumina due to van der Waals forces but unfortunately did not increase the strength of the composites on account of interfacial reactions with SiO_2 contained within the alumina fibres.

Madeleno describes a method for coating carbon fibres with nickel using electrolytic and electroless methods[31]. An acceptable thickness window for nickel occurred whereby a

coating of < 0.2μm produced a patchy coating, but a coating of > 0.6μm deposited in dendritic form. Apparently no fibre/matrix interfacial reaction was observed but reaction did occur between the matrix and the coating to produce $NiAl_3$ intermetallics. The best tensile strengths were obtained from coatings applied by cementation but these strengths were still less than that of the uncoated fibres.

Titanium carbide has been applied by a fairly exotic dipping method to carbon fibres incorporated in both Al-Mg and Al-Si matrices[32]. Once again tensile strengths were slightly below these predicted. The coating remained stable in the Al-Mg alloy but reacted significantly in the Al-Si matrix to form $Ti_7Al_5Si_{12}$, which was stated as not being detrimental to the bulk mechanical properties of the composite.

The conclusion to be drawn from this section is that some fibre/matrix interfacial reaction may be expected with uncoated fibres. However, fibre coatings can also induce the formation of complex intermetallics through reaction with a molten matrix. In some of these cases desired composite properties may be degraded rather than improved.

3.4 APPLICATIONS OF METAL MATRIX COMPOSITES

The potential applications of metal matrix composites are currently determined by production economics. The reason that the squeeze cast components from Toyota are so successful is basically due to the advantages of mass production in depressing component costs. Automotive engineering is a massive industry and is an ideal target area for metal matrix composites. Dinwoodie discusses the potential in this field with specific reference to incorporating the Al_2O_3 reinforcement produced by ICI[33] into aluminium. Projected uses included connecting rods, piston pins, cylinder liners and valve components.

British Aerospace have considered metal matrix composites along with other composites as candidates for structural airframes to be used in their HOTOL re-entry vehicle[34]. The outer space theme is continued in a number of publications where metal matrix

composites are considered as ideal candidate materials. Orbital cycling tends to induce severe thermal variations in structural trusses. Specific reinforcement may eliminate and reduce distortion by tailoring a composite such that it exhibits a zero coefficient of expansion[35]. In addition aluminium-based components could act as bumper plates to protect a satellite's delicate equipment from damage by micrometeorites.

The dimensional stability of metal matrix composites have made them suitable materials for sensitive components such as camera barrels for UV satellite telescopes, together with the framework on which to mount the camera in space[36].

Aluminium metal matrix composites have been researched as fusion reactor materials, mainly because of their high strength at elevated temperatures. The effect of radiation has also been examined for Al/SiC composites, where excellent stability under irradiation was observed[37].

The resistance of metal matrix composites to hard object impact damage has been discussed by Awerbuch[38]. Metal spheres were projected at the composite plates at speeds up to 4000ft/s. For Al/Boron composites cracks reduced mechanical strength by up to 50%. Titanium reinforced with Borsic fibres demonstrated much better damage tolerance, showing only a 20% degradation in strength. The projectile speeds and the affiliation of the author (Wright-Patterson Airforce Base) would presumably indicate the interest in these materials for armour plating applications and bird strike protection for jet engine components.

The final application discussed in this section is that of composite hull structures for submersible vehicles. This application is most closely allied to the interests of this project's sponsors (DRA Holton Heath). These structures have been built from epoxy-based polymer composites[39], filament wound around a suitable mandrel. However, the stringent requirements of the Royal Navy are most suitably met by a hull structure manufactured from a metal matrix composite. The design remit of these components is basically to increase the resistance to buckling. In simple terms this would increase the

collapse depth of a submersible vehicle and thereby expand its potential theatre of operations.

It is anticipated that these large structures will be cast using the Liquid Metal Infiltration method developed within the DRA.

3.5 JOINING METALS USING POLYMERIC ADHESIVES

3.5.1 Introduction

Historically, adhesives have been used in very advanced pieces of high-tech engineering. The best early example is probably the composite bow, evolved concurrently in Central Asia, Eastern Europe and India. Animal products were boiled down forming a product that enabled the various components of the bow to be assembled; sprung wood, cartilage and tree-bark were all held together by this natural adhesive.

From these early examples of adhesive science until well beyond the industrial revolution, adhesives themselves tended to be relegated to more mundane fields. However, the use of adhesives has become well established recently, mainly through advances in the various fields of polymer chemistry and polymer engineering. Indeed, adhesives and glues are now so ubiquitous that they are largely ignored or considered as examples of low-technology. The largest current market examples are: *packaging* (seaming, labels, corrugated boarding), *tapes* (surgical, masking, insulating), *construction* (acoustic panelling, joint cements, tiling, dry wall lamination), *transportation* (vehicle trim attachment, roof bonding, vehicle assembly, seals and gaskets).

Most engineering products or processes rely on the joining of components together in order to assemble a larger, more complicated, structure. Traditionally the techniques used for joining have relied on a certain amount of sustained substrate damage; for example, drilling prior to mechanical fastening, melting during welding.

It has long been realised that mechanical fastening methods do not distribute engineering loads evenly. As a result of the local nature of these methods high stresses can be generated over small areas during use. The application of adhesives, especially, can significantly reduce these local stress concentrations by helping to spread the loads over a larger area. In addition to this, adhesives can also be used as sealants, thus conferring a degree of corrosion protection to the joint in question. This is of course the preferred method of joining in many branches of engineering nowadays, the supplementation of traditional joining methods with adhesive bonding.

With the development of more advanced resin materials the number of advanced applications of polymers in adhesion has grown very quickly. A confidence gap has traditionally existed between adhesive engineers and design engineers, but a large expansion of the "adhesive" knowledge-base has begun to close this gap. Indeed examples of both primary and secondary structural adhesive joining may be found today in many critical areas such as aerospace, sub-marine and automotive engineering.

Structural adhesive bonding appears to be expanding rapidly. In 1979, structural bonding accounted for 10-15% of the volume consumption of adhesives. Predictions stated that this figure would grow by about 8% per year through the 1980's[40].

3.5.2 Theories of Adhesion

If two plane surfaces are brought together, then intimate contact is only made at a few points across their interface. Most of the volume in between them is occupied by air. To obtain a more intimate contact, pressure in the form of a load must be applied. This will cause some deformation of the substrates and produce contact areas instead of contact points. When the load is removed, some of the energy applied, stored elastically in the substrates, is dissipated by breaking some of the contact points again. An adhesive will displace the air and fill the volume between the substrates, enabling good contact between the adherend and the adhesive. Most adhesives will set or cure into the solid state, thus allowing the transfer of stress between substrates.

For complete accuracy, adhesion theories must explain the wide range of phenomena that occur in a bonded joint. These include molecular structure and behaviour of adhesive and substrate, thermodynamic and kinetic properties of surfaces and the distribution of stress inside the joint.

At present there are four main theories that have been proposed as explanations for the behaviour of adhesives. None of these theories offers a comprehensive or unified explanation, indeed to do so would require the inclusion of many inaccurate generalisations. It is accepted therefore, that a number of different mechanisms may operate, either separately or synergistically, to give *good adhesion.*

a) Mechanical Interlocking

Mechanical interlocking was an early theory used to explain adhesive behaviour and arises from the rather instinctive idea that an adhesive will flow into and around surface asperities, cure, and then provide strength, due to physical hindrance and interlocking, along a labyrinthine surface/adhesive interface. Joint strength, in this example, is derived from the amount of work required to break off interlocking adhesive members.

Related to this notion is the fact that if there is a sharp change in modulus between adhesive and substrate (as with a smooth, flat surface), the adhesive would have difficulty containing the concentration of stress at the interface without fracturing itself. A rougher surface finish may be more effective in transferring or dissipating this stress concentration[41]. The increased surface roughness also increases the effective area available for bonding.

The adhesion of polymers to metal substrates has been examined by a number of groups. A lengthy and particularly systematic series of studies was performed by Packham et al[42,43]. Work was originally performed on anodized aluminium using a 180° peel test with low density polyethylene as the adhesive film. Changes in the peel strengths of polyethylene bonded to sealed and unsealed anodized surfaces indicated that penetration

of the polymer into the porous anodic structure had occurred. Variations of peel strength with thickness of anodized film also seemed to support the idea that pore penetration was important. In fact the adhesion of polyethylene to sealed anodic films was shown to be lower that to unsealed films if antioxidant was added to the polyethylene (the role of polymer oxidation is discussed in 3.5.2 b) Adsorption Theory). The second paper by Packham et al provides evidence based on scanning and transmission electron microscopy of adhesively bonded films. Bonded specimens were placed in 50% w/v NaOH in order to dissolve away the aluminium substrate, leaving behind polyethylene "replicas". Tendrils of polyethylene indicated that pore penetration, and hence a degree of mechanical interlocking, had occurred.

Subsequent work on the adhesion of polyethylene to copper substrates also showed the importance of topography in adhesion[44]. Copper specimen surfaces were oxidized chemically to produce thick, black, films of CuO. Peel strengths of polyethylene to the fibrous CuO films were good, approximately 1.4 Nmm^{-1}, compared with 0.2 Nmm^{-1} on chemically polished copper substrates.

A series of experiments were run to eliminate any oxidative effect on the polyethylene. Antioxidant, added to the polyethylene, still gave good peel strength results on the rough oxide surface. Electrolytic reduction of the oxide film to Cu_2O, whilst maintaining surface morphology, also gave good peel strengths[45,46,47].

Separate work at the Admiralty Research Establishment has also demonstrated the variation in single-lap shear strength of adhesively bonded specimens with differing surface morphology[48,49].

Specimens that had been hard anodized in cold sulphuric acid (≈-5°C) were subjected to a number of post-anodizing chemical etches. These etches produced a number of anodic oxide topographies. The bond strength results were compared to those obtained by using conventional aluminium surface pre-treatments, such as degreasing, NaOH etching, mixed Chromic/Sulphuric acid etching, chromic acid anodizing and phosphoric acid

anodizing. The various oxide morphologies were compared, and the importance of tailoring surface topography in order to obtain sufficiently high bond strengths was established[50].

Early work by Jennings[51] also examined the bond strength of adhesives as a function of surface roughness. Samples were joined using a butted tensile configuration and results showed that a sand-blasted surface gave consistently higher bond strengths than the as-received material. In addition, the same tests were performed using a highly oxidizing mixed acid etch, comprising chromic and sulphuric acids. The effect of this acid treatment was to increase bond strengths in all cases compared to unetched specimens. This leads to the interesting speculation relating to whether micro-, or macro-, surface roughness is important.

The plating of metals onto plastics, mainly for lower cost decorative applications, has been a large unit-volume section within the polymer industry. Some workers have speculated that surface topography, and hence an implied component of mechanical interlocking, is important in the electroplating of plastics, notably ABS[52]. In high impact strength plastics, a common feature is the presence of a rubbery phase that is based on butadiene, which may be co-polymerised with either acrylonitrile or styrene. The process relies on a mixed chromic/sulphuric acid etch in order to plate a metal onto the plastic substrate. This etch removes the rubbery phase and produces a porous, rugous surface. After sensitization, the rough surface is plated with copper. If this sample is pyrolyzed or placed in an oven to burn off the polymer, a copper replica of the surface is left behind. Examination of this replica yielded detailed information concerning the extent of the surface roughness of the ABS after etching and provided some support to the postulation that mechanical interlocking has a part to play in the promotion of a good adhesive bond.

A final example of mechanical interlocking, quoted by Wake[53], concerns fillings in dental practice. Traditional fillings were made by drilling a cavity with a base that was wider than the cavity opening. Amalgam filled the cavity which expanded on hardening to give a true, mechanically interlocked fixing. However, modern polymeric

developments have allowed the introduction of acrylic materials. These acrylics bond chemically with dentine and enamel, eliminating the need for extensive drilling and filling. This implies that other phenomena and processes may indeed be important in an application requiring adhesion.

b) Adsorption Theory

The adsorption theory has gained wide acceptance as a general explanation for the adhesion of surfaces. It proposes, in brief, that mating surfaces will adhere provided that thorough intermolecular contact is obtained between those surfaces. The forces that are usually present and act in such a situation are van der Waals and London (or Dispersion) forces. These forces exist universally and if small enough intermolecular separations are obtained, powerful interfacial attractions ought to occur, irrespective of the chemical nature of the two phases in contact. The exact nature of the materials governs the magnitude of these dispersion forces, the highest being between two dielectrics. The magnitude of the dispersion forces between a metal and a dielectric tends to be at an intermediate level.

Huntsberger has calculated the force of attraction between two parallel, plane plates at separations of 10, 100Å and at molecular contact[54]. Even with a separation of the order of 10Å, attractive forces of the order of 10^2MPa might be expected.

This type of calculation was also performed for a polyethylene/iron interface[55]. van der Waals forces alone accounted for a tensile strength of 175,000 psi, which was at least an order of magnitude larger than the actual measured tensile strength. The reason for this discrepancy is because an adhesive bond generally fails due to the presence of discontinuities and the growth of a catastrophic crack. The inference of these theoretical calculations is that if molecular contact were attainable, reasonably high joint strengths could be expected from the interaction of dispersive forces alone.

These calculated results are significantly higher than those measured under experimental conditions. An attempt has been made by Kinloch to explain the discrepancy in the measured data compared to the calculated figures; cracks, voids, defects and geometric aspects of joint design are all thought to contribute to a reduction in effective attractive force[56].

Huntsberger[54] performed an experiment to ascertain the peel strength of poly (n-butyl methacrylate) adhered to a steel substrate. Samples bonded at 150°C for one hour exhibited higher bond strengths that those bonded at 100°C for one hour. An explanation was given in terms of differing degrees of interfacial contact. The samples bonded at the lower temperature had not attained interfacial equilibrium, the interface may have contained many small discontinuities. The samples bonded at the higher temperature had reached, or were close to reaching, interfacial equilibrium where non-wetted regions were too small (or too few) to be significant. It was suggested that stress concentrations did not occur inside the joint bonded at higher temperatures, only at the joint edges. These results, amongst others, led Huntsberger to observe that wetting and bonding were synonymous. He was careful to state that his conclusions were inferred and hence constituted an hypothesis, direct evidence being unavailable.

The idea of joint strength being dependant on the wetting of a substrate led to the concept of the critical surface tension for wetting (γ_c). In order to obtain a reasonable adhesive bond, the adhesive must have a surface tension less than the substrate value of γ_c at any given temperature.

Kinloch[56] points to some publications that support and others that conflict with this concept, he suggests, however, that practical test methods may be unsuitable for the confirmation of purely theoretical ideas.

The thermodynamic work of adhesion W_A can be related to surface free energies by the Dupré equation:

$$W_A = \gamma_1 + \gamma_2 - \gamma_{12}$$

This equation states that W_A is the sum of the surface free energies of the solid and liquid, minus the interfacial free energy[57]. Assumptions need to be made to use the Dupré equation in this form. The assumptions made basically state that the surface energy of the liquid does not change when it solidifies isothermally, and that shrinkage stresses are ignored. Under these conditions, the Dupré equation may be applied to solid adhesive/substrate interfaces.

The conventional method for measuring values of γ_1 etc is by the contact angle method. This method is relatively simple in theory, although more difficult to perform in practice. It relies on the shape assumed by a sessile drop of liquid at rest on a solid surface. The angle shown θ in figure 1 is the contact angle. Obviously, maximum adhesion will occur when the work of adhesion, W_A, is at a maximum.

Other forms of bonding may occur between adhesive and substrate in addition to the dispersion forces present. Sykes and Hoar[58] examined the adhesion of polyethylene to aluminium and copper substrates. Peel strengths on bright copper surfaces are quite low compared to the strengths on aluminium surfaces. It was suggested that copper inhibited the oxidation of polyethylene, thus preventing the formation of active groups in the polymer. However, if polyethylene is oxidized before application to a copper substrate, then increased peel strengths were noted.

Bikerman[59] had previously postulated the presence of a weak boundary layer at the interface of a system bonded with polyethylene. This layer was reportedly composed of a segregated layer of low molecular weight polymer. Sykes and Hoar suggested that when polyethylene was oxidised, the active groups might reduce the influence of Bikerman's weak boundary layer. This might be effected by the active groups crossing the boundary layer and acting as links from the polymer to the metal surface. Oxidized polyethylene contains -C=O- groups which are capable of being chemisorbed onto the substrate surface, producing a higher degree of adhesion. It is possible that in order to remove the polymer coating (or adhesive), the chemisorbed links must be broken, either by fracture

of the carbon-carbon backbone, or pulling the chemisorbed chain out of the polymer matrix. In order to achieve the latter, work must be performed against the van der Waals forces that act along the chain lengths.

Primary interfacial bonding has been shown in a number of studies to contribute significantly to the levels of adhesion in a bonded joint. Workers, amongst them Kinloch[56], consider, for instance, that primary chemical bonding is a pre-requisite for environmentally stable (or durable) adhesive bonds. Modern surface sensitive techniques like x-ray photoelectron spectroscopy and secondary-ion mass spectroscopy, have been employed to try to provide direct evidence for the presence of chemical bonds between adhesive and substrate.

The use of adhesion-promoters, or coupling agents, is a field that has been investigated thoroughly using surface analytical techniques. These agents are used to increase joint strength and durability by chemically interacting with both the adhesive and substrate. The oldest known coupling agents are the chrome complexes of methacrylates. The complex is thought to react with adherend surface-hydroxyl groups. More recently organic titanate compounds have been used as coupling agents, but the most common of these agents are the *silanes*. These compounds have two functional chain-end groups which may be simply represented as:

$$X_3\text{-Si-}(CH_2)_n\text{-Y}$$

where X is an hydrolysable group that can react with a metal or metal oxide, and Y is an organo-functional group designed to be resin- or adhesive-compatible. Silanes are used as a size, coated onto glass fibres prior to incorporation in a resin matrix, as a priming layer on the surface of a metal substrate prior to adhesive bonding, or as part of the adhesive formulation itself.

The accepted mechanism for their chemical interaction arises from the formation of a SUBSTRATE-O-SI- bond. Kinloch and Gettings[60], using secondary ion mass spectroscopy (SIMS) analysis on silane-primed mild steel substrates, isolated the $FeOSi^+$ radical

species. They also isolated the $FeOSi^+$ and the $CrOSi^+$ radicals on silane-primed stainless steel substrates. This, they stated, provided evidence for the existence of primary interfacial bonding, in the form of -Fe-O-Si-- and -Cr-O-Si-- bridges between the polysiloxane and metal oxide substrate.

It is worth highlighting Wake's observation relating to the work of Packham et al. He points out that the mechanical contribution to the adhesion of polyethylene to anodized aluminium is significant, but the actual retention of polymer in an anodic pore-cell must be due to the interaction of dispersion forces in the polymer and on the cell walls.

Adsorption theory is important therefore, and offers a fairly broad explanation for the interaction of an adhesive with a substrate.

c) Diffusion Theory

Diffusion theory became popular and was propounded chiefly by the Russians, especially Voyutskii[61]. The theory is based on the supposition that high (chain length) polymers adhere to each other, and themselves, by the diffusion of polymer molecules across their interface. Essentially, this theory relates to the adhesive bonding of polymers to polymers, particularly if the polymer and substrate are the same material.

Early Russian workers (Zhukov and Talmud, 1935) coined the term *autohesion* for the adhesion of a material to itself. In order that sufficient diffusion occurs, certain conditions must be satisfied with respect to the polymer chains concerned: i) the molecules must be sufficiently mobile and, ii) the molecules must be mutually soluble.

Adhesives can be supplied in various forms, some in suspension for instance, some in solution. In these cases the adhesive must be allowed to dry out after application. For the diffusion theory to operate effective adhesion may only take place if the interface is destroyed by mutual diffusion of the adhesive molecules. Polymer molecules must therefore be compatible (especially important if the polymers are dissimilar) for this effective diffusion to take place. The actual movement of molecules is quite small and in

a high chain length polymer with a repeat unit of thousands, only tens of repeat units may actually move across the interface. The degree to which a polymer molecule can diffuse into another polymer must depend strongly on the size and aspect of available "pores". These "pores" are the spaces in and around a chain molecule and are known as the free volume of a polymer.

Diffusion between dissimilar polymers is not thought to be common. Huntsberger[54] describes an experiment where a mixed solution of polymethylmethacrylate (PMMA) and polystyrene (PS) in toluene was left to stand, the solvent was then allowed to evaporate. The resulting thin films of PMMA and PS were peeled apart, a spectrophotometry technique was used to assess the composition of these films, and no evidence of interdiffusion was found. The experiment seemed to indicate that interdiffusion was not applicable in a broad sense.

The diffusion of polymers across an interface involving a metal substrate is questionable, although porous oxide structures may exhibit this effect. Moth[62] has noted examples where the bond strengths of acrylic-bonded anodized aluminium increase with time. Coupons were tested after the normal cure of 24 hours and after 6 months. Diffusion of the acrylic adhesive into the porous anodic aluminium oxide is possible, but more likely, is the fact that the adhesive exhibits significant post-bonding cure after the recommended 24-hour period. In other words the adhesive continues to cure over the months following the initial bonding operation.

d) Electrostatic Theory

The concepts in this theory were developed and proposed mainly in Russia, by Deryaguin. Electrostatic theory of adhesion supposes that a charge transfer occurs across an interface which results in the formation of an electrical double layer. It can be shown in a dark-room that adhesive tapes, stripped rapidly from glass substrates, produce electrical discharges. Deryaguin treated the adhesive and glass substrate as two plates of a capacitor. Separation of these plates leads to a separation of charge which gives rise to a

potential difference, which is dissipated as a spark. Deryaguin appeared to have made a number of false assumptions concerning the dissipation of the work of adhesion. Visco-elastic response of the polymeric materials was ignored and this lead to a general lack of enthusiasm for the theory.

The concept of an electrostatic component of adhesion should not, however, be completely ignored. The Xerox machine and dust filters are reminders that particles, at least, may adhere to a surface by this method. Additives to proprietary polymeric materials may have some influence on the formation of an electrical double layer. The charge carrying bodies in polymers are not exactly known; adhesion levels of substrates and polymers have been compared to those between substrates and polymers that have been radiation polymerised from purified monomers, have been suggested[56,57].

To conclude, the electrostatic theory of adhesion undoubtedly has applications but ought to be put into perspective. The theory can account for some degree of adhesion but cannot be used as a unifying explanation for the adhesive behaviour of polymers.

3.5.3 Structural Adhesive Bonding

The American Standards Group define a structural adhesive as basically a bonding material that transfers loads between adherends exposed to service environments typical of the structure involved. Structural adhesives fall into a group of materials that give high strength bonds (say greater than 1000 psi). However, a structural adhesive must also demonstrate durability, this is implicit in the definition given earlier. Studies have therefore been carried out (many sponsored by the military) to attempt to discover what processes govern corrosion resistance and crack propagation under environmental conditions[63,64]. Aerospace applications in the tropics and various marine applications have been targeted as critical in the past, however most structural adhesives nowadays tend to exhibit corrosion protection, usually conferred by including corrosion inhibitors in the formulation of the adhesive or primer, if used.

In February 1975 the US Air Force awarded contract No F33615-75-C-3016 to the Douglas Aircraft Company. This programme was entitled "Primary Adhesively Bonded Structure Technology - PABST" and provided a high profile to the subject of structural adhesive bonding. An airframe fuselage was chosen for manufacture and assembly with adhesives as it provided scope for cost and weight savings in both acquisition and service. Various fields were identified for research including adhesive selection, structural evaluation and manufacture/inspection. The programme was a large one but the conclusions can be summarised briefly; it was possible to design and produce the individual components of a fuselage and successfully bond them into a single structure; cost savings of some 20% were achieved; corrosion resistance was increased; reduction in numbers of rivet holes reduced the likelihood of fatigue crack growth. It is important to realise the significance of this programme as it managed to take basic concepts of adhesion and put them into the context of a realistic production environment.

The potential of adhesive technology may be illustrated by studies carried out by the Lockheed Missiles and Space Co concerning the suitability of some structural epoxy adhesives for outer space applications. Generally a typical space structure would be required to sustain only moderate loads and adhesives would appear to be an ideal choice of joining media due to their high efficiency and weight saving characteristics. However, the adhesive would need to be able to sustain the conditions of creep experienced during periods of storage on earth, launch and orbital manoeuvering. The adhesive must have an ability to accommodate widely varying strains, exhibited by the metals they join, produced under large ranges of solar heating and cooling. Finally, the adhesives must not out-gas in space as they may contaminate sensitive payload equipment[65]. Room temperature cure resins appeared to offer better properties than their elevated-cure counterparts.

More recently, attention has been focussed on structural adhesives for repair work. It appears that this field is emerging because it is common practice to keep aircraft in operation long after their predicted service lives are finished. The service life is extended

in this fashion mainly because upgrading existing technology is cheaper than purchasing new aircraft. Repair work can fall into three categories, depot, field and battle. These reflect differing levels of desirability; battle repairs in military aircraft can only be temporary as they tend to adversely affect airworthiness; field repairs often depend on operator skill and repair environment. In the field, limitations may also be experienced in terms of adhesive cure and storage facilities (i.e availability of freezers for storing low-temperature cure adhesives and autoclaves for high-temperature cure adhesives). In view of these limitations only a repair performed at a fully equipped depot would attempt to return an aircraft to unrestricted service[66]. A number of desirable characteristics have been formulated for repair adhesives, these include: storage stability; quick cure at lower temperatures; insensitivity to bond line thickness; and finally mix ratio insensitivity (for adhesives with multi-part formulations). Correct choice of fillers and additives in the adhesive formulation would presumably go some way to achieving most of these requirements.

Other groups have also researched repair adhesives[67,68], and have shown that the fatigue life, for example, of a cracked composite component can be greatly increased by using composite patching. Hot cure adhesives seem to offer better properties but cold cure adhesives are easier to apply by less highly skilled operators, offering adequate temporary repairs and enabling restricted flights from the field to a depot. Choice of repair adhesives appears to lie between epoxy and acrylic resins.

a) Surface Treatment of Aluminium Adherends

The main driving force for structural adhesive bonding for the last 40 years has undoubtedly been the aerospace industry. The very rigorous safety requirements in this area have necessitated research into adhesive bonding, and surface preparation has been identified as one of the single most important considerations. Obviously, it is important for the adhesive to wet the substrates being joined. Successful wetting of a substrate depends on, amongst other things, surface chemistry and topography. Therefore, many

different types of surface treatment have been devised in order to promote conditions that lead to wetting and hopefully to strong, durable joints. Successful adhesive bonds may only be achieved on surfaces that are very clean. Handling, rolling of sheet product and contaminants picked up during storage all contribute to the formation of an oily layer on the metal surface. Before any subsequent surface modification can be realised this surface soil must be removed, either by solvent cleaning, abrasion or chemical etching. Many manufacturers claim to be able to bond through oily layers but long-term bond strengths under these conditions are never high.

The current research is being focussed on aluminium, a material which is of special interest to the project sponsors. Therefore, it is useful to describe surface preparations for aluminium and its alloys.

Due to the electronegative nature of aluminium, a strongly adherent oxide film tends to form on exposure to the atmosphere or when exposed to an oxidising media. Values for the thickness of this film vary but a typical thickness could be 3nm. This value may increase up to 100nm in a humid environment.

When bonded without surface treatment, an aluminium specimen may show reasonable initial bond strengths. On exposure to a moist environment the bond strength may even rise due to plasticization of the adhesive. Lengthy exposure to moisture will inevitably result in bond failure, mainly due to hydrolysis of both the adhesive and the barrier oxide, resulting in the breaking of the chemical link between the adhesive and substrate[69]. Therefore, a typical surface treatment would seek to modify this barrier film in such a way that, not only is the initial bond strength increased, but there is also a corresponding increase in durability (or resistance to hydrolysis/corrosion).

The types of surface pre-treatment available to an adhesive engineer range from simple surface cleaning to complex oxide enhancement, through etching to anodising[70]. Generally, the more effective methods remove most, or all, of the naturally forming

barrier oxide, replacing it with a thicker, artificially-grown oxide, perhaps of more uniform structure.

Surface pre-treatments can be extremely complex. For example, previous work at ARE Portland by Arrowsmith and Clifford[71] lead to the development of a 4-stage process for aluminium that involved: a degrease, a caustic etch, sulphuric acid anodising, and finally a post-anodising hot phosphoric acid dip. Other types of anodising have been performed, chromic acid anodising (CAA) is generally preferred in the UK, whilst phosphoric acid anodising (PAA) is preferred in the USA. The chromic acid anodising process tends to produce dense but thinnish coatings (approx 2.5μm) which may also be dyed or impregnated, and is widely used in the aerospace industries.

Phosphoric acid anodising was developed as a pretreatment to adhesive bonding by the Boeing Corporation. The structure of the oxide is different to that formed in chromic acid anodising in that it exhibits a much more open and porous nature, strongly dependent on its base alloy microstructure[72].

The importance of surface treatment has been realised for some time now, however, an American group led by Venables was instrumental in formulating the inter-dependences of oxide type and morphology on the strength and durability of an adhesive bond[73]. A mixed acid etch (FPL) was used to prepare the aluminium specimens prior to bonding. Based on chromic and sulphuric acids, this etch proved useful on its own and also as a sensitizing etch prior to anodising. Workers in the Ministry of Defence (UK) have also examined this type of surface treatment with particular reference to its use prior to anodising[74]. Details of the etch procedure are explained in the Experimental section of this work.

The known history, relatively good performance and reproducibility of the FPL etch led to the inclusion of this pre-treatment in the adhesion program for this project.

b) Epoxy Adhesives

The epoxy resins that comprise the functional part of these adhesives can vary enormously in their physical and chemical properties, depending upon their composition. This composition can range from aromatic to aliphatic, cyclic or acyclic, mono- or multi-functional (i.e one, or many, oxygen rings present in the molecule). The common thread linking all of these compounds however is the 3-membered, oxygen-containing epoxy group, sometimes known as the *oxirane* group. This group can be conveniently represented as:

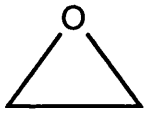

The epoxy adhesives have been formulated successfully to meet a number of essential pre-requisites. They usually cure with minimal loss of volatiles, removing the need for fume and solvent treatment equipment. Epoxies exhibit some shrinkage at the bondline upon cure, however this can be minimised by the inclusion of well chosen filler compounds.

Due to the essentially complex nature of the epoxy molecule, both polar and non-polar moieties co-exist. This leads to their excellent adhesion to a number of varied substrates such as steel, glass, aluminium etc.

A certain amount of "ring-strain" exists in the oxirane structure shown earlier. The need to release some of this ring strain explains why both nucleophilic and electrophilic curatives react and work so well with this compound group. This "ring-opening" confers high crosslink density, which when coupled with the ability to participate in hydrogen bonding means that epoxies have good strength and creep resistance (this is the reason why monofunctional epoxy materials are not generally used as they produce quite low crosslink densities).

Being a single part adhesive, with the catalytic curing agent present in the formulation, it is important that the catalyst does not begin to operate at ambient storage temperatures. Cure agents are carefully chosen to be either insoluble in the epoxy at room temperature, or, to be non-functional at room temperature. In each case a certain threshold temperature has to be reached before the cure takes place. Catalysts always have some type of residual, low grade action even at room temperature. Therefore most single-part epoxies need to be stored at refrigerant-type temperatures. Catalysts tend to be nitrogen-containing compounds such as amines or cyanamides.

The toughening phase present in the epoxy adhesive is a co-polymer of butadiene and acrylonitrile. The acrylonitrile increases the strength and chemical resistance of the butadiene. The butadiene provides the toughening by existing as a discrete phase within the adhesive. Invariably, the butadiene will have some functional group present that is capable of co-curing with the epoxy adhesive.

c) Acrylic Adhesives

Acrylic adhesives are now produced by a large number of companies such as, Ciba Geigy, Goodyear, Du Pont, B.F Goodrich and many more. This widespread interest points to, and would seem to reflect, the potential of these materials. Figures indicate a relatively small share of the adhesives market in terms of annual material consumption (approx 10%), indicating that acrylic adhesives are yet to achieve their perceived potential. An acrylic adhesive basically consists of three components: a monomer, a toughener and a catalytic cure compound.

Monomeric materials are generally based upon monofunctional methacrylates. The lower crosslink density exhibited by these monomers is useful for toughening the adhesive. Monofunctional monomers are quite volatile but are important for a number of reasons; they cure quickly and consistently, they have a higher T_g than higher-alkyl derivatives and they have a solvent ability. This solvent ability is quite critical as it allows the adhesives to

be used on contaminated surfaces such as oily steel and aluminium. An example of a lower-alkyl monomer could be[75,76,77]:

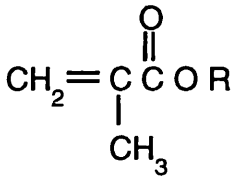

where R could be CH_3 or CH_2CH_3

Tougheners used in these adhesives are usually some type of rubbery phase, existing discretely in the acrylic matrix. This toughening mechanism is similar to that used in epoxy technology. Polybutadiene/acrylonitrile rubber may be used[78] but the most common toughening phase is chlorosulphonated polyethylene. Various side-chain groups are grafted onto the polyethylene molecule, such as vinyl-monomers. These monomers then participate in chemical reactions between the rubbery phase and the acrylic matrix, enhancing the toughening effect of the rubber.

The curing process is very complex for acrylic adhesives, the chemistry of which goes well beyond the scope of this project. However, in brief, curing is achieved by coating one side of the adhesive joint with a *primer*. This primer is formulated to contain hydroperoxides together with a condensation product of an amine and an aldehyde. The condensation product gradually reduces the peroxides to free radical species, which then take part in a sequence which leads to the polymerisation of the acrylic under essentially anaerobic conditions. In effect the acrylic is a two-part adhesive which requires priming, but not mixing, before application.

d) Adhesive Joints

The basic requirement for a high strength adhesive bond is that intimate contact occurs between the adhesive and the substrate. This intimate contact needs to be established right down to a molecular level. In order to achieve this, the adhesive must be capable of being spread conveniently and uniformly across an adherend, it must displace any air that may become entrapped and also be able to operate in the presence of any contaminants existing on the specimen surface.

In order to design a safe and durable adhesive joint, some predictions have to be made concerning the future load regimes and environmental conditions experienced by that joint. This is a very difficult type of prediction to make, but a designer has some basic rules to rely on, rules that have been refined through much experience. These can be summarised as follows[79]:

- maximum bond area should be used.
- the joint should be stressed in its strongest direction, i.e shear or tension.
- stresses in the weakest direction, i.e peel and cleavage, should be minimised.
- allowance should be made for residual stresses such as thermal mismatch.

The various preceding sections describe different ways in which the strength of an adhesive bond may be affected by its environment. This includes, of course, both its physical and chemical environment. It is important to realise that the strength of an adhesive bond is not a deterministic quantity. In other words bond strength cannot be predicted solely from knowing what the adhesive and substrate will be in advance. The factors and interdependences are too complex; bond strengths are generally predicted along statistical lines, based on large quantities of specimen testing and years of experience.

A generalised relationship has been produced that is useful to study, simply because it lists the most important factors governing the strength of a bonded joint. This generalisation can be expressed as:

$$F_{meas} = f\,[\,M, W_A, E, G, \mathcal{G}_c, \Delta H_{surf}, \delta_1\text{-}\delta_2, r, \nu(t)]$$

This expression states that the measured strength of an adhesive bond, F_{meas}, is a function of:

- M, the mechanics of the joint
- W_A, the work of adhesion
- E, Young's Modulus of the substrate
- G, Shear Modulus of the adhesive
- $\mathcal{G}_c$, Fracture resistance of the materials
- ΔH_{surf}, the strength of the interfacial chemical bonding
- $\delta_1\text{-}\delta_2$, solubility parameter or degree of mutual solubility
- r, the surface roughness
- $\nu(t)$, viscosity profile of the adhesive during cure

Some or all of these variables are interdependent and give a good idea as to the complexity of trying to predicted the behaviour of an adhesive bond.

The benefits of using adhesives are readily understood but a certain amount of thought must be given to their limitations. A number of points have been listed that question the reliability and are supposed to have limited the wider use of structural adhesives. The list, as compiled by DeVries and Anderson[80], is as follows:

- Which test method allows the mechanical quality of an adhesive to be evaluated?

- How can test results be compared with results from other tests, performed perhaps under differing conditions?

- How are test results related to the performance of a real in-service component?

Questions also need to be asked relating to the quality or strength of the adhesive. The authors referred to previously state that tests need to be performed on the adhesive alone for the following reasons:

- In order to compare the mechanical properties of a group of adhesives.

- Testing as a means of "batch checking" (e.g deterioration of adhesive quality with age, etc?).

- To check and compare the effectiveness of surface preparations and pretreatments.

- A means to determine parameters that may subsequently be used to predict adhesive performance.

The type of problems just mentioned, and the ideas that have limited the application of adhesives, are topics that have concerned the large producer and user corporations. These may go beyond the scope of this programme but it is important to view developments in adhesive technology in a broader context.

3.5.4 Adhesive Bonding of Metal Matrix Composites

Although the benefits of metal matrix composites are widely perceived, their potential for successful application has yet to be realised. This is especially true in the field of adhesive bonding. Through the period of this programme no publications were available on this subject, only in the last year or so have researchers acknowledged the importance of the area and have begun to produce papers about their work.

One of the first publications found in this subject was by workers at the US Army Materials Technology Laboratory[81]. Particulate composites were used comprising of aluminium alloy 6061 reinforced with SiC particles. A number of surface pretreatments were then examined, including the FPL etch used in this project. Not surprisingly the materials responded very differently to these treatments compared with unreinforced materials. The most relevant result in this work was the response of the composites to the FPL etch. Apparently there was much selective etching around the particulate reinforcement coupled with the formation of craters and cavities in the matrix alloy. The result of this selective etching was to leave particles standing proud from the matrix surface. This observation matches well with the observations in this project concerning the response of materials with complex microstructures to the FPL etch. Thick specimens were tested in shear and good bond strengths were obtained, probably on account of the higher strength of composite specimens resisting bending during testing. Future work by this group intended to examine the durability of similarly bonded composite specimens.

Similar studies are currently being carried out in the UK on adhesive bonding of various aluminium alloys. Work by Davis and Ritchie[82] has looked at some of the alloys that are likely to be used as matrix materials for metal composites, e.g Al-2.25% Mg.

This paper was a modelling exercise for samples that had been anodised in chromic and phosphoric acid. The porous anodic oxide was infiltrated by a mobile adhesive and this infiltrated layer was then considered to be a "micro-composite". The intended interest of the research group was eventually to examine surface pretreatments for metal composite materials.

3.6 DIFFUSION BONDING

3.6.1 Diffusion

Diffusion is a fundamental material process that controls how, and how fast, many reactions or transformations occur. Diffusion gives rise to a reduction in the Gibbs free

energy of a system and usually occurs where a chemical potential gradient is present. Atoms will tend to diffuse along a chemical potential gradient from regions where the chemical potential of a species is high to regions where the potential is low. This effect can be represented by the diagram in figure 2 where high initial concentrations of two species are gradually homogenised by diffusion across an interface. The manner in which this process may take place is described in the following sections.

Direct Interchange: This process is shown schematically in figure 3a) and 3b). The energy required for this type of process can be quite high, however temperature is an important consideration as the magnitude of vibrations displayed by an atom bear directly on its ability to become involved in a direct interchange. The process shown in the first example in figure 3a) is more difficult than the Zener ring shown below as there is much more geometric constraint acting on the atom about to jump. This geometric effect is lessened if a ring of atoms succeed in moving in the same circular direction at the same time. In this way an atom may make net movement in a specific direction via a series of position changes.

Vacancy Diffusion: Most metals or alloys contain point defects such as vacancies which are induced during casting and fabrication processes. Figure 4a) shows a vacancy position in a close packed plane, and an example of a possible direction of atom movement. It should be noted that diffusion of atoms via a vacancy process is equal to the diffusion of vacancy sites in the opposite direction to that of the atoms involved.

Figure 4b) shows the unit cell of a face centred cubic crystal and an example of how an atom within the cell can jump from one position to another. This kind of jump can usually only occur if the thermally induced vibrations of the four shaded atoms are sufficient in amplitude to allow the arrowed atom to pass.

Interstitial Diffusion: Metal elements added to an alloy formulation often exist in solid solution, occupying interstitial sites within a crystal lattice. Open structures such as face centre cubic crystals have well defined vacancy sites which can house other atoms. If the

solute atoms are sufficiently small they can occupy these positions without distorting the lattice. Once again, if the thermal vibrations give enough of a push the solute atoms may move from one interstitial site to another in a manner shown in figure 4c). The curve shown below the diagram indicates the free energy of the lattice during the interstitial movement, it is obvious that a significant energy barrier must be overcome before diffusion can occur.

The elements studied in this programme, aluminium, silicon, copper and silver are all fcc structures and would behave in this manner. Aluminium is the major alloying element under study and has an atomic radius of 1.82Å; silicon, copper and silver have atomic radii of 1.46, 1.57 and 1.75Å respectively and could occupy interstitial sites with varying degrees of imposed lattice strain.

The vibrational energy of an atom is proportional to temperature and therefore this tends to be one of the most important considerations for diffusion processes.

3.6.2 Introduction to Diffusion Bonding

Diffusion bonding is a joining technique mainly used in space and aerospace engineering. The technique is a difficult one to perform to high standards for a number of reasons which will be discussed later. Diffusion bonding often relies on equipment that has a high capital value e.g high vacuum machinery; accurate control over processing parameters such as environment and applied load is usually necessary. Having said this, the method has been known for some time, forge welding for example was a popular method of sword manufacture for at least 2000 years.

In the aerospace industry particularly, unnecessary weight is viewed as a particular problem and research often involves addressing this factor alone. The alloys mainly used for aircraft applications tend, therefore, to be the light alloys especially aluminium. Some aluminium alloys rely heavily on their unique strength-to-weight ratios for competitiveness and anything that reduces this ratio is usually avoided. As a result some

joining techniques have been developed that allow lighter structural frames to be assembled by eliminating the need for mechanical fasteners.

In addition to these weight-penalty considerations, environmental resistance and maintenance of microstructural integrity must also be addressed. For example, conventional welding can totally destroy the required microstructure of an alloy in the region known as the heat affected zone (HAZ). In this area there may be a reduction of mechanical properties which is sometimes considered a necessary trade-off against ease-of-assembly or ease-of-repair.

The fine-grained, metastable structure of a rapidly solidified aluminium alloy (or any other RS alloy) is especially sensitive to temperature, and assembly of this type of material is preferred well below the normal temperatures of brazing even. Aero-engineers have therefore tended to look towards lower temperature techniques to avoid these problems. Diffusion bonding has a number of perceived advantages and these have been variously listed by a number of authors but include the following[83]:

- possibility of parent metal strengths
- large bond areas possible
- low distortion and good dimensional control
- absence of corrosive fluxes
- ability to join thick and thin sections
- possibility of joining dissimilar metal and powders
- more efficient component design

The principles of the technique are relatively simple and may be divided into 3 stages:

- initial surface contact

- surface deformation

- elimination of original interface

The first two stages are closely related. Contact may either be initiated before the surfaces have been heated up, in which case the thermal expansion of the components initiates the surface deformation, or after heating, in which case the surface deformation is controlled completely by the subsequent application of a known load. As this section usually occurs under load at high temperatures, it is reasonable to assume that the deformation is a creep-type process and hence is diffusion controlled.

However, it is well known that films, either oxides or contamination, exist on the surfaces of metals. It is essential to disperse these films for good metal-to-metal contact to be achieved. Successful interruption of these films would then hopefully enable the third point in the list to be achieved.

It is theoretically supposed that macro-deformation is not required for a successful diffusion bond. Surfaces need to be in close contact, close enough to be within the range of interatomic distances. This enables the metal (or other) atoms to migrate between the surfaces. If two surfaces were perfectly clean and perfectly matched, topographically, a perfect diffusion bond should result. In practice some pressure needs to be applied to break up these films in localised areas, allowing the joining process to begin.

The final elimination of the interface is diffusion controlled and one or more of 4 mechanisms may contribute. These mechanisms have been listed as follows[84]:

- atom transport occurs across the interface by volume diffusion[85].

- recrystallisation and subsequent grain growth results in the formation of a new grain structure at the interface. The low yield strength of recrystallising grains then allows atomic contact to occur at almost zero loads[86].

- surface diffusion and/or sintering cause the interfaces to grow together[87].

- surface films are dissolved by the metal substrates and thus eliminate the barriers to diffusion[88].

On the basis of these points, Schwartz[84] postulated the following simplistic basic model for a successful diffusion bond:

Two surfaces are brought together under load. The combination of high load and/or high temperature will bring about intimate surface contact on account of the plastic flow exhibited by the surface asperities. A bond is achieved at the points on the metal surfaces where contact occurs. Over a period of time at elevated temperature recrystallisation and grain growth may occur, increasing the degree of interfacial contact. This process of grain growth serves to increase the disruption of any surface films. Dissolution and removal of remnant oxides then results in increased joint strength. This theory is obviously simplified and does not seek to explain all diffusion bonds, indeed, it can only explain in part the processes occurring in this work.

This project has looked at the use of dissimilar metal foils as bonding aids, together with the effect of bonding temperature. The metal substrates originated from cast ingots and were therefore highly heterogeneous in nature. Perfect interfacial grain growth could not be expected to occur in such complex systems and so different explanations have been postulated for the microstructures observed. The processes occurring here will be discussed more fully in later sections.

The current and past literature has been grouped along two broad themes, joining of metals to metals and the joining of metals to ceramics. The diffusion bonding of a metal matrix composite could fall into either or both of these categories. The reason for this is that the type of bonding occurring will depend heavily upon the state of the surfaces prior to joining.

If an ideal metal composite specimen manufactured by Liquid Metal Infiltration is available then there would probably be a skin of matrix alloy completely surrounding the

reinforcement. In this case the joining technique would certainly be metal to metal. However, as a result of the manufacturing route, or some secondary processing such as finishing, some of the reinforcement may be laid bare. In this case, due to the exposed fibre or particulate reinforcement, the joining technique would necessarily involve metal to ceramic bonding.

3.6.3 Early Diffusion Bonding Programs

Diffusion bonding became a realistic production process mainly through advances made in the American space programs of the late 1950's and 1960's. Initially, diffusion bonding was not envisaged as a structural joining technique in the sense that a joint would need to bear significant loads. The process was developed in response to other needs, for example the construction of complex component shapes in thin sheet material.

A number of early Apollo Program applications have been published[89]. The basic design requirement for the first example in this report was for an aluminium baseplate to radiate away the heat generated by the electronic equipment attached to it. The thickness of the plate/sheet material was usually of the order of 0.025", and coolant passages of width 0.085" were machined under the sheet. Conventional joining technology such as brazing or soldering were considered unsuitable as the filler material blocked the cooling passages and rendered the component useless. Interestingly, the group used a thin film of silver plate on the bonding surface, this was to prevent the formation of oxide material during joining that would inhibit the successful formation of a sound joint. This arrangement was finally considered to be unsuitable however (30-65% scrap rates) as the galvanic effect of the silver coupled to the aluminium resulted in localised corrosion in the coolant channels. The second example described was a much larger-scale radiator designed to cool the whole of an Apollo cabin. In this design, sheets with pre-formed coolant passages needed to be joined to a curved panel (the module exterior). Roll bonding was chosen, in this case a graphite stopoff material was applied to the plates in the correct pattern, this allowed certain areas only to bond during hot-rolling, the next stage of the

process. This hot rolling effectively joined specific areas of the sheet material in a diffusion process. The areas left unbonded by the graphite stopoff were then hydraulically inflated inside a die to control the degree of bulging. This type of process combines forming and joining and has subsequently become known as "superplastic forming/diffusion bonding". This combination of mechanisms accounts for many of the diffusion bonded components in service today, the difference between the Apollo example and modern superplastic forming is of course the amount of strain sustained by the metal/alloy. Careful choice of alloy and control/refinement of the microstructure can allow up to 1000% strain, unlike that quoted above which would only have been of the order of 50%.

The McDonnell Aircraft Company undertook a series of evaluation trials in the 1970's to demonstrate the cost and weight advantages obtained by combining diffusion bonding with superplastic forming. The program, sponsored by the US Air Force was known as BLATS (Built-up Low-cost Advanced Titanium Structures)[90]. The aft fuselage structure of a fighter aircraft was chosen as the subject of a major re-design using the technologies just mentioned. The choice represented a high performance use of a titanium structure, produced using state-of-the-art techniques. The re-design sought to meet all of the structural and functional requirements of the existing mature design, thus allowing true performance and cost comparisons to be made. Previous studies performed by McDonnell seemed to indicate that manufacturing costs in particular could be significantly reduced by the high material utilization exhibited by this forming/joining approach. In fact, after a period of development work, the fuselage section was successfully manufactured. The diffusion bonding technique enabled the saving of 150 detailed parts and 5000 fasteners, with all the implications of better load distribution by eliminating the need for rivets. In total costs were reduced by 53% and weight by 38%. A similar approach was adopted for the manufacture of the jet nozzles on the same aircraft. Costs were reduced here too, but significantly, it was shown that the manufacture of a more complex shape was possible (the jet nozzles were highly curved structures with reversing curvatures in places).

In the mid 1970's interest in metal matrix composites began to grow and one of the first projected applications was for jet turbine blades. Initially major problems were encountered simply making these complex hybrid materials.

One of the first methods devised was to lay up alternate layers of fibres and matrix alloy and subject the whole preform arrangement to high temperature, solid-state pressing[91]. The main aim of this method was to produce a net-shape component that required only minor finishing. This method allowed preforms to be laid-up and complex shapes such as turbine blades to be made. Apart from the increased tooling pressures the method was exactly analogous to that used for the manufacture of complex polymer composite components. The high temperatures enabled enough plastic flow of the matrix material around the fibres to consolidate the preform. Similar techniques have been used for fibres within a powder matrix and also for fibres coated with a thick layer of matrix metal. Some studies have been cited in this paper relating to single-lap shear data for some joints that had been made using an Al-Zn-Mg alloy (7039) containing boron fibres ($20\%_{vol}$). The surfaces of the joints had been coated with silver as a joining aid but the measured strengths were quite low. It was suggested that the reason for this low strength was not in fact a joining problem per se, but actually a manufacturing problem as the composite material seemed to exhibit poor interlaminar shear strength. This is an interesting result as it indicates that the chosen manufacturing route, i.e diffusion bonding, was not suitable. This may not be surprising when one considers the tenacious nature of the barrier oxide present on all the aluminium surfaces. It was suggested that it would not be possible to solid-state diffusion bond an aluminium composite as the amount of plastic deformation required to form a bond would result in wholesale breakup of the fibre reinforcement.

3.6.4 Diffusion Bonding of Metals to Metals

For convenience, this section has been sub-divided into two smaller sections. The applications of diffusion bonding are varied and involve coupling surfaces that may be

either similar or dissimilar. A device or component may not always be joined to a surface of the same material, hence the distinction.

Works quoted in the literature are varied and sometimes relate to quite obscure systems, so examples have been chosen that represent familiar materials.

a) Diffusion Bonding of Metals to Similar Metals

Diffusion bonds obtained when joining copper to itself have been studied by Derby et al[92]. The material was chosen for a number of reasons: physical data is well documented for copper, which was useful as the group was validating a mathematical model they had developed earlier; copper is not protected by a tenacious oxide film which would inhibit any diffusion bonding, also under normal bonding conditions copper readily dissolves its oxide; finally, diffusion bonding is considered a potentially useful technique for joining copper due to the difficulties encountered when using conventional welding techniques. The copper was quite pure, having used phosphorous as a de-oxidant. The group recognised the importance of surface preparation prior to diffusion bonding. After initial contact a number of mechanisms compete during the process, bulk and/or surface diffusion and creep. The degree of bonding was examined by measuring the fractional bonded area and then looking at the interface produced at the bond-line. Much of the argument concerning which mechanisms are acting seems to rely on the shape of the voids produced at the bond-line. Creep mechanisms alone would leave angular voids (simple flattening of asperities followed by more plastic deformation). Diffusion along the surface of the void or through the bulk would tend to round off the corners of the voids. This rounding action is a manifestation of the Joule-Thompson effect, where a sharp neck radius will have a greater diffusion driving force; more diffusion from the neck results in a net mass transfer which will eventually blunt the neck, resulting in a larger neck radius and therefore a lower driving force. Stable conditions would presumably be reached if the void became spherical. The group made the conclusion that, not surprisingly, a number of phenomena probably contributed to the bonding process. If

the temperature was raised then diffusion, being thermally activated, would play a dominant part. This was borne out by the observation that sharp voids typical of a creep dominated process were obtained when bonding at 500°C, voids produced at 700°C had rounded edges indicating a diffusion-aided process. However, pressure giving rise to creep at the interface could result in increased diffusion due to the Joule-Thompson effect described above.

A number of papers concerning diffusion bonding have been published by workers at the RAE Farnborough. The nature of the work was, not surprisingly, aerospace engineering and followed previous studies performed on the superplastic forming and diffusion bonding of titanium. If there is careful control over their microstructure certain aluminium alloys can be made to exhibit superplasticity. The advantages of combined superplastic forming and diffusion bonding include better load distribution and weight reduction, these had previously been demonstrated on American military aerospace programs. It was thought that the aluminium alloys used in the wider field of commercial aircraft manufacture could also benefit from this technique[93]. This particular piece of work was mainly concerned with jigging design for both the manufacture and the testing of a diffusion bond. For the manufacture of a bonded specimen a plunger-type arrangement was used that allowed the monitoring of compression load and degree of imposed strain. This type of tooling was used as the basis for equipment used in this project and is described in the Experimental chapter. More attention had to be made to the testing of diffusion bonded specimens. The type of samples were designed to be tested as single-lap shears specimens and it was important to ensure that the bond-line was kept in shear. Bending moments would induce peel forces into the interface and would have reduced the apparent strength of the joints. This was also a consideration that had to be made with the experimental work carried out later in this thesis. Results of shear tests indicate good bonds sustaining approximately 150 MPa. The load vs. strain curves of the test itself indicated a peak followed by drop-off before failure. This implied a degree of plastic shear before failure. The effect of surface finish was discussed and it was shown that a progressively finer finish gave higher shear strengths. These strengths started at

about 100 MPa for roughly ground surfaces and increased through lapped and as-clad surfaces to 180 MPa for polished surfaces.

The move towards alloys with greater strength to weight ratios has resulted in the development of a new range of aluminium alloys containing lithium as a primary alloying addition. The excellent properties of these alloys has aroused much interest, especially in the USA.

Al-Cu-Mg alloys have been used in aerospace applications for nearly 35 years and the newer Al-Li alloys were considered as possible replacements[94]. Even though the Al-Li alloys are 4-5 times more expensive they could still be considered in high cost applications where expense is less of a penalty than weight. The quoted cost in 1990 of US $7900/kg for placing an object in a low space orbit is an ideal example of the incentive to reduce component weight. However Al-Li could not be welded satisfactorily under laboratory conditions and often exhibited hot shortness or weld porosity on actual components. These problems have also been compounded by the tendency of Al-Li alloys to show localised lithium depletion as a result of exposure to severe temperatures or melting.

These problems led the group at RAE to examine the possibility of diffusion bonding Al-Li alloys[95]. The environment experienced by these alloys would be much less severe for diffusion bonding than conventional welding. It was found that reasonable bond strengths were obtained (≈190 MPa) but optical micrographs revealed a visible planar interface for each of the specimens presented. However polished macro-specimens did reveal a degree of plastic shear in the substrate which would indicate the existence of a good bond. It was suggested that the planar interface caused the shear strengths to be lower than expected, probably due to a lower resistance to intergranular fracture along that interface. A quantitative comparison was made to adhesive bonding, stating that the diffusion bonded joints were some seven times stronger. This may not be a surprising result but adhesive bonding was considered a highly likely candidate for joining the Al-Li alloys for low temperature applications. The group at the RAE probably felt that diffusion bonding

could compete and should also be considered as a likely joining technique for this difficult range of alloys.

Work involving the diffusion bonding of Al-Li alloys was continued by the research group at the RAE in a study that identified two types of fracture in the lap-shear joint[96]. Intergranular fracture appeared to be the predominant mode of failure, rough fracture surfaces corresponding to the contours of the grain boundary surfaces. The second fracture mode was characterised by a peel type of failure, this did not carry much of the applied load and occurred due to bending moments that were induced just before complete failure. If the problem of intergranular fracture of diffusion bonded Al-Li joints is not eliminated then the use of this joining method for these materials may be very limited.

The joining of aluminium and its alloys have been examined, especially using coatings of silver on the joining surfaces[97]. Silver was used because the coating should have had similar mechanical properties to the underlying substrate. Coatings were applied by an electrolytic method and the diffusion bonding was carried out in the solid state, up to about $0.8T_m$ for the base metal. Similar observations are made to other groups in the field, basically relating to:

- improved contact between the surfaces
- reduction of interface porosity
- reduced interface oxidation

When diffusion bonding pure aluminium, intermetallic compounds were apparent in the region of the bond, particularly a needle-like phase described as the δ phase. This Widmannstätten structure forms when a solid solution, of high silver content adjacent to the bond-line, cools down after joining is completed. An Al-Si alloy was also bonded and the same δ-phase Widmannstätten structure was formed. No evidence was found for a

ternary reaction between the aluminium, silver and silicon. No bond strengths were quoted, the quality of a joint was considered on its metallographic merits.

Titanium possesses a surface oxide like that on aluminium but it can be dissolved in the metal at the temperatures used for diffusion bonding. The temperature is higher than that used for aluminium which means that the pressures and bonding times can be less. Some of the first components produced industrially were manufactured in titanium and have seen widespread application in the aero industry. An example of the type of process engineering is given in the paper by Schwartz[98]. Examples of components are described for various applications, such as engine inlets, vanes and engine casings. These components were required to withstand hot, corrosive conditions making titanium an ideal choice of material. Significant weight savings were attained when a hollow, webbed engine inlet was manufactured by diffusion bonding. Previously, the component had been machined from a solid block and sheets of protective facing material had to be electron beam welded onto the component substrate. The cost of this production route was also reduced by using the simpler one-stage diffusion bonding technique.

The brittle nature of the ceramic fibre reinforcement in metal matrix composites means that little deformation can be tolerated during manufacture and subsequent processing. A number of production techniques have been developed that do not rely on massive deformation of these materials, some of which are described by Sakamoto[99]. Some of the problems associated with diffusion bonding as a joining method were discussed, as distinct from diffusion bonding as a means of manufacturing bulk metal matrix composites. The discussion is somewhat superficial but does make the distinction between the degree of plastic deformation required to consolidate a metal matrix composite during manufacture, and the amount of plastic deformation sustainable by the reinforcement without damage in a metal matrix composite during joining.

Early examples of metal matrix composites were primarily manufactured by diffusion bonding. "Green" tapes were made by wrapping metal foils around a drum and then winding fibres over these foils. Acrylic or styrene adhesives were applied to hold the

fibres in place whilst the completed tapes were cut to shape. These foil/fibre tapes were than laid up and laminated in the correct fashion and vacuum bagged. Final consolidation would be carried out using a HIPping furnace to produce the component. The component could be quite complex and the size was dictated by the HIPping capacity of the furnace equipment. A number of problems were encountered when using this method. Large linear defects tended to form at the join between adjacent tape laminae as a result of incomplete diffusion bonding. Also, the polymer adhesives were burned off by the high temperatures but could not always escape from the HIPping vacuum bags. This could result in the formation of voids within the component or the contamination of joining surfaces. This type of problem was more serious with aluminium components than titanium.

Perhaps the most publicised components made by this route are the space shuttle trusses. These are structural tube members designed to carry high loads. Metal foils and fibre tapes were wrapped around a mandrel arrangement and then inserted into an outer mandrel. HIPping was then applied and the whole component was consolidated by diffusion bonding. Secondary processing costs were extensive, though, as the mandrels could only be removed by machining and chemical etching. End fittings were joined by a more conventional route, electron beam welding. The estimated cost of 1 truss was $20,000.

A more systematic study has been carried out on the diffusion bonding of samples of an Al-Mg-Si alloy (6063) reinforced with $15\%_{vol}$ alumina short fibres[100]. The material used for joining was in rod form that had been made by centrifugal casting followed by extrusion. The joining process involved butt joints with or without a foil interlayer placed on one of the faying surfaces. This was then heated by a radiant resistance heater comprising of a molybdenum foil. The whole apparatus was placed in a vacuum of 10^{-2} Pa. The effect of surface finish was studied and appeared to follow the results found by the group at the RAE Farnborough, i.e bond strengths were in the ascending order of wire brushed < lathe turned < electropolished. In other words a smoother surface tended

to produce better bond strengths. The highest strength attained was some 80% of the tensile strength of the base material. In a parallel series of studies it was found that the bond strength of the unreinforced matrix alloy was almost independent of surface finish. This anomaly was explained by the presence of fibre debris at the interface of diffusion bonded composites. This debris was produced by aggressive surface finishing like wire brushing. Microstructural examinations revealed that some bond-line reinforcement occurred for the electropolished specimens. This was concluded to be a result of protruding fibre-ends being pushed into the facing bonding surface. Increased electropolish times decreased the bond strengths due to excessively protruding fibres, breaking on contact with the other faying surface, and then the broken remnants residing in the bond-line. Bonding experiments were carried out without the use of foil interlayers. It was noted that it was only possible to obtain equivalent bond strengths within a limited range of temperatures and pressures. In addition a large amount of plastic deformation was required at the interface to obtain a good joint. The results of diffusion bonding with foil interlayers were interesting. All testing was carried out at temperatures above those required to form a liquid phase, i.e above the solidus and eutectic temperatures. The bond strengths were generally higher with less deformation at the bond-line.

b) Diffusion Bonding of Metals to Dissimilar Metals

As has been mentioned in the introduction to this section, metals do not necessarily have to be diffusion bonded to themselves. Diffusion welding/bonding can be a candidate technique for joining dissimilar metals, under these conditions it may be possible to avoid some of the problems experienced when trying to fusion weld some of the metals that are metallurgically incompatible. Incompatibility may arise through differences in reactivity or melting temperatures.

Examples of this are described by Johnson et al where interest was directed at the manufacture of laminated sheets for structural applications[101]. Primary sheet material was Ti-6%Al-4%V and the interleaf sheets were made from 6061 aluminium alloy. The

primary sheets were surface treated with a mixed acid etch that consisted of HF and HNO_3. The secondary interleaf foils were lightly abraded before diffusion bonding. Vacuum bagging was carried out within minutes of these surface pretreatments to minimise the effects of surface contamination and oxide growth. Bonding was carried out at 524°C for around 1 hour at 4000 psi (27.6 MPa). The research group managed to produce diffusion bonds for this configuration of sheet material. Subsequent testing showed failure within the aluminium alloy interlayers and not at the interface itself, which was considered a success. Metal laminates are considered important an materials with potentially high fracture toughness. Some diffusion bonded laminate samples were quoted as having K_c values over 50% higher than their monolithic relatives. Weak interlayers may be important for having crack arresting capabilities.

The bonding of aluminium alloy A2017 (Al-Cu-Mg) to titanium has been investigated. This project continued the interest of T. Enjo in the diffusion bonding of metals, both with and without intermediate foils[102]. The alloy A2017 is very difficult to weld using conventional fusion techniques, it has a high susceptibility to weld solidification cracking. Other techniques needed to be found and diffusion bonding seemed ideal. Previous studies by the authors had shown that this alloy could be successfully diffusion bonded to itself by operating just above the solidus, i.e where solid and liquid phases coexisted. Titanium was chosen as a candidate for dissimilar metal bonding as it exhibited similar strengths to A2017. The bonding technique has been described in the previous section (molybdenum radiant resistance heater and hydraulically applied pressure). The liquidus temperature for the aluminium alloy was determined by using differential thermal analysis. Weld solidification cracking was avoided by maintaining pressure at the bond-line until complete solidification of the sample had occurred. The strengths obtained were generally good, rising to a maximum of 240 MPa for bonding carried out at 850K. At this temperature approximately 7% of the aluminium alloy was in a liquid state. A uniform layer of intermetallic (4μm thick) was produced at the interface which appeared to contain aluminium, titanium and also copper. The copper was part of the alloy composition. Fracture of the joint during testing took place within this intermetallic layer.

A comparison was made to the diffusion bonding of commercially pure aluminium to titanium in which an intermetallic compound is also formed but does not reduce the joint strength. For this configuration fracture occurred within the pure aluminium base metal. The presence of copper in the later study seemed to produce a much more brittle intermetallic.

This piece of work was followed up by Enjo's group[103]. The impurity levels within the aluminium alloys appeared to have an effect on the strength of the diffusion bonds. This effect was related to the formation of the intermetallic compound at the interface, the thicker the intermetallic the weaker the joint. Silicon was added as an impurity to the aluminium and there was an immediate effect on the intermetallic formed. When the silicon reached a certain level ($2\text{-}7 \times 10^{-3}$ mass%) the growth of the intermetallic was severely inhibited. It was postulated that the presence of silicon reduced the ability of aluminium to diffuse towards the titanium and form this compound.

The final paper examined in this section is of particular interest as it examines the nature of diffusion bonds formed between copper and aluminium. This work was carried out by Calvo using commercially pure base metals under regimes quite similar to those examined for this thesis[104]. The authors propose a three stage model that describes the bonding process. The first stage is localised point contact at the interface, usually over an area significantly smaller than the maximum possible. This first stage is dominated by yield and creep mechanisms coupled with initial disruption of the aluminium oxide film. Increased initial bonding pressures produced increased initial contact between the bonding surfaces. This observation was confirmed by the larger area of intermetallic compounds formed at the interface with increasing pressure. The proposed model here begins to differ from the ideas postulated by Partridge et al at the RAE; Calvo suggests that increased initial contact and oxide disruption via asperity shear mechanisms is more effective for a rougher surface, the other group prefer to postulate the advantages of a polished, smooth surface for greater contact. When this contact is made, though, the area grows rapidly due to creep.

The second stage of diffusion bonding is characterised by the onset of mass transport, which begins when the barriers to diffusion are removed or broken down (oxide films). In this stage interfacial voids tend to spherodise and intermetallic compounds are nucleated. The nucleation sites for these compounds are at the points where the two metals are in contact. These compounds grow and eventually form continuous layers. As the flat, lenticular voids spherodise, then the driving force for diffusion at the neck of the voids is reduced and the movement of atoms begins to slow down.

The final stage begins with the spherodisation of the interfacial voids. At this point bulk diffusion and diffusion along the interface dominate. Diffusion of vacancies results in the shrinkage of the voids, although completion of this process is lengthy.

A number of different intermetallic compounds were identified at the interface, these included Cu_9Al_4, CuAl and $CuAl_2$. The presence of these compounds has been confirmed in the course of this program Whilst the cited paper concentrated on bonding bulk materials a similarity exists with this thesis' experimentation when using copper foils between aluminium alloy specimens. The copper foils are obviously not bulk specimens but on a micro-scale could be considered so.

3.6.5 Diffusion Bonding of Metals to Ceramics

The technology of ceramic production has improved and there has been a general increase in the application of structural ceramics, i.e ceramic parts or components that can sustain a load. Under these circumstances, the characteristics of a ceramic may lead to its selection as a small part or component within a larger group or structure. It is necessary, therefore, to integrate the ceramic into that structure, usually by a joining technique. Strength and vacuum tightness are often the primary requirements of a metal/ceramic joint. The successful combination of a metal/ceramic bond may be critical in any one of the following applications:

- electronic/electrical componentry

- catalyst design and construction
- high hardness tooling
- metal matrix composites[105]

Novel joining processes have been developed in response to the lack of success when using conventional joining techniques. The non-wetting nature of many ceramics to liquid metals has been the most significant reason why fusion welding is not a successful joining method. This problem must still be addressed even if a liquid phase diffusion bond is attempted.

The problem of wettability may be sidestepped to a certain extent by careful modification of the joining surfaces. For example, a mixture of metal and ceramic powders (e.g Mo and MnO_2) may be added to the ceramic surface of a ceramic/metal joint. This powder mixture is applied and fired to form a glassy mixture. The metal content of this glassy mixture makes it more wettable than the original ceramic surface alone.

A variation of this surface modification is described by Beraud et al[106]. The study was based on Cu/Al_2O_3 bonding, i.e Al_2O_3 with copper foil inserts. Instead of modifying the ceramic surface with a metal as described above, they modified the metal by forming a ceramic on its surface. This was performed simply by oxidising the copper and growing a Cu_20 film to various thicknesses. When bonding was carried out at about 1065°C the Cu_2O and copper formed a liquid eutectic phase, which then wet the Al_2O_3 specimen surface and promoted surface contact. Optimal strengths were obtained for Cu_2O films of between 3 and 10μm. At thicknesses above this, porosity was induced in the liquid phase which then resided at the interface.

Other methods include electroplating, vapour deposition and, most commonly, TiH_2 activation. This last example involves the application of titanium hydride as a powder followed by dissociation at about 400°C to produce a wettable titanium film. Complex

variants exist on this technique that involve the use of sacrificial materials that melt to form eutectics with either, or both, the TiH_2 coating and the metal part of the joint.

Solid phase bonding may be preferred as the materials can be kept at temperatures below those at which thermal degradation occurs. Lack of contact may accommodated between the surfaces by the deformable nature of the metal or foil used. Aluminium foils have been fairly widely used, for example the solid state bonding of steel to Al_2O_3 (for Na-S batteries), and quartz to steel (laser components).

Aluminium oxide has been diffusion bonded to titanium as a combination material for dental applications[107]. The individual materials have been used separately with much success in dentistry. As a combination the best properties of each should be available such as the formability and high strength of the titanium together with the corrosion and wear resistance of the aluminium oxide. This reference was mainly a very detailed study of the application of various metallographic techniques for imaging these systems. However some pertinent observations were made regarding the nature of the interface and the phases produced at the bond-line. $TiAl_3$ and TiAl were both formed and bonded specimens showed extensive cracking through these intermetallics on cooling due to the major differences in thermal expansion. Different bonding temperatures were examined and an coarsening of titanium grain size was noted at a bonding temperature of 1300°C compared with 1200°C. At even higher temperatures (1500°C) complete embrittlement of the bond-line resulted, the difference in thermal expansions also led to the production of deformation twins in the titanium on cooling.

A model system has been studied where a sandwich-type construction of two pieces of Al_2O_3 were separated by a 500μm foil of pure aluminium. The samples were abraded and degreased then bonded at 600°C and 50MPa. Subsequent heat treatments were a soak at 400°C for 30 minutes then a 4 hour anneal at 200°C. The anneal was found to be necessary as all other specimens had zero bond strength otherwise[108]. Bond strengths were measured for as-received and lapped samples but although the lapped specimens had a slightly greater average strength (32MPa c.f. 20MPa) the scatter of the data almost

appears to make the result distributions overlap. Higher bond strengths of approximately 50MPa were obtained by taking the bonding temperature above the melting point of the aluminium foil. An interesting result was described which relates to the effect of bonding temperature on joint strength. Up to 480°C there was no particular effect of temperature on final strength, however above this temperature the measured strengths began to rise. It was found that above 480°C, the aluminium foil deformed and was compressed to about 100μm. The amount of contact made between the foil and the ceramic obviously depended on the degree of foil deformation, this contact area governed the quality of the diffusion bond subsequently achieved.

Ceramic/metal combinations required for a specific application appear in the literature. Alumina and steel joined with an aluminium foil insert have been studied as a combination for use in electrical and vacuum components[109]. The materials were assembled in a heated vacuum press apparatus. The specimen geometry was a truncated cone, a sandwich construction where the outer materials were Al_2O_3 with steel as the central insert. The steel and Al_2O_3 was separated by thin aluminium foil inserts. The strength of the bonds increased with temperature. Those bonds produced at 496°C, 542°C and 594°C fractured at the interface between the alumina and the aluminium foil. However, bonds produced at 625°C were stronger still and failed at the interface between the steel and the aluminium. Layers of intermetallic formed at each of these temperatures, the thickness of the intermetallic layer increased with temperature. A similar effect was noted with fabrication time. Growth of the intermetallic between the aluminium and steel seemed to be the dominant failure consideration and conditions that promoted the growth of this layer increased the risk of failure in that brittle layer. Bonding environment had a significant effect on the measured strengths. Joining performed in an argon atmosphere decreased the thickness of the aluminium/steel intermetallic but also led to a drop in bond strength, from 50MPa down to 17MPa. Bonding in air brought about a reduction of strength to practically zero, indicating the significance of an oxidising environment.

The influence of foil-choice has also been investigated for diffusion bonding metals and ceramics[110]. Samples of Al_2O_3 were joined with various thin layers of metal foil as inserts (aluminium, Al-Mg, silver, copper, nickel). This type of joining was redefined as thermo-compression bonding, a term yet to catch on. Faying surfaces on the ceramic and foils were abraded to a standard finish and degreased. The group showed that there was a threshold temperature for each foil below which no bonding would take place. Beyond this threshold, the measured bond strengths increased to a maximum. The reason for this rise in bond strength was not explained but it was hypothesised that the increased temperature gave rise to increased contact area and therefore lead to an increase in metal/ceramic bonding. This would be balanced, though, by increased thermal stresses arising from the thermal mismatches at the higher temperatures. It was suggested that for a metal/ceramic couple, diffusion bonding required some form of chemical reaction. To investigate this Al-Mg foils were used in addition to pure aluminium foils. It was hoped that the small amount of magnesium present in the alloy foils would encourage the formation of the $MgAl_2O_4$ spinel and thus give a stronger joint. Bond strengths increased in the range 44 to 60MPa when using the following foils: Al, Al-1% magnesium, Al-4.5% Mg. The samples were tested and the fracture surfaces had a dark, reacted appearance. However, it was suggested that the spinel, if produced, would be sub-micron in nature due to the lack of any conclusive electron-optical data.

Thermal expansion mismatches often appear as the cause of joint failure in diffusion bonding. The phenomena can occur when bonding metal to metal but, not surprisingly, it appears most often when diffusion bonding metals to ceramics. It can be a problem, not only when the samples or components are cooled after joining, but also if they are used at elevated temperatures. Under these conditions the components would likely experience severe thermal cycling coupled with repeated thermal shock. In aggressive environments, a bond which was suffered from high residual stresses would also become susceptible to stress corrosion cracking. Suganuma specifically examined various joint configurations with the view to reducing the adverse effect of thermal mismatch[111]. The results quoted in this paper involve both finite element calculations and experimental data. Cylindrical

"coin"-like samples were joined together using a HIPing furnace; residual stress vs. sample diameter seemed to rise to a maximum, after which the stress reduced to a constant value, independent of increasing diameter. The thickness of ceramic coating on the steel substrate was also significant, residual stress rose to a maximum value above a ceramic thickness of 6mm. This trend was confirmed when the strength of a diffusion bonded joint was shown to drop off with increasing ceramic thickness. This implied that ceramic coatings on metal substrates may be more stable than bulk bonded specimens.

Some other suggestions were made by Suganuma[112] that may help to reduce the residual stresses in a joint. Soft metals may be incorporated so that they may plastically deform when a residual stress is imposed on them. Alternatively a number of foils of differing thermal expansions may be used. These foils would deform to different extents and protect the bond-line from failure. Foam metals, metal grids and soft solders were also suggested as possible solutions. A composite interlayer with a constantly changing coefficient of thermal expansion could also be used, this could be manufactured from a combination of metal and ceramic powders, mixed using a "Graded Powder" method.

A useful variation of metal/ceramic diffusion bonding has been carried out where the investigation centred on the use of titanium and titanium hydride powder instead of foil inserts[112]. Al_2O_3 substrates were joined together via a titanium insert coated with an layer of TiH_2 powder. This hydride powder decomposed to give metallic titanium under the influence of heat, the resulting titanium powder then sintered to give, hopefully, a fully dense continuous interlayer. As a comparison, an Al_2O_3 component was joined with an identical insert coated with commercially pure titanium powder. This butt-type of joint was mechanically tested in 4-point bend. After fabrication it was shown that the strengths of the joints made with the hydride powders were higher than those of the pure titanium starting material. This increase in strength was attributed to the higher activity of the hydride powder and also to the ability of the powder to compensate for residual stresses. Even so, the samples always fractured at the ceramic/powder interface and the joints were therefore significantly weaker than the ceramic they were joining.

The effect of alloying additions in braze materials has been investigated[113]. SiN workpieces can be joined together with an aluminium filler metal, the strength of which was apparently sensitive to small additions of magnesium and silicon. The study concluded that magnesium was detrimental to the joint strength because it promoted the formation of a stable film of Al_2O_3 between the SiN and the filler metal. Also, a spinel was formed between the aluminium and the silicon in the workpiece. This spinel was not usually a problem, however, when a film of Al_2O_3 was formed there were always instances of fracture at the interface of the spinel and the Al_2O_3. In comparison, silicon additions to the filler metal were generally beneficial. Apparently, a non-crystalline layer of SiO_2-Al_2O_3 was produced at the filler metal/workpiece interface which resulted in increased joint strengths. It was noted, though, that too much silicon reduces the plasticity of aluminium and excess additions may have altered the ability of the aluminium to relax the thermal stresses induced upon cooling.

The importance of residual stresses has been highlighted by Yamada in a paper describing the joining of Al_2O_3 to steel with an Al-Si interlayer[114]. Joints were tested and, after reaching a maximum, were shown to be independent of the thickness of foil interlayer. The bonds consistently failed at the interface between the Al-Si foil and the steel. This was taken as an indication that the ultimate strength of the assembly depended on the strength of any intermetallic formed at this interface. Cracks induced at the interface on cooling, for example, would have reduced the strength of this interface and hence reduced the effectiveness of the joint. The paper noted that the residual stress decreased with increasing foil thickness, indicating an ability for the foil to absorb residual stresses, but, the formation of a brittle intermetallic at the Al_2O_3/steel interface ultimately dictated the strength of the joint.

Diffusion bonding is anticipated to play a vital role in the nuclear industry and is described in the final two papers of this section. Ceramic materials are hoped to be used in fusion reactors because of their excellent refractory properties. However, the extreme temperatures generated in this environment must be dissipated away from the insulating

tiles inside a reactor. To facilitate this, metal heat sinks are bonded to the ceramic tiles. This is obviously a service-critical design where failure of the assembly could mean catastrophic failure of the reactor[115]. Typical ceramics examined in the paper were Al_2O_3 and partially stabilised ZrO_2. The substrates were austenitic steel. Once again a foil was used between the surfaces, in this case Al-Mn-Si. The foil alloy was chosen because of its good adhesion to both Al_2O_3 and ZrO_2. TEM examination of the interface showed high dislocation densities indicating considerable strain in the vicinity, together with the formation of a fine grained reaction layer. Attention was brought to the interface between the foil and the steel. Apparently the silicon in the alloy foil reacted with nickel-containing steels and this reaction would have to be taken into account in order to produce good diffusion bonds.

Vanadium is considered as a structural material in nuclear applications[116]. However, vanadium has a high affinity for gaseous elements. This allows the permeation of tritium and lowers the alloy's resistance to oxidation. The properties of the alloys may be improved by alloying additions or, more pertinently, by surface modification. The range of surface treatments available include coating and bonding with ceramics. What makes vanadium attractive in this respect is that it's coefficient of thermal expansion is similar to that of Al_2O_3. The coefficient of thermal expansion can be made closer still by judicious alloying additions of certain elements such as titanium and chromium. Diffusion bonds obtained between vanadium and Al_2O_3 showed fracture solely in the Al_2O_3, also in a mixed type of mode within the Al_2O_3 and at the Al_2O_3/V interface. It was proposed that the fracture occurred within the Al_2O_3 because the ceramic had been degraded through thermal stress. For the mixed mode type of failure, the measured strength was seen to reflect the interface strength and that of the degraded Al_2O_3.

3.6.6 Liquid Interphases in Diffusion Bonding

Many of the papers referred to previously refer to the use of interlayers to produce a better diffusion bond. In many cases the benefits arise through the presence of a ductile

layer deforming and thus improving interfacial contact when bonding in the solid state. Intermetallic compounds may also be formed by solid state diffusion, these compounds may be strong but, being naturally brittle, are sensitive to thermal contractions induced on cooling and they often fracture under these conditions.

Some papers mention the formation of a liquid phase during the bonding process. This type of bonding is very important and is closely related to the content of the latter section of this thesis. In some of the previous references the formation of a liquid phase was merely Adventitious, being merely a useful development. Not many papers exist specifically related to this topic, however some of the more relevant are reviewed.

An earlier section in this part of the literature review talked about diffusion bonding as a method for manufacturing metal matrix composites. Generally the metal tape and fibre preforms had to sustain high degrees of deformation such that the metal flowed and surrounded the fibres. The volume fraction of fibres therefore had to be kept reasonably small so that this deformation could happen, however, the high loads often led to fibre breakup. Niemann et al. developed a lower pressure technique to reduce this problem of fibre breakup. The technique involved the use of physical vapour deposition coatings of copper laid onto the aluminium tapes[117]. The aim of the process was for a thin surface layer of copper to diffuse into the aluminium matrix and form a eutectic phase when heated above 1018F (approx 550°C), a technique coined as eutectic bonding. This technique resembled conventional brazing in that joining is effected by a liquid phase, however the method differed because the liquid was formed by diffusion into the metal matrix and not by the simple liquation of a low melting point filler metal. The process conditions were gradually altered and optimised and the authors stated that it was possible to fabricate laminated structures of metal matrix composites by coating monolayer foils with about 20μm of copper. Fibre degradation was kept to a minimum by reducing the time that the laminates were exposed to elevated temperatures.

Alloys containing a dispersion of oxide have attracted some attention for their potential as strong, heat resistant alloys. General welding techniques were not considered effective

due to a tendency for the weld zone to lose its strength at high temperatures. Diffusion bonding was therefore considered as an alternative[118]. However the authors were worried that even for liquid phase diffusion bonding some of the oxide dispersion would coagulate at the interface and result in the formation of a line of weakness. The samples for this study were very complex in nature. The alloy substrates were basically a nickel alloy with additions of chromium, titanium, aluminium, iron, carbon and an oxide dispersion of Y_2O_3. The insert metal was also a nickel alloy but with additions of boron and silicon to lower its melting point. The interlayer was manufactured in the form of a ribbon rapidly solidified on a rotating drum. Metallographic examination of these liquid phase diffusion bonded specimens showed that the oxide had indeed coagulated at the interface. Lower temperature tensile tests all fractured along the path of the coagulated particles, but higher temperature tests exhibited failures in the base metal. Samples notched in the bond zone compared favourably in terms of strength and elongation with the base metal, the boron, nickel and silicon from the ribbon insert were thought to be responsible.

Liquid diffusion bonding has also been applied to titanium structures. The combination of the advantages of both brazing and conventional diffusion bonding have been used to assemble titanium honeycomb structures[119]. These liquid diffusion bonded honeycomb structures had, at the time of the paper, seen service in 5000 Pratt and Whitney engine ducts and also in 325 large fan exit cases for Rolls Royce RB211 jet engines. The process involved the insertion of a thin Cu-Ni interlayer between the titanium workpieces. On heating with modest pressures a ternary eutectic was formed containing titanium, copper and nickel. This eutectic bridged the component workpieces and initiated diffusion. It was possible to assemble components with integral foil inserts and complex shapes could be manufactured. The foil used in this process was very thin indeed, <0.001" made by a patented process. Exact details are scarce in this publication as it was probably intended to advertise a new product.

Instantaneous liquid phase bonding was another variation developed by a Japanese team in a study that covered a wide range of differing materials[120]. The actual process itself involved heating up the samples as rapidly as possible in an inert atmosphere to such a temperature where the lowest melting point liquid first formed. At this point bonding was completed very quickly and the samples were then cooled rapidly. The rapid cooling was to try to avoid the formation of a brittle layer. The unusual method of heating the faying surfaces is what makes this paper so unusual. If the metals to be joined were dissimilar, then each faying surface could be heated independently to any temperature and then brought into contact. If, for example, one of the metals had a much higher melting point than the other, then this first metal could be heated to above the melting point of the second. The surfaces would then be rapidly brought into contact and the higher-temperature surface should cause melting by direct conduction in the opposite side giving rise to rapid, extensive wetting.

The 2017 series of aluminium alloys (Al-Cu-Mg) are high strength materials and of great interest but are difficult to join by welding due to their susceptibility to weld cracking. As an alternative a solid state technique was considered by Enjo et al[121]. True solid state joining techniques generally require heavy deformations in order to disrupt the Al_2O_3 film on any aluminium alloy surface. Separate foil inserts also change the chemistry of the samples in the bond zone. Therefore, Enjo decided to attempt to bond the 2017 alloys at temperatures just above their solidus. A hot stage optical microscope was used to observe *in situ* metallographic changes and the solidus was determined by differential thermal analysis (DTA). It was decided that significant amounts of liquid phase were not produced at temperatures below 830K. Above this point a large endotherm was observed on the DTA. Microscopic examination showed no recrystallisation across the interface until bonding temperatures of 853K were reached. Under these conditions, maintaining bonding pressure as the liquid cooled was found to be beneficial as it tended to reduce the tendency of the alloy to crack on solidification. For temperatures above 868K, joints fractured in the base metal but strengths were reduced, indicating a degradation of alloy properties. This degradation was linked to the amount of liquid phase produced. High

magnification microscopy showed voids forming at grain boundaries in the vicinity of the bond. This porosity was interpreted as a sign of grain boundary sliding where cracks and voids were produced but were unable to be removed by subsequent vacancy diffusion. Many combinations of materials were examined and the conclusions may be summarised in the following points. Weld times were much shorter than conventional diffusion bonding times. Good diffusion bonds were obtained with low pressures. Pure aluminium bonded to titanium fractured at the interface but pure aluminium bonded to a plain carbon steel fractured away from the bond-line in the aluminium, ie giving parent metal strength. An Al-Mg alloy also demonstrated fracture away from the bond-line together with some plastic deformation in the Al-Mg alloy. The team joined some high strength aluminium alloys (A2024) and obtained very good bond strengths of around 240MPa when diffusion bonded to a titanium alloy.

Finally, a "transient" liquid phase method is described by Iino[122]. As with previous techniques, this relied on the production of a molten phase for example at the interface of a Ti-Ni bi-layer. As titanium diffuses quickest into nickel, compared with vice versa, the titanium would diffuse away and after a period of time the local concentrations of titanium would fall to below that of the liquidus line. Further diffusion would decrease the titanium concentration even more, the result would be a zone whose local melting point was higher than previously. This effect was used by Iino to join samples of pressureless sintered Si_3N_4. The foil arrangement was basically Ti/Ni/Ti, where the nickel was 1000μm and the titanium was 5μm thick. As a comparison samples were bonded with a simple nickel layer of the same thickness. Bend tests confirmed that the combination of foils produced good strengths (≈234MPa) which exhibited fracture in the ceramic bulk. The samples bonded with just a nickel layer fractured at ≈56MPa and along the interface. The point was made that any technique relying on the formation of a liquid phase will only work if that liquid will wet the faying surfaces, in this case it must wet both a ceramic and a metal.

4. SCOPE OF THE INVESTIGATION

The aim of the programme is to study and compare the adhesive bonding and diffusion bonding of metal matrix composites as manufactured by liquid metal infiltration (LMI). The first part of the programme concerned itself with a study of matrix alloy materials. A high strength heat-treatable casting alloy, ARE 415, will be examined and also an aluminium/silicon casting alloy A357 chosen as the primary matrix material for the metal composite system.

Since it is well established that surface design is particularly important for adhesive bonding, techniques will be applied to develop optimal surface topography such that strong adhesive bonds are achieved with epoxy and acrylic resins. A joint geometry will be determined to carry out suitable mechanical tests. The effect of metallurgical condition of the matrix material on measured shear strength will be investigated for adhesively bonded joints, and particular attention will be paid to the locus of failure in the joints in order to determine the effectiveness of the surface treatment.

Apparatus will be designed and manufactured to enable specimens to be diffusion bonded. Initially, samples of the aluminium/silicon matrix alloy will be joined using metal foil inserts as bonding aids and the effect of time, temperature and pressure on bonding will be studied. A test-jig will be designed and manufactured to carry out single-lap shear tests using a suitable test-piece geometry. Test data will be analysed to determine a set of conditions that may lead to the successful joining of these materials. An attempt will be made to correlate microstructural features with the mechanical strength of the diffusion bonds. Data obtained from the joining of unreinforced metal will be applied to reinforced metal composite in order to determine the feasibility of the process for bonding metal matrix composites. Microstructural studies will be carried out to determine the effect of reinforcement media and orientation of reinforcement, on joint integrity. These observations will be contrasted and compared with data gathered for unreinforced metal.

5. EXPERIMENTAL

5.1 MATERIALS

5.1.1 Unreinforced Metals

The manufacturing route used to produce MMCs involved a type of low-pressure die-casting and, therefore, casting alloys were required. Obviously casting-type alloys have much more heterogeneous microstructures and they may be expected to behave differently to wrought alloys when surface preparations are carried out.

A component produced using this casting route would usually take the form of a composite array surrounded by a skin of matrix material. This skin could be advantageous for a number of reasons; for example, it may be wear resistant, corrosion resistant or it may indeed act as an aid to joining. In effect, if two composite components were placed together, the process would actually require the joining of the two skins of matrix material.

Therefore initial experimental work was carried out on three unreinforced alloy systems, all supplied by ARE Holton Heath: i) Commercial purity aluminium, ii) an Al-Si alloy designated A357, and, iii) an Al-Cu-Zn-Ag-Mg alloy, designated ARE 415.

Commercial Purity Aluminium: aluminium in this form comprises the bulk of commercial production and in terms of composition may contain up to 1% impurities, rarely exceeding 99.9% purity. Typical impurities, which are raw-material dependant, may be sodium, iron and silicon, gallium, titanium, vanadium, manganese and copper.

Al-Si alloy A357: silicon is one of the most common additions to aluminium alloys for a number of reasons. Silicon additions impart fluidity to a melt, improving both casting and welding behaviour, also, improved mechanical properties are obtained through the formation of heat-treatable compounds. The presence of discrete particles of pure silicon

(in the form of a eutectic) also tends to confer some measure of wear resistance to the material; this property alone has made Al-Si materials important in the automotive industry where they are used widely for reciprocating components.

Aluminium and silicon form a simple eutectic series, as shown in figure 5)[123], with a maximum solid solubility of silicon in aluminium, of 1.65% at 577°C, the eutectic temperature.

Chemical analysis of A357 gave the following composition:

Al	Si	Mg	Fe	Ti	(Cu, Cr, Ni, Zn, Pb
rem	7.22	0.38	0.13	0.05	Sn, Be < 0.01 wt%)

A357 is described as a medium strength casting alloy, typical mechanical properties include:[124]

Density:		2.98 g/cm^{-3}
Elastic Modulus	Tension	71.7 GPa
	Compression	72.4 GPa
Tensile Strength	Sand Castings	262-283 MPa
	Permanent Mould Castings	283-317 MPa
Elongation	(typical range)	3-5%

The microstructure of A357 alloy is shown in figure 6a) and b). The specimen has been lightly etched in 10%$_{vol}$ NaOH in order to bring out some topographic detail. The silicon in the eutectic regions is plainly visible standing proud from the aluminium grains.

Al-Cu-Zn-Ag-Mg alloy ARE 415: chemical analysis of ARE 415 has given the composition:

Al	Cu	Zn	Ag	Mg	Mn	Ti
rem	4.11	1.60	0.65	0.47	0.30	0.22

This alloy was developed jointly at Bath University and the Admiralty Research Establishment, Portland, Dorset. The presence of copper, zinc, silver, and magnesium greatly enhance the alloy's response to an ageing treatment. This results in high strength and generally improved mechanical properties, unusual in a casting alloy.

The microstructure of ARE 415 is shown in figure 7a) and b). Figure 7a) is an optical micrograph of an etched specimen showing significant segregation of second phase material at the grain boundaries. The second phase was studied using electron probe microanalysis and was found to be $CuAl_2$. Figure 7b) is a backscattered electron image, the light coloured shading at the grain boundaries represents more evidence of heavy coring in the grains. The microprobe traces in figure 7c) indicate the effect of the coring on element distribution across a grain. Small increases in concentration of silver and zinc are apparent, but the most significant variation is in the copper content which becomes much higher towards the grain boundary

a) Metallurgical Condition of Metals

Alloy samples were used in either one of three different metallurgical conditions: as-cast (as-received), solution treated or peak hardened.

A357 Alloy: in order to achieve the solution treated condition, the Al/Si alloy A357 was soaked in a muffle furnace for 12 hours at 540°C and then quenched into boiling water.

An ageing curve was not available for this alloy so an experiment was carried out to evaluate whether or not the alloy A357 responded to an ageing treatment. Small samples of solution treated alloy were left in an oil bath in a muffle furnace at 160°C, samples were then removed at hourly intervals.

The hardness of the samples taken from the furnace was measured using a Leco M-400 hardness tester (load of 500gf applied for 20 seconds). Each hour six values of hardness were measured on the specimen that had been removed, the hardness values were averaged and these average readings were plotted against $\log_{10}$ time, the graph is shown

in figure 8a). The alloy does not have a great response to an ageing treatment, however there is a definite increase in hardness probably due to the formation of Mg_2Si. By inspection, the peak was judged to have occurred after 7 hours at 160°C and subsequent specimens were prepared accordingly from the solution treated condition.

ARE 415 Alloy: previous work performed at Bath University has established the optimum conditions for both solution treating and ageing of alloy ARE 415[125]. The solution treatment basically comprised of a two-stage process. Specimens were heated to 500°C and left to soak at this temperature for 6 hours. Specimens were then ramped up to 525°C and left to soak at this higher temperature for 24 hours.

Peak hardening follows the curves shown in figure 8b). The curve shown at temperature 170°C has a more sharply defined peak and it was decided to follow this method. Samples were heated for 4 hours at 170°C after which they were judged to have reached their peak hardness.

5.1.2 Metal Matrix Composites

Liquid Metal Infiltration (LMI) was used to fabricate the specimens for this project. The details of the technique are still commercially confident but a schematic of the apparatus is shown in figure 9. Inspection of the diagram will reveal that the process is really just a variation of injection casting/moulding, the only difference is that the die can contain a flexible array of fibre preforms. The process allows the casting of many metal types and some success has been achieved with aluminium, zinc, magnesium, copper and their respective alloys.

a) Matrix Alloy

The alloy chosen as the matrix for the MMC composite system was A357, the aluminium/silicon casting alloy. The reason for this choice was the combination of the alloy's advantages, described earlier. These advantages include casting fluidity, medium strength, good wear properties, weldability and its current widespread commercial use.

b) Reinforcement with PAN-based Carbon Fibre

Much interest has been shown in the production and use of carbon fibres over the past 30 years or so. Early work was performed at the Industrial Research Institute in Japan, followed closely by patents published by the Royal Aircraft Establishment, Farnborough, in 1964.

Carbon fibres are generally considered to be strong and have a low density, thus enabling a material to be made that demonstrates a high specific modulus (E/ρ). There are a number of engineering properties displayed by carbon fibres that also make them desirable as a composite reinforcing system, such as:[126]

- good fatigue resistance: capable of withstanding $1x10^6$ cycles at 70% of UTS
- wear resistance: dry graphitic parts are comparable to well lubricated metal bearings ($1x10^{-6}$ wear coefficient).
- damping characteristics: acoustic and mechanical waves may be attenuated in 1/10th of the time of metal systems.
- thermal stability: dimensional changes may be as little as 1/50th of that in metals.

Speciality carbon fibres have therefore been developed that exhibit one or more of the following:

- stiffness
- lubricicity
- electrical/thermal conductivity
- low-to-negative thermal expansion coefficient

PAN-based precursors have become the major starting material for carbon fibre production because they have faster turn-round times and higher yields (e.g 65%). The processing of carbon fibres manufactured from PAN precursors follows three different steps:

Stabilisation: Acrylic precursors contain, typically, 85% of acrylonitrile together with polymeric residuals and small amounts of spin bath chemicals. Therefore, before any processing can be performed the spun fibres need to be *stabilised.* This is carried out in a furnace at about 200°C. The purpose here is to induce polymer cross-linking, with or without the involvement of oxygen, which results in the formation of a desired graphitic precursor structure. The stabilisation may be performed under tension to reduce the effects of shrinkage porosity.

Carbonisation: this step involves heating the stabilised precursor for up to 20 hours in a furnace at about 1000°C, under either inert or mildly oxidising conditions. The aim is to burn off all unwanted polymeric materials and volatile impurities (e.g ammonia, CO_2, hydrocarbon gases), leaving behind an essentially completely carbonaceous material.

Graphitisation: this final process simply converts the carbonaceous precursor material into a graphitic material. The heating is performed under an inert atmosphere at high temperatures (up to 3000°C) for about 10 minutes. Graphitic nuclei are formed in the precursor, the basal planes of which are parallel to the direction of the polymer chains.

5.2 ADHESIVE BONDING

5.2.1 Structural Adhesives

Two widely available adhesives were used for the bonding operations, these were:

Acrylic adhesive

Permabond F241: a rubber-toughened acrylic adhesive used, together with an initiator, to give bonds that exhibit high resistance to tensile, peeling, shear and impact forces (manufactured by Permabond Ltd, Eastleigh).

Cure cycle: 24 hours at room temperature; curing was initiated by contact with a catalyst painted as a very thin film on one of the two bonding areas.

Epoxy Adhesive

Scotchweld 7823: This is a single part, thermo-setting, toughened epoxy adhesive. The adhesive is formulated to give high strength bonds on a variety of surfaces and is claimed to give good environmental resistance (due to the incorporation of soluble corrosion inhibitors in the formulation). Scotchweld 7823 contains 100% solids by weight and has a thixotropic consistency that allows use on vertical or sloping surfaces. The FPL mixed acid etch is recommended as the surface pre-treatment by the manufacturers (3M Corporation Inc).

Cure cycle: the adhesive was applied to either one of the two adherends, the joint was then assembled together with spacer beads (Ballotini), clamped and placed in an oven. Samples were pre-heated for 10 minutes at 100°C, followed by the final cure of 45 minutes at 165°C.

Thickness of Adhesive Bondline

There were two distinct requirements for bond line thickness, depending upon which adhesive was being used. The acrylic, F241, is designed to function best in quite narrow bond lines. Therefore the adhesive was applied, the specimen was clamped to maintain alignment and simply left to cure. Final bond line thicknesses were typically up to 100μm.

The 3M adhesive (Scotchweld 7823) is rather different, however, being designed to have a space filling capacity. The adhesive, therefore, could be prepared with slightly thicker bond lines. To facilitate this, small spherical glass beads known as Ballotini were incorporated sparingly into the bond line. One or two were placed at each corner of the bonded overlap, together with one or two in the centre of the bonded area. The Ballotini were nominally 250-400μm in diameter and this dictated a standard, final bondline thickness. These spheres are shown in figure 10.

The Ballotini beads served another important function. When the epoxy adhesive is placed in a hot oven, it tends to become much more mobile just before the cure process begins. Under the pressure of aligning clamps there would be a tendency for the soft adhesive to be squeezed out of the bondline before any curing could take place. The Ballotini beads incorporated in the bondline were therefore able to bear the load of the aligning clamps. This enabled a standard bondline thickness to be maintained without complete loss of adhesive during curing.

5.2.2 Preparation of Specimens

Surface Finish

The specimens were ground using a Struers Planopol machine that allowed up to 8 samples to be prepared at the same time. This method enabled larger numbers of specimens to be prepared quickly to the same thickness and surface finish. Progressively finer abrasive pads were used until a standard 600-grit finish was obtained. This finish was chosen to match as closely as possible that which is used on industrial scales. It was considered that a mirror finish (say approx 1μm) was an unrealistic expectation for most industrial components. If samples were required for optical microscopy then they were polished using a 6mm diamond slurry followed by 1μm and 0.25μm diamond paste. Final finishing was achieved by applying a momentary polish with colloidal silica. Any debris or suspension fluid was removed by ultrasonic cleaning with detergent and alcohol.

Chemical Etching of Aluminium Alloy Specimens

Chemical treatment of adherend surfaces is an established type of surface pre-treatment in both the United States and Europe. Many different methods exist, including techniques ranging from degreasing through acid etching to acid anodising. Degreasing is essential particularly when bonding metal sheet which may have become oily during rolling.

A mixed acid etch was chosen as the bonding pre-treatment for a number of reasons. Firstly, it improves bond strength when compared to untreated aluminium[127]. Secondly, it is and has been, an established technique for many years and standards exist covering the technique. Thirdly, it is a technique that does not require a large investment in equipment (unlike anodising which needs specially designed busbars, refrigeration, stabilised power supplies etc). Fourthly, it is relatively straight forward to administer and is repeatable. Finally, the research group had experience with this solution in previous work covering the anodising of aluminium alloys.

The exact type of etch is covered under Defence Standard 03-2 Method O. In the UK this type of solution is known simply as a mixed-acid etch because the solution comprises both sulphuric and chromic acids in its formulation. In the US the etch is known as the FPL etch, named after the Forest Products Laboratories that originally developed its formulation. Concentrated sulphuric acid is gradually dissolved in distilled water to give the required concentration. Then, chromic acid is added in the form of sodium dichromate ($Na_2Cr_2O_7.2H_20$). Traces of copper and aluminium, in sulphate form, are added to artificially age the solution (known in the USA as an "optimized" solution)[128].

Due to the aggressive nature of the etch, a stainless steel bath was made from welded sheet material in order to contain the solution. It was necessary to perform the etch at slightly elevated temperatures, therefore the outside of the stainless steel tank was lagged with 2" thick expanded polystyrene insulation. A monolayer of polypropylene spheres was laid on top of the solution to minimise evaporative losses.

A Gallenkamp ThermoStirrer was used to agitate the solution and maintain the required temperature of 65°C. Samples were left in the solution for 20 minutes after which they were removed, rinsed in distilled water and dried thoroughly. Samples were bonded immediately to reduce the possibility of contaminating the newly etched adherend surfaces.

5.3 DIFFUSION BONDING

5.3.1 Development of Apparatus

No facilities were initially available for diffusion bonding, so equipment had to be designed and fabricated at DRA Holton Heath. It was decided to modify and equip an Instron testing machine such that samples of modest size could be bonded under controlled temperatures and loads.

Figure 11 is a schematic diagram which illustrates the apparatus used to perform the diffusion bonding. The arrangement was a simple one, push rods were turned out of solid stainless steel bars ensuring that the working faces and the end fittings were closely parallel to each other. The rods were 45mm in diameter and operated within a muffle furnace that had a 50mm bore.

A groove was machined along the side of each rod which connected with a blind hole drilled just below the working face. A k-type thermocouple was cemented into this groove-and-burrow arrangement, this enabled the temperature at a central position in each working face to be monitored at all times. In addition a thermocouple was positioned within the working area between the steel rods, this monitored the ambient furnace temperature in the region of the specimens.

The small gaps at the end of the furnace between the rod and the furnace wall were plugged with Rockwool to minimise heat losses during bonding.

The upper steel push rod was fixed to the Instron cross-head together with the muffle furnace. To extract the bonded specimens the furnace and top rod were simply raised leaving the specimen exposed on the lower rod.

Calibration: the load cells used during diffusion bonding were universal tension/compression type cells. These were calibrated with standard weights supplied by Instron to give accurate zero and full-scale deflections on the chart plotter.

Later in the programme an external plotter had to be used instead of the one integrated into the tensile machine. In order to calibrate this plotter, the low voltage output from the load cell was diverted to the new plotter, via an accurate digital voltmeter. The standard Instron weights were used again, with voltage outputs measured for each weight. In this way, it was possible to define accurate full scale deflections on the external plotter that gave representative data concerning loading profiles during bonding.

In addition, the digital voltmeter itself recorded voltage maxima for each bonding operation. It was therefore possible to validate the peak load values appearing on the external plotter by comparing the plots with voltmeter maxima.

The muffle furnace was a 3-zone type and therefore had a power supply with 3 controllable channels, one to the resistance coil in each zone. Operating this type of furnace is usually quite straight forward but some effort had to be made to obtain a bonding zone that had an predictable temperature distribution. If this type of furnace is used horizontally it is possible to set the outside coils to "buffer" the central coil and thus produce an isothermal zone for the specimens. Because the furnace was used vertically it was much more difficult to achieve a stable region within the vicinity of the sample, the power requirements for each zone varied significantly, more power was needed for the lower coil, less for the centre coil and less still for the top coil. In addition, the stainless steel rods acted as heat sinks, conducting heat away from the bond zone. Care had to be taken in particular to insulate the load cell from heat conducted through the bottom rod.

A transient temperature plotter was used to construct a series of temperature profiles within the bond zone of the furnace. Temperature data were sent from the 3 permanent thermocouples and also from a thermocouple embedded in a dummy sample. The control settings were adjusted such that the smallest possible temperature difference appeared between the three thermocouple readings. Having done this, the control settings were each increased by the same amount and the system allowed to come to equilibrium. Once equilibrium was reached the three temperatures were plotted and the process was repeated for a range of temperatures. This data is shown in figure 12. It can be seen that

there is a constant relationship between the top bar, the bottom bar and the furnace environment. The effect of the heat conduction away from the bonding zone is apparent by the small temperature lag exhibited by the bars and the furnace itself.

The steel push rods were always preheated to the appropriate temperature before a bonding run and when the correct temperature was reached the furnace was raised and the samples were placed on the bottom push-rod. The furnace was then lowered over the samples and allowed to come back up to the correct temperature. In practice the bottom bar was always the last to warm up, so when this thermocouple reached a suitable value the bonding process proceeded. It was usually necessary to wait for about 5 minutes for the bottom bar to heat up after loading a specimen.

Once the furnace arrangement was complete it was noted that there was an advantage to using large steel rods. Their heat capacity gave them significant thermal inertia, in other words they helped to maintain relatively constant bonding conditions when they had been allowed to come to equilibrium.

5.3.2 Preparation of Specimens

a) Alloy Specimens

A 600-grit finish was chosen as a suitable surface finish for diffusion bonding. These specimens were prepared by hand using the same preparation materials as for adhesively bonded samples. Alloy specimens required for microscopy were polished by using a 6mm diamond slurry followed by 1μm and 0.25μm diamond pastes. Final finishing was achieved by a rapid polish with colloidal silica.

b) Composite Specimens

Composite specimens were cut to shape using a bronze cut-off wheel whose perimeter was coated with embedded diamonds. A slow feed speed was used, together with Aquicut lubricant all through the cutting process. This helped to remove debris and

reduce the opportunity for fibre pullout and surface damage. The diamond wheel gave a fine surface finish which was considered adequate for diffusion bonding.

The preparation of samples for microscopy involved slurry grinding followed by polishing with diamond pastes on clothes with little or no knap. This type of flat polishing cloth helped to reduce relief polishing which is often a problem when preparing multi-component systems of different hardnesses.

c) Foil Inserts

Pure metal foils were obtained from Goodfellow Metals, these had been laser tested and were guaranteed free of pinholes.

Copper foils were etched in $10\%_{vol}$ H_2SO_4 to remove any residual oxide, followed by a rinse in distilled water and acetone. Diffusion bonding was carried out immediately to preempt the formation of an oxide film.

Aluminium is reactive enough to form an oxide film immediately after caustic etching so the aluminium foils were simply degreased in acetone prior to bonding.

Silver foils were also etched ($10\%_{vol}$ HNO_3), water rinsed and degreased prior to bonding.

5.4 MECHANICAL TESTING

A metric Instron 1195 was used to perform the single-lap shear testing, the cross-head speed was varied depending on the type of joint being tested. A cross-head speed of 20mm/min was used for adhesive bonds and 5mm/min for diffusion bonds.

5.4.1 Joint Design

In normal service conditions a design engineer would attempt to keep an adhesive bond in shear when under load. This is because adhesive bonds are more resistant to shear

loading than tensile or peel modes. As a result, most adhesive bonding is evaluated by using one form of shear test or another.

In consequence, a single-lap shear type of test specimen was chosen to evaluate adhesive bond strength in this project. In this type of test the load is applied in the plane of the adhesive, producing a sliding motion of the substrates relative to one another. This geometry is simple to fabricate and simple to test although quantitative interpretation of single-lap shear data can be ambiguous.

Aluminium alloy samples were machined from as-received ingots. The three types of alloy were all used; commercially pure aluminium, Al-Si alloy A357 and Al-Cu-Zn-Ag-Mg alloy ARE 415. Samples were machined to a thickness of 10mm, allowing a bonding area of 200mm^2 (i.e width 20mm, overlap 10mm). The samples needed to be quite thick for two main reasons. Firstly, machining is a costly and wasteful process, much material would have been lost in attempting to manufacture thin specimens. Secondly, thicker specimens lead to greater stiffness and therefore less tendency to bend and induce peel forces in the bondline.

Care needed to be taken when testing thick specimens such as those used in this program. If the ends of the sample are gripped and pulled to destruction, a bending moment will induce peel forces at the bondline. This would tend to give a lower value of bond strength for the simple reason that the adhesives used are weaker in peel than in shear. Therefore, spacer blocks were attached to the ends of the specimen to attempt to keep the test unidirectional. The arrangement of the test specimen and spacer blocks is shown in figure 13a). The effect of a bending moment induced by asymmetric loading is shown in figure 13b).

Similar geometric considerations were necessary for diffusion bonded specimens as for adhesively bonded samples. During shear testing, the applied load had to be kept in the plane of the bond-line. It was not possible to attach spacer blocks to the specimens, so a diffusion bonded sample was prepared with two diamond-sawn slits cut just through the

bond-line. In effect this allowed the entire sample to be gripped and the area between the slits was tested in shear. This type of specimen is analogous to, and is compared with, the adhesively bonded specimens; the diffusion bonding arrangement is shown in figure 14b) where the shading represents the area under test.

5.4.2 Design of Lap Shear Test Jig

The size of the diffusion specimens placed some constraints on the test methods used to ascertain lap shear strengths. The sample width was too small to use any of the conventional gripping devices standard to the Instron 1195 so a jig was designed and built that bolted onto existing tooling. A schematic diagram of the test jig is shown in figure 15.

This arrangement basically consisted of a pair of sliding barrels. The top of the specimen was connected to the upper barrel which remained stationary during the test. The bottom of the test piece was connected to the descending cross-head by a stainless steel pin placed in a hole bored through the bottom barrel. A pair of slots machined into the top barrel allowed the bottom stainless pin to descend with the cross-head and thereby place the sample in shear. A series of locknuts were used to restrain the workpiece during testing. The barrels were rigidly fixed in their positions to ensure that no torque was transferred to the test-piece.

5.5 MICROSTRUCTURAL ANALYSIS

5.5.1 Optical Microscopy

Optical microscopy relies on the vertical illumination of a suitable specimen by a light source whose rays are directed onto the sample by a partially silvered mirror. Reflected light is the re-directed through a series of glass optics to an objective eye-piece where a final image is formed. The resolution of a light microscope is a function of the wavelength of the light being used and is of the order of $2x10^{-7}$m. The resolution of the

unaided human eye is approximately $2x10^{-4}$m, dividing this by the previous figure for the microscope resolution gives a maximum useful magnification of around 1000 times for a typical optical microscope[129]. This magnification equates to objects of micron dimensions or just smaller. Resolution can be lost by imperfections within the optic geometries (spherical aberration) and also by the varying focal points of the different colour components of visible light (chromatic aberration). Chromatic aberration can be reduced somewhat by using appropriate filters that provide illumination within a more narrow band of wavelengths. Filtering the light source can also increase the effective contrast of an image on certain photographic recording media.

5.5.2 Scanning Electron Microscopy

When an incident electron beam hits a specimen, energy is lost due to inelastic scattering of the electrons. This type of scattering is likely to give rise to emissions from the specimen, which are in turn used to produce images in the electron microscope. Figure 16 schematically shows these effects.

Computer-based Monte-Carlo simulations have shown that incident electrons can be scattered within a region in a solid as show in figure 17. This region is known as the interaction volume and it is here that secondary radiations will be generated.

For the purpose of analysis in the SEM, the most important interactions are those that generate secondary electrons, backscattered electrons and x-rays.

Secondary electrons are generally those that escape from the specimen surface with energies less than about 50 eV. They tend to be either escaping electrons that have gained some energy through inelastic scattering of the primary beam (figure 18), or indeed may even be remnants of the primary beam itself that have been scattered toward the surface of the specimen. Secondary electrons may also be generated by interaction with escaping backscattered electrons, these however are far less numerous than those formed by the primary electron beam. Having such low energies, secondary electrons can only escape

from a layer close to the specimen surface (≈10-20nm). These secondary electrons are thus heavily influenced by the state of the surface and are therefore used to gather topographical information.

Primary electrons that escape from the surface with significant fractions of their incident energies are known as backscattered electrons. Being more energetic than secondary electrons (≈tens of keV) they tend to emerge from deeper within the specimen (≈150nm). Backscattered electrons may be sensitive to orientation and atomic number of the specimen but they are relatively unaffected by the topographical nature of the specimen surface.

X-rays are also produced as a result of interactions between incident electrons and the specimen (or more precisely, the orbital electrons of atoms in the specimen). When an atomic electron is ejected by an incident electron, it leaves its host atom in an ionised, higher energy state. In an attempt to reduce the energy of the atom, a higher energy electron may drop into the vacancy created by the ejected electron. During this process the electron will lose energy which may result in the production of an x-ray.

The Pauli Exclusion Principle states that electrons in a shell cannot all exist in that same orbital. The result is that an orbital shell will consist of sub-orbital levels, with clearly defined energy states. Therefore, when an electron from a higher level fills a vacant electron position, the energy lost relates directly to the energy difference between the occupied and previously-occupied levels. Therefore, the emissions formed by electrons "shedding" energy also have clearly defined energy levels, and are known as *characteristic x-rays*.

Alternatively, an electron may be emitted from a higher level orbital in order to reduce the energy of the atom, these are known as *Auger* electrons. Auger electrons are also energetically characteristic of the material from which they were ejected. Whilst sophisticated apparatus exists to harness these electrons for chemical studies, this type of analysis was not performed in this programme.

In addition to characteristic x-rays, continuum x-rays are produced by the "braking" effect experienced by the incident electrons which do not interact directly with the atomic electrons, but are rapidly slowed down in the vicinity of the nuclear field. The x-rays subsequently emitted by this process can include a range of energies which are not characterised by the particular species of atom, thus producing "white" or "background" radiation.

The background radiation when combined with the characteristic x-rays form the x-ray emission spectra of the material, in which the characteristic x-rays appear as peaks above the continuum.

The scanning electron microscope (SEM) has greater resolution (≈10nm) than the optical microscope, and also little sample preparation is necessary for many of its applications. The operation of an SEM requires an energetic electron beam to be directed at the specimen, this beam may be characterized by its accelerating voltage, typically 5-40 keV.

As described in a previous section, various interactions occur when an energetic electron beam hits a specimen. In the SEM, secondary or back-scattered electrons are primarily used for analysis. The secondary electrons, not being particularly energetic, are surface sensitive and provide topographic data. Back-scattered electrons come from deeper within the sample and are more energetic, thus, they are less surface sensitive and yield more chemical information.

X-ray detection equipment may be attached to an SEM to enable more detailed chemical analysis to be performed.

5.5.3 Electron-Probe Microanalysis (EPMA)

An electron probe microanalyser (EPMA) is basically an SEM-type machine that has been built specifically for the analysis of characteristic x-ray emissions. Operating a similar regime of accelerating voltages as an SEM and using EDS and/or WDS detecting facilities, detailed qualitative and quantitative chemical data may be extracted from many

different types of specimen. Modern software control allows reproducible analysis conditions, such as specimen tilt, position and operating umbrellas (e.g accelerating voltages and beam currents).

Measurement of energy, or wavelength, of a characteristic x-ray provides a means for identifying, chemically, the source of the x-rays. Additionally, the measurement of x-ray intensity may provide information concerning the concentration of a chemical species. These analyses may be performed using two related techniques: i) Energy Dispersive Spectrometry, or ii) Wavelength Dispersive Spectrometry.

a) Energy Dispersive Spectrometry (EDS)

The detecting system of an energy dispersive spectrometer (EDS) consists of a lithium-doped, silicon crystal. The presence of lithium reduces the effect of impurities in the silicon and promotes semi-conducting behaviour. A thin coating of gold (200Å) is evaporated onto the surface of the silicon crystal, this forms an electrical contact and allows the application of a negative bias voltage to the detecting face. The crystal is usually capable of detecting x-rays up to 15 keV.

The signal currents in the detector must be amplified for accurate measurement. To achieve this a Field Effect Transistor (FET) is mounted close to the detector. Noise may be picked up by thermally induced vibrations in both the detector and the FET. In order to reduce these effects to a minimum, the assembly is maintained under high vacuum at liquid nitrogen temperatures. The amplified current is fed into a multi-channel analyser, in which the signal is separated by a pulse-height analyser. Each separate channels relates to the number of x-rays of equivalent energy.

b) Wavelength Dispersive Spectrometry (WDS)

Wavelength dispersive spectrometry (WDS) is a technique in which the lattice planes of an analysing crystal diffract characteristic x-rays, according to Bragg's Law, which can be expressed by:

$$n\lambda = 2D \sin\theta$$

where λ, D, and θ, are the wavelength of the x-ray, the interplanar spacing of the crystal and the Bragg angle, respectively.

The diffracted x-rays are collected by a detector and the x-ray intensity is plotted as a function of the Bragg angle θ, hence the x-ray spectrum is obtained. For example, by setting the crystal to a known Bragg angle (θ), the characteristic x-radiation of a particular element (i.e known λ) in a specimen can be examined.

Commonly, a WDS system will incorporate up to 4 different crystals. Traditional crystal materials such as quartz, gypsum and mica, have largely been superseded by synthetic organic and metallo-organic crystals. These organic-based crystals are constructed layer by layer, on a molecular level, using a process pioneered by Langmuir et al[130], whose name has been given to this type of thin film production.

The most common detector used in wavelength dispersive spectrometry is the gas-proportional counter. The device is simple in its construction, being basically a metal tube fitted with insulating end-pieces, incorporating a coaxially mounted anode wire of very smooth finish. The sealed tube is filled with a noble gas, such as argon, and fitted with a window to allow the x-rays to enter the device.

When x-rays enter the system they interact with the electrons in the gas. These interactions induce a small electrical pulse in the wire, the magnitude of which is proportional to the energy of the characteristic x-ray.

The window of a WDS detector is usually made of beryllium. This is because beryllium is transparent to x-rays (except at low x-ray energies) and can withstand the aggressive pressure environment of a vacuum system. Where beryllium is unsuitable, thin plastic windows may be used instead.

c) EM Method for Characterising Oxide Film Thicknesses

It has been suggested that a possible reason for any improvement in adhesive bond shear strength after FPL etching is, in part, related to a modification in film thickness of the barrier oxide. It was therefore considered important to ascertain by how much the FPL etch enhanced the thickness of the barrier oxide. Various techniques exist for this kind of analysis, but one in particular was chosen because previous work and expertise existed in the School of Materials Science at Bath. The method involved a measurement and subsequent comparison of characteristic x-ray intensities, these values being taken from both etched and unetched alloy specimens and also from an aluminium oxide (Al_2O_3) standard.

As described previously, x-rays may be produced as a result of the bombardment of a specimen by energetic electrons. These x-rays originate from within a volume of a few cubic microns; the x-ray depth distribution is a function of both the atomic number of the specimen and the electron accelerating voltage. The variation of intensity of generated x-rays with depth has been shown to follow the curve illustrated in figure 19a), often called a $\phi(\rho z)$ curve.

An approach by Bishop[131], followed by Love and Scott[132], treated the x-ray distribution in a simple fashion. They adopted a rectangular x-ray profile, figure 19b), and showed that this could be used in quantitative microanalysis, provided that an accurate mathematical expression for the mean depth of generation, $\rho\bar{z}$, was found.

The parameter, $\rho\bar{z}$, may be defined thus:

$$\rho\bar{z} = \frac{\int_0^\infty \phi(\rho z)\rho z d\rho z}{\int_0^\infty \phi(\rho z) d\rho z}$$

Sewell et al (1985), quoted in Scott and Love's book, produced the following equation for $\rho\bar{z}$ from Monte Carlo calculations:

$$\rho S_m = \rho\bar{z}(2.4) + Z(0.07) + \frac{(1.04 + 0.48\eta)}{\ln U_0}$$

where Z = atomic number

η = backscatter coefficient. Electrons are backscattered and hence unable to generate x-rays, η is therefore dependant on the type of specimen.

U_0 = overvoltage ratio = (energy of incident electron beam)/(critical excitation energy of target atom)

ρS_m is known as the electron range and can be found from the expression:

$$\rho S_m = \frac{A}{Z}\left[(0.773 * 10^{-5})J^{1/2}E_0^{3/2} + (0.735 * 10^{-6})E_0^2\right]$$

Where:

A = atomic weight

J = mean ionisation potential = 0.0135.Z

E_0 = incident electron energy

In using this simplified rectangular model, a constant intensity of x-ray generation is assumed up to a depth $2\rho\bar{z}$ whereupon the intensity falls to zero.

The total intensity of x-rays generated may be obtained by integrating under the ϕ(ρz) curve, viz:

$$\int_0^\infty \phi(\rho z)d\rho z$$

However, x-rays will be absorbed on their way out of the specimen (before they can be measured) and an absorption term must be included such that the total intensity of

emitted x-rays becomes :

$$\int_0^{\infty} \phi(\rho z)\exp(-\frac{\mu}{\rho}.\rho z.\cos ec\psi)d\rho z$$

where:

$\frac{\mu}{\rho}$ = mass absorption coefficient,

ψ = take-off angle.

For the simple rectangular model the intensity of emitted x-rays can therefore be given by the expression:

$$I = \int_0^{2\rho\bar{z}} k\exp(-\frac{\mu}{\rho}.\rho z.\cos ec\psi)d\rho z$$

$$I = \left[\frac{-k\exp(-\frac{\mu}{\rho}.\rho z.\cos ec\psi)}{\frac{\mu}{\rho}.\cos ec\psi}\right]_0^{2\rho\bar{z}}$$

$$I = \frac{k - k\exp(-\frac{\mu}{\rho}.2\rho\bar{z}.\cos ec\psi)}{\frac{\mu}{\rho}.\cos ec\psi}$$

Consider now an aluminium specimen with a thin layer of surface oxide, Al_2O_3, see figure 20a). The intensity of oxygen characteristic x-rays emitted from this thin layer is measured, and then compared to those emitted from a pure Al_2O_3 standard, figure 20b).

An assumption is made that the x-ray distribution functions are similar for aluminium and Al_2O_3, i.e both of the rectangular profiles the k-values are the same.

Hence we may write:

$$\frac{I_{spec}}{I_{stan}} = \frac{\int_{0}^{\rho z_1} k\exp(-\frac{\mu}{\rho}.\rho z.\cos ec\psi)d\rho z}{\int_{0}^{2\rho\bar{z}} k\exp(-\frac{\mu}{\rho}.\rho z.\cos ec\psi)d\rho z}$$

Where:

ρz_1 = mass thickness of the analysed film.

I_{spec} = intensity of x-rays emitted from specimen.

I_{stan} = intensity of x-rays emitted from Al_2O_3 standard.

By assigning values of ρz_1, i.e by changing the limits of integration, a series of values of x-ray intensity may be calculated for thin films of known thickness. These results, after normalising to I_{stan}, may then be plotted as a curve of the form:

$$\frac{I_{spec}}{I_{stan}}.vs.Thickness$$

Thus in practice, the unknown thickness of an oxide layer may be calculated. This method involves taking characteristic x-ray intensity measurements from the unknown oxide film using electron-probe microanalysis. These specimen measurements are then compared against those taken from a standard of the same composition as the film. The ratio of x-ray intensities emitted from the specimen and standard is calculated, these measurements are then compared with a calibration curve such as that shown in figure 21, provided by Dr G. Love in the School of Materials Science at Bath University. The oxide thickness is then simply read directly off the curve.

6. RESULTS - ADHESIVE BONDING

6.1 RESPONSE TO FPL ETCH

The mixed acid (FPL) etch enhances the thickness of the barrier oxide present on all aluminium alloys. All previous work using this method of surface treatment had been performed using wrought alloys which can exhibit microstructures that are relatively homogeneous. This programme focuses on alloy samples fabricated using a novel casting technology, the specimens exhibited the microstructures normally present in cast materials such as coring and eutectic colonies. It was therefore expected that these microstructures would react differently to a standard surface etch treatment.

6.1.1 Commercially Pure Aluminium

The absence of alloying elements in commercially pure aluminium leads to a simple microstructure and, as the micrographs in figure 22 show, the material responds in a fairly homogeneous manner to the FPL etch.

The etch pits produced by the FPL solution are some 2μm in diameter. Close inspection of the surface reveals a finer structure still. This type of surface is considered ideal for adhesive bonding, the etch effectively roughens the surface and thereby increases the area available for wetting by the adhesive.

6.1.2 Al-Si Alloy [A357]

The eutectic structure of this alloy reacted violently to the FPL etch, as evidenced in figure 23. Aluminium in the region of the eutectic was deeply etched and there is some evidence of attack in the centre of the grains as well.

It has been shown that alloy A357 responds in a modest way to a solution and ageing treatment. It could be expected then that a change in alloy microstructure will bring about a change in response to the FPL etch. This is confirmed in figure 24 where much less

surface damage is apparent after the alloy has been solution treated. Some eutectic silicon seems to have been etched out of the matrix and there is still some evidence of pitting within the grains.

The modest response to ageing in this alloy does not indicate a great change in microstructure between the solution and peak hardened states. The micrograph in figure 25 confirms this observation as there is little difference in this and the etch structure produced on solution treated material.

6.1.3 Al-Cu-Zn-Mg-Ag Alloy [ARE 415]

ARE 415 is a very complex alloy containing a number of additions that act together to induce a significant response to ageing. The as-cast material is typical of foundry-type alloys exhibiting highly cored grains, segregation and porosity.

The response of this alloy to the FPL etch is shown in figure 26. The $CuAl_2$ second phase at the grain boundaries has been severely etched, as have some areas within the grains. Once again the pitting is apparent within the grains.

The structure produced by the FPL solution is slightly different to the Al-Si alloy in that the etch around the grains is more "clean", leaving deep furrows rather than the very rough regions amongst the silicon eutectic.

The 415 alloy has had a special 2-stage solution treatment devised for it to enable the dissolution of the alloying elements. The elimination of coarse casting defects, particularly, has an effect on the action of the FPL etch and the structure produced is shown in figure 27a). The catastrophic effect of the etch is reduced and damage is limited to areas that are probably porous already.

Figure 27b) shows an etched sample of peak aged 415 alloy. The magnification is slightly different to the previous micrograph so comparison is not so simple. However,

the apparently decreasing evidence of large scale chemical attack could be linked to the formation of a more uniform microstructure.

6.2 OXIDE FILM MEASUREMENTS

Two methods were employed to measure the oxide thickness on pure aluminium and FPL-etched pure aluminium. The first was essentially semi-quantitative, the second more fully quantitative.

All measurements were performed using a Jeol JXA 733 "Superprobe". The operating conditions for the microprobe were:

- Accelerating voltage 10 KV
- Beam Current 3.0×10^{-8}A
- Magnification 3600
- Diffracting Crystal LDE1

X-ray intensity data were measured in counts per second (cps, also known as count rate) and were either noted down or presented using a chart recorder. The full scale deflection of the chart recorder was chosen to accommodate the count rate.

6.2.1 Method 1: Comparison of Peak Heights

In this method, the maximum intensity of characteristic oxygen x-rays was obtained by driving the WDS crystal and thereby scanning the specimen through the entire oxygen peak. Peak results were compiled for pure, polished aluminium and these were compared to the peak intensities measured from FPL-treated pure aluminium.

In this way a quick, visual measurement was possible. The oxygen characteristic peaks are shown in figure 28. By a straight comparison, the peaks of the FPL-etched pure aluminium look to be some 2 to 3 times higher than those of the unetched, polished pure

aluminium. By induction, the enhanced oxide produced by FPL etching could be expected to be some 2 to 3 times thicker than the barrier oxide.

The exact thickness of the barrier oxide existing on the surface of all aluminium specimens is not that widely reported. A preference seems to exist for using an estimated figure of something less than 10.0nm. By using this as a base figure for the natural oxide film present on an as-polished specimen, and comparing it with the peaks shown in figure 28, it may be possible to infer that the oxide film arising from the FPL etch is somewhere between 10 and 30nm. This value can obviously be used only as an estimate.

Therefore, in order to attempt to find an accurate measure of the thickness of the oxide produced after the mixed acid etch, a more precise quantitative method was required.

6.2.2 Method 2: Use of Calibration Curve

Samples of as-polished aluminium and FPL-etched aluminium were placed in the EPMA, along with a suitable standard (in this case a sample of pure Al_2O_3, i.e the same composition as the barrier oxide).

The operating conditions for the EPMA were the same as those described earlier in this section. The maximum intensity of generated x-rays was measured in counts per second as the crystal scanned through the characteristic oxygen peak. This measurement was taken a number of times and the averaged for each specimen. The results are shown below:

	Oxygen X-ray Intensity (cps)	Average (cps)	Background Intensity (cps)
Alumina Standard	5150 5250	5200	100
Pure Aluminium	150 160 165	160	30

	275		
	285		
FPL etched	305	290	40
Aluminium	300		
	300		

The average values (in cps) for each category, corrected for background thus become:

Alumina	5100
Polished Pure Aluminium	130
FPL Etched Pure Aluminium	250

The ratios of I_{spec} / I_{stan} therefore become:

Polished Pure Aluminium $\frac{130}{5100} = 0.03$

FPL Etched Aluminium $\frac{250}{5100} = 0.05$

A calibration curve was employed to convert these ratios into meaningful numbers, the curve has been shown in figure 21. From this curve, oxide thicknesses were calculated to be:

Specimen Type	Oxide Thickness (nm)
Aluminium	6.8
FPL Etched Aluminium (optimised at 65°C)	14.2

This value of 14.2 nm falls within the band of values indicated by the qualitative method described earlier involving the comparison of x-ray peak heights.

6.2.3 Effect of FPL-etch temperature on oxide thickness

The relevant standards quote an optimum temperature for operating the FPL etch. If the operating temperature is too low, the oxide formed will not be sufficiently thick to ensure good bond durability. In order to determine the effect of temperature on oxide thickness, the FPL etch bath was lowered to +40°C, this being some 25°C lower than that required for this process. Samples of commercially pure aluminium were then etched for an identical period of time in this lower-temperature solution. The oxide film on the low temperature etched specimen was then analysed in the EPMA in exactly the same way as previously, using the same electron microprobe operating conditions.

Characteristic oxygen x-ray intensities were recorded, averaged and then corrected for background radiation as follows:

	Oxygen X-ray Background Intensity (cps) (cps)		Average Intensity (cps)
	220		
	210		
Low-temp	210	210	28
FPL etched	210		
Aluminium	200		
	210		

$\therefore$ Average value corrected for background = 182 cps

Al_2O_3 standard intensity as before = 5100 cps

The ratio $\frac{I_{spec}}{I_{stan}}$ becomes: $\frac{182}{5100} = 0.04$

Applying this $\frac{I_{spec}}{I_{stan}}$ ratio to the same calibration curve gives a value for oxide thickness for the low temperature, non-optimized FPL etch. This value is noted and may be compared to those values calculated in the previous section, such that:

Specimen Type	Oxide Thickness (nm)
Aluminium	6.8
FPL Etched Aluminium (optimised at 65°C)	14.2
FPL Etched Aluminium (non-optimised at 40°C)	9.6

It is clear therefore that the FPL etch does indeed build up the thickness of the oxide film present on the aluminium surface. It is also clear that operating the FPL etch at incorrect temperatures will result in the formation of a significantly thinner oxide film. The effect of this reduction in barrier film thickness would become manifest in durability tests, where the ingress of water gradually degrades bond strength.

6.3 SINGLE-LAP SHEAR TESTING OF ADHESIVE BONDS

Alloy samples were bonded for single-lap shear testing as described previously. They were then tested to destruction on an Instron 1195 and the load reached at failure was recorded for each specimen.

Two types of adhesive were used, a cold-cure acrylic and a hot-cure epoxy. The acrylic was a new formulation from Permabond Ltd and was included as a comparison to the epoxy which is the type of adhesive of most interest to the research group at DRA Holton Heath.

The results obtained in this series of tests are tabulated in figures 29-35. A students t-test was performed on each group of results in order to test the null hypothesis that the mean values were the same, i.e that they originate from the same distribution of results. This is a convenient way of statistically determining whether heat treatments, for example, affect the measured bond strength.

The tests were conducted at a 95% confidence level and the results are given in the form of a probability rating. If the null hypothesis were true, i.e that the mean values were the same, then the value of the T-statistic calculated through the test must be less than t, the test statistic found from lookup tables. The value of t is fixed and depends on the sample size and the confidence level at which the test is performed. The results are actually given in the form of a test probability between 0 and 1 (see P(T<=t) in the t-test data), in other words how probable it is that the distributions are the same for a given confidence level.

The t-tests were initially performed by hand, but have been re-calculated using the analytical tools available in Microsoft Excel. Strength data were tabulated in the spreadsheet and t-tests were performed on the appropriate sample ranges. The program automatically took into account mean values and standard deviations when it performed the calculations.

6.3.1 Epoxy Adhesive

This adhesive is of particular importance to the DRA at Holton Heath. The adhesive has many in-service uses, notably as a structural sealant for torpedo hull sections. For this reason a range of bond tests was performed, both etched and unetched specimens have been tested to ascertain the effect of the FPL etch on measured bond strength.

The number of combinations of possible t-tests is quite large so the tests have been performed in the two most relevant ways, firstly between etched specimens in different metallurgical conditions, secondly between etched and unetched specimens in the same metallurgical condition. The first method examines the effect of metallurgical condition on bond strength and the second examines the effect of the FPL etch on joint strength.

a) Commercially Pure Aluminium

This material was included as a test reference. The results for etched and unetched pure aluminium are shown in figure 29. The unetched samples gave an average load at failure of 3225N whilst the FPL etched samples had a higher average value of 4405N.

The t-test performed on the results shows that the etched and unetched mean values are significantly different, in other words this confirms the data stated in the literature that the FPL etch improves the lap shear strength of adhesively bonded specimens. The scatter in results is quite low, 9% of the mean for the unetched samples. This scatter is reduced to 4.5% for FPL etched specimens.

b) 415 Alloy

Failure loads are tabulated in figure 30. The effect of metallurgical condition is tested in figure 31. There is no statistical similarity between the as-cast, solution treated and peak aged samples. The bond strength falls off significantly for solution treated samples (from 6240 to 4610N) but climbs again to 5700N after an ageing treatment has been performed. Although the as-cast and peak aged samples' means are quite close (6240 and 5700N) there is only a 13% probability of these samples being similar. The standard deviations for these data are smaller and tend to lie in a band about 11-14% of failure load, roughly half the scatter magnitude found for the acrylic adhesive.

The effect of FPL etching is shown in the t-tests from figure 32. In all cases the measured failure loads were shown to be statistically higher for unetched specimens. This is an interesting result as it basically contradicts the published data for this type of surface treatment. Also, the unetched specimens exhibit less scatter than the etched samples. The magnitude of the standard deviations lies in a narrow band of the order of 3-7% of the average failure load.

c) A357 Alloy

The results for this alloy are tabulated in figure 33. The t-tests for the etched samples in figure 34 show a significant dependence on the metallurgical condition of the samples. The results show that the solution treated specimens have higher failure loads (8450N) than the as-cast material (5010N). Peak ageing appears to bring about a reduction in bond

strength down to 7030N compared with solution treated alloy. The standard deviations lie in the range of 12-19% of the average failure loads.

The effect of FPL etching is tested in figure 35. The results are essentially the same as those found for the 415 alloy, the FPL etch reduces the bond strength in all cases. The closest sets of values between etched and unetched samples was for solution treated A357 alloy. In this case there was a 68% probability of the values being similar. Once again the scatter in unetched results is lower than for etched samples (7-11% of average failure load), with the notable exception of the unetched solution-treated data, however in a sample set of 3 results one incongruous data point can offset the standard deviation by a substantial amount. Under these circumstances the question has to be asked as to whether that point is representative when compared to the trends exhibited by other samples.

d) Air Entrapment

A novel technique was used to investigate to what degree the metal surface was wetted by the adhesive. This method involved bonding the adherend to a glass microscope slide with epoxy adhesive and curing the joint in the usual manner. Examination of the glass slide using low-power optical microscopy gave valuable information relating to the processes occurring during adhesive cure. An example of this experiment is shown in figure 36a) where significant quantities of porosity are visible through the glass slide. Additionally the SEM micrograph in figure 36b) shows blow-holes of significant size residing within the remnant adhesive spew fillet after fracture in a shear test.

6.3.2 Acrylic Adhesive

a) FPL Etched 415 Alloy

The results of single lap shear testing are given in figure 37. Average failure loads for as-cast, solution treated and peak aged material are 4320, 2710 and 3390N respectively. The

highest scatter, as given by the standard deviation, occurred for peak aged samples and at 950N represented nearly 30% of the average failure load.

The t-tests for this alloy are shown in figure 38. It can be seen that in each test there is less than a 10% probability that the result are related, in the case of the as-cast and solution treated alloy the probability approaches zero.

b) FPL Etched A357 Alloy

The results for this alloy are given in figure 39. The as-cast, solution treated and peak aged materials have the following failure loads; 3820, 4180 and 4220 N. Visual inspection shows that the solution treated and peak aged materials have similar mean values. This significance of this is borne out by the t-test in figure 40 where a probability P(T<=t) of the sample distributions being the same is 0.89 or 89%.

The standard deviations for the data relating to the acrylic adhesive are quite high. Results for the Al-Si alloy and also the Al-Cu-Zn-Mg-Ag alloy show deviations between 600 and 950 N, between 14 and 30% of the mean values of failure load.

All of the adhesive bond strengths have been plotted in figure 41. The results have been separated into graphs relating to the two alloys examined in this part of the programme.

6.4 FRACTOGRAPHIC OBSERVATIONS

6.4.1 Epoxy Adhesive Joints

After single-lap shear testing, fractured samples were examined to attempt to establish the locus of failure. To the naked eye and under a low powered microscope, the adhesive appeared to fail at the metal/adhesive interface, i.e clean areas of metal where observed on each fracture surface.

It was decided to use the EPMA to try to see if a thin film of polymer was left behind on what appeared to be clean metal. In order to make subsequent measurements simpler,

samples of commercially pure aluminium were bonded and then shear tested. This choice of alloy enabled the measurement of one, and only one, Kα x-ray type.

a) Method 1

The LDE1 crystal was tuned to look specifically for carbon and area scans were conducted over "clean" metal fracture surfaces. The micrograph is shown in figure 42a). The photograph does not have much detail, but, even allowing for statistical noise on the detectors it seems to indicate the presence of a fairly uniform carbon film. The presence of this residual carbon based film implies that the adhesive has failed cohesively, i.e, within the adhesive and not at the interface.

The micrograph in figure 42b) is constructed in a similar way to the previous two except that the detecting crystal was set to measure oxygen x-rays. The photograph indicates an almost homogeneous oxygen source. There is some oxygen present in the adhesive but it is possible that some of the oxygen x-rays being shown in this figure originate from the enhanced aluminium oxide lying just below the adhesive film.

b) Method 2

A similar type of measurement and calculation was performed on this thin carbon film as that carried out on the oxide earlier. The method attempted to measure the attenuation of characteristic aluminium Kα x-rays emitted from a pure aluminium substrate. The reasoning being that the presence of a thin carbon film would impede the emission of characteristic x-rays from the alloy beneath.

The intensity of aluminium Ka x-rays were measured from a bonded specimen and compared with a polished sample of the same purity aluminium. Scans were carried out on areas roughly 80μm x 80μm.

Examples of intensities are as follows:

	Aluminium X-ray Intensity(cps)	Average Intensity(cps)
Aluminium standard	22500 22625	22560
Aluminium + polymer film	17200 18400	17800

The ratio $\frac{I_{spec}}{I_{stan}}$ becomes: $\frac{17800}{22500} = 0.8$

(we shall subsequently use $\frac{I_{spec}}{I_{stan}} = 0.8$)

This ratio value tells us that some 20-21% of aluminium Kα x-rays have been attenuated by the adhesive film.

The absorption of the aluminium Kα x-rays may be expressed as follows:

$$I = I_0 \exp(-\rho t.\frac{\mu}{\rho})$$

where:

ρt = mass thickness of the adhesive

$\frac{\mu}{\rho}$ = mass absorption coeff. for aluminium Kα radiation.

So:

$$\ln(0.8) = -\rho t.\frac{\mu}{\rho}$$

We shall take 2 values of $\frac{\mu}{\rho}$, one for pure carbon and one for pure oxygen. The reason for this is that the precise composition of the adhesive is unknown, but contains both

carbon and oxygen. The two values would therefore give the two widest boundaries of film thickness.

$\frac{\mu}{\rho}$ for C = 557 for aluminium Kα

$\frac{\mu}{\rho}$ for O = 1503 for aluminium Kα

So,

for carbon, when $\frac{\mu}{\rho}$ = 557, thickness t = 4.00 x 10^{-3} mm

and,

for oxygen, when $\frac{\mu}{\rho}$ = 1503, thickness t = 1.48 x 10^{-3} mm

In order to obtain these values the assumption has been made that the polymer density ρ = 1.00.

If the film comprised entirely of oxygen, it would need to be some 1.48 x 10^{-3} mm to explain the amount of x-ray attenuation measured. This is obviously not possible, an examination of the base formula for a di-functional epoxy adhesive (figure 43) shows the presence of only 4 oxygen atoms in the molecule. The true value of film thickness is probably somewhere between the values given for carbon and oxygen-only layers.

6.4.2 Acrylic Adhesive Joints

After lap shear testing the acrylic specimens left behind discernible quantities of remnant adhesive. These effects are shown in figure 44, 45 and 46.

a) A357 Alloy

The fracture surfaces of a sample of FPL-etched Al-Si alloy is shown in figure 44. The lower magnification micrograph clearly shows the heavily etched eutectic regions on the

surface. The centre of the grains are shown in the higher magnification micrograph in figure 44b).

b) ARE 415 Alloy

A specimen of etched 415 alloy bonded with acrylic adhesive is shown in figure 45. The cored regions removed by the FPL etch are visible at the edges of the micrograph. Etch pits are also visible within the grain. A higher magnification of this is shown in the photograph below.

The micrographs in figure 46 demonstrate the type of failure occurring in the bondline at the acrylic adhesive. The top photograph shows a classic mixed-mode type of failure. Other areas exhibit failure within the adhesive itself.

6.5 ADHESIVELY-BONDED COMPOSITE MATERIAL

Composite specimens of aluminium/silicon alloy A357 reinforced with a 0/90° arrangement of carbon fibres were manufactured by Cray Advanced Materials. The geometry and bonded area (20x10mm) of the single-lap shear specimens was similar to the unreinforced metal specimens discussed earlier except that the composite material was in plate form 3mm thick, additionally the same epoxy adhesive manufactured by 3M was used to prepare bonded joints. In order to determine the effect of the acid etch, samples were bonded with surfaces prepared to a 600 grit finish and also with the FPL treatment. Figure 47 shows an SEM micrograph of composite material simply prepared on a grinding wheel. Areas of matrix material are visible in places together with significant quantities of fibres exposed by the mechanical preparation. Regions of "dry" fibres are also visible indicating that the composite had been poorly infiltrated during manufacture.

Composite specimens were prepared using the FPL etch under conditions described previously and the resulting topographic structures are shown in figure 48a) and b). There

is no evidence for the presence of matrix alloy at the sample surface, this had obviously been removed by the etch. The higher magnification micrograph in figure 48b) shows some small debris particles which were identified by EDS analysis to be primary silicon, probably originating from the Al/Si matrix alloy. Gaps can clearly be seen between the fibres which may have permitted ingress of the FPL solution, chemical attack by the etch below the composite surface may also have been possible.

Single-lap shear results were lower than those of unreinforced alloy material in all cases. The specimens demonstrated either one or both of two possible failure modes, the first was a type of subcutaneous interlaminar fracture in which the adhesive appeared to pull away a layer of composite material from the bonded area, the resulting damage covered most of the bonded surface and is shown in the collage in figure 49. The second failure type was a simple through-section crack occurring at the edge of the overlap area, also shown in figure 49 (arrowed). No joints failed either within the adhesive or at the composite/adhesive interface.

7. DISCUSSION - ADHESIVE BONDING

7.1.1 Pure Aluminium

The differences in alloy composition produced different responses to treatment by the FPL etch. The absence of significant alloying additions made commercially pure aluminium an ideal reference material. Exposure to the FPL solution produced an even etch with a scalloped structure with the etch pits roughly 2μm in diameter, figure 22. Finer detail is just visible within the etch pits themselves and has been variously reported as small oxide flakes or nodules, see for example Venables[73]. These nodules can serve to increase the effective area available for bonding by an adhesive. This type of structure has also been noted by Arrowsmith and Moth[74] for Al-Mg wrought alloys. In the case of wrought alloys the etch pits were slightly smaller (≈1μm diameter) but had an identical shape and distribution. The similarity in etch topographies demonstrated that the treatment was being performed correctly and served as a calibration before more complex alloys were etched in the solution.

The use of the FPL solution produced higher initial bond strengths than unetched specimens. The increase was of the order of 36% of the unetched values. This observation is in general agreement with a number of authors' work, notably Arrowsmith and Moth[49], who also note the benefit of the FPL etch when adhesively bonding aluminium specimens. The increase in the load measured at failure was also accompanied by a reduction in scatter of results, the average strength was 4400N the standard deviation was ±200N, a relative error of ±4.5%, see figure 29. The observed reduction in scatter of results is consistent with published data showing that the FPL etch is a beneficial pretreatment for adhesive bonding.

In addition to surface roughening the FPL etch produced a thickening of the oxide on the aluminium surface. Typical values for oxide thickness given by Kozma and Olefjord[133] lie between 4 and 5.5nm, depending upon which technique has been used to take the

measurements. If an average value of 5nm is used for the barrier oxide then it is reasonable to assume that the FPL oxide thickness is some three times this figure, i.e ≈15nm. The final figure is derived from the method for estimating oxide thickness by comparing oxygen peak heights in the microprobe. The data were in accord with measurements taken using the quantitative method described in section 6.2.2 which gave values for FPL oxide thickness of around 14nm. The figure is low compared with some published in the literature; for example, figures of 40nm are quoted by J. C. McMillan[134], Venables[73] and Bethune[69]. However these authors all use the same model and diagram, so it is reasonable to assume that they have all referred to the same published material. Kozma and Olefjord quote a spread of results for FPL oxide thicknesses and their figures vary between 5 and 60nm. Our value of 14.2nm measured by microprobe analysis falls well within this spread of results.

Errors in film thickness may be explained by reference to the topography developed by the FPL etch. Venables[73] propounded that oxide tendrils stretched some 40nm away from the substrate and this would account for their values of 40nm for the thickness of the FPL oxide. The small oxide protrusions and the gaps between them are much smaller than the x-ray generation volume induced in the specimen by the electron beam. The analysis technique used in the electron microprobe is not sensitive to these dimensions and would tend to see an "average" oxide which appears to be more uniform but not so thick.

Fractographic analysis of pure aluminium specimens that had been bonded with epoxy adhesive showed a smooth adherend surface after testing. Chemical analysis performed in the electron microprobe indicated a uniform distribution of remnant adhesive on the specimen surface, between 1 and 4μm thick, see section 6.4.1. The data suggested that the locus of failure was close to the substrate but within the adhesive itself. This deduction accords with the observations of Bascom[135] and also Gettings and Kinloch[60]. Workers examined the bonding of steel and aluminium with epoxy adhesives and in both cases affirmed that the locus of failure in the joint was just inside the adhesive. A thin

residual layer of epoxy material was left behind on the surface of the aluminium but we found no evidence for failure or weakness within the oxide film confirming that the FPL oxide is strongly adherent and readily aids wetted for adhesives.

The bond strength of FPL etched epoxy-bonded aluminium (1100) was 22MPa, see figure 29, which is a significant proportion of its yield strength (34MPa). The fact that samples of pure aluminium exhibited some degree of permanent deformation after testing therefore is not surprising given the low yield strength of the material. As a consequence bending induces peel stresses within an adhesively bonded joint which significantly lowers the measured shear strength of the system.

7.1.2 ARE 415

Alloy ARE 415 responded in a vigorous manner to the FPL treatment and exhibited significant removal of material and pitting within the grains. Deep etching was apparent around the grains, see figure 26, which indicates preferential chemical attack in the cored regions of the alloy. The effect is due to larger concentrations of alloying elements such as copper, zinc and silver in these areas, as shown in figure 7, which locally raise chemical activity. The small amounts of copper which are generally added to the FPL etch solution help to produce a uniform etch structure, as well as helping to speed up the etch process. The enhancing behaviour of copper in the FPL solution is discussed by Kozma and Olefjord[133] who state that additions of no more than $1.6x10^{-2}M$ of $CuSO_4$ can double the etch rate. It is possible that the higher concentrations of copper in the cored regions of the grains act in this way by locally speeding up the etching process. The evidence for pitting within the grains of the as-cast material can be explained by localised attack on either intermetallic phases or regions of micro-segregation. This is a reasonable assumption in an alloy with such a complex composition.

The significant removal of surface material by the FPL etch had a profound effect on the strength of the bonded joints. In all cases the strengths were lower than the unetched samples. It is our contention that the effect is associated with air being trapped within the

bond-line of an adhesive. This possibility was referred to by Huntsberger in his treatise on adhesion[54] where he proposed that recesses in a substrate would remain unfilled by the adhesive, and thereby reduce the area available for bonding. A method for observing the effect was suggested by Bascom and Cottington[136] which involved the bonding of a specimen to a glass slide, thus it was demonstrated in this programme that quantities of air are indeed trapped within the very rough surface of the specimens when the viscous epoxy is applied to the etched adherend. Furthermore, when the epoxy was cured at a relatively high temperature the trapped air expanded and outgassed into the adhesive. With the commencement of curing the bubbles and trails left by the escaping gas were preserved as a network of connected porosity, see figure 36. The porosity not only reduced the effective bonded area but also acted as a series of ready-made cracks. Clearly, it follows that the strength of these epoxy joints would be improved if the problem of trapped air were reduced or eliminated. There are a number of ways to do this. Firstly, the joints could be preheated at an intermediate temperature to encourage outgassing whilst the epoxy is in a mobile state before curing. Secondly, and perhaps more practically, a priming system could be used. Ideally this would take the form of an epoxy monomer that would be chemically compatible with the adhesive and would be mobile enough to fill in all of the roughened metal surface. The priming monomer could then combine with the adhesive during the curing process.

The broken test specimens all left a remnant of epoxy adhesive on the adherend substrate and there was no evidence for failure of the joints within the oxide film. This observation indicated that the FPL etch was still performing in the correct manner although the benefits of the enhanced oxide were being undermined by the formation of a porous adhesive joint as a result of outgassing from the deeply etched sample surfaces.

Samples of FPL-etched 415 alloy demonstrate significant differences in bond strengths depending upon the metallurgical condition of the alloy. The strength was highest for as-cast metal and lowest for solution treated material with an intermediate value for alloy in the peak aged condition. The as-cast material would probably be in a condition

resembling that of partially heat treated alloy, with some coarse precipitation at the grain boundaries and perhaps some finer precipitates within the grains themselves. In this case the yield strength of as-cast material is higher than the solution treated which would explain the higher bond strengths of the former. Although 415 is a casting alloy its properties are similar to the heat treatable wrought alloy 2024, which has high strength in the fully heat treated condition (≈420MPa) but a low strength in the solution treated condition (≈120MPa). Therefore the drop in bond strength for the solution treated samples, 23MPa compared with 31MPa (as-cast), could be explained by the fact that the material has been homogenised by the heat treatment and its yield strength has been reduced as a consequence. In practice this could mean that the slightly softer material could bend during the test and hence induce some peel forces into the joint. Based upon the assumption that the properties of 415 alloy are similar to a wrought 2024 alloy, its yield strength would increase to approximately 320MPa in the naturally aged condition (T4) and further still to around 420MPa in the artificially aged condition (T6)[137]. It is therefore concluded that the rise in bond strength from solution treated to peak aged condition is due to the higher yield strength of aged material, rendering the material less susceptible to bending during mechanical testing.

7.1.3 A357

As-cast A357 alloy also produced a heavily etched structure after FPL treatment. The regions most heavily attacked were the colonies of eutectic where the aluminium offers preferred sites for chemical attack. The alloy formulation of A357 includes 0.5% (total) of magnesium and iron and the small etch pits present within the aluminium-rich grains may be related to these alloying additions as inclusions and intermetallic particles formed from these elements.

The solution treatment appeared to spherodise slightly the silicon particles and this change in geometry could have affected the surface energy exhibited by the particles, explaining the slight reduction in FPL etch damage. The aluminium grains do not show much

evidence for pitting which may be explained by the removal of alloying additions into solution. The A357 alloy includes a small addition of magnesium in order to promote a moderate ageing response by inducing the formation of Mg_2Si. However, the relatively small ageing response observed in A357 (from $70H_v$ to $100H_v$) does not imply a great change in microstructure and this is borne out by the similar response of aged material to the FPL solution as that noted in the solution treated condition.

The aggressive effect of the FPL etch on A357 alloy produced a unilateral reduction in bond strengths in a manner comparable with the 415 alloy. Outgassing of entrapped air at the bond-line again was in evidence and explains the reduction in bond strength in the same manner as previously described. The effect of metallurgical condition was slightly different to that found with the 415 alloy. The yield strengths of as-cast and solution treated metal are quite similar (approximately 200MPa) and therefore the bond strengths would be expected to be similar in the as-cast and solution treated condition. However, the lower bond strengths recorded with the as-cast material may be due to the effect of bond-line outgassing arising after FPL etching, the less heavily etched samples in the solution treated and aged condition resulting in a reduction in air entrapment. The high bond strengths reached by solution treated A357 (around 42MPa) appears to be surprising when compared with the solution-treated 415 alloy which showed a decrease in bond strength (23MPa). The reason for this behaviour can be explained by the nature of the silicon eutectic in A357 which is in the form of interconnected silicon colonies[138]. This silicon structure can support a load and enable the soft aluminium grains to resist deformation. In this way the possibility of samples bending during testing is reduced.

In data relating to epoxy adhesives presented by Nickolson[139] epoxy bond strengths in the range of 20MPa were given for aluminium and carbon composite specimens bonded with an unmodified epoxy resin. The addition of fillers and toughеners to the resin were found to increase the bond strengths to 41MPa, Nickolson stating that bonded aluminium samples had similar strengths to these composite materials. The highest bond strengths reached by epoxy bonded samples in the present programme was 42MPa. This was for

unetched, solution treated A357 alloys and obviously compares favourably with the data presented by Nickolson.

7.1.4 Acrylic Adhesive

All specimens bonded with acrylic adhesives demonstrated lower bond strengths compared with epoxy adhesives. Unlike epoxies, however, the locus of failure was more variable and mixed mode failures were common. The phenomena are shown in figure 46a where shearing of the acrylic adhesive is combined with a large area of interfacial failure to leave bare the surface of the aluminium adherend. This implies that the acrylic adhesives are failing both cohesively and adhesively, i.e within the adhesive and also at the adhesive/metal interface. The fractographic results show a measure of cohesive failure and the tabulated shear results indicate a lower bond strength which would point to the fact that the acrylic is a less strong polymer under these conditions. Also, the degree of interfacial failure suggests that the acrylic is less able to wet the FPL oxide effectively. No evidence was however found for failure within the FPL oxide which, once more, indicated that the etch produced a strongly adherent film that was resistant to fracture.

It was noticeable that heavily etched areas of the alloy specimens were much more successfully penetrated by the acrylic compared with the epoxy due to its lower viscosity and the longer time (24 hours) before the adhesive hardens and cures, which allows trapped gas to escape. Fractography showed that, in general, the aluminium grains were stripped of adhesive whilst significant quantities of acrylic remained within the etched areas. Thus the penetrating action of the adhesive enhances the strength of the bond by conferring a degree of mechanical interlocking after adhesive cure. Particular references to this type of strengthening have been made by Gent and Lin[140], Evans and Packham[44] and Jennings[51]. The strength of a mechanically interlocked bond is generally due to the work required to break the embedded strands of adhesive. In the present samples the benefits of mechanical interlocking were offset to a certain extent by the interfacial failure of the adhesive in areas where penetration had not occurred.

The metallurgical condition of the 415 and 357 alloy specimens had an effect on the bond strength of the acrylic joint in the same way as the epoxy joint. Although the strengths were lower than the epoxy joints, it can be argued that specimens experienced some measure of bending during testing which induced peel forces and lowered bond strength. Indeed, some specimen deformation was visible during bond testing although it did not always result in permanent deformation of the specimen after testing.

The highest mean value for shear strength with an acrylic adhesive was found to be 21MPa for as-cast 415 alloy, which compares well with those observed by Arrowsmith and Moth[49] on Al-Mg alloys using acrylic adhesives. These authors quote lap shear strengths of 14-22MPa depending on the surface pretreatment, values comparable with those found in the present programme.

7.1.5 Composite Material

The FPL etch had a significant effect on the surface of composite material when compared to conventional grinding methods. A 600 grit finish exposed the fibre reinforcement in various places but left discernible evidence of the presence of matrix alloy. FPL etching apparently removed all traces of alloy at the surface of the composite leaving behind a layer of fibres denuded of matrix material. In both of these cases the roughened appearance of the composite surface appeared to favour good keying for the adhesive, interfacial failures may not have been expected if the adhesive was strongly bonded to the composite surface.

During testing, however, all specimens failed within the composite material itself and not within the joint. Examination of the fracture surfaces revealed two types of failure that occurred either separately or together. The first failure involved the formation of a crack at the edge of the sample overlaps which propagated through the specimen thickness. This type of failure has been described previously by Matthews, for example, in single-lap shear joints[141], in all-metal specimens failure can occur by the formation and subsequent deformation of plastic hinges at these positions. In the case of the composite material it is

suggested that matrix alloy may have been deformed during the test but the stiff fibres cracked because they were unable to accommodate the strains experienced during loading. Support for this explanation is given by the fact that stress concentrations are known to occur at these positions in a single-lap shear test. The effect of these stress concentrations would be to magnify the load experienced by the fibre bundles thus leading to fibre cracking, this in turn would produce a concentration of load on a smaller sample cross-section and so on. The adverse effect of stress concentrations can be reduced somewhat by machining either a scarfe or a reverse taper onto the ends of the overlap, together with the construction of an adequate adhesive spew fillet.

The second type of failure was basically of the interlaminar-type. This failure starts with the formation of a small crack at the overlap edges in much the same way as has just been described. Such a crack then finds a convenient low energy path in which to propagate, usually at right angles in a subcutaneous fashion along the fibre lengths. Failure in this manner can be explained by the poor infiltration of matrix alloy into the reinforcement during composite manufacture. A badly infiltrated 0/90° composite has many hundreds of pre-existing longitudinal "cracks" where fibre bundles are relatively free of matrix material. The effect of this type of failure would be to lift off a surface layer of composite which then remains adhered to one side of the joint, this is indeed what happened and figure 49 shows an entire overlap which has had this layer of material lifted off revealing the fibrous reinforcement beneath. This is a fairly typical type of failure for composite material during single-lap shear testing and is in agreement with observations noted by Hart-Smith in Matthews' book "Joining Fibre-Reinforced Plastics"[142].

Some feel for the mechanical properties of the composite material may be obtained from the mechanical tests. Samples that failed solely by through-section cracking could be considered to be tensile-type failures. Typical loads at failure were 3000N across a sectional area of 60mm^2 (20x3mm) giving a strength of around 50MPa. This result is not fully representative because of the geometry of the lap-shear specimens and of course the presence of any stress concentrations, however the result is well below that expected

for the tensile strength of these composite materials. Similarly, a measure of the interlaminar shear strength may be derived for samples that failed solely in this way. Loads at failure were typically 2500N over a bonded area of 200mm^2 (20x10mm) which gives an interlaminar shear strength of 12.5MPa. It is suggested that the major contributory reason for the apparently low mechanical properties is failure to manufacture high quality, well infiltrated metal matrix composites.

It was therefore difficult to divine the effect of the FPL etch on lap-shear strength because both etched and unetched specimens failed within the composite material and not at, or within, the adhesive joint. Under these circumstances the adhesive bond was apparently stronger than the material it was joining and the test provided more information relating to the integrity of the material rather than the effectiveness of the surface treatments.

8. RESULTS - DIFFUSION BONDING

8.1 MODEL DIFFUSION BONDING EXPERIMENTS

Specimens were prepared using standard metallographic methods, finishing with 600-grit silicon carbide paper. The samples were then degreased and ultrasonically cleaned before bonding. The micrographs were all taken in the SEM using backscattered electrons to give better atomic number contrast.

8.1.1 Aluminium + Copper

The specimens were bonded using the apparatus described in the Experimental section at temperatures close to the eutectic for aluminium and copper i.e 548°C. A strain of 10% was applied and the specimens were removed after 30 minutes.

The structures obtained from this experiment are shown in figure 50a) and b). The reaction layer formed is roughly 300μm wide and has cracked during cooling. Small "teeth", approximately 10μm in size, are visible on the copper side of the reaction layer.

Figure 51 shows a higher magnification view of the copper side of the reaction layer. A thin reaction layer is visible together with the globular features. Energy dispersive (EDS) x-ray analysis was performed on the structures visible in this micrograph to determine their chemical composition. The x-ray data for the thin reaction band marked "A" is shown in figure 52 showing $62\%_{at}$ copper and $37\%_{at}$ aluminium. Analysis of the globular products, marked "B" is given in figure 53 and has the composition $31\%_{at}$ copper and $68\%_{at}$ aluminium.

Figure 54 is a view of this eutectic colony taken at the aluminium side of the reaction layer. The $CuAl_2$ + aluminium eutectic can be seen to be growing along a planar front.

Figure 55 shows five spot analyses taken at incremental steps away from this planar front and into the aluminium. The purpose was to determine how far the copper had diffused

into the aluminium. The first value, taken close to the reaction front indicates some 5.5%$_{at}$ copper in solution. The amount of copper in solution decreases away from the reaction front, the final value is 0.177%$_{at}$ copper some 20μm into the pure aluminium.

8.1.2 A357 Alloy + Pure Copper

The next experiment was performed at 525°C between a sample of pure copper and a sample of Al-Si alloy. A strain of 10% was applied but the associated stress relaxed almost totally after only a minute or so, indicating the presence of a liquid phase, see figure 56a). The micrograph in figure 56b) shows the presence of intruding structures along the copper interface. The microstructure away from the interface and into the aluminium alloy is quite complex, showing evidence of at least two phases.

Figure 57 is a higher magnification of the interface structure. Once again there appears to be an intermediate reaction band formed between the copper and the globular phase. ED analysis of this reaction layer, marked "A", is given in figure 58 and appears to be the same as that in the previous experiment, i.e the δ phase with 61%$_{at}$ copper and 38%$_{at}$ aluminium.

Analysis of the globular phase marked "B" is shown in figure 59 and indicates the presence of $CuAl_2$. The other, smaller, grey phase has the same composition.

Figure 60 shows the ED data from the dark phase and indicates the presence of primary aluminium with some copper in solution (approx 2.5%$_{at}$). The data also shows the presence of some silicon.

This ternary eutectic mixture consisted of aluminium, silicon and $CuAl_2$ and extended some distance into the aluminium alloy sample (0.5cm) indicating massive reaction. Micrographs were therefore taken at the outer limits of this reaction front. Figure 61a is an optical micrograph, and figure 61b is a backscattered SEM micrograph of this reaction zone.

8.2 DIFFUSION BONDING WITH COPPER FOILS

On the basis of the model experiments some work was carried out bonding A357 alloy with copper foils. In these cases there is not an infinite supply of copper, instead a thin 20μm foil is used. Two cases are possible for this combination of materials, one below the ternary eutectic temperature of 525°C where reactions occur in the solid state; and one above the ternary temperature where liquid reactions occur.

8.2.1 Solid State Reaction

Samples of the alloy A357 were bonded at 510°C for 30 minutes and an applied strain of 10%. An optical micrograph of the bond-line is shown in figure 62. A number of layers, symmetric to a central band are visible. The central band is unreacted pure copper (i.e foil remnant) which appears a characteristic burnished colour under the microscope.

ED analysis of the two other layers are shown in figure 63 and figure 64. These data reveal that the band marked "A" has the composition 56%$_{at}$ copper and 43%$_{at}$ aluminium. The outer band marked "B" has the composition 36%$_{at}$ copper and 63%$_{at}$ aluminium, which is tolerably close to the $CuAl_2$ intermetallic compound found already.

a) Effect of Bonding Time

Samples of A357 alloy were then bonded under identical conditions for 60 minutes instead of 30 minutes at 510°C. An optical micrograph of the bond-line is shown in figure 65. The copper foil remnant has been consumed leaving behind a duplex type of band.

ED analysis revealed that the composition of these layers was the same as the previous specimen bonded for 30 minutes. In other words the inner layer had the composition 56%$_{at}$ copper and 43%$_{at}$ aluminium, whilst the outer layers had the composition 36%$_{at}$ copper and 63%$_{at}$ aluminium. Thermal stresses induced during cooling have cracked the interface, the crack has been limited to the 56%$_{at}$ copper + 43%$_{at}$ aluminium layer.

b) Effect of Imposed Strain

In order to investigate the effect of loading conditions for these samples, the amount of applied strain was altered for specimens bonded at the same temperature of 510°C. The results are shown in the macro photographs in figure 66.

The top photograph shows a sample bonded with 5% applied strain. The bond area is clearly visible, its brightness implying a crystalline fracture surface. The bottom macro shows a sample bonded at 10% applied strain and indicates a significantly larger bonded area. Unused copper foil remnants are visible around the edges of both specimens.

8.2.2 Liquid State Reaction

The next option for diffusion bonding with copper foils is to induce a liquid phase at the interface. In order to obtain this liquid the bonding temperature needed to be taken above the ternary eutectic temperature of 525°C for aluminium, silicon and copper.

The two optical micrographs in figure 67 show a sample bonded using a liquid phase at the interface. The top micrograph indicates that the bond-line is less visible but a curious structure has formed at the edge of the specimen. The lower photograph is a higher magnification of this structure showing not only remnant foils but also large grey silicon particles and the ternary eutectic microstructure typical of this liquid system.

The optical micrographs in figure 68a) and 68b) demonstrate the two types of morphology present along the interface. The first micrograph indicates that there has been some coarsening of the silicon in the vicinity of the bond-line. The second micrograph (at x1000 magnification) shows that there is some evidence of attempted grain growth across the interface. However small pockets of debris seem to be trapped at the bond-line.

Figure 69 is an ED trace of an aluminium grain present at the bond-line after the ternary liquid has formed and been removed from the interface. The data shows that some silicon is present, either in solid solution in the aluminium, or existing as very small discrete

particles. The ED traces also show that there is a significant amount of copper present in solution in the aluminium ($\approx 2.8\%_{at}$).

Figure 70 is a schematic representation of how a liquid phase could be formed at the interface and then removed to another part of the specimen.

Figure 71a) and 71b) demonstrate this observation in practice. The upper macro shows a liquid phase formed at the bond-line of a sample bonded at 525°C with a 20μm copper foil. The small bead in the same photograph shows, for reference, a bead of ternary material that has been ejected completely from the bond-line. The lower optical micrograph at x50 magnification shows a cross section of just such a eutectic bead *in situ*.

Figure 72a) and 72b) are backscattered SEM images showing the type of microstructures typical in this Al-Si-Cu liquid phase. Figure 73a), b) and c) show this structure in more detail. The top micrograph is another backscattered image which has had the contrast adjusted in order to attempt to image the details that are just visible within the grey phase. ED analyses were performed on the white phase marked "A" and the grey phase marked "B". The ED spectra in figure 74 and figure 75 indicate that the white phase is $CuAl_2$ and the grey phase is aluminium with some $2.8\%_{at}$ copper and $0.73\%_{at}$ silicon.

An x-ray map for silicon has been constructed in figure 73b). It is apparent that the fine lathe-like structures in the top image are probably primary silicon, sub-micron in width.

The bottom micrograph shown in figure 73c) is a composite double-exposure of the previous two images, superimposed over each other and exposed at the same time. The technique shows that the ternary eutectic mixture comprises of aluminium rich grains, $CuAl_2$ particles and discrete silicon.

8.3 DIFFUSION BONDING WITH SILVER FOILS

The format of the work with silver foils followed the same format as that of the copper foils, i.e solid and liquid state bonding.

8.3.1 Solid State Reaction

Samples of Al-Si alloy were bonded at around 540°C under an applied strain of 10%. The backscattered images in figure 76a) and b) show the microstructures resulting from this process. The position of the original foil is visible, as are the dark images of the silicon eutectic colonies in the A357 alloy. There is a slightly bright aura on either side of the foil which could indicate the presence of a heavy element in solid solution in the aluminium alloy. The higher magnification image in figure 76b) shows that silver has diffused from the parent foil into the aluminium matrix. The small white particles denote silver-containing areas around the silicon particles.

ED analysis of the foil in figure 77 shows that it has been converted to the intermetallic Ag_2Al in a manner analogous to the consumption of a copper foil to form $CuAl_2$. The dark phase occurring at intervals along the matrix/foil interface has a complex composition shown in figure 78.

8.3.2 Liquid State Reaction

Raising the bonding temperature takes the conditions towards those that favour the formation of a liquid mixture. This is confirmed by the results shown in figure 79a) and 79b) where the sample was bonded at 560°C. The remnant silver foil has disappeared leaving aluminium grains in contact with each other. The white phase in the backscattered image is silver-rich. The micrograph in figure 79b) is a higher magnification view showing the transport of liquid product around the silicon particles.

Figure 80 is a macro view taken in the SEM using backscattered electrons. This image shows the final position of the liquid phase. Bright areas occur along the bond-line and

within the regions of porosity. Surface diffusion can be seen up the outside edges of the sample.

A bead of liquid material was formed when using silver foils in the same manner as that formed with copper foils. A bead was taken, mounted and placed in the microprobe for x-ray chemical analysis. Figure 81a) and b) show microstructures typical of those obtained for this expelled liquid bead. The structures are quite complex, exhibiting dendritic formations and particles in a range of sizes and compositions.

A higher magnification image is shown in figure 82. Some of the white phases (marked "A") have been analysed and the ED spectra is shown in figure 83. The data implies that this phase is in fact the intermetallic Ag_2Al.

A backscattered micrograph of one of the large grains is shown in figure 84. A Widmanstätten structure is visible at the periphery of the grains. X-ray analysis was performed at positions in the centre of the grains where no Widmanstätten was present. The results are given in figure 85. From this data the grains seem to be mainly aluminium with a high degree of silver in solid solution ($\approx 19\%_{at}$).

Angular precipitates were visible at various places in the expelled bead. An example of one of these precipitates is shown in figure 86. Its dark colour in the backscattered image implies that it is comprised of a an element with a low atomic number. ED analysis of this phase in figure 87 indicates that the precipitate is primary silicon.

8.4 DIFFUSION BONDING COMPOSITE SPECIMENS

The transverse microstructure of the composites used in this study is shown in figure 88a) and b). The higher magnification optical micrograph shows a relatively good distribution of fibres with small regions of poor infiltration, notably in areas where fibres touch and the melt has not been able to penetrate.

However, the lower magnification micrograph shows the essentially heterogeneous distribution of reinforcement within the matrix. Portions of the fibre bundles are visible, separated by regions of matrix material. The dark coloured fibres with the elliptical sections are glass wefts used to bind the fibre bundles together.

The morphology of the alloying silicon is different to that in the conventionally cast 345 alloy. The primary silicon has become needle-like instead of the slightly more spheroidal morphology usually expected in this alloy.

The longitudinal sections of the composites are shown in figure 89. In the lower magnification micrograph small regions of poor infiltration are visible. The higher magnification micrograph shows a region of good infiltration with just one or two visible pores.

Two combinations of bonding geometry are possible when joining metal matrix composites, matching transverse sections and matching longitudinal sections. These are shown schematically in figure 90.

8.4.1 Transverse Sections

Transverse composite sections were joined under conditions similar to those for unreinforced materials, i.e at 525°C with a 20mm Cu foil. The resultant microstructures are shown in figure 91a) and b). The higher magnification optical micrograph shows a complex banded structure formed at the interface between the specimens. The three layers are marked A, B and C respectively. EDS analysis of these layers are detailed in figure 92-94. The first analysis in figure 92 shows that band A is metallic copper. Band B has the composition 62%$_{at}$ copper and 32%$_{at}$ aluminium, this δ phase has been found previously in unreinforced samples bonded with copper foils. The composition analysis of layer C is shown in figure 94 and is $CuAl_2$.

The lower magnification micrograph in figure 91 shows a long stretch of the bond-line and indicates the fairly uniform, continuous nature of the interface reaction band. This

photograph shows an interesting phenomena marked with the arrows on the left of the figure. In this position the intermetallic band has grown into the regions of matrix alloy between the fibres.

The bonding conditions of the transverse section metal matrix composites were changed in order to reduce the possibility of producing a brittle intermetallic structure. A combination of foils was used, 20μm copper sandwiched by two 20μm aluminium foils. The temperature was increased to 550°C to ensure foil liquation.

The results of this are shown in figure 95a) and b). The higher magnification backscattered SEM image shows that the interface has indeed been altered, with evidence of the metal filling the bond-line. The white phases were identified as $CuAl_2$ except for the angular precipitate marked "A". The ED spectra and composition of this phase is shown in figure 96. The compositional data points to the formation of a complex iron- and chromium-containing intermetallic. Some fibre damage is also evident in the backscattered micrograph.

The extent of the fibre damage at the interface is shown in figure 95b). At every point along the bond-line there are broken fibres which indicate that the strain sustained by the specimen should be reduced. In addition to this observation it is worth noting that there is also a complete absence of interfacial bond-metal. This is surprising as the two micrographs shown in this figure were taken from the same specimen and demonstrates the inconsistent nature of the bonding process.

8.4.2 Longitudinal Sections

The second possible bonding geometry is shown in figure 97a) and b). These longitudinal specimens were joined under the same conditions as the previous transverse specimens, i.e Al/Cu/Al foil combination at a temperature of 550°C. The difference between this sample and the transverse section is immediately apparent. The bond-line has been arrowed and is less discernible, the backscattered information indicates a white

phase distributed around many of the fibres near the bond-line. Figure 97b) is also a backscattered micrograph and shows in more detail the white phase and its distribution. A higher magnification micrograph of this is shown in figure 98 and shows that the white phase occurs to a certain extent around all of the fibres in the field of view. ED analysis of the white phase was performed at the position marked "A". The spectrum and chemical data are shown in figure 99. The white phase is most likely to be $CuAl_2$, this information together with the distribution of the $CuAl_2$ around many fibres indicates the formation of the binary Al/Cu eutectic in these areas.

The longitudinally bonded specimens also demonstrated bond-line regions with differing microstructures. Figure 100 shows two optical micrographs of a different position along the same bond-line. The lower magnification micrograph provides striking evidence for the production of a liquid phase at the interface. This phase has formed at the bond-line and has then found a route penetrating the region between two fibre tows. The higher magnification micrograph shows the morphology of the liquid phase and is typical of the $CuAl_2$ eutectic.

Figure 101a) and b) show two macro-views of fractured composites that have been bonded longitudinally. Large regions of the fracture surfaces show unreacted fibres, this bright phase is $CuAl_2$ that has formed in areas associated with matrix metal in the composite.

The damage sustained by a longitudinally oriented composite bonded with 10% applied strain is shown in figure 102. Fairly significant cracking is evident within the specimen.

8.5 LOAD VERSUS TIME CHARACTERISTICS DURING BONDING

Load profiles were recorded during each bonding run to determine whether any information could be gathered that related to processes occurring at the bond-line. Typical examples of these profiles are shown in figure 103. The vertical red line running down

through each curve indicates the position at which the load cycle was completed (2.5% strain per minute was the slowest cross-head movement possible on the Instron).

All specimens exhibit some degree of relaxation after the load has been applied. The oscillatory nature of the latter half of curves 103a) and b) indicates the sensitivity of the load cell to the thermostatic switching of the furnace working to maintain a constant temperature.

8.5.1 Alloy Specimens

Figure 103a) concerns the load profiles for samples of alloy A357 and pure aluminium bonded at 510°C with a 20μm copper foil. The two curves follow the same basic shape with the notable exception of the peak load sustained by the material. The alloy A357 reached a load of ≈10MPa at 10% strain whilst the lower modulus pure aluminium reached ≈4.5MPa at 10% strain. Load relaxation follows the peak in both cases, reaching a level of roughly half the peak height by the time the bonding process was finished.

Samples of A357 alloy bonded at 525°C with a 20mm copper foil exhibit the loading profile shown in figure 103b). The shape of the curve is generally similar to that of the samples of A357 alloy bonded at 510°C except that the peak load attained was slightly lower at 8.9MPa. Relaxation and thermal cycling are both evident in the latter part of the load curve. The biggest difference between the profiles lies in the first part of the curve where a dip is apparent. This dip appeared on all such specimens bonded at 525°C and also for samples of A357 alloy bonded with silver foils at 560°C. For alloy samples bonded with copper foils at 525°C the dip appeared at a load of about 5.5MPa roughly 1 minute after the initiation of loading.

8.5.2 Composite Specimens

Figure 103c) shows that large differences are visible in the load curves produced when bonding composites specimens under similar conditions. Both longitudinal and transversely bonded samples exhibit a linear rise in load up to the point where the

maximum strain has been applied (10%). The transversely bonded samples reach a peak load of ≈44MPa whilst the longitudinal specimens reach a peak load of ≈17MPa. After this the transverse specimens relax in a linear fashion to a point not far below the peak load. The longitudinally bonded specimens relax to a level of about half the peak load but not in a linear manner. Neither composite samples show sensitivity to thermal fluctuations within the furnace during bonding.

8.6 SINGLE LAP SHEAR TESTING

Alloy samples were diffusion bonded and tested using a single-lap shear jig. The values of load at failure were recorded and converted to a stress by dividing by the bond area ($10x5mm^2$). The results are given in figure 104. This figure shows samples of A357 alloy bonded with both 20 and 10μm copper foils at 510 and 525°C. In addition some results are presented for pure aluminium bonded at 560°C just above the eutectic temperature.

Students t-tests were performed on the data in a similar manner to the adhesive bond results and these tests are given in figure 105.

8.6.1 A357 Alloy + 20μm Copper Foils

Specimens with 20mm copper foils were bonded in the solid and liquid states, i.e at 510 and 525°C. The results in figure 104 indicate that the average load at failure for 510°C is 1558N (31MPa) with a standard deviation of 334N. The samples bonded at 525°C sustained an average load at failure of 2372N (47MPa) with a deviation of 437N.

The standard deviations of these results represent some 18% and 21% of the average values for 510 and 525°C respectively.

These results are obviously quite different and this is supported by the t-test which affirmed that the mean values only had a 1% probability of originating from the same sample set. This t-test is shown in figure 105a).

8.6.2 A357 Alloy + 10μm Copper Foils

As in the previous section, samples were bonded at 510 and 525°C with 10μm copper foils. The specimens diffusion bonded at 510°C had an average load at failure of 785N (15MPa) with a standard deviation of 214N. Samples bonded at 525°C showed a higher load at failure of 1005N (20MPa) with a standard deviation of 236N.

The standard deviations for 10μm copper foils were higher than for 20μm copper foils. At 510°C the deviation represented some 27% of the mean value whist for samples bonded at 525°C the deviation was 23% of the mean.

The t-test confirmed that the sample sets of 10μm copper foils at 510 and 525°C were indeed different, the probability was 28% that the results came from the same distribution (i.e 72% probability of the results being significantly different). This t-test is shown in figure 105b).

8.6.3 Pure Aluminium + 10μm Copper Foils

The pure aluminium samples showed low bond strengths with the average load at failure only 563N (11MPa). The standard deviation was 284N and this is some 50% of the mean value.

The effect of foil thickness on bond strength was investigated in a final pair of t-tests performed for samples bonded at the same temperature but with different thicknesses of copper foils. Data was taken from the results tables in figure 104 and the t-test results are shown in figure 105c) and d). The results of the t-tests show that at both 510 and 525°C there is a significant reduction in bond strength when using a thinner (10μm) copper foil

8.6.4 Shear Test Profiles

Four of the test results in figure 104 have been marked with an asterisk. The load versus time curves of these samples were recorded during shear testing and are shown in figure 106 and 107. The highest strength sample in figure 106 demonstrates a smooth increase

in load up to the point of fracture. All of the other samples show some degree of stepwise fracture which indicates cracking in the sample before final fracture.

9. DISCUSSION - DIFFUSION BONDING

9.1 DIFFUSION BONDING A357 ALLOY USING COPPER FOILS

Extensive reaction took place at the interface when specimens of A357 were bonded in the solid state at 510°C and 5% strain with copper foils. Figures 62 and 65 show that continuous bands of intermetallic compounds have formed, consistent with a significant amount of diffusion having taken place. It follows that the barrier-like qualities of aluminium oxide must have been overcome for these reactions to take place and this is most likely to have been achieved by mechanical damage during bonding. Asperities originating from surface preparation were pressed together during loading which subsequently suffered severe plastic shearing. The shearing action broke up the aluminium oxide and led to intimate contact between areas of fresh metal. Once contact was made on an atomic scale, the high temperatures in the furnace encouraged diffusion and then chemical reaction between the copper and the aluminium. This explanation of the mechanisms occurring during these experiments is supported by the observation that an increase in applied load during bonding (from 5% to 10% strain) resulted in a significant increase in bonded area, see figure 66, the bonded area almost doubling under these circumstances. In addition, the edges of the sample which experienced a lower load showed evidence of completely unreacted copper, implying that in these areas there had not been an effective breakup of the barrier oxide. The explanation of oxide breakup promoting diffusion is supported by Derby[92] who ascribed effective diffusion to just such a mechanism.

Electron-probe microanalysis of the intermetallic phases formed in these samples (figures 63 and 64) revealed the central phase as ζ_2 (56.5%$_{at}$ copper, 43.5%$_{at}$ aluminium) surrounded by $CuAl_2$ (θ phase, 36%$_{at}$ copper, 64%$_{at}$ aluminium). The thin remnant of pure copper at the centre of the bond-line was consumed when exposed to the bonding conditions for a longer period of time. Reference to the phase diagram in figure 108 confirms the likelihood of these intermetallics forming at the bond-line and under

equilibrium conditions it would be reasonable to assume that these phases occur in the order γ_2, δ, ζ_2, η_2 and θ, with the most copper-rich compound forming nearest to the source of copper atoms, i.e the foil in this case. The η_2 phase (CuAl), forming between the ζ_2 and θ phases, was not apparent using the analytical methods in this programme. This does not preclude its existence as the phase may reside in the form of a very thin layer, much smaller than the excitation volume generated by an electron beam in a substrate. The copper-rich phases, γ_2 and δ, were not identified in foil-bonded samples of A357, probably for the same reason. However, the δ phase was present as a thin reaction layer in samples of both pure aluminium and A357 bonded to a block of pure copper, figures 57 and 58. The presence of the more copper-rich phases could be ascribed to the plentiful supply of copper atoms from a large block of pure metal (acting as an "infinite" source) compared with a thin foil insert. Similar phases have been identified by Calvo[104] when diffusion bonding pure copper and aluminium in the solid state, although the intermetallics took the form of small nuclei growing in isolated positions where local disruption of the aluminium oxide had occurred. In Calvo's study, the samples were bonded at around 1.9MPa pressure and it is apparent that the continuous banding produced in this thesis can be explained by the higher bonding pressures (8MPa) causing increased oxide disruption along the bond-line and therefore increased metal-to-metal contact.

Samples of A357 alloy bonded at 510°C in the solid state with copper foils showed lower bond strengths than those bonded at 525°C in the liquid state. A maximum shear strength for A357 joined with a 20μm copper foil in the solid state was 31MPa. The macro photographs in figure 66 show the effect of applied load on effective bonded area also indicate the locus of failure during shear testing. In each case, the samples bonded in the solid state fractured through the intermetallic reaction band formed at the bond-line. This observation confirms the view that the intermetallic structures which are formed are brittle. Evidence of cracks formed as a result of thermal stressing during cooling is given in figure 65, in this case the crack is confined to the central ζ_2 phase which indicates that this phase is the most brittle of those formed. Cracks may possibly exist before

mechanical testing which would explain the lower strengths measured in these specimens. It may be feasible to consider this type of bonded specimen as a metal/ceramic joint on account of the formation of brittle intermetallic compounds. Nicholas and Crispin[111] have noted tensile strengths of 50MPa for alumina samples bonded with copper foils and if the assumption is made that shear strength is approximately half of the tensile strength then Nicholas' data would be consistent with a shear strength of some 25MPa. It may therefore be argued that the bond strengths measured in the present work of 15-31MPa compare favourably with those of Nicholas.

If the bonding temperature is raised to 525°C then a completely different mechanism appears to dominate the joining process. At these temperatures a liquid phase is formed which is then ejected from the bond-line, see figure 71. The formation, followed by ejection, of a molten phase indicates rapid liquation of the copper foil at the bond-line. This liquation can only occur if there is sufficient diffusion of the copper into the alloy substrate which confirms that the barrier oxide has been successfully disrupted by the action of the applied load during bonding. Evidence for instantaneous liquation is provided by the sudden relaxation in applied load in the load vs. time curve in figure 103b. The momentary dip after approximately 1 minute and a load of 800lbs (5.5MPa) occurred reproducibly each time a specimen was bonded under these conditions and gives an indication of; a) the load levels required to cause oxide break-up to facilitate diffusion of the foil into the alloy surfaces; b) the time it takes for diffusion to occur to form a liquid phase.

The microstructure of the ejected material in figure 72 is further indication of the formation of a molten phase. Its presence can be explained by reference to the aluminium/silicon/copper phase diagram, e.g Mondolfo[143], showing that a ternary eutectic mixture of aluminium, silicon and $CuAl_2$ is formed at 525°C. Analysis of the ejected material (figures 73-75) confirmed that this ternary mixture was indeed formed. Support for these observations were noted in the work of Abbott and Parker[144] and also in an early publication by Gwyer and Phillips[145], both groups of which identify the

ternary eutectic mixture as having a similar microstructure to that noted in this programme. The reaction mechanism was duplicated in an experiment where A357 was bonded to pure copper and the same phases were formed, figures 56-61. It appears that the mechanism involved the migration of copper around the surfaces of the silicon eutectic in the A357 alloy, the particles providing regions where surface diffusion is rapid. Once the copper concentration was high enough the low melting point ternary mixture formed and was ejected as a liquid from the bond-line under the influence of the applied load. No large intermetallics were found of the type identified in the solid state bonding. It may be expected that the barrier oxide, which must have been broken up for the liquid to have formed, was flushed out with the ejected material. Little published work is available describing this type of bonding, most authors have studied solid state bonding or limited their comments on liquid phase bonding to superficial mechanistic considerations. However, Iino[122] mentions the ejection of a liquid metal phase when bonding ceramic materials with metal foils and ascribes better bonding to the increased contact area which follows the formation of a liquid and its subsequent removal from the interface by the bonding load.

The samples exhibiting this type of behaviour displayed higher bond strengths than those joined in the solid state, the highest being 46MPa. Also, it was noted that strengths were higher for 20μm foils compared with 10μm foils. The strengths are comparable with those quoted by Zhang[120] who noted tensile strengths of 100MPa for aluminium joined to titanium via a liquid phase technique; these tensile results approximate to shear strengths of around 50MPa. Partridge[83] shows higher shear strengths for diffusion bonded aluminium (90MPa), using alloys clad with pure aluminium, plated with silver and joined in an inert gas environment. The shear strength of A357 base material is approximately 100MPa which is just over double the shear strengths attained by bonded specimens in the current programme. The fact that the bond strengths are lower than the parent metal indicates that the failure mechanism is dominated not by base metal properties but probably by an artefact induced by the joining process. Specimens fractured at the bond-line in all cases with no major evidence of ductile shearing which

would otherwise indicate grain growth and hence a fully developed interface, figure 109. Fracture along the bond-line can be explained in two ways. Firstly, remnants of copper foils were evident at the edges of the specimen, figure 67, which were a black colour consistent with the presence of copper oxide. By virtue of their shape they could act as crack initiation sites during testing. Secondly, there was evidence of local coarsening of the A357 silicon eutectic at the bond-line figure 68a, to form a line of defects along the interface between the specimen surfaces. The coarsening of the silicon may be explained in two ways; firstly, and less likely, the particles grow by Ostwald ripening, which involves mass transfer by detachment of atoms from smaller particles followed by diffusion through a matrix and subsequent growth of larger particles. This process is one that occurs mainly by diffusion in the solid state and could be expected to take some time to complete, a time-scale longer than that of the bonding process described in this work. Secondly, the coarsening may be explained by coalescence which involves dispersed particles being moved around such that they make contact and merge by a mechanism similar to sintering. Of the two processes the second is more likely because any liquid phase formed at the interface is likely to move the silicon particles around in a vigorous manner encouraging contact and coalescence. Both of these methods of coarsening have been propounded and modelled by Meyers with particular reference to the A357 alloy[146].

9.2 DIFFUSION BONDING A357 ALLOY USING SILVER FOILS

The interface of samples of A357 bonded in the solid state with silver foils showed very little change in dimensions across the bond-line. The thickness of the interfacial layer was 10μm, the same value as the initial thickness of the foils, figure 76. Electron-probe microanalysis of the interlayer identified the phase Ag_2Al indicative of the diffusion of aluminium into the foil itself. The presence of this intermetallic is confirmed by the phase diagram shown in figure 111 which shows a range of compositions for this phase. In addition the silver diffused away from the foil, particularly around the particles of silicon eutectic close to the bond-line. The diffusion of aluminium into the foil and the diffusion

of silver away from the foil may have had a compensating effect such that the interlayer had similar dimensions to the starting foil thickness. Dark precipitate material was evident at the interfaces between the Ag_2Al phase and the A357 alloy and appeared to be a complex structure containing oxygen, magnesium, silver and aluminium, figure 78. The presence of the dark precipitates formed a plane of weakness between the Ag_2Al layer and the A357. In all cases bonded specimens fractured interfacially, figure 110. The presence of both clean metal and intermetallic on the fracture surface implied that the locus of failure passed from one side of the Ag_2Al layer to the other, probably via the dark globular interfacial precipitates illustrated in figure 76. This is slightly different from that of solid state bonded copper foils which failed completely within the intermetallic layers. The maximum strength reached by samples bonded with a 10μm silver foil in the solid state was 30MPa, higher than that obtained when using an equivalent thickness of copper foil (bonded in the solid state) but still below the shear strength of the A357 base material.

Raising the temperature of the bonding conditions induced the formation of a liquid phase in a similar way found when using the copper foils. The load vs. time curve displayed the same dip relating to a relaxation of applied load at the point of liquation. The liquid phase was not expelled in as vigorous a fashion as the copper eutectic, manifested by the appearance of smaller beads of ejected material. It remained mainly within the sample and rapidly flowed around aluminium grains at the interface and around silicon particles in the eutectic colonies, figure 79. In addition, the liquid phase found paths of interconnected porosity and left traces remote from the bond-line and along the outside of the specimen, figure 80. The difference in microstructure may be explained by the higher diffusion of silver within aluminium compared with copper. Samples bonded in the liquid state using a silver foil were generally stronger than the equivalent copper samples, a maximum shear strength of 70MPa was obtained compared with 46MPa for copper foils. The bond strength is slightly less than the 90MPa values quoted by Partridge and Harvey[83]. The interface produced after bonding in the liquid state introduced a planar defect along which a crack could propagate, figure 79. Specimens fractured at the bond-

line and therefore indicated the sensitivity to such planar-type defects and discontinuities at the interface. The diffusion of silver into the aluminium in the region of the bond-line is not thought to promote a significant increase in local strength through solid solution hardening or precipitation hardening.

Analysis of the liquid ejected from the bond-line identified the presence of aluminium (containing silver at the limit of solid solubility), silicon and Ag_2Al. The analysis of the material is in agreement with Mondolfo[143] who states that a ternary mixture of this composition and not a ternary compound is formed under these conditions. Evidence for the Widmanstätten morphology of the Ag_2Al phase (figures 84 and 86) is in agreement with the findings of Gomez de Salazar[97] who noted this δ structure in samples of aluminium that were diffusion bonded with thin coatings of silver on the specimen surfaces. Incidentally, this phase has been described variously as γ by Mondolfo and ζ by Hansen in his book "The Constitution of Binary Alloys".

9.3 DIFFUSION BONDING COMPOSITE SPECIMENS USING COPPER FOILS

The transverse sections of composite materials were bonded with copper foils at 525°C under conditions that would have been expected to form a liquid phase. Instead, continuous bands of intermetallic compounds were formed and unreacted copper remained, effects comparable with those found using solid state bonding. The bands appeared in the order of copper, δ and $CuAl_2$ (θ), moving from the foil towards the matrix, figures 92-94. The intermetallic compounds formed only in regions where there was sufficient matrix material to react with the copper foil, figure 91a), which gave an indication to the limited extent of metal/foil reaction in composite specimens. In other regions intermetallic compounds grew into the sample particularly in infiltrated areas between fibres (careful examination of figure 91b shows this). Thicker foil combinations consisting of copper and aluminium and the use of a higher temperature (550°C) succeeded in promoting the formation of a liquid phase which then filled the gap between the composite specimen surfaces, figure 95a. Various structures form within this liquid

such as aluminium, $CuAl_2$ and precipitates of complex chemistry probably originating from casting defects, figure 96. However, the presence of defects at the bond-line such as fibre-end damage, coupled with the geometry of the fibres resulted in regions of the bond-line that showed no remnants of an interfacial liquid phase, figure 95b. The liquid formed in these areas has simply been removed from the bond-line, probably by capillary action, into the long crack-like defects running away from the interface. Composites bonded in this way exhibited no mechanical strength at all, fracturing immediately during testing or simply on removal from the bonding apparatus. The reinforcement of the matrix metal by the carbon fibres is demonstrated by referring to the load/time profile in figure 103c. The load sustained by the specimens during bonding was much greater than the unreinforced alloy metal, the values peaked at about 44MPa for transversely bonded composite material, figure 103c.

Longitudinally bonded composites formed a less clearly defined interface. Liquation of the foil occurred which rapidly spread away from the interface around the edges of the fibres in the vicinity, figure 97. The cracks which were induced during bonding and voidage due to poor infiltration, a characteristic of this material, provided easy paths for the transport of the liquid phase. Various points along the bond-line were filled with the liquid phase and were microstructurally consistent with the formation of the $CuAl_2$ eutectic, figures 98 and 99. The silicon appearing at various places does not appear to have taken part in the liquation as it remained in an unmodified morphology, figure 100b. The distribution and extent of composite defects may be indicated by the position of the $CuAl_2$ liquid eutectic mixture identified in the electron-probe microanalyser, the eutectic could be considered as a marker under these circumstances because it tends to accumulate in the defects within the material, figure 98. It is postulated that the liquid reaction of the copper foils can only take place in regions of the composite that contain areas of matrix material. Support for this is given in figure 100a which shows the formation of an interfacial liquid phase, additionally the liquid has penetrated the gap between two fibre tows and has started to react in the matrix-rich regions between these tows. There was no

apparent reaction at exposed fibres, planar defects are shown in figure 100b where the liquid phase has been unable to wet the fibre surfaces. The restriction of interfacial reaction to regions of matrix metal is clearly evidenced in figure 101, an observation which supports the view that fibres are essentially inert under these bonding conditions and take no part in the process. Indeed the inability of molten metals to wet ceramic fibres is a problem that has limited the successful production of metal matrix composites for many years. During testing the composites fractured at the interface in all cases and displayed no significant strengths. The longitudinally bonded composite material did not sustain as high a load during bonding as the transverse material, a peak was reached at 17MPa figure 103c), which may explain why the specimen suffered some damage during the bonding operation, figure 102.

10. CONCLUSIONS

10.1 ADHESIVE BONDING

Electron-probe microanalysis confirmed that the application of the Forest Products Laboratory (FPL) etch to aluminium specimens induced the formation of an oxide film 14nm thick. The enhanced FPL oxide was some three times thicker than the native barrier oxide whose thickness was confirmed by electron-probe microanalysis to be close to 5nm.

The FPL etch induced a reproducible scalloped surface topography on pure aluminium. However, the etch induced highly preferential chemical attack on the alloys A357 and ARE 415 which was characterised by deep pitting. The FPL solution reacted vigorously with the eutectic areas in A357 and the cored regions and eutectic of ARE 415. Local etching of intermetallic particles within the grain structure took place in both alloys.

Samples of pure aluminium demonstrated higher single-lap shear strengths after etching in the mixed acid FPL solution. Conversely, all samples of A357 and ARE 415 exhibited lower bond strengths after etching in the FPL solution. The reduction in bond strengths were attributed to air entrapment in the heavily etched specimens leading to insufficient wetting of the adherend surface.

The metallurgical condition of alloy material had an effect on the shear strengths of the adhesively bonded joints. Specimens with lower yield strengths, such as solution treated ARE 415, tended to deform during shear testing and consequently exhibited lower shear strengths. The reduction in bond strengths was ascribed to the samples' reduced resistance to peel forces induced during mechanical testing.

A maximum shear strength of 42MPa was achieved with solution treated A357 alloy bonded with epoxy adhesive. This result compared favourably with published data. Samples of material bonded with epoxy adhesive reproducibly fractured within the epoxy

resin and close to the metal/adhesive interface. This result confirmed previous data which described cohesive failure of epoxy adhesives used to bond other materials, such as steels.

Samples bonded with acrylic adhesive demonstrated mixed modes of failure, typified by combinations of clean areas of interfacial failure and sheared adhesive regions identified as cohesive failure. Penetration of the acrylic adhesive into heavily etched areas of the adherends confirmed the less viscous nature of the acrylic compared with the epoxy adhesive. This penetration was thought to confer a modest degree of mechanical interlocking within the adhesive joint.

A maximum shear strength of 21MPa was shown by the acrylic adhesive with as-cast ARE 415. This value also compared favourably with data published for other aluminium alloys bonded with acrylic adhesives.

The benefit of the FPL etch when applied to composite material was not fully determined due to consistent failure of the composite substrates before the adhesive, irrespective of surface pretreatment. Failure of the composite occurred by either tensile cracking, interlaminar cracking or a combination of both.

Initial results indicate that the composite studied is currently only capable of attaining a fraction of its maximum potential. Mechanical properties could be markedly increased by improving fibre infiltration during manufacture.

10.2 DIFFUSION BONDING

Specimens of A357 bonded in the solid state at 510°C with 20μm copper foils produced a continuous band of intermetallics at the bond-line. Electron-probe microanalysis identified the phases as ζ_2 (56.5%$_{at}$ copper, 43.5%$_{at}$ aluminium), θ ($CuAl_2$, 36%$_{at}$ copper, 64%$_{at}$ aluminium).

An increase in applied bonding load, from 5% to 10% strain, almost doubled the effective bonded area. This was attributed to increased deformation of surface asperities leading to better contact between the bonding surfaces.

A maximum shear strength of 31.5MPa was achieved with samples bonded at 510°C with 20μm copper foils. The use of a 10μm copper foil produced weaker joints, the maximum value reached was 15.7MPa. Fracture occurred within the intermetallic bands in all these cases.

Samples of A357 bonded with 20μm copper foils at 525°C produced stronger bonds, a maximum strength of 46MPa was attained. The increase in shear strength was attributed to the formation of a liquid phase at the bond-line which increased wetting and contact between the bond surfaces. Samples of A357 bonded at 525°C with 20μm copper foils fractured at the bond-line between the specimens in all cases. Electron-probe microanalysis identified the composition of the liquid phase formed at the bond-line to be a ternary eutectic mixture of aluminium, silicon and $CuAl_2$.

A357 alloy bonded with 10μm silver foils at 540°C formed a continuous intermetallic at the bond-line comparable to the structure formed when bonding with copper foils in the solid state. Electron-probe microanalysis identified the composition of the intermetallic compound to be Ag_2Al, the δ phase. A maximum shear strength of 30MPa was reached for samples bonded with silver foils in the solid state. In all cases the samples fractured at the interface between the δ phase and the base metal.

Specimens of A357 bonded with 10μm silver foils at 560°C produced stronger bonds, the highest value was 70MPa. The increase in bond strength was attributed to the formation of a liquid phase which promoted contact between the specimen surfaces. Also, the silver foil material was removed more fully from the bond-line probably due to the increased diffusion of silver in aluminium compared with the copper foils. These samples fractured at the bond-line in all cases. Analysis of the liquid material formed

when bonding 10μm silver foils at 560°C revealed a ternary eutectic mixture comprising aluminium, silicon and Ag_2Al.

Composite specimens sustained higher bonding loads (up to 44MPa) compared with alloy material. As a result damage was incurred at the fibre-ends for transversely-bonded composites and cracking through the material was evident for longitudinally-bonded specimens.

Transversely-bonded composites showed limited reaction with copper foils when bonded at 525°C. The formation of intermetallic structures was restricted to inter-fibre areas of the composite that allowed contact between matrix metal and the foil. Intermetallic compounds were identified as δ ($62\%_{at}$ copper, $38\%_{at}$ aluminium) and θ ($CuAl_2$, $32\%_{at}$ copper, $68\%_{at}$ aluminium).

Composite specimens bonded transversely at 550°C with thicker foil combinations formed a liquid phase at the bond-line. The liquid was either removed from the bond-line by capillary action along the fibres or remained at the bond-line in isolated areas. The liquid phase was analysed as the eutectic comprising aluminium and $CuAl_2$.

Longitudinally-bonded composites also formed a liquid phase. This was attributed to the presence of more matrix metal in contact with the foils. The liquid phase was removed from the bond-line by capillary action around the fibre/matrix interfaces or via defects in the composite material. The liquid phase was identified as the eutectic consisting of aluminium and $CuAl_2$.

In all cases the carbon fibre reinforcement was essentially inert and took no part in the bonding process. These diffusion bonded composite materials showed no mechanical strength under any orientations or bonding conditions.

11. FURTHER WORK

Further experiments should be carried out on the adhesive bonding of metal matrix composites. However, these experiments will have to await the production of higher quality metal matrix composites in order to make a more rigorous evaluation of surface pretreatments.

Similar requirements exist vis a vis diffusion bonding before a systematic study may proceed.

For successful diffusion bonding of metal matrix composites studies need to be completed relating to the degree of damage tolerated by the composites. This dictates strongly the loading regimes permitted during bonding. In general studies should try to keep temperature as low as possible because the higher the temperature the greater the extent of oxidation of aluminium surfaces.

Investigations will need to be carried out concerning the type of interlayers used for diffusion bonding. Intermetallic compounds are generally undesirable and work should be aimed at assessing insert materials that produce a liquid without deleterious phases, for example, alloy foils such as Al-4% Cu. Additionally, foils from the 2000-series of alloys could be used, the presence of magnesium may have a role to play in controlling the formation of an oxide film on aluminium substrates.

12. REFERENCES

1 Chou, T.W, Kelly, A., Okura, A.; Composites, 16, (1985), 187-206.

2 Girot, F., Quenisset, J.M., et al.; Comp. Sci. and Tech., 30, (1987), 155-184.

3 Mortensen, A., Cornie, J.A., Flemings, M.C.; J. Metals, (Feb 1988), 12-19.

4 Tanikawa, E., Takeyama, S.; Proc. 4th Jpn-US Conf. Comp. Mats., Lancaster, Pennsylvania, 1988, 449-457.

5 Modi, O.P., Yegneswaran, A.H.; J. Mat. Sci., 23, (1988), 83-92.

6 Ehrstöm, J.C., Kool, W.H.; J. Mat. Sci., 23, (1988), 3195-3201.

7 Mahanty, G., Tiwari, A.N; Key Eng. Mats., 29-31, (1989), 747-754.

8 Quigley, B.F., Abbaschian, G.J., et al.; Met. Trans. A., 13A, (1982), 93-100.

9 Karandikar, P.G., Chou, T-W.; J. Mat. Sci., 26, (1991), 2573-2578.

10 Ahmad, I., Barranco, J.; "Advanced Fibres and Composites for Elevated Temperatures", The Metallurgical Soc. of AIME, 1980, p180-204.

11 Technical information supplied by the Toaz Corporation Inc., USA.

12 Bader, M.G., Clyne, T.W.; Comp. Sci. and Tech., 23, (1985), 287-301.

13 Nagata, S., Sakamoto, M.; Mat. and Design, 10, (1989), 153-158.

14 Aghajanian, M.K., Rocazella, M.A., J. Mat. Sci., 26, (1991), 447-454.

15 White, J., Willis, T.C.; Internal Tech. Memo., Alcan Research Labs, Banbury, 1988.

16 Tsunekawa, Y., Okumiya, M.; J. Mat. Sci. Letts., 6, (1987), 191-193.

17 Lagacé, H., Lloyd, D.J.; Canadian Metallurgical Quarterly, 28, (1989), 145-152.

18 Abis, S., Donzelli, G., J. Mat. Sci. Letts., 7, (1988), 51-52.

19 Deonath, Rohatgi, P.K.; J. Mat. Sci., 15, (1980), 2777-2784.

20 Ohori, K., Watanabe, H.; Mat. Sci. and Tech., 3, (1987), 57-60.

21 Imai, T., Nishida, Y.; J. Mat. Sci. Letts., 6, (1987), 1257-1258.

22 Stacey, M.H., Mat. Sci and Tech., 4,(1988), 227-230.

23 Balasubramanian, M.; J. Mat. Sci., 22, (1987), 3864-3872.

24 Dhingra, A.K.; Phil. Trans. R. Soc. A., 294, (1980), 559-564.

25 Saggese, M.E., Scott, V.D.; Mat. Sci and Tech., 4, (1988), 871-875.

26 Cappleman, G.R., Watts, J.F.; J. Mat Sci., 20, (1985), 2159-2168.

27 Chernyshove, T.A, Kobeleva, L.I.; J. Mat. Sci., 20, (1985), 3524-3528.

28 Hall, I.W.; J. Mat. Sci. 26, (1991), 776-781.

29 Fishkis, M.; J. Mat. Sci., 26, (1991), 2651-2661.

30 Abraham, S., Pai, B.C.; J. Mat. Sci., 27, (1990), 2839-2845.

31 Madeleno, U., Liu, H., et al., J. Mat. Sci., 25, (1990), 3273-3280.

32 Himbeault, D.D., Varin, R.A.; Composites, 20, (1989), 471-477.

33 Dinwoodie, J.; SAE Tech. Paper Series, 870437

34 Warwick, G.; Flight International, 5 Mar 1988, 24-25.

35 Thompson, D.F., Babel, H.W.; 34th Int. SAMPE Symp., (1989), 759-769.

36 Lane, M., Hseih, C.; 34th Int. SAMPE Symp., (1989), 7798-809.

37 Kohyama, A., Sato, S.; J. Nuc. Mats., 179-181, (1991), p 254-258.

38 Awerbuch. J.; J. Comp. Mats., 10, (1976), 231-257.

39 Chin, H.B., Prevorsek, D.C.; Proc. 4th Jpn-US Conf. Comp. Mats., Lancaster, Pennsylvania, 1988, 953-962.

40 Schroff, G.; "Mechanical Joining-U.S Markets and Technologies"; Research Report 633, SRI International, Menlo Park, California, (1980).

41 Good, R.J.; J. Adhesion, 4, (1972), 133

42 Packham, D. E., Bright, K., Malpass, B. W.; J. Appl Poly Sci, 18, (1974), 3237-3247

43 Idem, Ibid; 18, (1974), 3249-3258

44 Evans, J. R., Packham, D. E.; "Adhesion", vol.1, (1977), ed. K. W. Allen

45 Idem; J. Adhesion, 9, (1978), 267-277

46 Idem, Ibid; 10, (1979), 39-47

47 Idem, Ibid; 10, (1979), 177-191

48 Arrowsmith, D. J., Clifford, A. W.; Int. J. Adh, 5, (1985), 40-42

49 Arrowsmith, D. J.; Proceedings International Adhesion Conference., 1984, p.27.1-27.4

50 Lindsay, N. J.; B.Sc Final Year Project Report, Dept. of Metallurgy, University of Aston, April 1986

51 Jennings, C. W.; J. Adh, 4, (1972),25-28

52 Koichi Kato; Polymer, 8, (1967), 33

53 Wake, W. C.; Adhesion and the Formulation of Adhesives, p. 73, Applied Science Publishers, London and New York

54 Huntsberger, J. R.; Treatise on Adhesion and Adhesives, 1, ed. R. L. Patrick, (Marcel Dekker, New York,) 1967

55 Fowkes, F.M.; Ind. Eng. Chem., 56, (1964), 40

56 Kinloch, A. J.; J. Mat. Sci., 15, (1980), 2141-2166

57 Wake, W. C.; Polymer, 19, (1978), 291-307

58 Sykes, J. M., Hoar, T. P.; J. Poly. Sci., Part A-1, 7, (1969), 1385-1391

59 Bikerman, J. J.; J. Appl. Chem., 11, (1961), 81

60 Gettings, M., Kinloch, A. J.; J. Mat. Sci., 12, (1977), 2511-

61 Voyutskii, S. S.; "Autohesion and the Adhesion of High Polymers", (J. Wiley and Sons, New York), 1963

62 Private communication, D.A Moth, DRA Holton Heath.

63 Benoliel, R. W.; in "Materials Synergisms", 10th National SAMPE Conference, Oct 1978, New York, p 873-888.

64 Rice, K. K., Mahoney, C. L.; ibid., p 351-361.

65 Mulroy, B. J., Mazenko, D. M.; ibid, p 416-424.

66 Cichon, M. J.; 34th Int. SAMPE Symposium, May 1989, p 1052-1065.

67 Chin-Long Ong; ibid, p 1067-1078.

68 Sivy, G. T; ibid., p 448-457.

69 Bethune, A. W.; SAMPE J., (1975), 4

70 Minford, J.D.; Adhes. Age, 23, (1980), 36

71 Arrowsmith, D. J., Moth, D. A.; Trans. IMF, 64, (1986), 91-94.

72 Arrowsmith, D. J., Moth, D. A., Maddison, A.; Trans IMF, 65, (1987), 38-44.

73 Venables, J. D., McNamara, D. K., et al.; "Materials Synergisms", 10th National SAMPE Conference, Oct 1978, New York, p 362-376.

74 Arrowsmith, D.J., Moth, D.A., Trans. IMF., 66, (1988), 112-114.

75 Briggs, P.C., Muschiatti, L.C.; US Patent 3,890,407 (1975).

76 Owston, W.J.; US Patent 3,725,504 (1973).

77 Bachman, A.G.; US Patent 4,429,088 (1984).

78 Owston, W.J.; US Patent 3,832,274 (1974).

79 Snogren, R.C.; Mech. Eng., May 1970, 33- .

80 DeVries, K. L.; Anderson, G. P.; "Bonded Joints and Preparation for Bonding"; AGARD Lecture Series N° 102, Harford House, London, 1979, p 3-1 to 3-25.

81 Bergquist, P.R., Petrie, S.P.; 22nd International SAMPE Conference, (Nov 1990), 815-825.

82 Davis, R.J., Ritchie, M.D.; J. Adhesion, 38, (1992), 243-254.

83 Partridge, P.G., Dunford, D.V.; "Advanced Joining of Metallic Materials"; 61st AGARD Symposium, Oberammergau, FDR, Sept 1985.

84 Metals Joining Manual, MM Schwartz, p 10-2,, (McGraw-Hill Inc), ISBN 0-07-055720-9.

85 Feduska, W., Horigan, W.L.; Weld. J., 41, (1962), 28-35,

86 Vaidyanath, L.R, Nicholas, M.G; Br. Weld. J., 6, (1959)

87 Tylecote, R.G., Wynne, E.J; Br. Weld. J., 10, (1963), 385-394

88 Wilford, C.F, Tylecote, R.F; Br. Weld. J., 7, (1960), 708-712

89 Haynes, C.W.; Metal Progress, March 1969, p. 83-86.

90 Schier, J.F., Dorr, D.J.; "Materials Synergisms", 10th National SAMPE Conference, New York, 1978, p 63-72.

91 Metzger, G.E.; WRC Bull., 20, (1975), 1-21.

92 Derby, B., Wallach, E.R.; J. Mat. Sci., 19, (1984), 3140-3148.

93 Harvey, J., Partridge, P.G.; J. Mat. Sci., 20, (1985), 1009-1014.

94 Pickens, R.P.; J. Mat. Sci., 25, (1990), 3035-3047.

95 Dunford, D.V.; Partridge, P.G.; Technical Report 89052, October 1989, RAE Farnborough.

96 Dunford, D.V. Partridge, P.G.; J. Mat. Sci., 26, (1991), 2625-2629.

97 Gomez de Salazar, J.M.; Prakt. Metallog., 25, (1988), 532-542.

98 Schwartz, M.M.; "Materials Synergisms", 10th National SAMPE Conference, New York, 1978, p 714-732.

99 Sakamoto, A.; J. Jap. Weld. Soc., 56, (1987), 20-29.

100 Enjo, T., Ikeuchi, Y.; Trans. JWRI, 16, (1987), 57-64.

101 Johnson, R.M., Goolsby, R.D.; "Materials Synergisms", 10th National SAMPE Conference, New York, 1978, p 802-811.

102 Enjo, T., Ikeuchi, K.; Trans JWRI, 14, (1985), 293-297.

103 Enjo, T., Ikeuchi, K.; Trans JWRI, 15, (1986), 61-68.

104 Calvo, F.A, Urena, A.; J. Mat. Sci., 23, (1988), 2273-2280.

105 Nicholas, M.G., Mortimer, D.A,; Mat. Sci. and Tech., 1, (1985), 657-664.

106 Beraud, C., Courbiere, M.; J. Mat. Sci., 24, (1989), 4545-4554.

107 Turwitt, M., Elssner, G.; Prakt. Metallog, 24, (1987), 560-569.

108 Derby, B.; Mat. Sci. Res., 21, (1986), 319-328.

109 Nicholas, M.G., Crispin, R.M; J. Mat. Sci., 17, (1987), 3347-3360.

110 Nicholas, M.G., Crispin, R.M.; Sci. Ceram., 14, (1988), 539-544.

111 Suganuma, K., Okamoto, T.; "Fundamentals of Diffusion Bonding"; ed Yoichi Ishida, pub. Elsevier, 1987, p71-87.

112 Ohmori, A., Arata, Y.; Trans JWRI, 18, (1989), 65-73.

113 Ning, X.S., Okamoto, T.; J. Mat. Sci., 26, (1991), 2050-2056.

114 Yamada, T., Yokoi, K.; J. Mat. Sci., 25, (1990), 2188-2192.

115 Muroga, T., Aono, Y.; J. Nuc. Mats., 179-181 (1991), p. 259-262.

116 Abe, K., Higuchi, T.; J. Nuc. Mats., 179-181 (1991), p. 766-770.

117 Niemann, J.T., Garrett, R.A.; Weld. J. Res. Suppl., April 1974.

118 Hirane, T., Morimoto, S.; Trans ISIJ, vol 24, (1984), B408-B409.

119 Norris, B.; Proc. Conference: "Designing with Titanium"; p83-86, Bristol, UK, 1986.

120 Zhang, Y-C,. Nakagawa, H.; Trans JWRI, 16, (1987), 17-29.

121 Enjo, T., Ikeuchi, K.; Trans JWRI, 13, (1984), 63-68.

122 Iino, Y.; J. Mat. Sci. Letts., 10, (1990), 104-106.

123 "Equilibrium Diagrams of Aluminium Alloy Systems", published by The Aluminium Development Association, London, 1961.

124 Metals Handbook (9th Ed), Vol 2, Properties and Selection: Non-Ferrous Alloys and Pure Metals, p 167. Published by the American Society for Metals (ASM).

125 S. Kerry and V.D. Scott; Final Report, "Microstructure and Mechanical Properties of High Strength Cast Aluminium Alloys", University of Bath, September 1985.

126 "Carbon and Graphite Fibres: Manufacture and Applications"; ed M. Sittig, pub Noyes Data Corp., New Jersey, USA, 1980.

127 "Bonded Joints and Preparation for Bonding", McMillan, J.C.; AGARD Lecture Series N° 102, Harford House, London, 1979, 7-1 - 7-30.

128 Arrowsmith, D.J., Moth, D.A., et al; Trans IMF, 66, (1988), 112

129 Newey, C., Weaver, G.; "Materials Principles and Practice", p. 73, (Butterworths, London), ISBN 0-408-02730-4.

130 Blodgett, K. B., Langmuir, I., Phys. Rev., 51, (1937), 964

131 H. E. Bishop; J. Phys. D: Appl. Phys., 7, (1974) 2009.

132 G. Love and V. D. Scott, J. Phys. D: Appl. Phys., 11, (1978), 1369.

133 Kozma, L., Olefjord, I.; Mat. Sci. and Tech., 3, (1987), 860-874

134 McMillan, J.C.; "Bonded Joints and Preparation for Bonding", AGARD Lecture Series 102, Harford House, London, 1979, pub. McMillan

135 Bascom, W.D., Timmons, C.O; J. Mat. Sci., 10, (1975), 1037-1048.

136 Bascom, W.D, Cottington, R.L; J. Adhesion, 4, (1972), 193-209.

137 Source Book on the Selection and Fabrication of Aluminium Alloys, (American Society for Metals, Ohio), 1978.

138 Chapman, A.R., Ph.D Thesis, School of Materials Science, University of Bath, 1992.

139 Nickolson, B.; 34th Int. SAMPE Symposium, May 1989, 631-642.

140 Gent, A.N., Lin, C-W.; J. Adhesion, 32, (1990), 113-125.

141 Matthews, F.L.; "Joining Fibre-Reinforced Plastics", p. 291, (Elsevier: London), ISBN 1-85166-019-4.

142 Matthews, F.L.; "Joining Fibre-Reinforced Plastics", p. 223 & 278, (Elsevier: London), ISBN 1-85166-019-4.

143 Mondolfo, L.M., "Aluminium Alloys: Structures and Properties", (Butterworths: London), 1976, p513.

144 Abbott, T.B., Parker, B.A.; J. Mat. Sci., 25, (1990), 2100-2106.

145 Gwyer, A.G.C., Phillips, H.W.L.; J. Inst. Metals, 40, (1928), 297-358.

146 Meyers, C.W; AFS Trans., 93, (1985), 741-750.

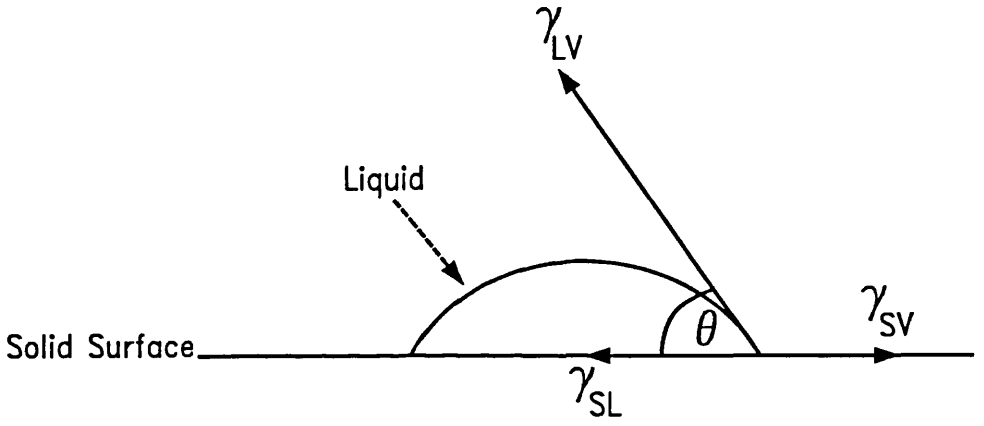

Figure 1 Surface tensions and contact angle for a sessile drop at rest on a solid surface.

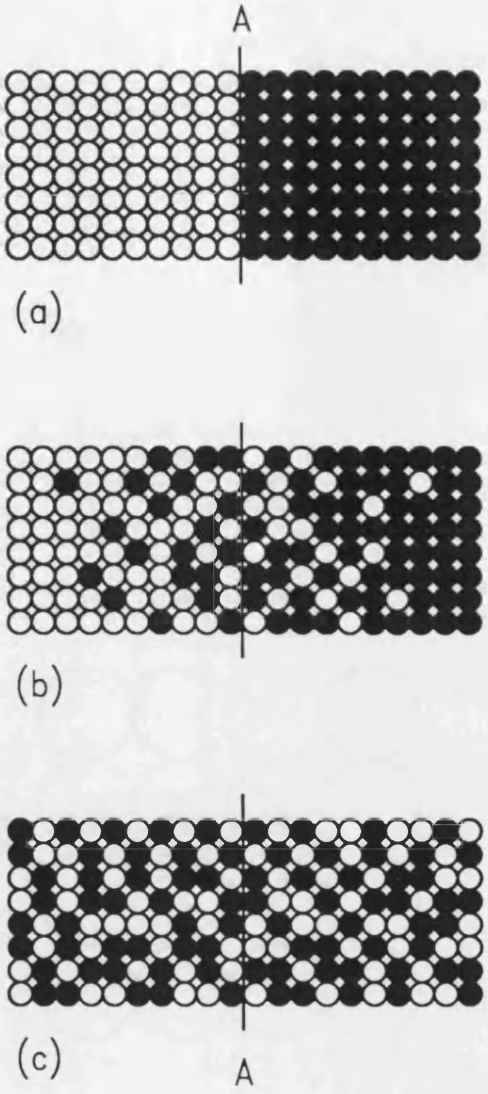

Fig 2 Atoms diffusing across an hypothetical boundary A–A

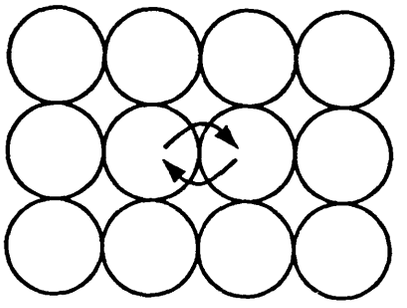

Fig 3a Direct interchange diffusion mechanism

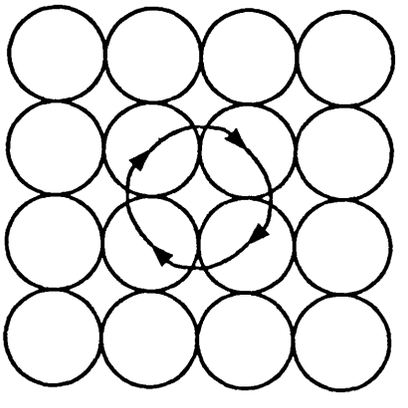

Fig 3b Zener ring mechanism for diffusion

Figure 4a: Movement of an atom into a vacancy position in an fcc lattice

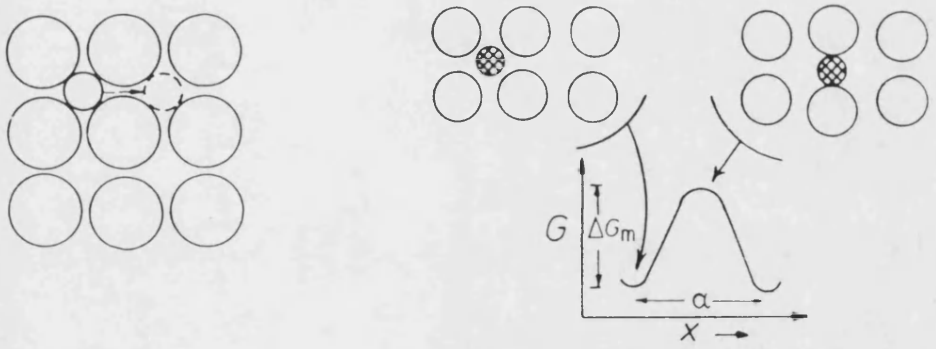

Figure 4b: Movement of an interstitial and the associated change in lattice free energy during the move

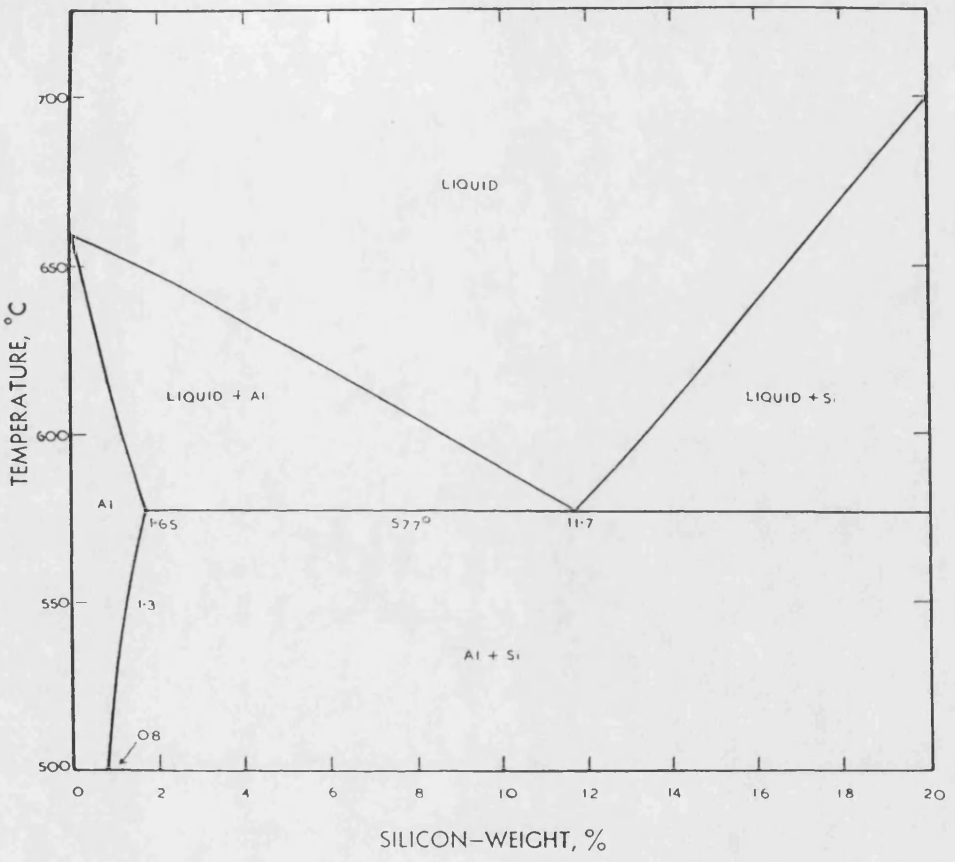

Figure 5: Aluminium / Silicon equilibrium phase diagram.

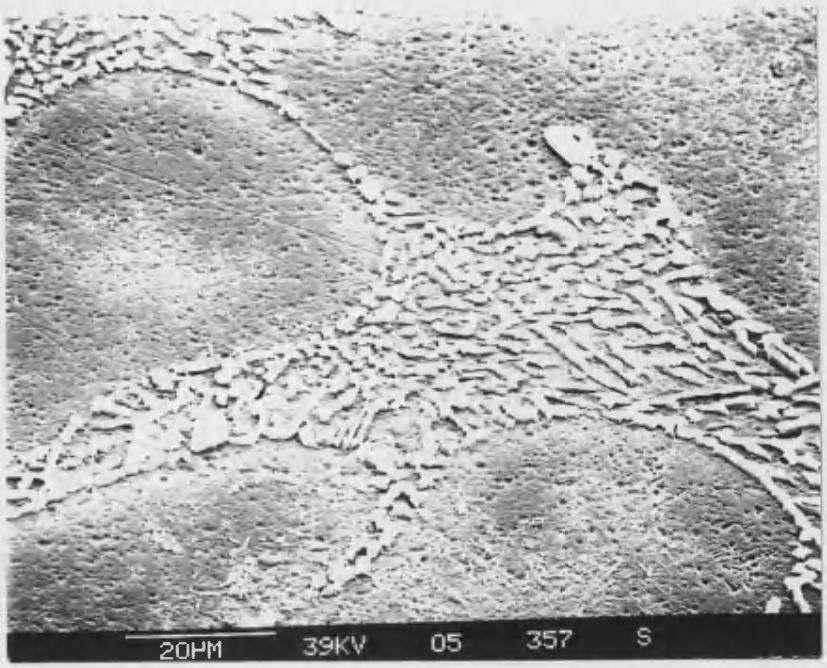

Figure 6a: Microstructure of A357 alloy, secondary SEM micrograph.

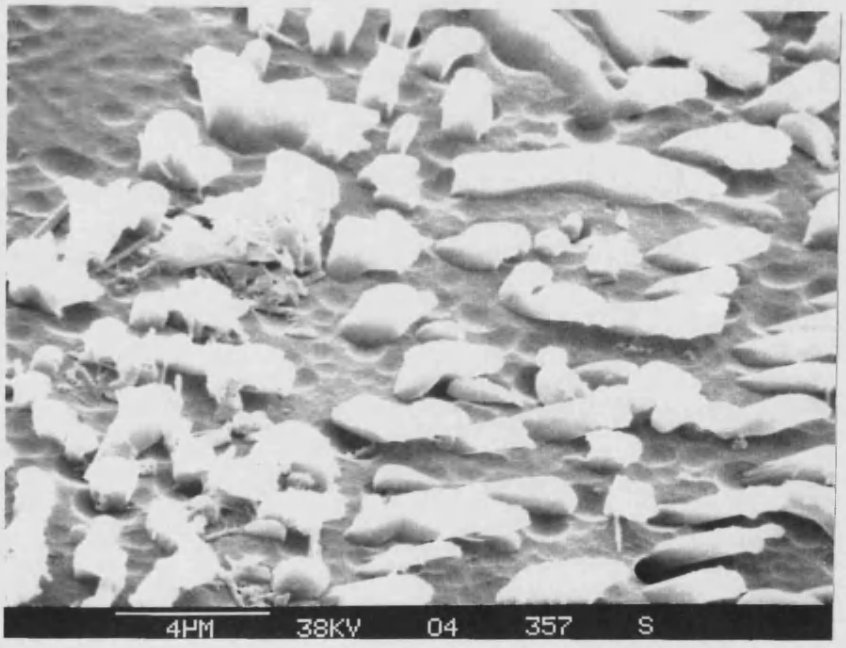

Figure 6b: Microstructure of A357 alloy, secondary SEM micrograph.

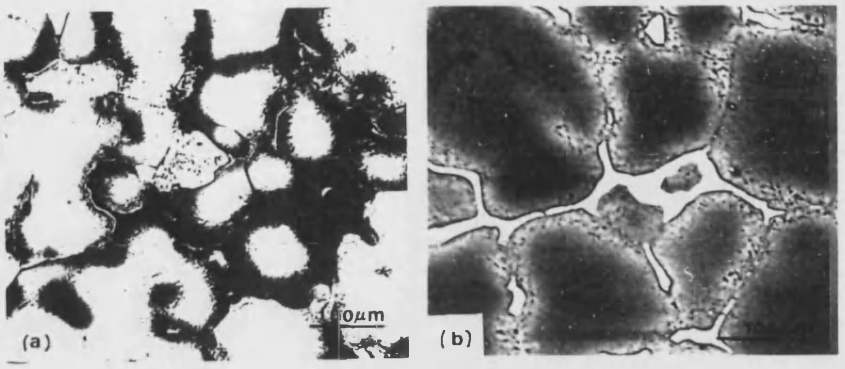

Figure 7 Optical (a) and backscattered (b) images of ARE 415 alloy

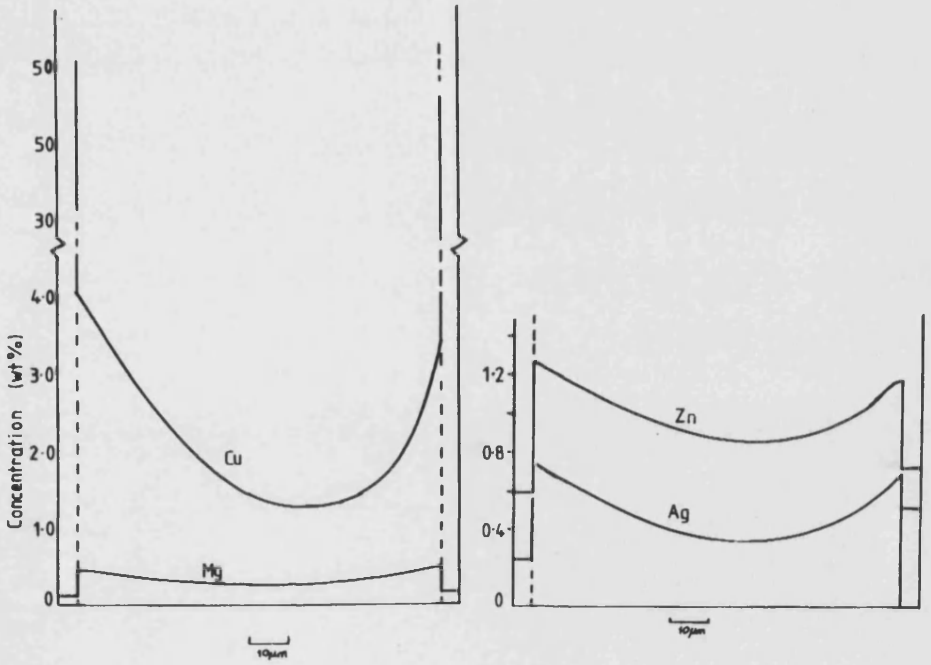

Figure 7 cont'd: Variation in chemical composition across a grain in ARE 415 alloy (After Scott & Kerry, University of Bath 1986)

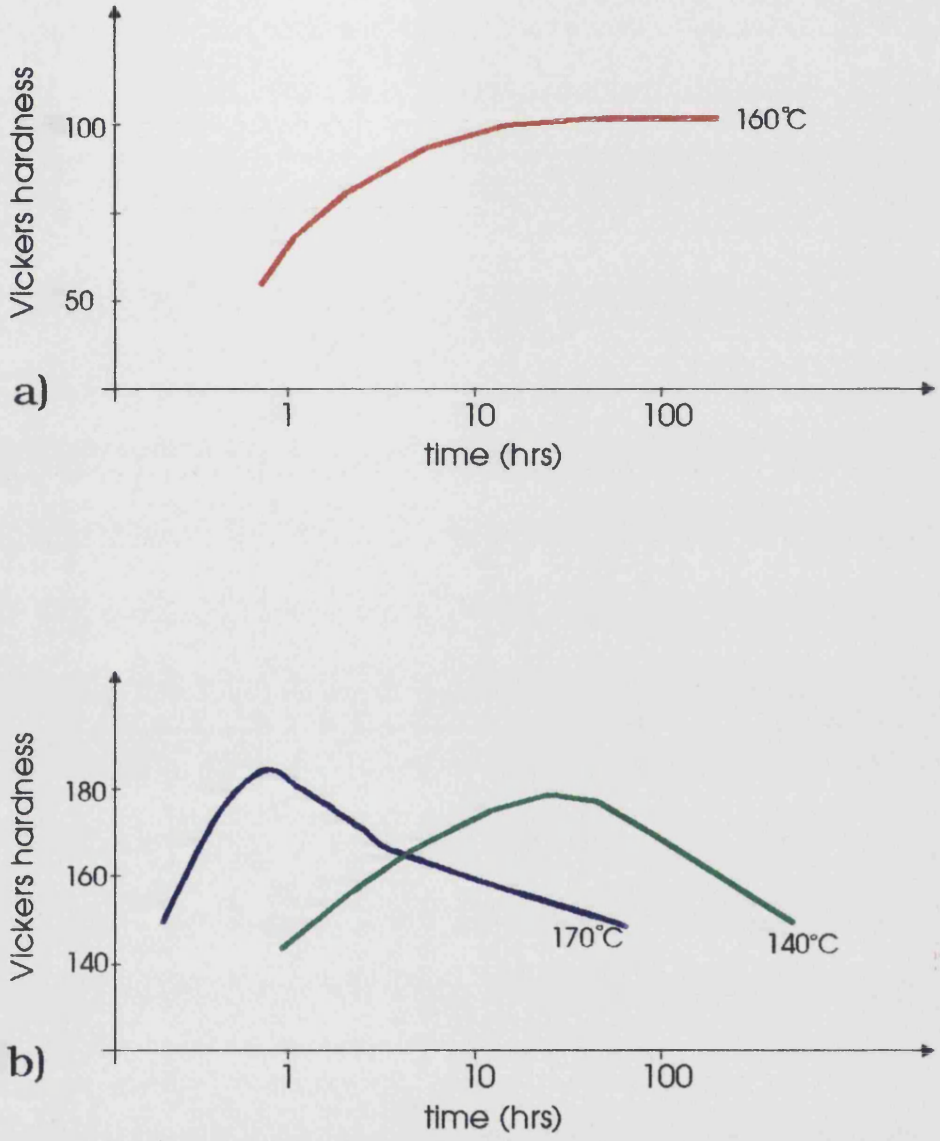

Figure 8: Hardening curves for a) A257 alloy and b) ARE 415

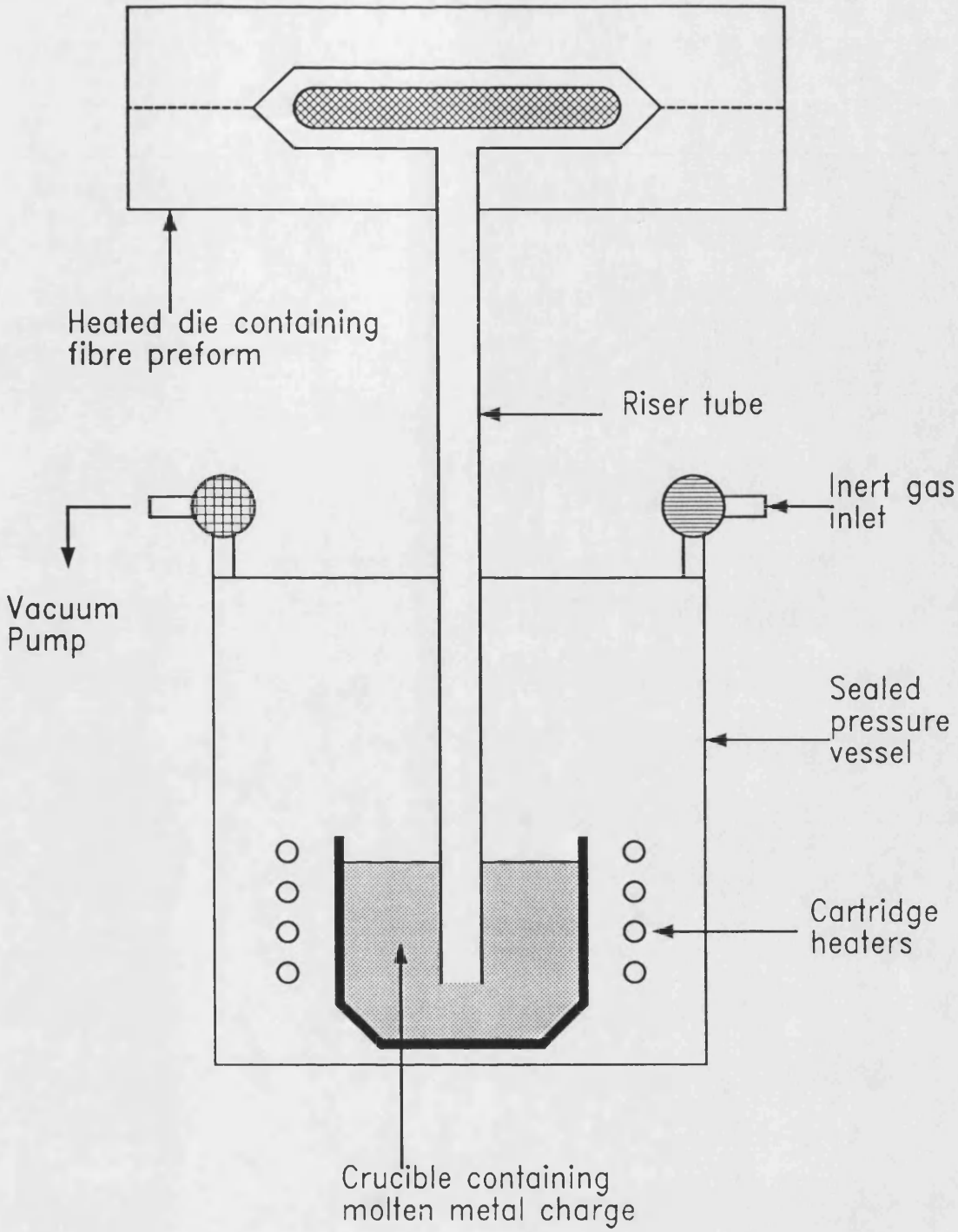

Fig 9 Schematic diagram showing Liquid Metal Infiltration (LMI) apparatus.

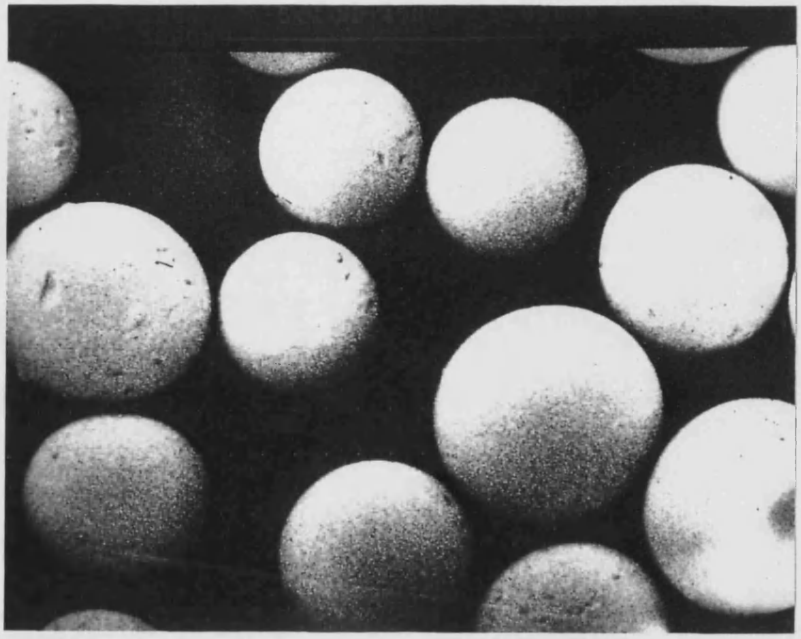

Figure 10: Glass "Ballotini" beads, SEM micrograph.

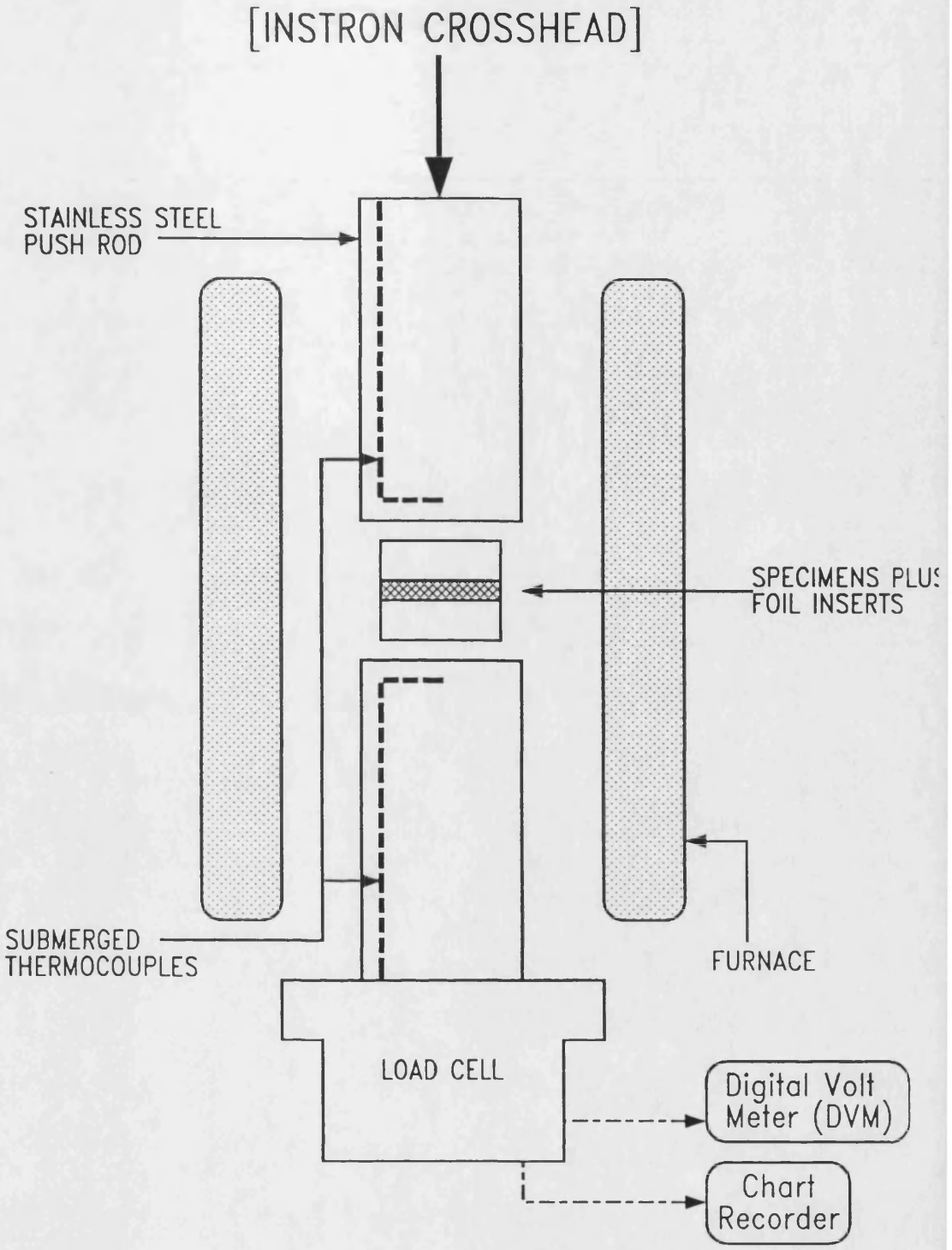

Figure 11 Schematic diagram of bonding apparatus.

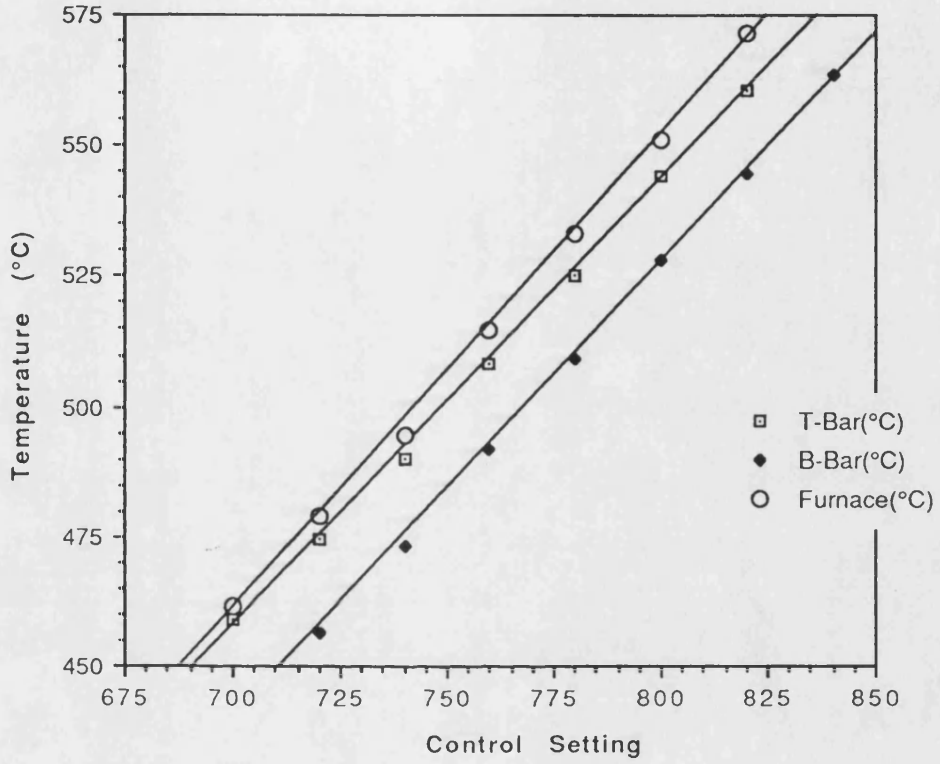

Figure 12: Calibration curve for 3-zone furnace

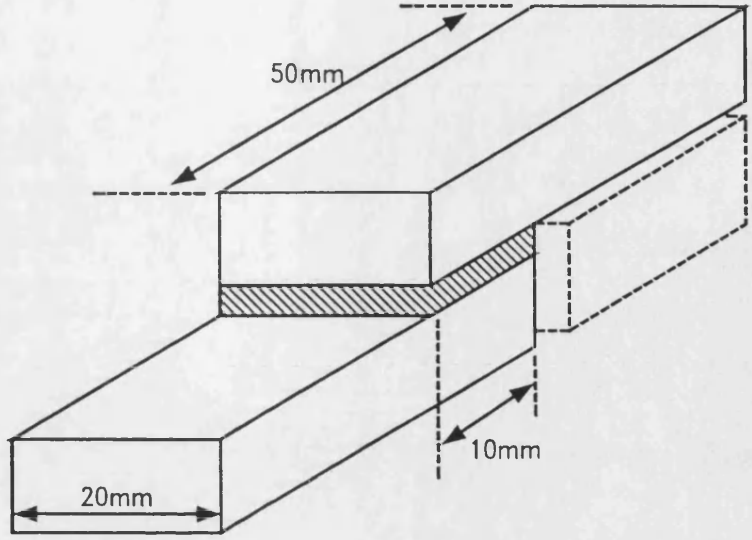

Figure 13a Schematic geometry of an adhesively bonded single–lap shear specimen.

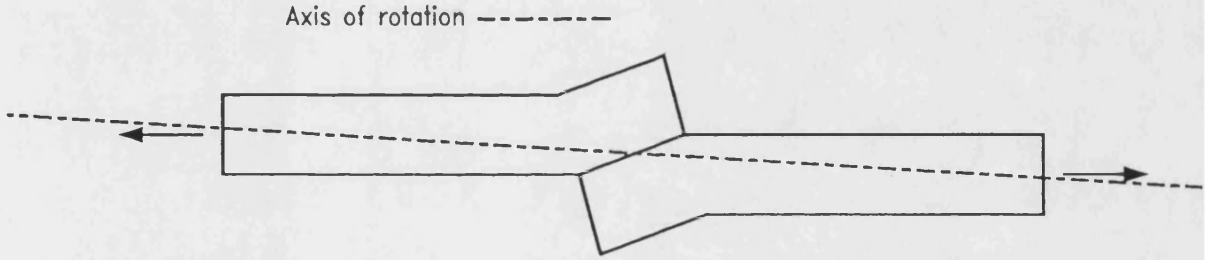

Figure 13b Bending moment induced by asymmetric loading during lap shear testing without spacer blocks.

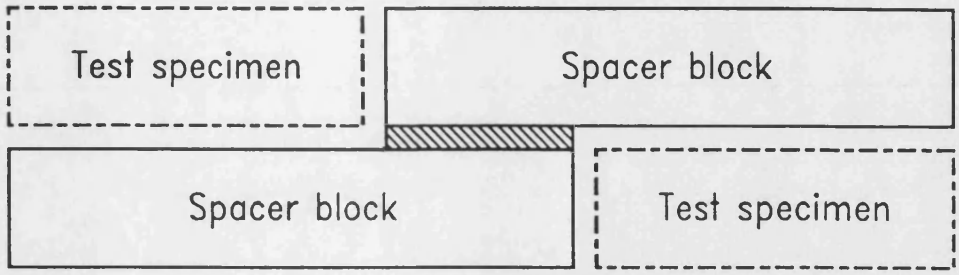

a) Adhesively-bonded test specimen

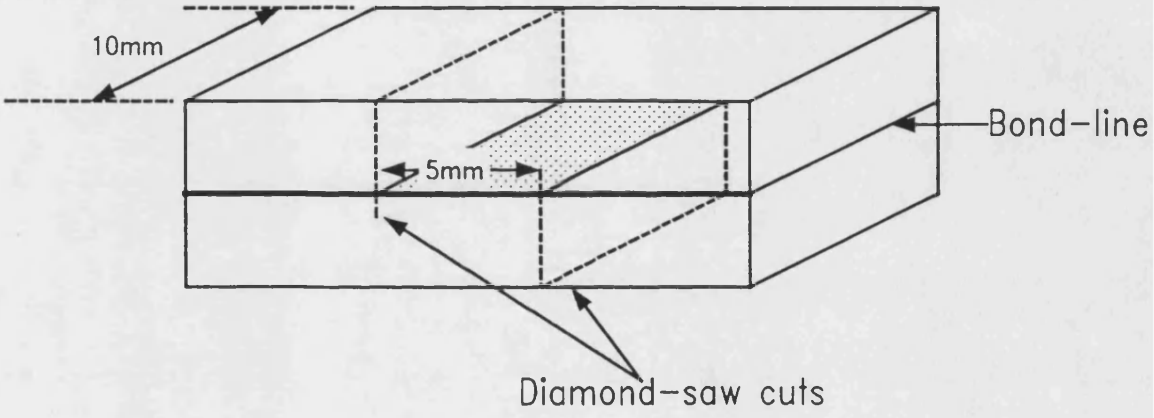

b) Diffusion-bonded test specimen

Fig 14 Side view geometries for shear-test specimens

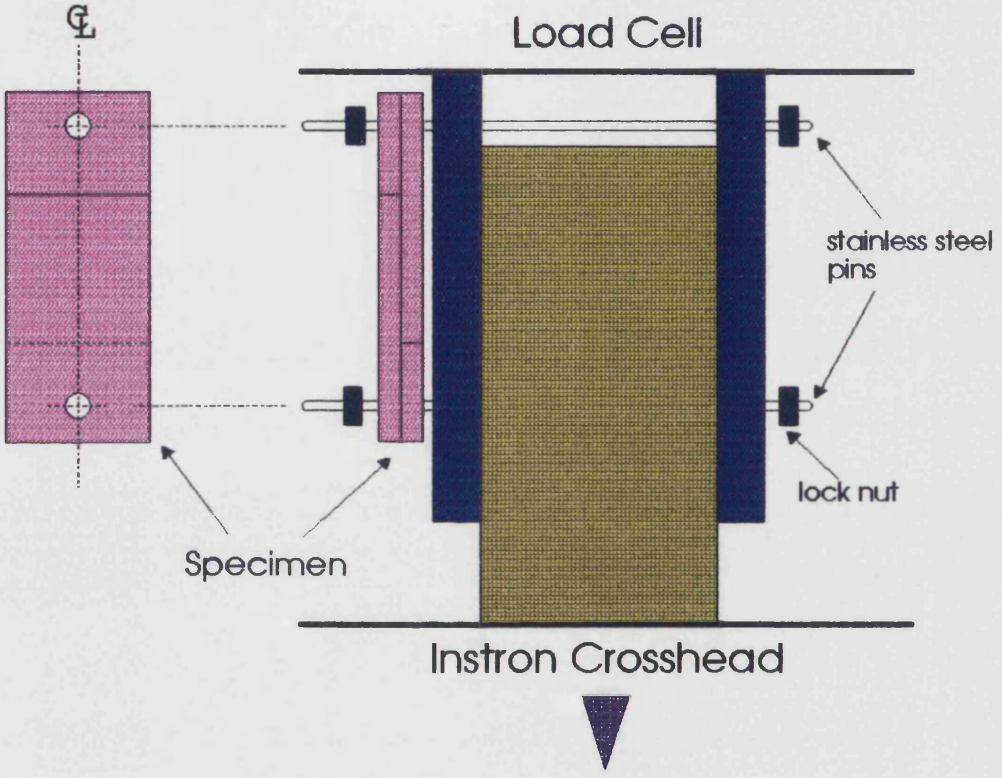

Figure 15: Schematic diagram showing apparatus used for testing diffusion bonds

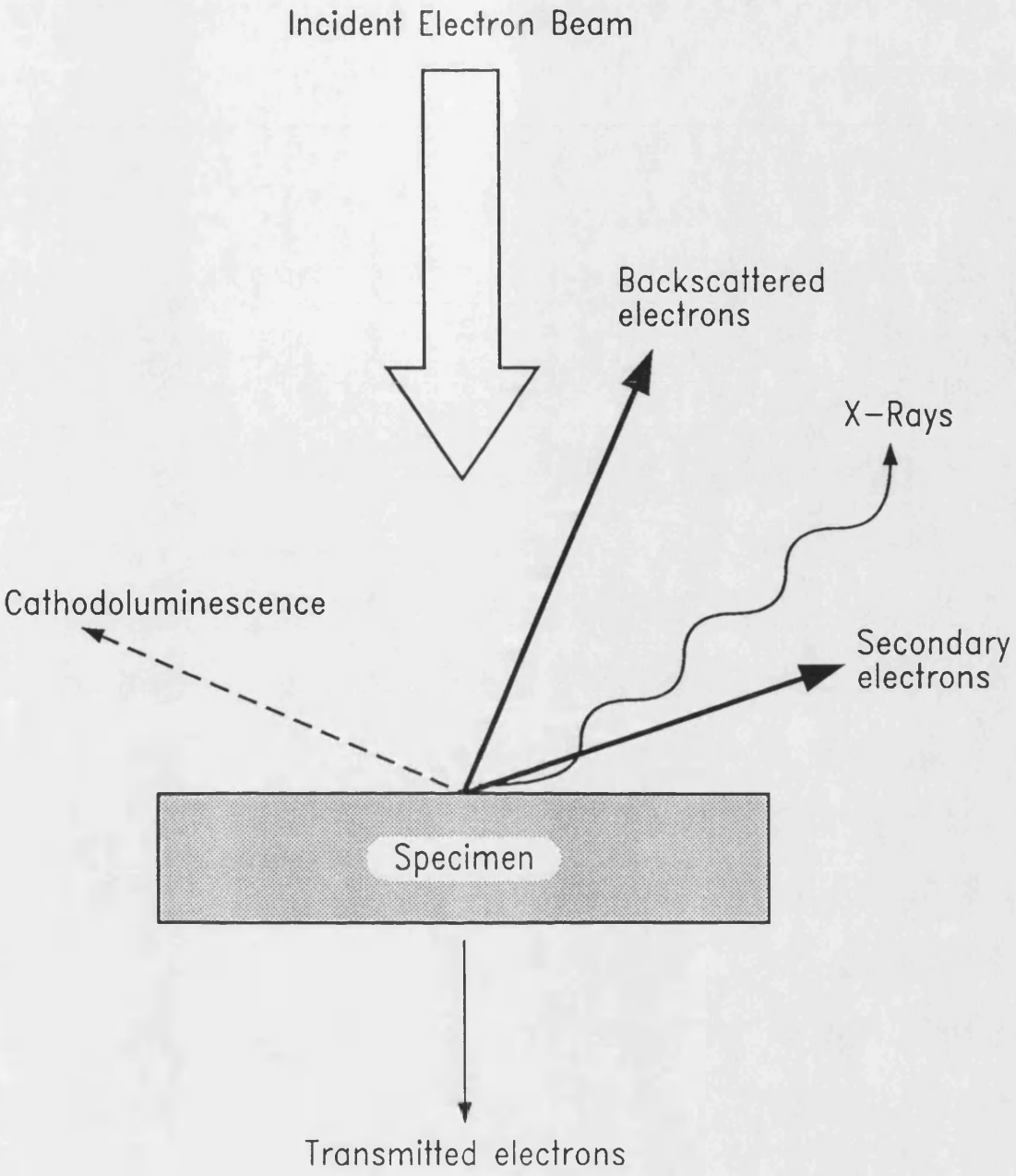

Fig 16 Signals arising from the interaction between specimen and incident electron beam

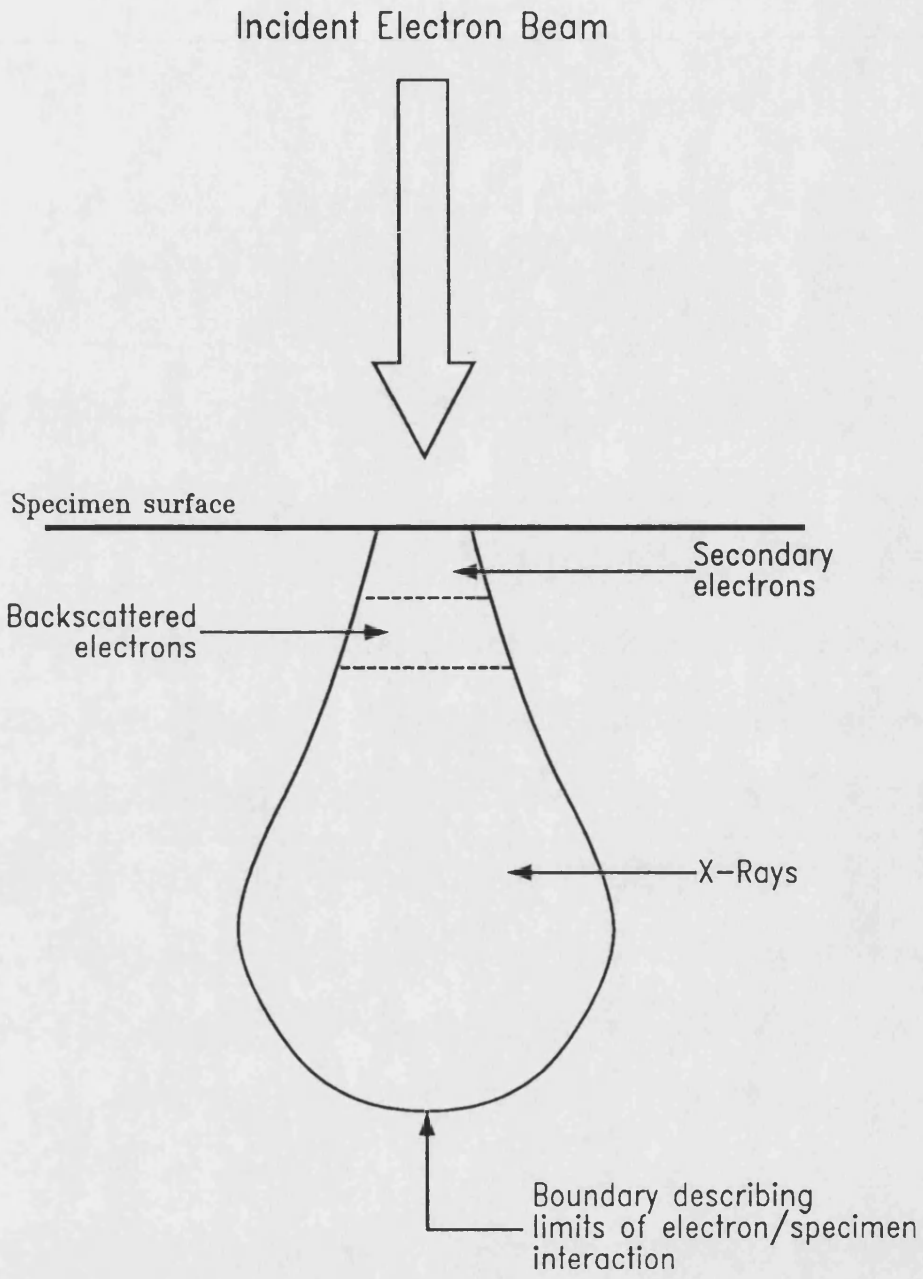

Figure 17: Schematic diagram of the x-ray generation volume within a substrate

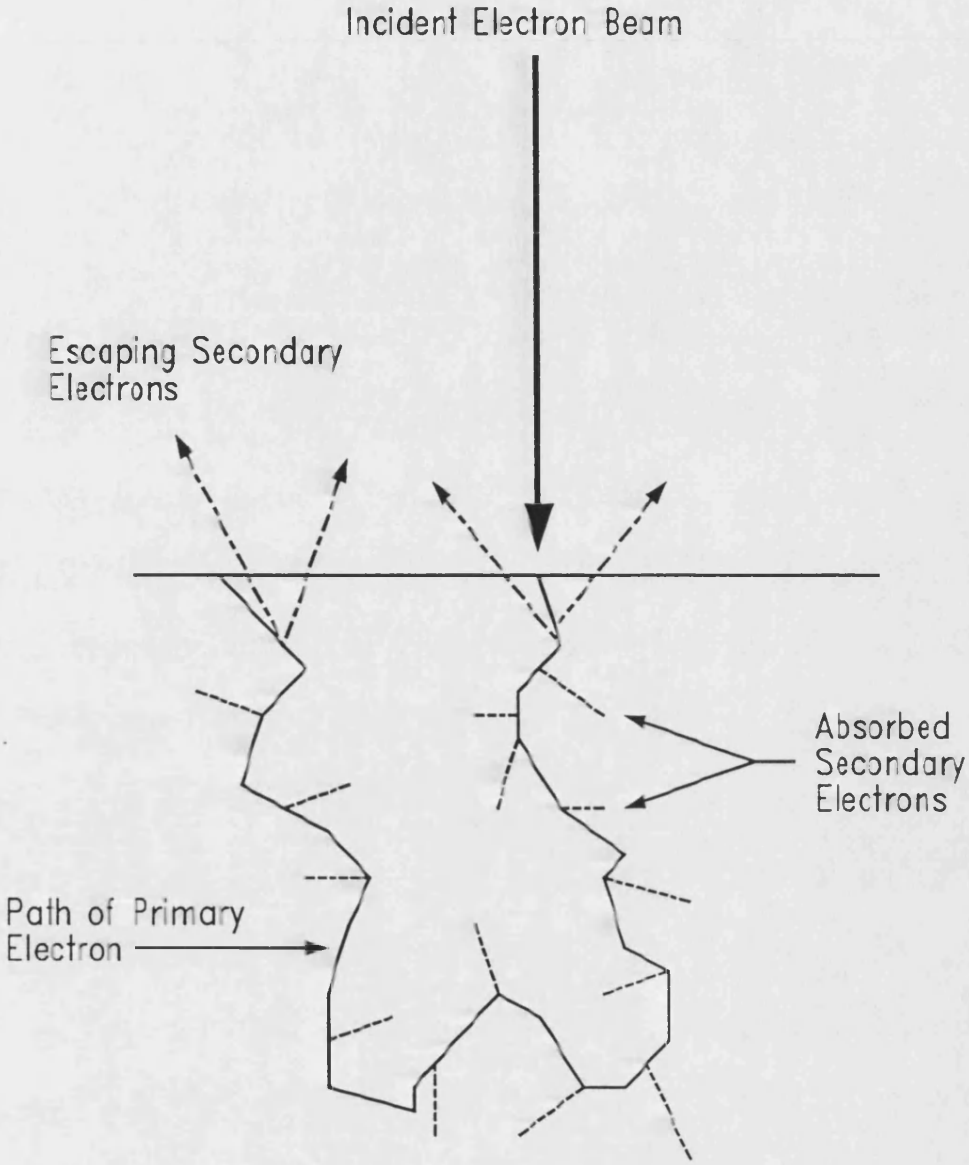

Figure 18: Schematic diagram of the path travelled by an electron in a substrate

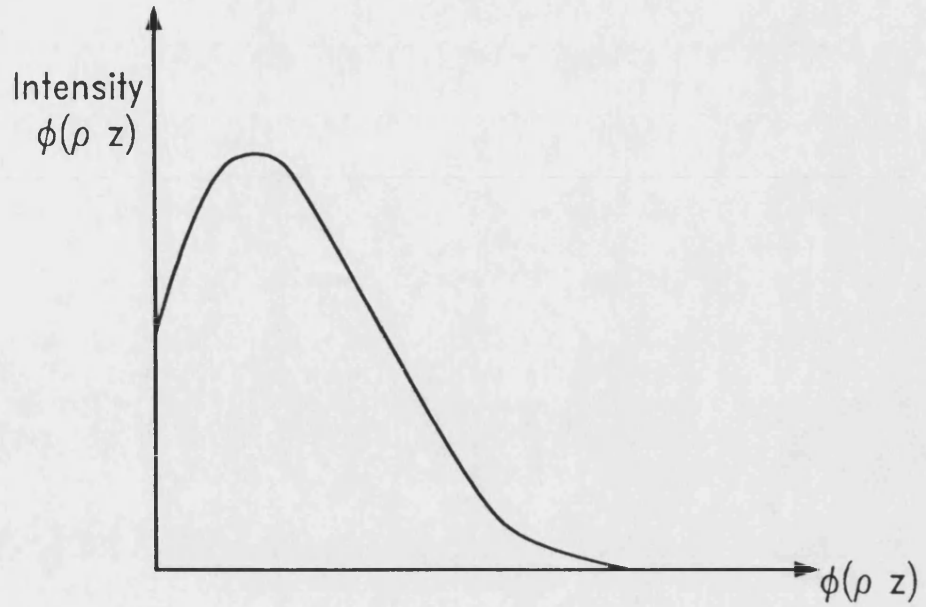

a) Curve showing X-ray intensity vs. Depth

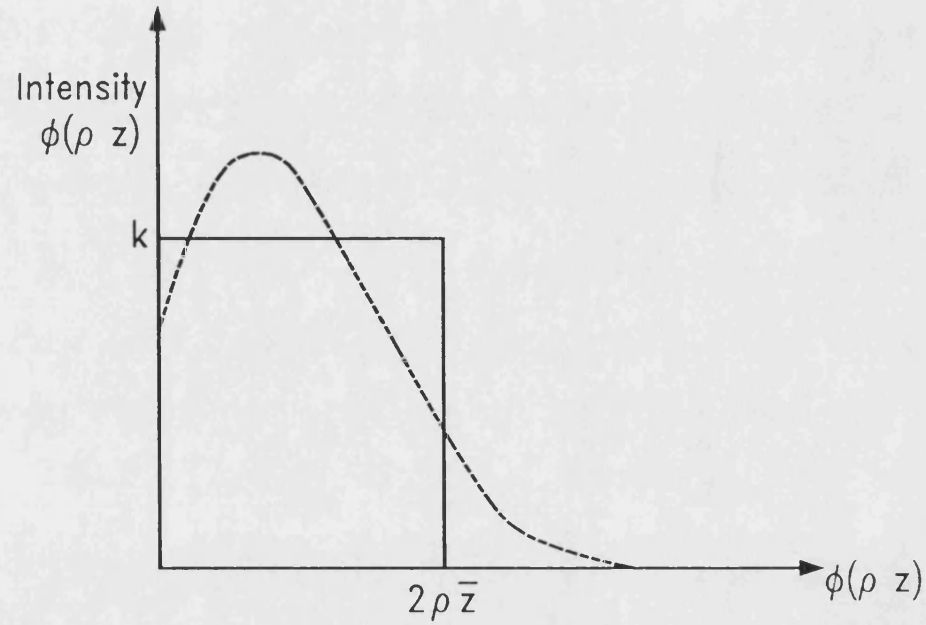

b) Rectangular model for X-ray generation with conventional model superimposed

Figure 19 Examples of $\phi(\rho\ z)$ curves

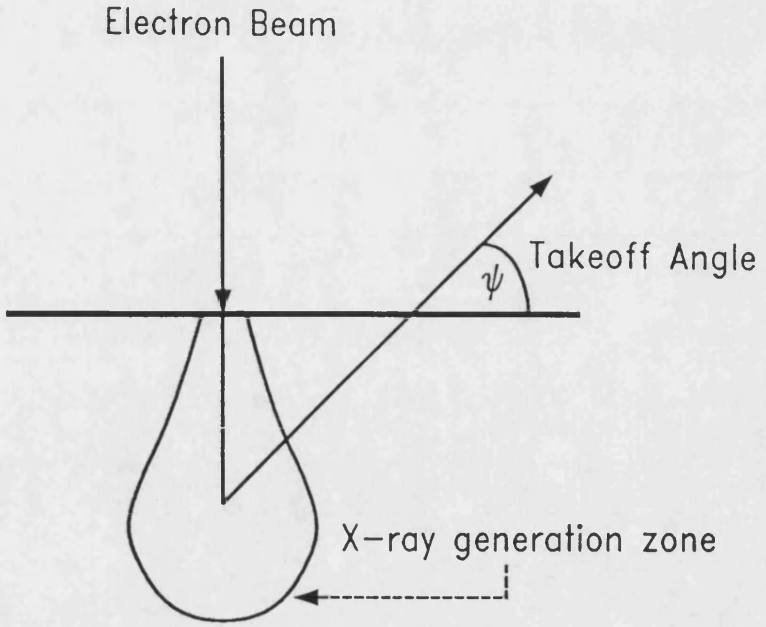

a) Measurement of characteristic Oxygen X-rays from an homogeneous Al_2O_3 standard

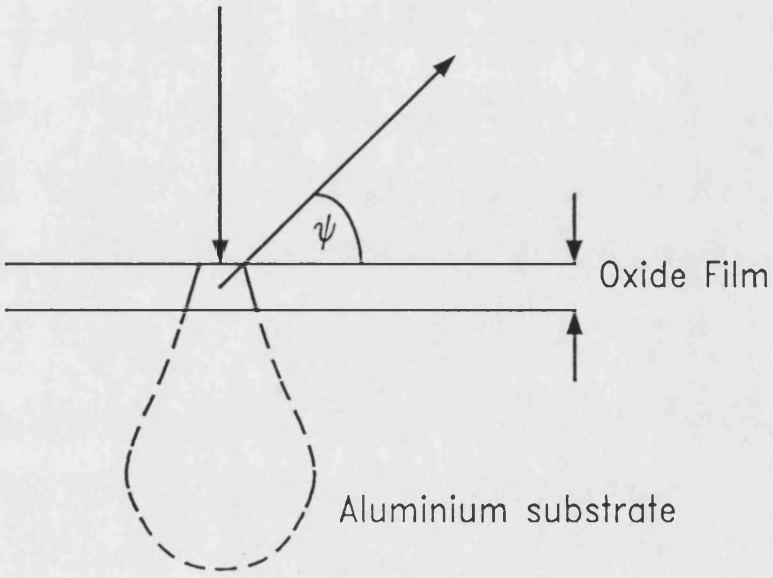

b) Measurement of characteristic Oxygen X-rays from a thin Al_2O_3 film on an aluminium specimen

Figure 20

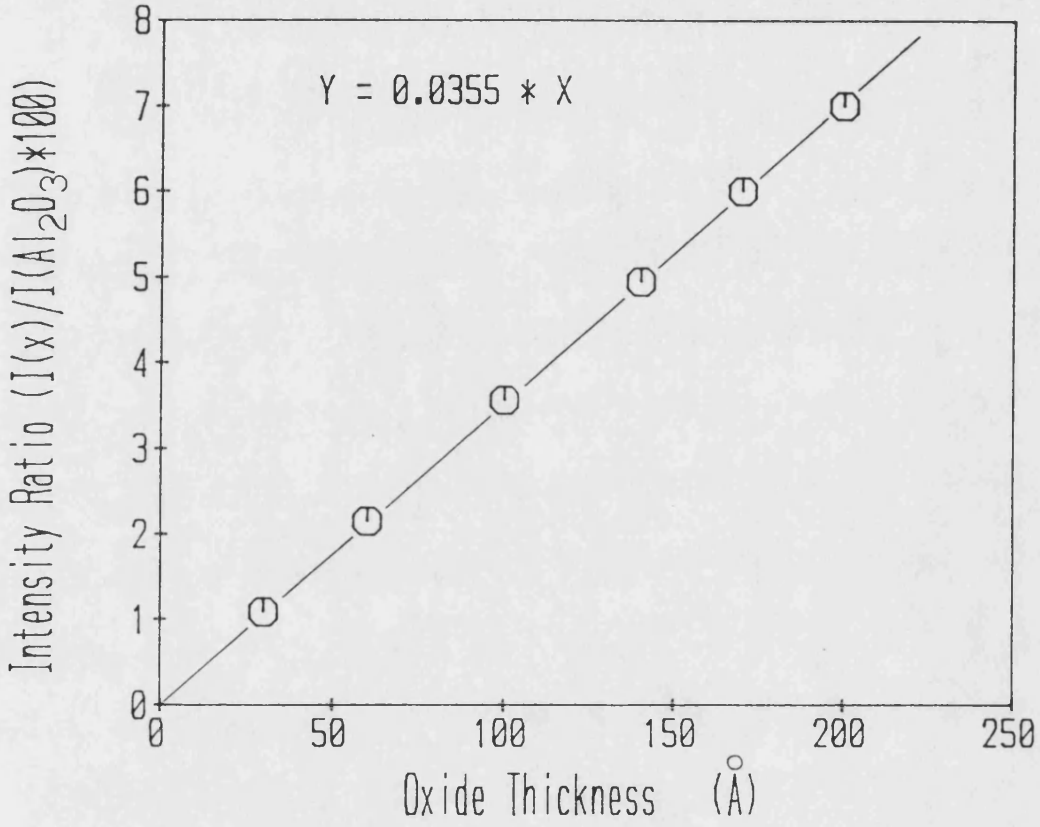

Figure 21: Calibration curve for determining thickness of oxide films in EPMA (Supplied by G. Love, University of Bath).

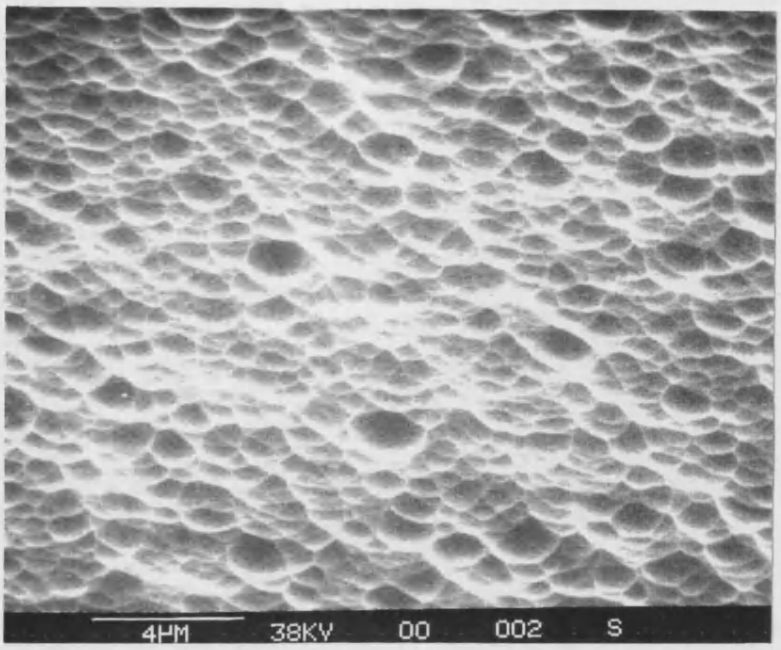

Figure 22a: Microstructure of FPL-etched pure aluminium

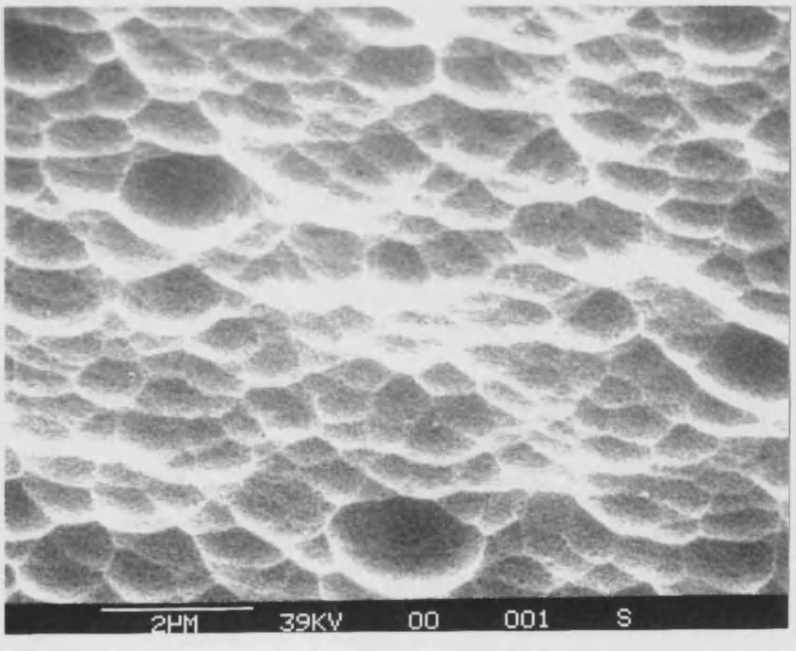

Figure 22b: Higher magnification of FPL-etched pure aluminium

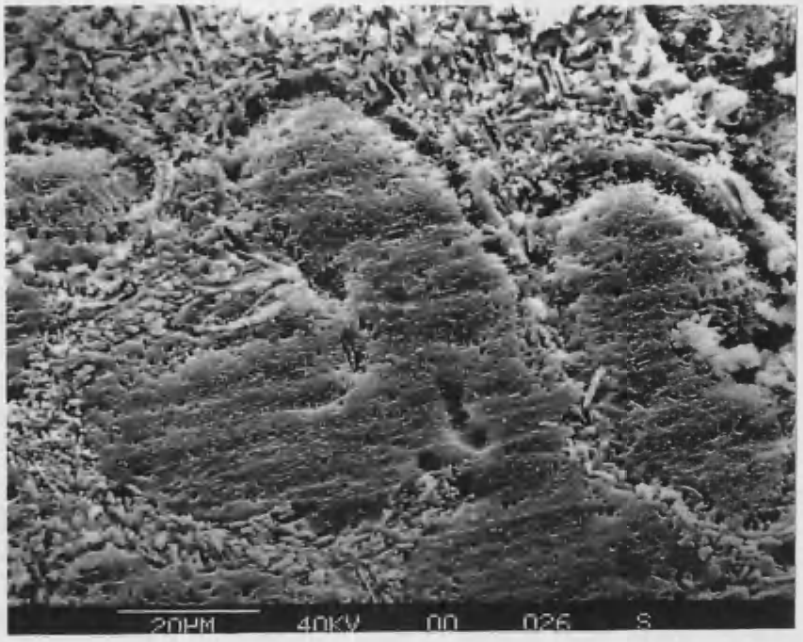

Figure 23a: Microstructure of FPL-etched as-cast A357 alloy

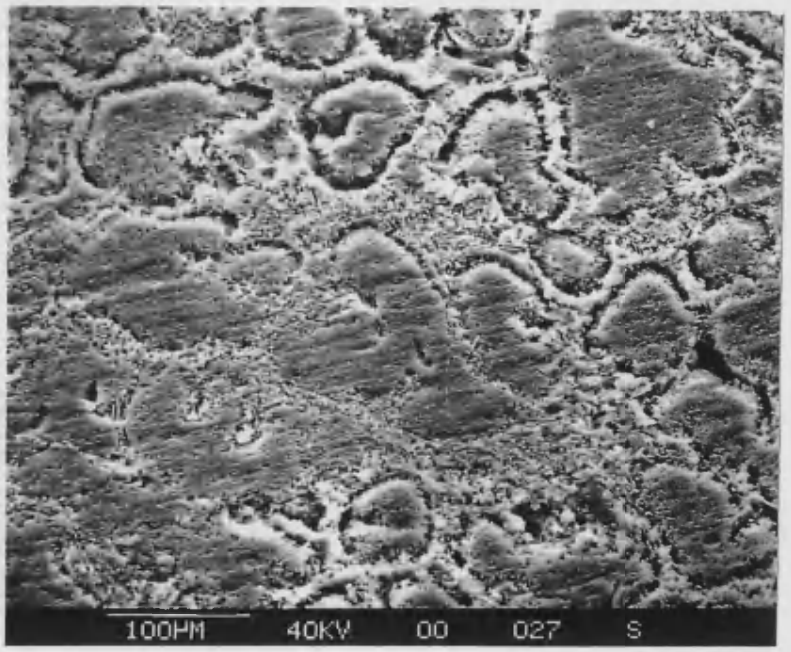

Figure 23b: Microstructure of FPL-etched as-cast A357 alloy

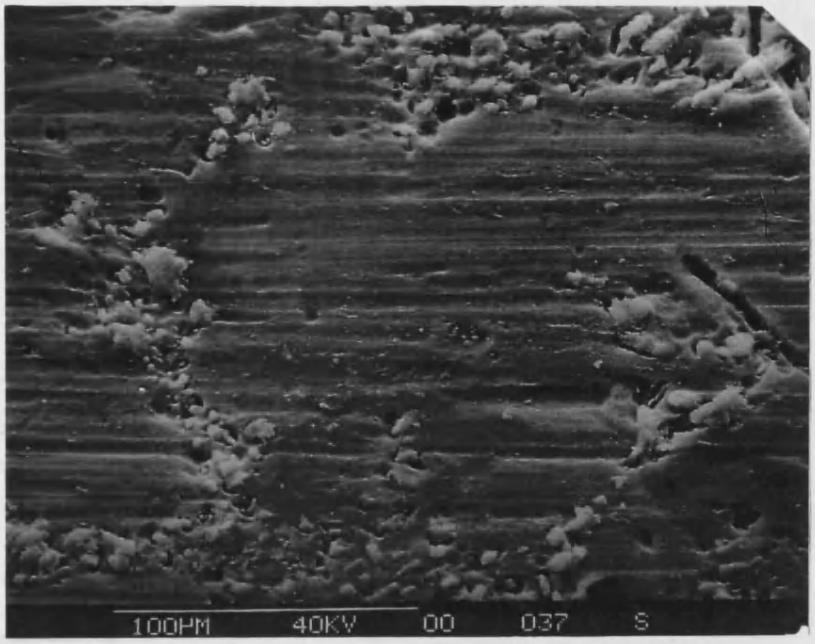

Figure 24a: Microstructure of FPL-etched solution treated A357 alloy

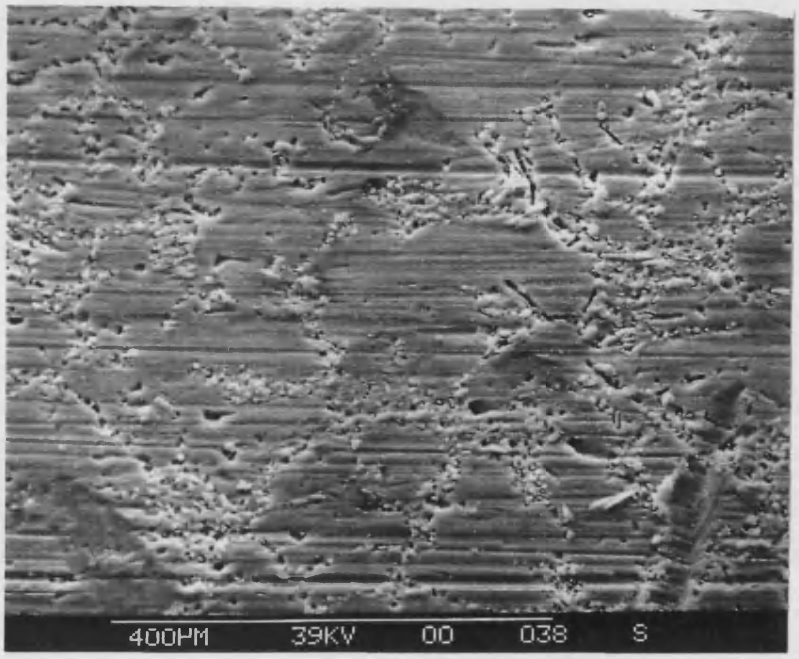

Figure 24b: Microstructure of FPL-etched solution treated A357 alloy

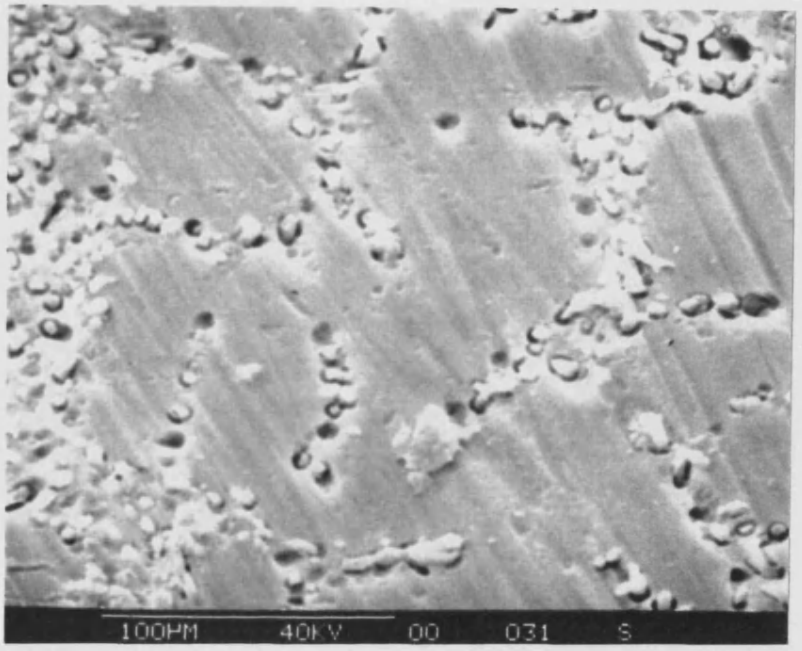

Figure 25: Microstructure of FPL-etched peak aged A357 alloy.

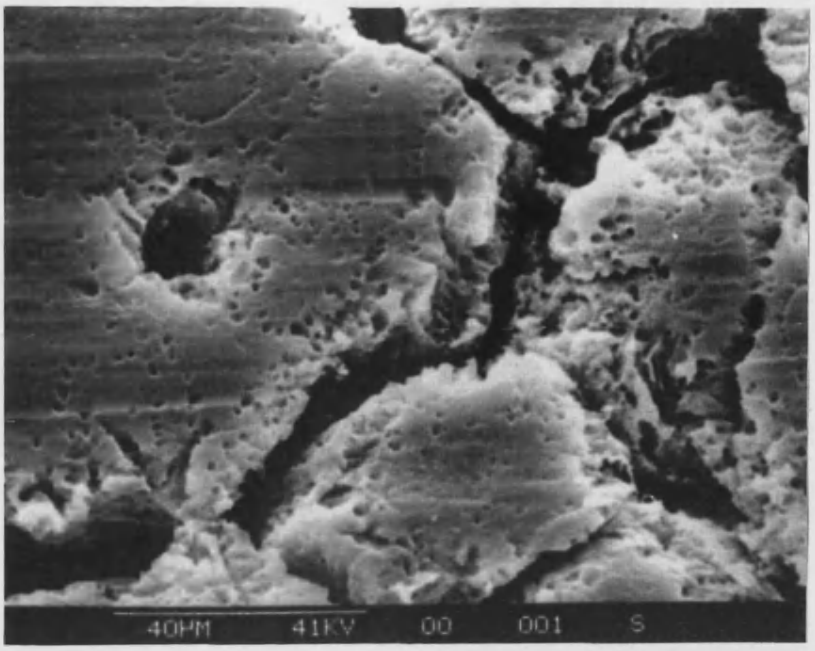

Figure 26a: Microstructure of FPL-etched as-cast ARE 415 alloy

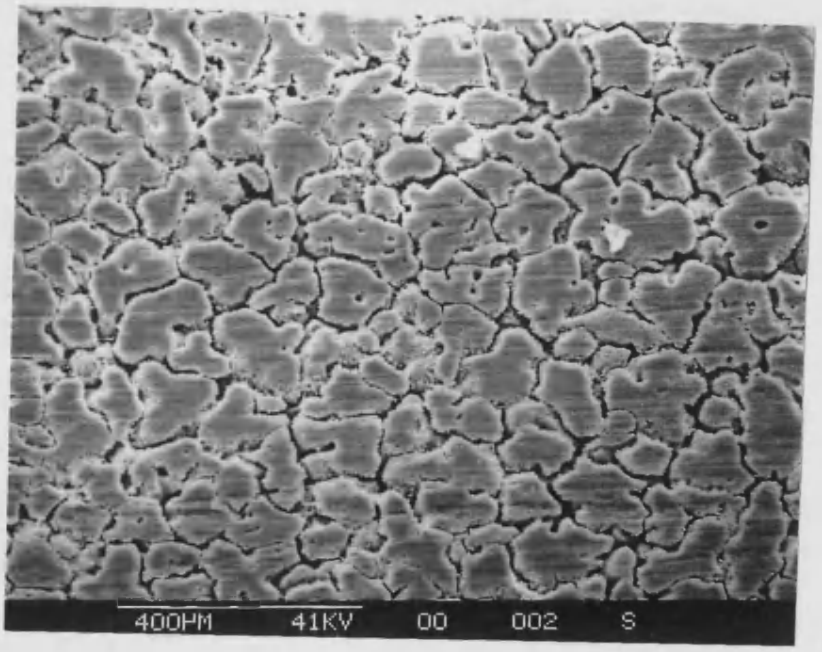

Figure 26b: Microstructure of FPL-etched as-cast ARE 415 alloy

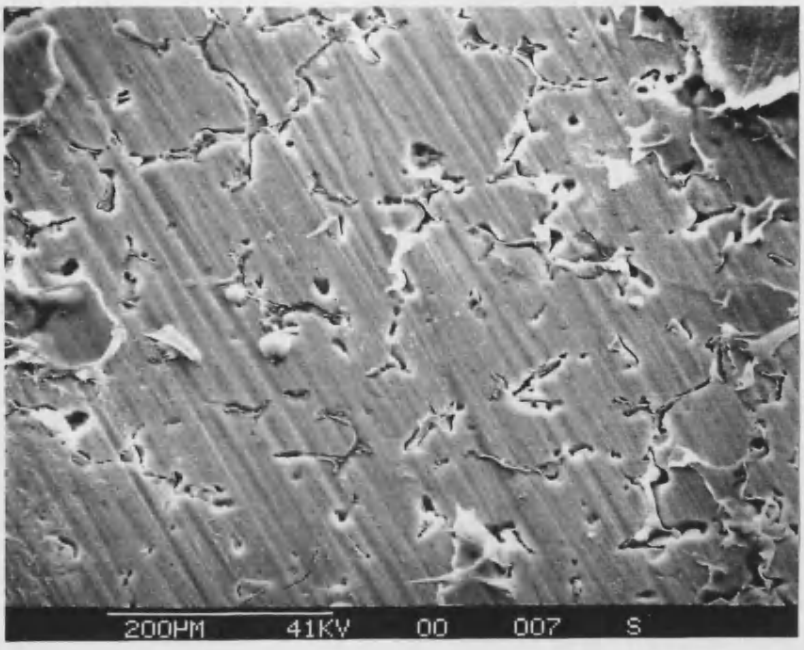

Figure 27a: Microstructure of FPL-etched solution treated ARE 415 alloy

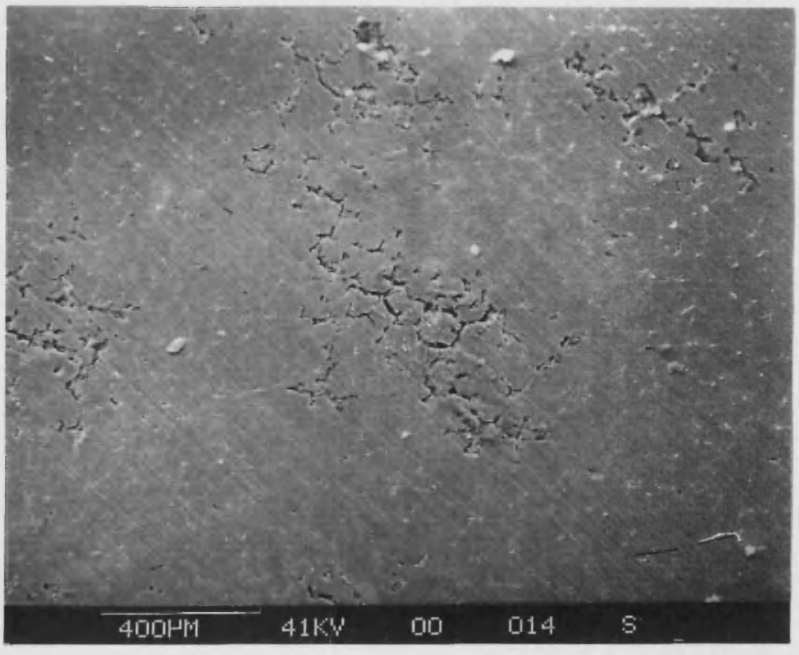

Figure 27b: Microstructure of FPL-etched peak aged ARE 415 alloy

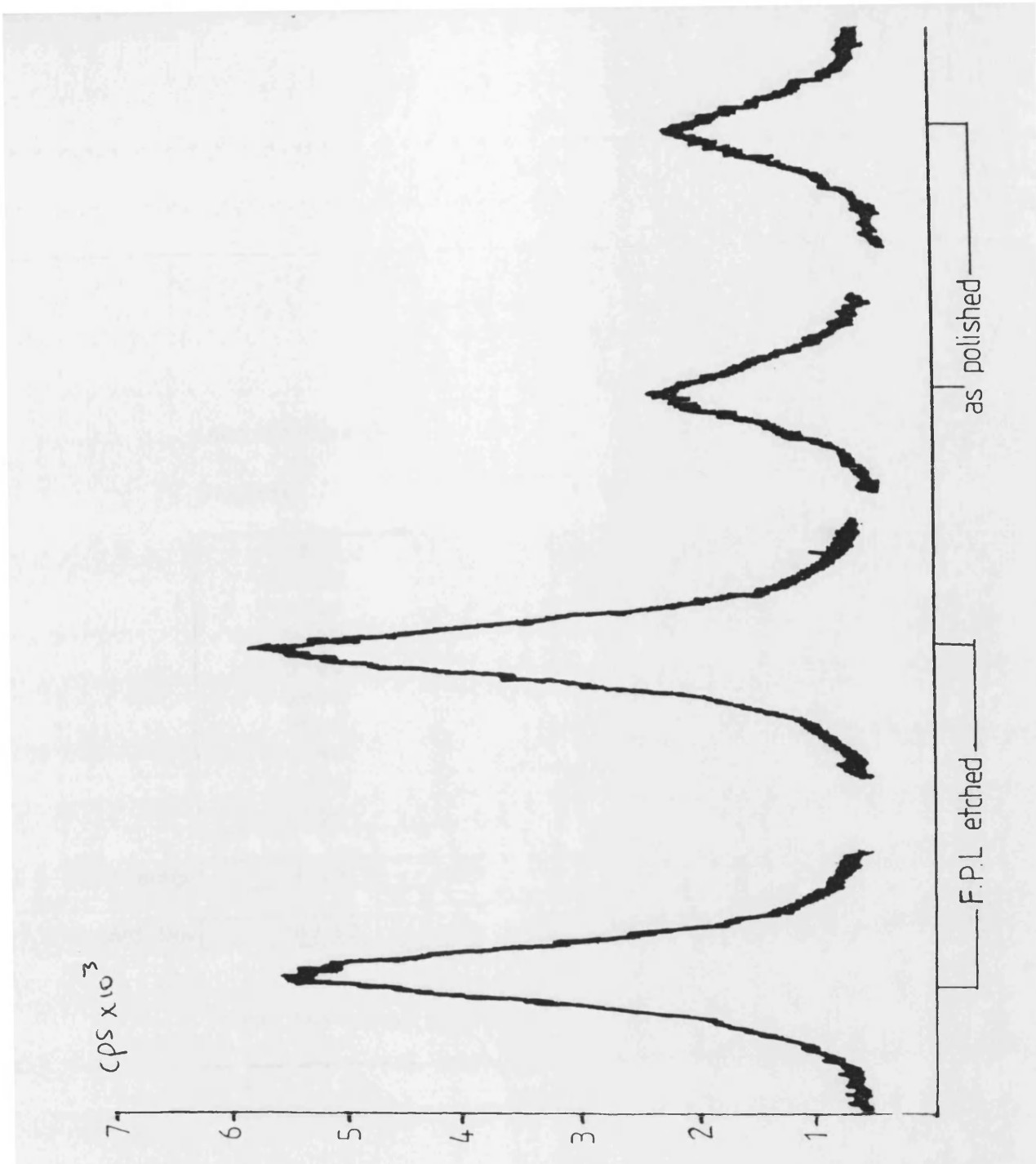

Figure 28: Characteristic x-ray peaks for oxygen taken from FPL-etched and as-polished aluminium

Load at Failure (N)

Unetched	Etched
2900	4000
3000	4300
3200	4200
2900	4500
3100	4450
3650	4600
3700	4500
3150	4350
3000	4750
3650	4400
Average 3225 (N)	4405 (N)
Std. Dev 303.52 (N)	199.31 (N)

t-Test: Two-Sample Assuming Equal Variances

	Unetched	*Etched*
Mean	3225	4405
Observations	10	10
df	18	
t	-9.75	
P(T<=t) two-tail	0.00	
t Critical two-tail	2.10	

Figure 29 FPL etched & Unetched Pure Aluminium (Epoxy Adhesive)

Load at failure (N)

FPL Etched

As Cast	S. Treated	Peak Aged
6550	4200	5400
5550	3400	4800
5600	4700	4900
7100	4300	6600
6800	5100	6700
5200	5900	5000
6500	4700	5700
6700	4600	6500
7200	5200	5100
5200	4000	6300
Average 6240	4610	5700
Std. Dev 734.78	660.98	721.11

Unetched

As Cast	S. Treated	Peak Aged
9000	7800	9050
8200	8500	8400
7800	8400	8000
9200	8150	8500
Average 8550.00	8212.50	8487.50
Std. Dev 572.28	270.13	374.79

Figure 30 Single lap shear strengths for 415 alloy & epoxy adhesive

t-Test: Two-Sample Assuming Equal Variances

	As Cast	*S. Treated*
Mean	6240	4610
Observations	10	10
df	18	
t	4.95	
P(T<=t) two-tail	0.0001	
t Critical two-tail	2.1	

t-Test: Two-Sample Assuming Equal Variances

	S. Treated	*Peak Aged*
Mean	4610	5700
Observations	10	10
df	18	
t	-3.34	
P(T<=t) two-tail	0.0036	
t Critical two-tail	2.1	

t-Test: Two-Sample Assuming Equal Variances

	As Cast	*Peak Aged*
Mean	6240	5700
Observations	10	10
df	18	
t	1.57	
P(T<=t) two-tail	0.13	
t Critical two-tail	2.1	

Figure 31 t-tests for FPL etched 415 alloy & epoxy adhesive

t-Test: Two-Sample Assuming Equal Variances

	Etched As Cast	*Unetched As Cast*
Mean	6240	8550
Observations	10	4
df	12	
t	-5.22	
P(T<=t) two-tail	0.00021	
t Critical two-tail	2.18	

t-Test: Two-Sample Assuming Equal Variances

	Etched S. Treated	*Unetched S. Treated*
Mean	4610	8212.5
Observations	10	4
df	12	
t	-9.77	
P(T<=t) two-tail	4.60E-07	
t Critical two-tail	2.18	

t-Test: Two-Sample Assuming Equal Variances

	Etched P. Aged	*Unetched P. Aged*
Mean	5700	8487.5
Observations	10	4
df	12	
t	-6.8	
P(T<=t) two-tail	0.000019	
t Critical two-tail	2.18	

Figure 32 t-tests for FPL etched and Unetched 415 alloy & epoxy adhesive

Load at failure (N)

FPL Etched

As Cast	S. Treated	Peak Aged
5500	9500	6300
3300	8100	6100
6100	9400	7700
5300	9300	8200
3800	6100	5800
5900	8500	8300
6100	9000	7300
4000	7800	6500
4500	8900	6700
5600	7900	7400
Average 5010	8450	7030
Std. Dev 975.14	980.05	833.13

Unetched

As Cast	S. Treated	Peak Aged
5900	7000	9800
5800	9500	8500
6800	9800	7400
Average 6166.67	8766.67	8566.67
Std. Dev 449.69	1255.21	980.93

Figure 33 Single lap shear strengths for 357 alloy & epoxy adhesive

t-Test: Two-Sample Assuming Equal Variances

	As Cast	*S. Treated*
Mean	5010	8450
Observations	10	10
df	18	
t	-7.46	
P(T<=t) two-tail	6.48E-07	
t Critical two-tail	2.1	

t-Test: Two-Sample Assuming Equal Variances

	S. Treated	*Peak Aged*
Mean	8450	7030
Observations	10	10
df	18	
t	3.31	
P(T<=t) two-tail	0.0039	
t Critical two-tail	2.1	

t-Test: Two-Sample Assuming Equal Variances

	As Cast	*Peak Aged*
Mean	5010	7030
Observations	10	10
df	18	
t	-4.72	
P(T<=t) two-tail	0.00017	
t Critical two-tail	2.1	

Figure 34 t-tests for 357 alloy & epoxy adhesive

t-Test: Two-Sample Assuming Equal Variances

	Etched As Cast	*Unetched As Cast*
Mean	5010	6166.67
Observations	10	3
df	11	
t	-1.83	
P(T<=t) two-tail	0.094	
t Critical two-tail	2.2	

t-Test: Two-Sample Assuming Equal Variances

	Etched S.Treated	*Unetched S.Treated*
Mean	8450	8766.67
Observations	10	3
df	11	
t	-0.42	
P(T<=t) two-tail	0.68	
t Critical two-tail	2.2	

t-Test: Two-Sample Assuming Equal Variances

	Etched P. Aged	*Unetched P. Aged*
Mean	7030	8566.67
Observations	10	3
df	11	
t	-2.47	
P(T<=t) two-tail	0.031	
t Critical two-tail	2.2	

Figure 35 t-tests for FPL etched and Unetched 357 alloy & epoxy adhesive

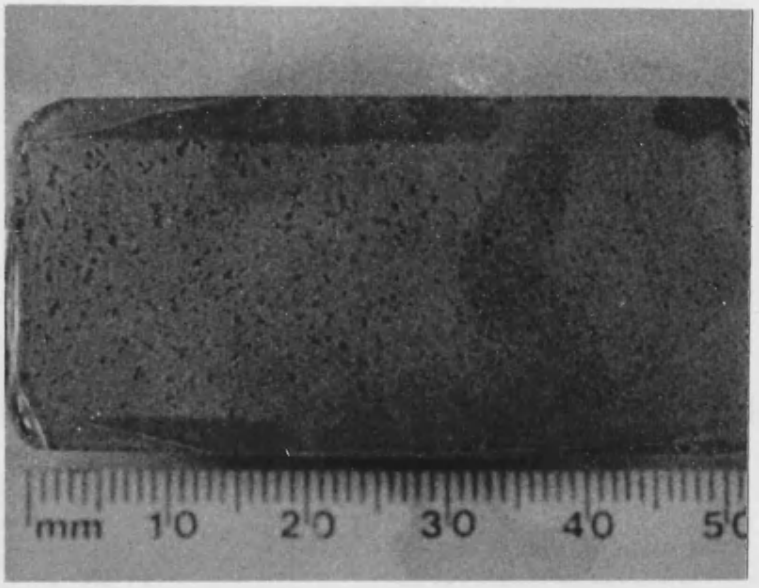

Figure 36a: Trapped/outgassed air visible through a glass slide adhesively bonded to a specimen of FPL-etched A357.

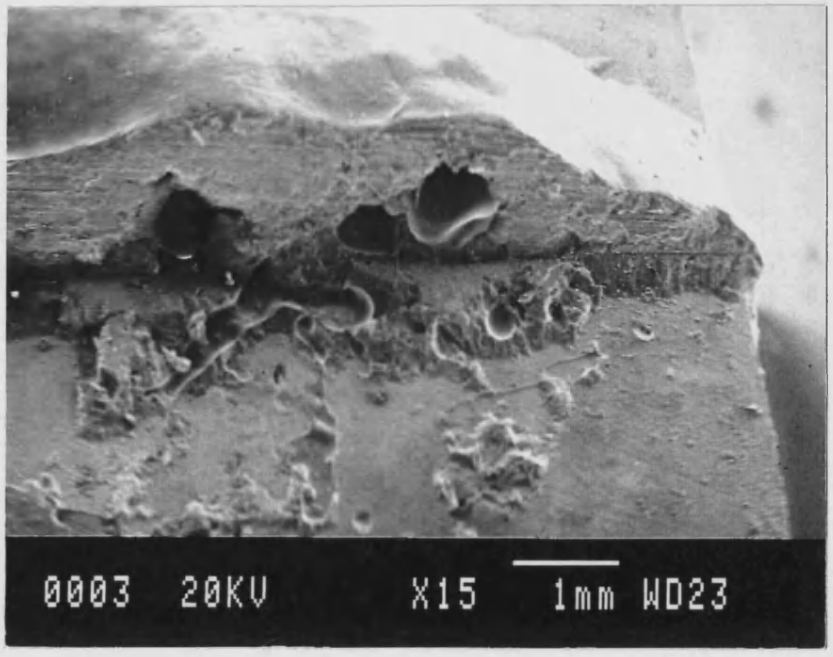

Figure 36b: Air pockets trapped within adhesive spew fillet, SEM micrograph.

Load at failure (N)

As-cast	S. Treated	Peak Aged
3200	1200	5500
4900	3200	3000
5100	2400	3100
4200	3600	2500
4700	3000	3300
3900	3100	4500
4200	2500	2400
4400	2700	2700
5200	2000	4100
3400	3400	2800
Average 4320	2710	3390
Std. Dev 646.22	683.30	950.21

Figure 37 FPL etched 415 alloy & acrylic adhesive

t-Test: Two-Sample Assuming Equal Variances

	As Cast	*S. Treated*
Mean	4320	2710
Observations	10	10
df	18	
t	5.14	
P(T<=t) two-tail	0.000069	
t Critical two-tail	2.1	

t-Test: Two-Sample Assuming Equal Variances

	S. Treated	*Peak Aged*
Mean	2710	3390
Observations	10	10
df	18	
t	-1.74	
P(T<=t) two-tail	0.098	
t Critical two-tail	2.1	

t-Test: Two-Sample Assuming Equal Variances

	As Cast	*Peak Aged*
Mean	4320	3390
Observations	10	10
df	18	
t	2.43	
P(T<=t) two-tail	0.026	
t Critical two-tail	2.1	

Figure 38 t-tests for 415 alloy & acrylic adhesive

Load at Failure (N)

As Cast	S. Treated	Peak Aged
5000	4200	4500
3000	3700	3900
4400	4900	5000
3600	3400	3500
4700	4800	3300
3300	3700	5100
4100	4700	3800
3900	5000	4600
2400	3300	3600
3800	4100	4900
Average 3820	4180	4220
Std. Dev 748.06	607.95	640.00

Figure 39 FPL etched 357 alloy & acrylic adhesive

t-Test: Two-Sample Assuming Equal Variances

	As Cast	*S. Treated*
Mean	3820	4180
Observations	10	10
df	18	
t	-1.12	
P(T<=t) two-tail	0.28	
t Critical two-tail	2.10	

t-Test: Two-Sample Assuming Equal Variances

	S. Treated	*Peak Aged*
Mean	4180	4220
Observations	10	10
df	18	
t	-0.14	
P(T<=t) two-tail	0.89	
t Critical two-tail	2.10	

t-Test: Two-Sample Assuming Equal Variances

	As Cast	*Peak Aged*
Mean	3820	4220
Observations	10	10
df	18	
t	-1.22	
P(T<=t) two-tail	0.24	
t Critical two-tail	2.10	

Figure 40 t-tests for 357 alloy & acrylic adhesive

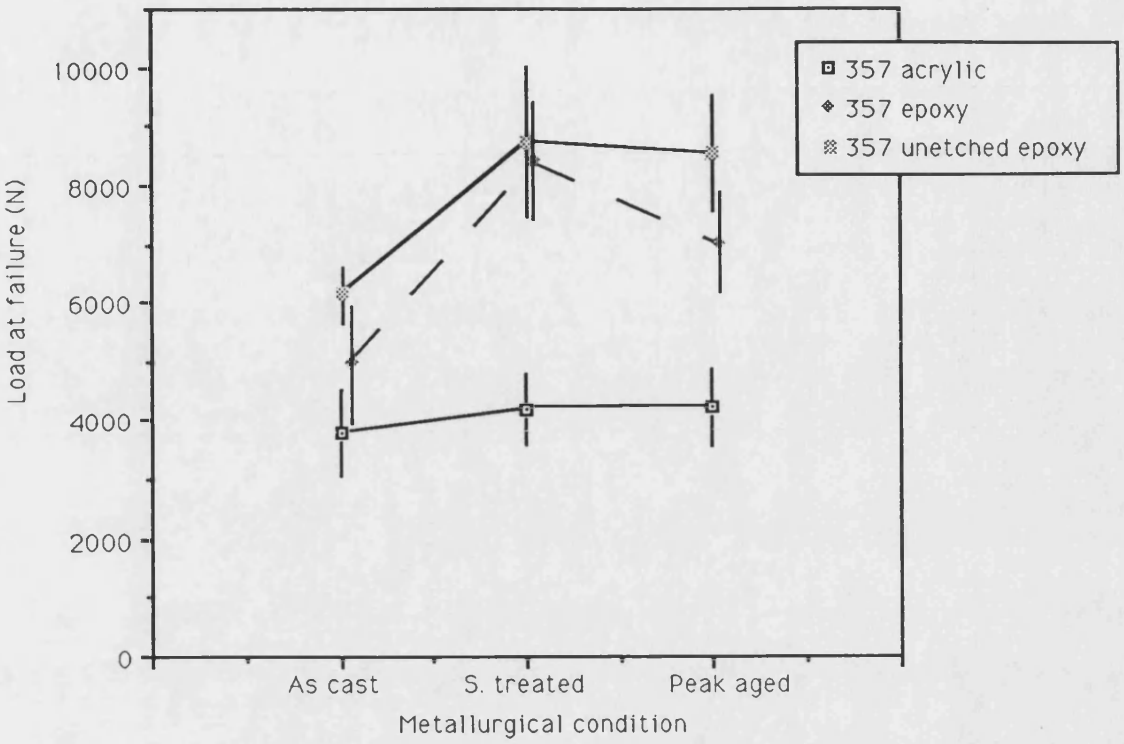

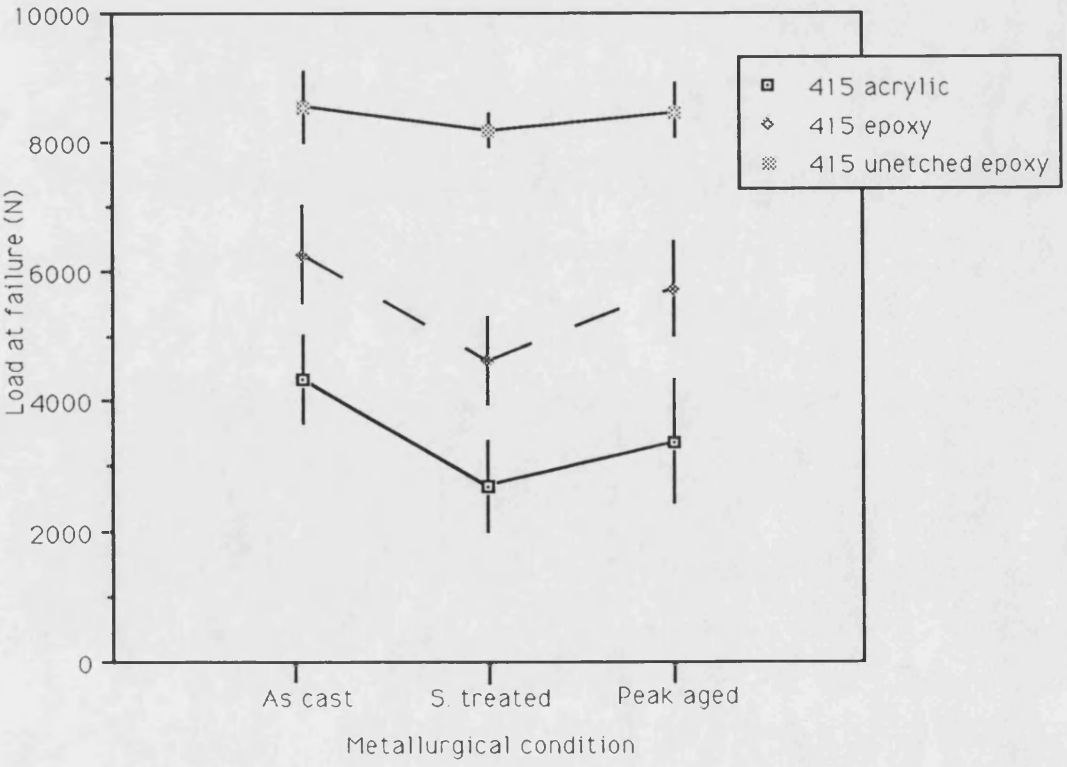

Figure 41: Graphical representation of adhesive bond data

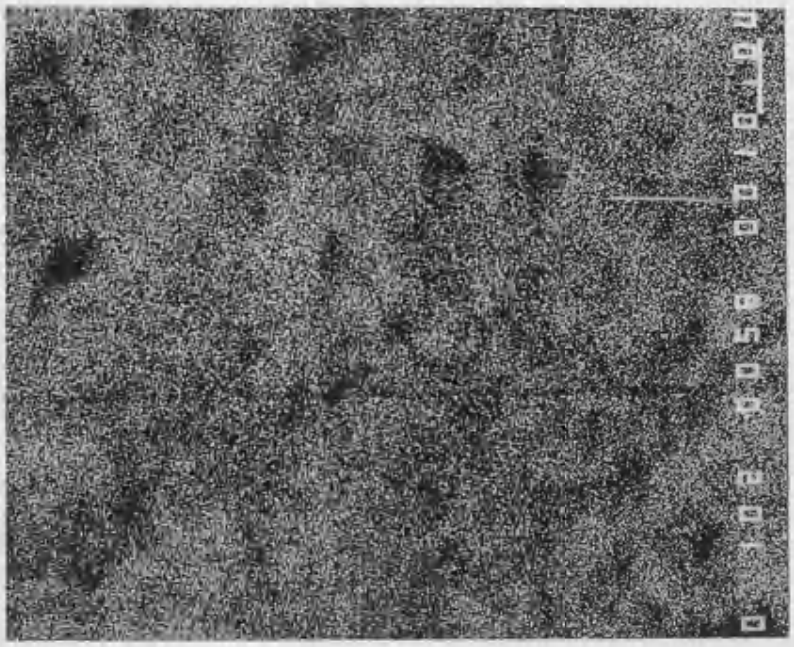

Figure 42a: X-ray map indicating distribution of carbon on sample. Magnification x1000

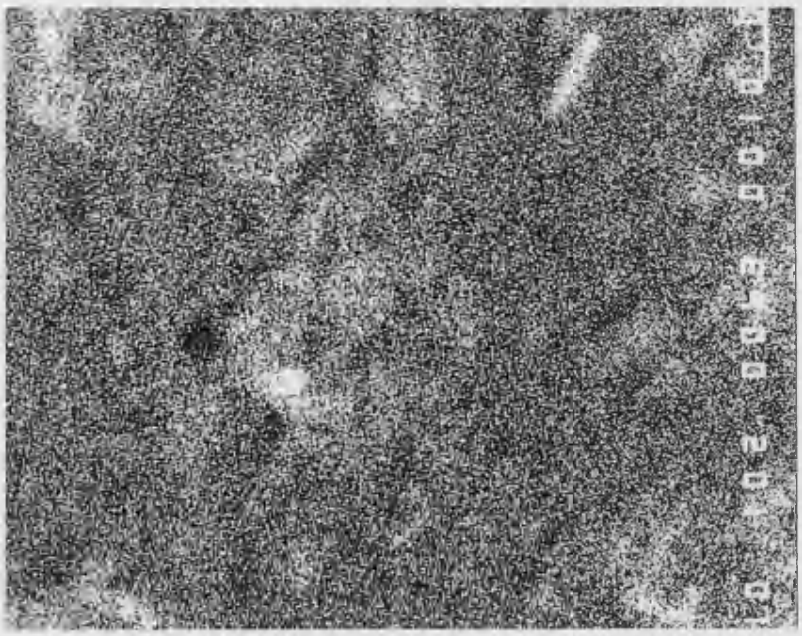

Figure 42b: X-ray map indicating distribution of oxygen on sample surface. Magnification x1000

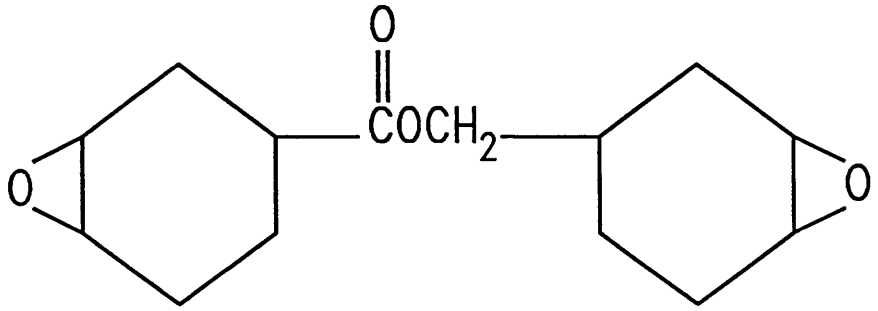

Figure 43: Example of a di-functional epoxy polymer

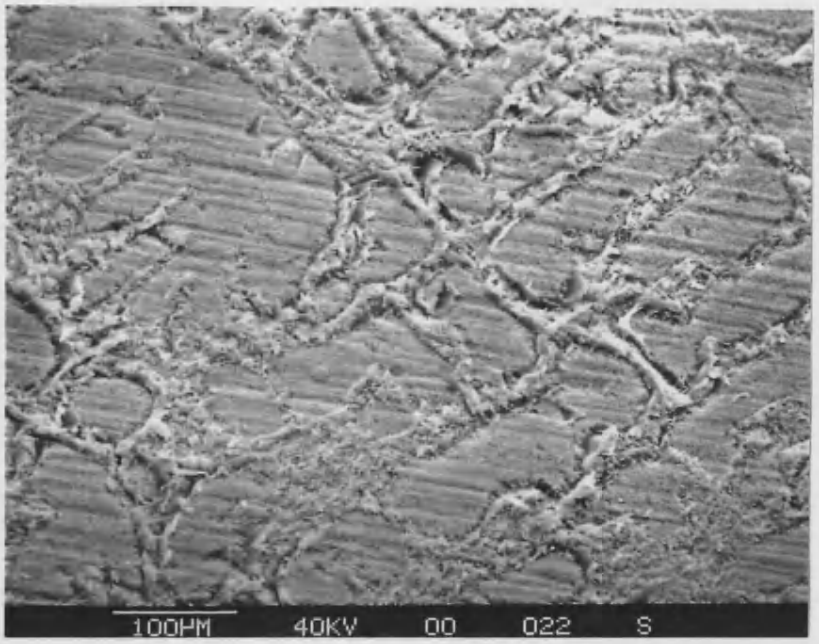

Figure 44a: Retained acrylic adhesive, FPL-etched A357 alloy

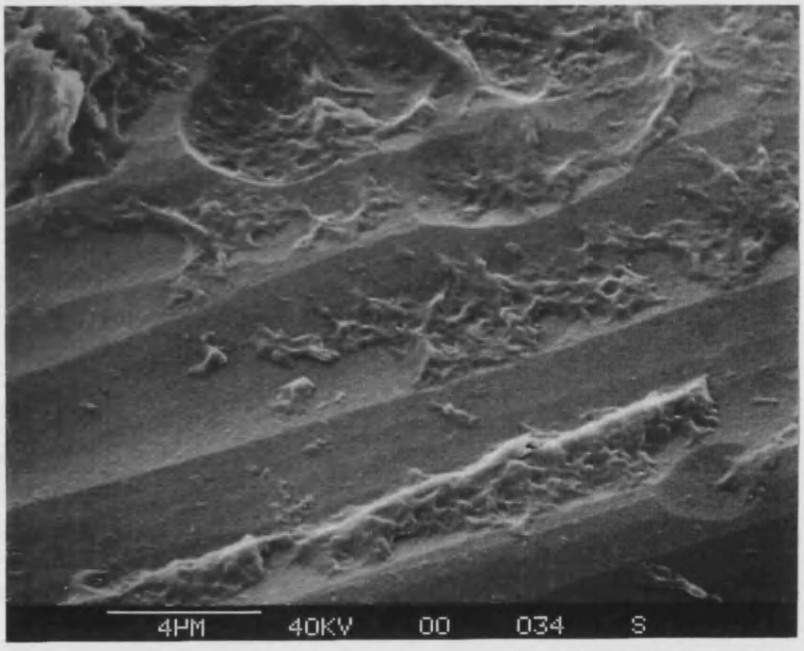

Figure 44b: Retained acrylic adhesive, FPL-etched A357 alloy

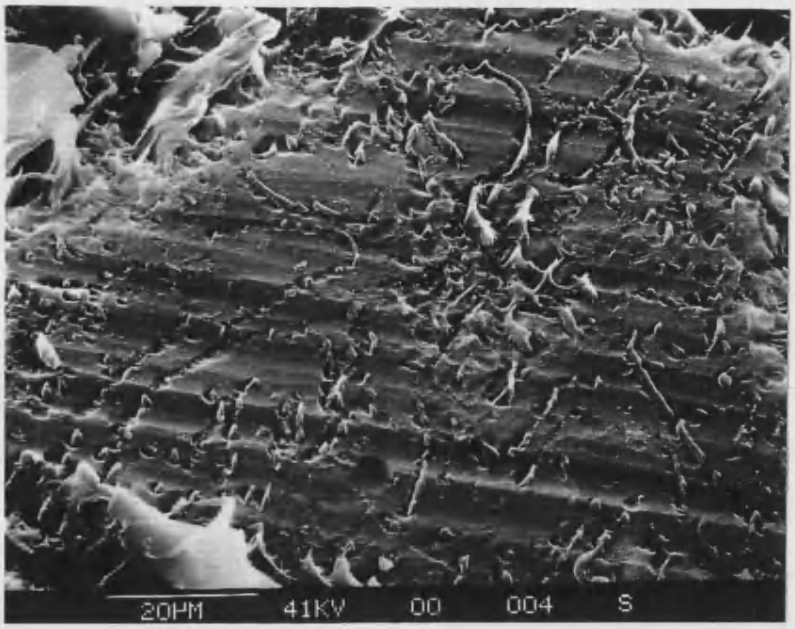

Figure 45a: Retained acrylic adhesive, FPL-etched ARE 415 alloy

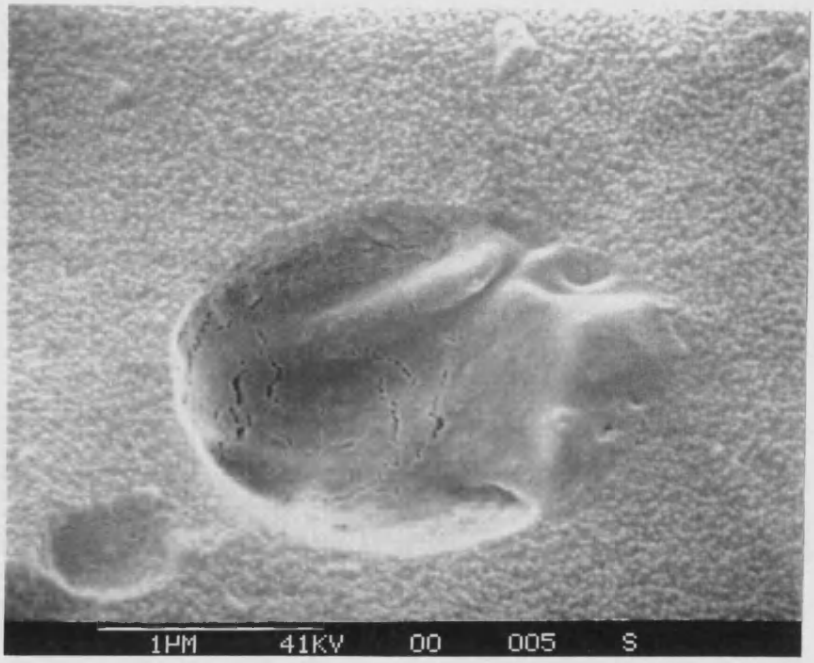

Figure 45b: Retained acrylic adhesive, FPL-etched ARE 415 alloy

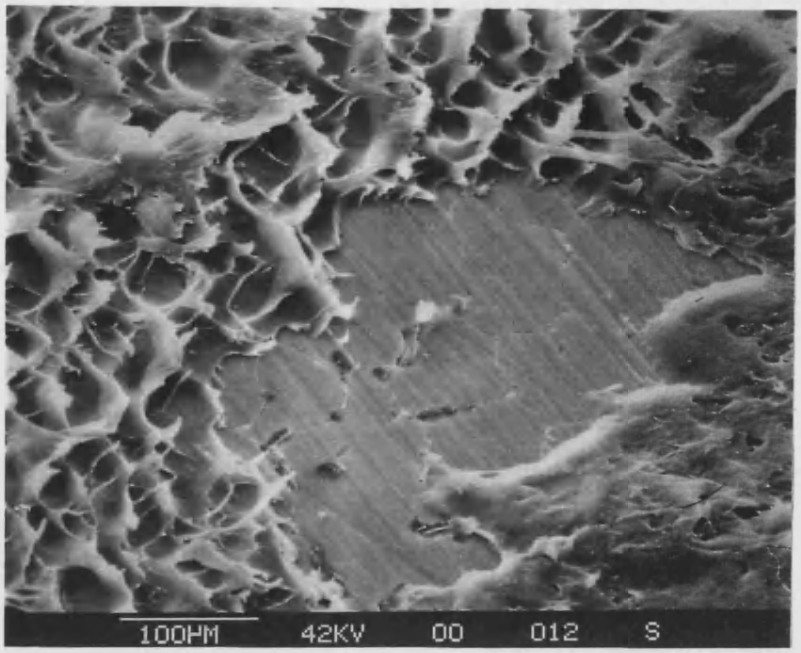

Figure 46a: Mixed mode failure, acrylic adhesive

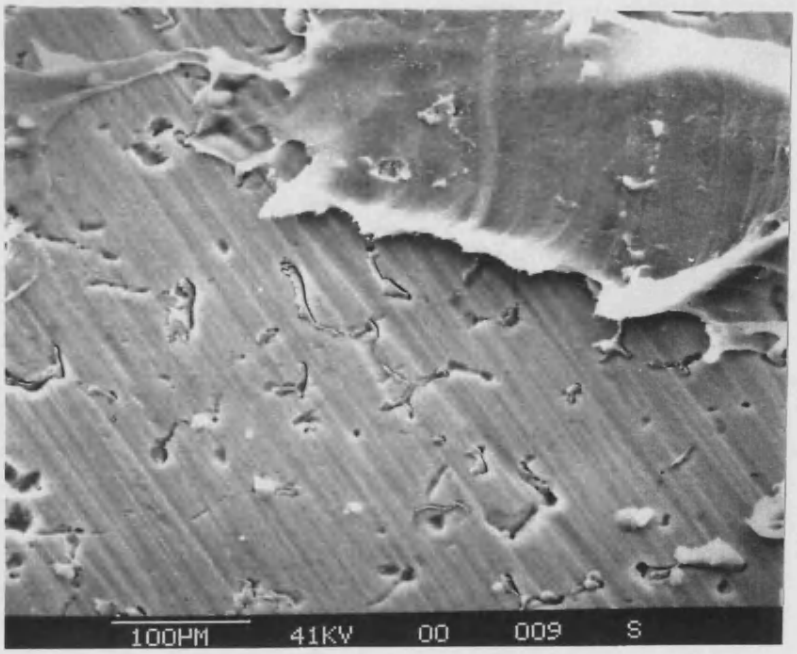

Figure 46b: Mixed mode failure, acrylic adhesive

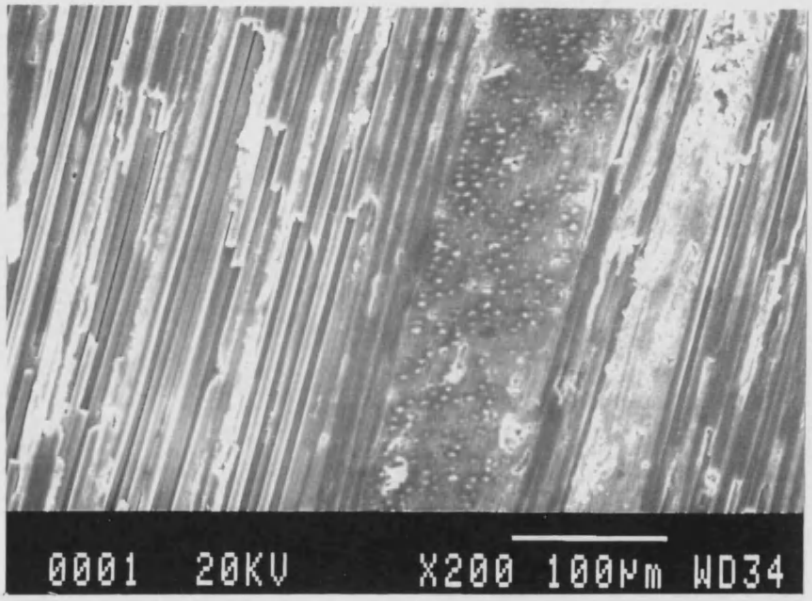

Figure 47: Surface of carbon-reinforced A357 mechanically prepared to a 600-grit finish, SEM micrograph.

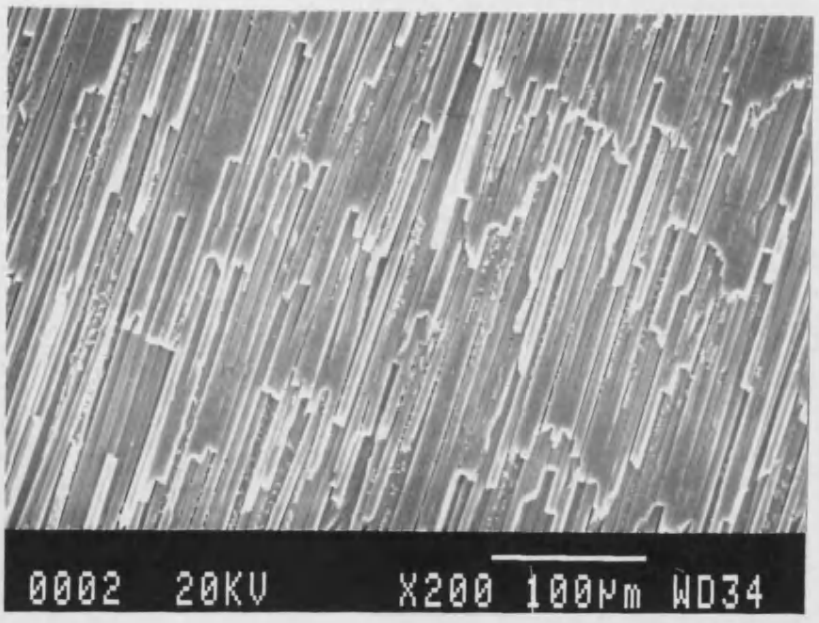

Figure 48a: Removal of matrix alloy from surface of carbon-reinforced A357 etched in the FPL solution, SEM micrograph.

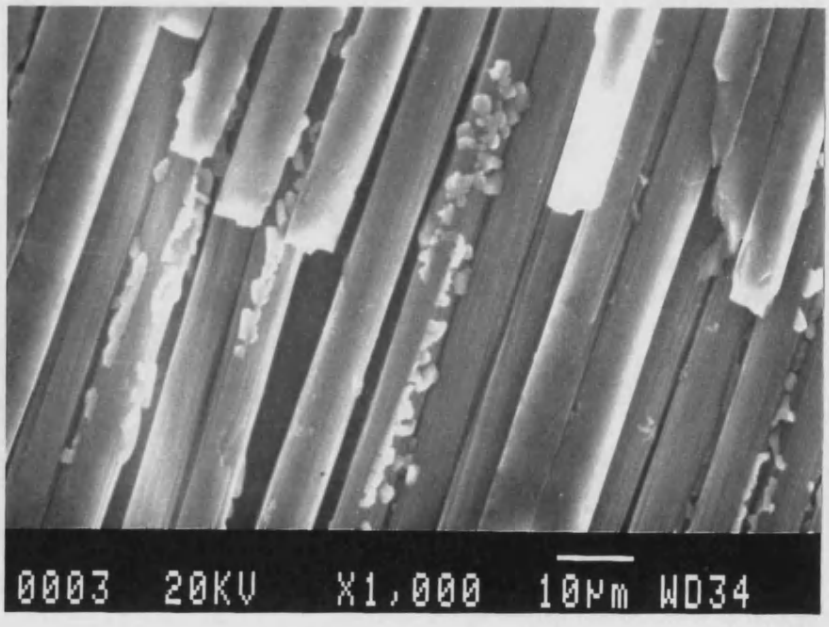

Figure 48b: Removal of matrix alloy from surface of carbon-reinforced A357 etched in the FPL solution, SEM micrograph.

Figure 49: Collage showing tensile- and interlaminar-type failures in adhesively bonded composite material, SEM micrographs.

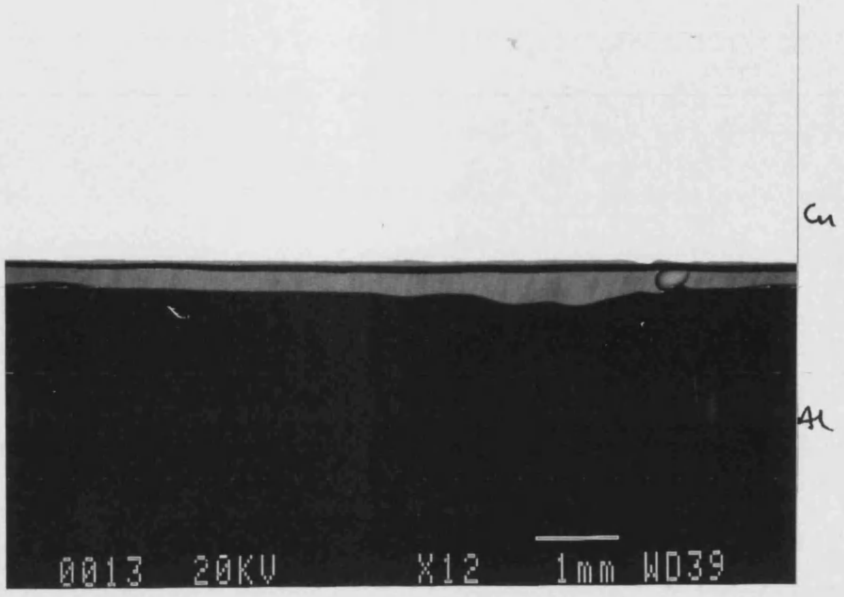

Figure 50a: Model diffusion bond, pure aluminium + pure copper

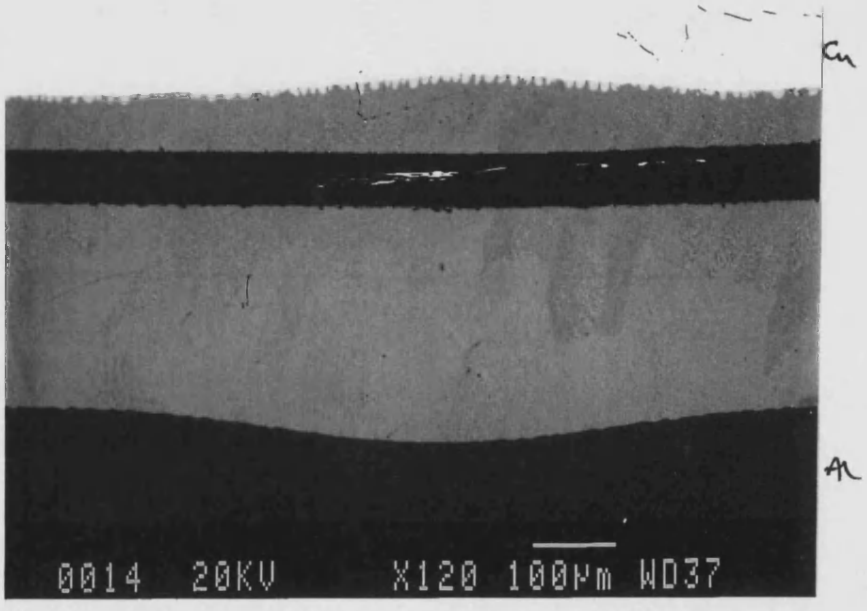

Figure 50b: Model diffusion bond, pure aluminium + pure copper

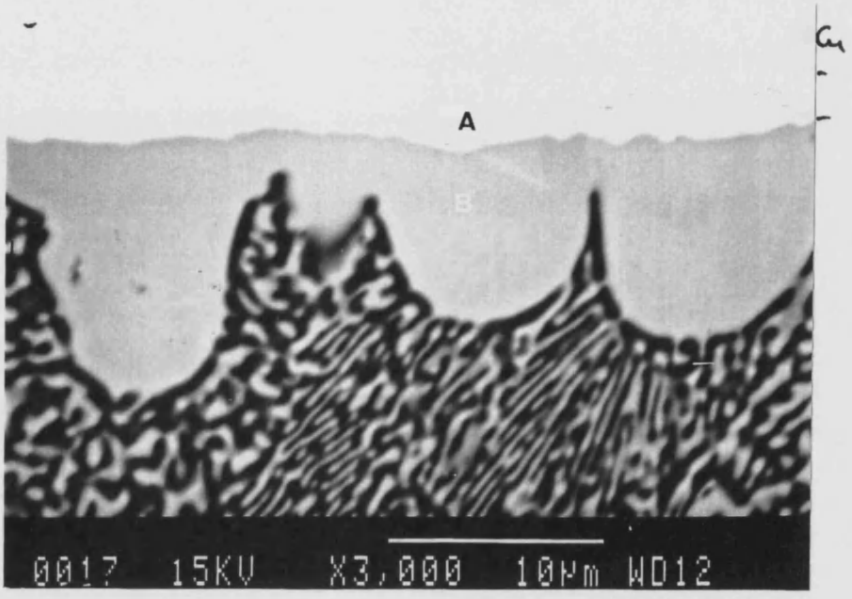

Figure 51: Structure of reaction layers formed during diffusion bonding of pure copper and pure aluminium, backscattered SEM micrograph.

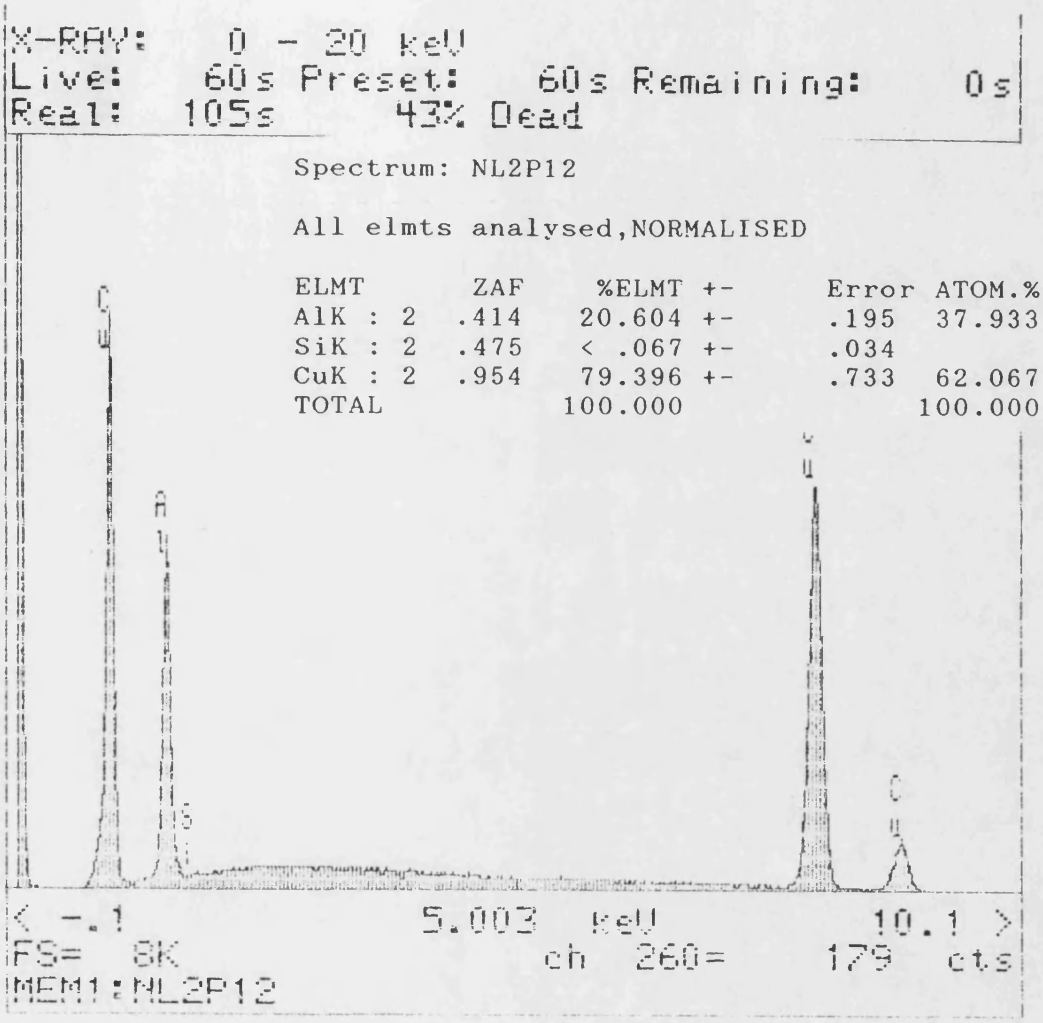

Figure 52: Energy dispersive spectrum for position A in figure 51, indicating formation of δ phase.

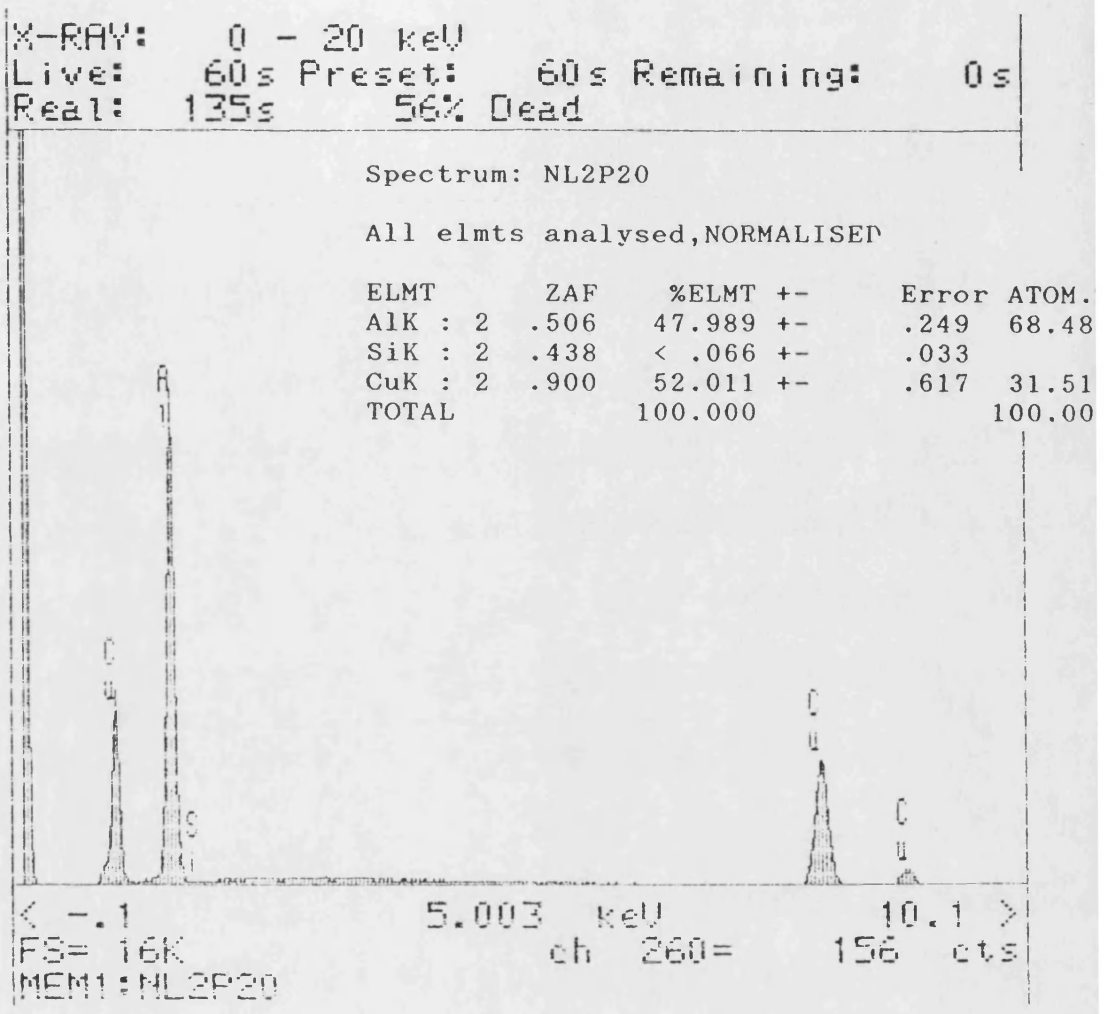

Figure 53: Energy dispersive spectrum for position B in figure 51, indicating formation of θ phase ($CuAl_2$).

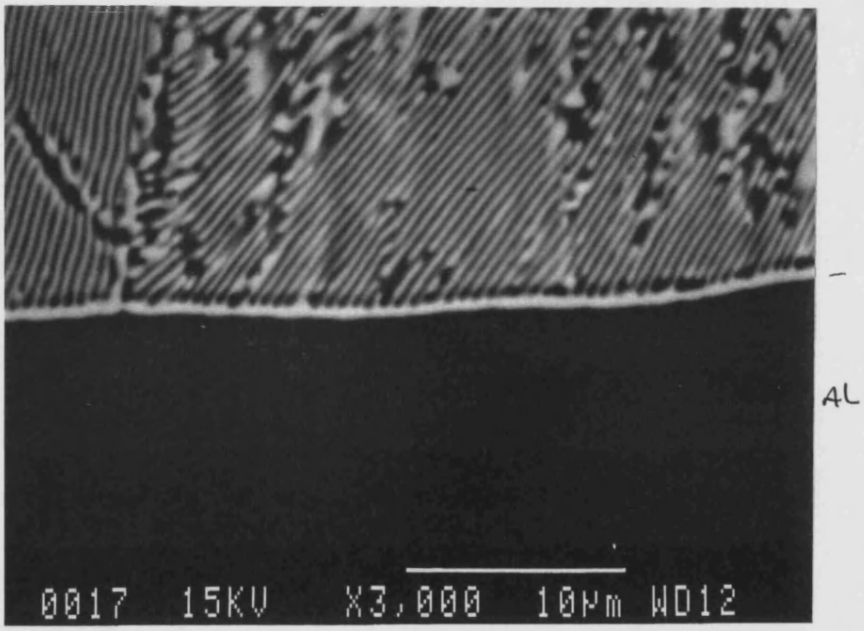

Figure 54: Backscattered SEM micrograph of interface between pure aluminium and $Al/CuAl_2$ eutectic.

Spectrum: NL2P30

All elmts analysed,NORMALISED

ELMT	ZAF	%ELMT	+-	Error	ATOM.%
AlK : 2	.809	87.794	+-	.267	94.423
SiK : 2	.394	< .062	+-	.031	
CuK : 2	.836	12.198	+-	.353	5.570
TOTAL		99.992			100.000

Spectrum: NL2P31 +5um into Al

All elmts analysed,NORMALISED

ELMT	ZAF	%ELMT	+-	Error	ATOM.%
AlK : 2	.912	94.974	+-	.244	97.802
SiK : 2	.387	< .065	+-	.032	
CuK : 2	.826	5.027	+-	.234	2.198
TOTAL		100.001			100.000

Spectrum: NL2P32 +10um into Al

All elmts analysed,NORMALISED

ELMT	ZAF	%ELMT	+-	Error	ATOM.%
AlK : 2	.969	98.321	+-	.241	99.280
SiK : 2	.384	< .064	+-	.032	
CuK : 2	.821	1.679	+-	.174	.720
TOTAL		100.000			100.000

Spectrum: NL2P33 +15um into Al

All elmts analysed,NORMALISED

ELMT	ZAF	%ELMT	+-	Error	ATOM.%
AlK : 2	.990	99.472	+-	.239	99.775
SiK : 2	.383	< .063	+-	.031	
CuK : 2	.820	.528	+-	.131	.225
TOTAL		100.000			100.000

Spectrum: NL2P34 +20um into Al

All elmts analysed,NORMALISED

ELMT	ZAF	%ELMT	+-	Error	ATOM.%
AlK : 2	.992	99.583	+-	.243	99.823
SiK : 2	.382	< .064	+-	.032	
CuK : 2	.820	.417	+-	.132	.177
TOTAL		100.000			100.000

Figure 55: Energy dispersive spectra taken at intervals away from the interface shown in figure 54.

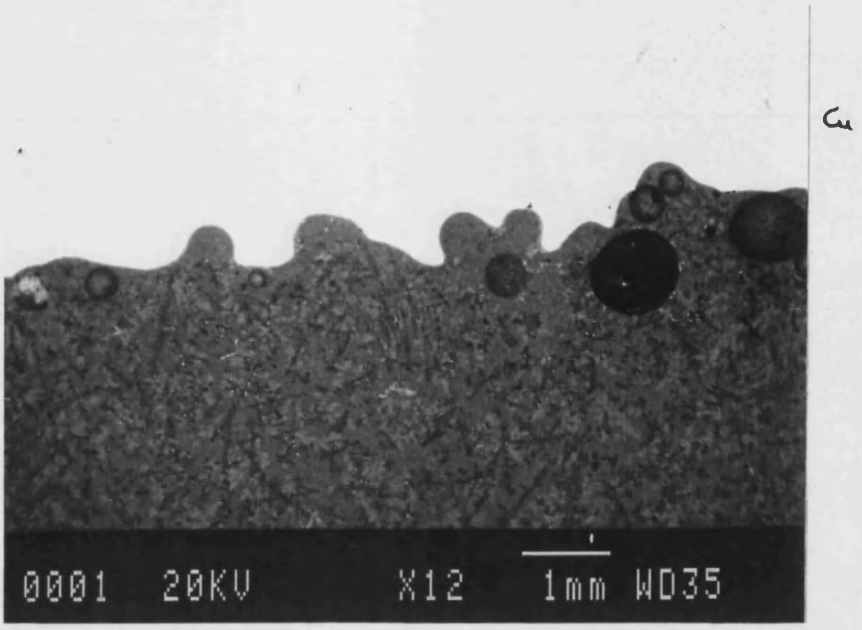

Figure 56a: Model diffusion bond, A357 alloy + pure copper

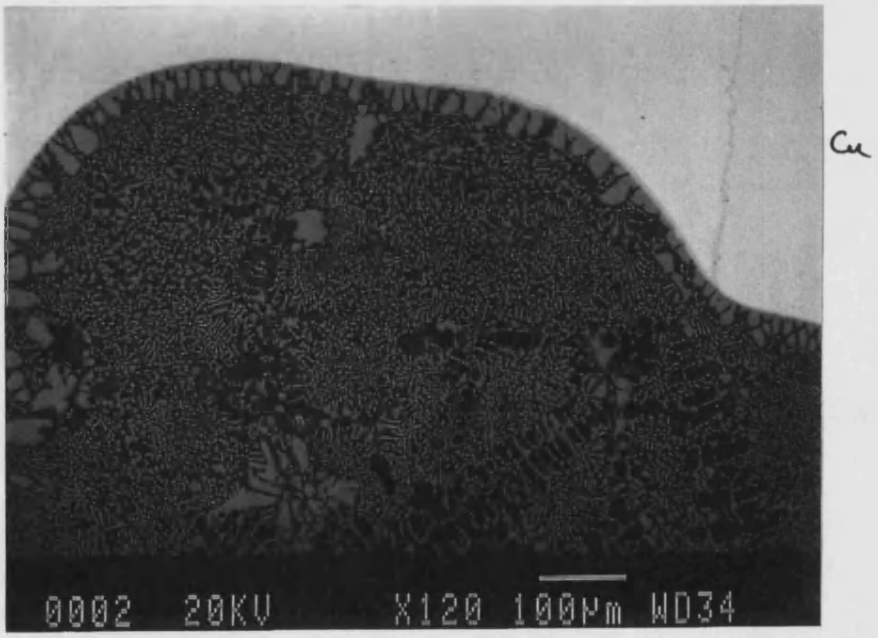

Figure 56b: Model diffusion bond, A357 alloy + pure copper

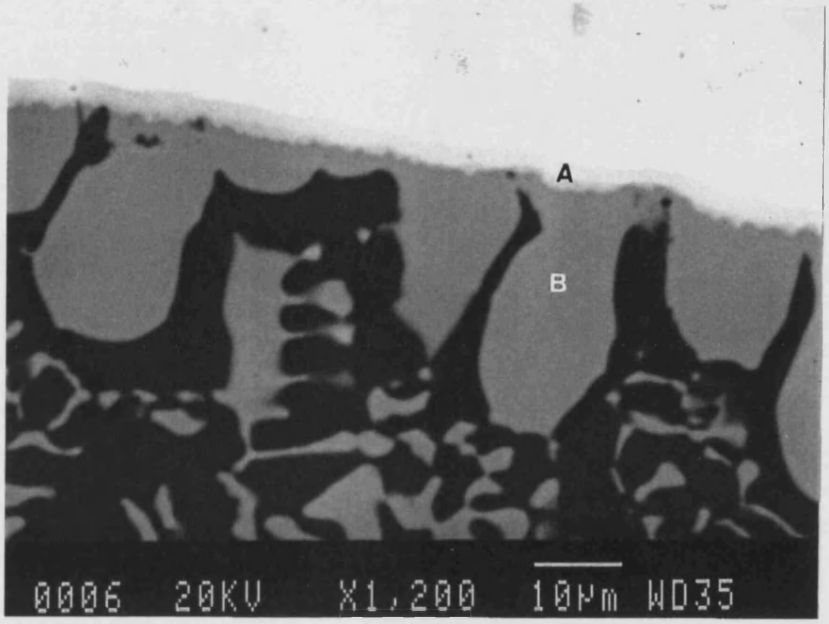

Figure 57: Structure of reaction layers formed during diffusion bonding of pure copper and alloy A357, backscattered SEM micrograph.

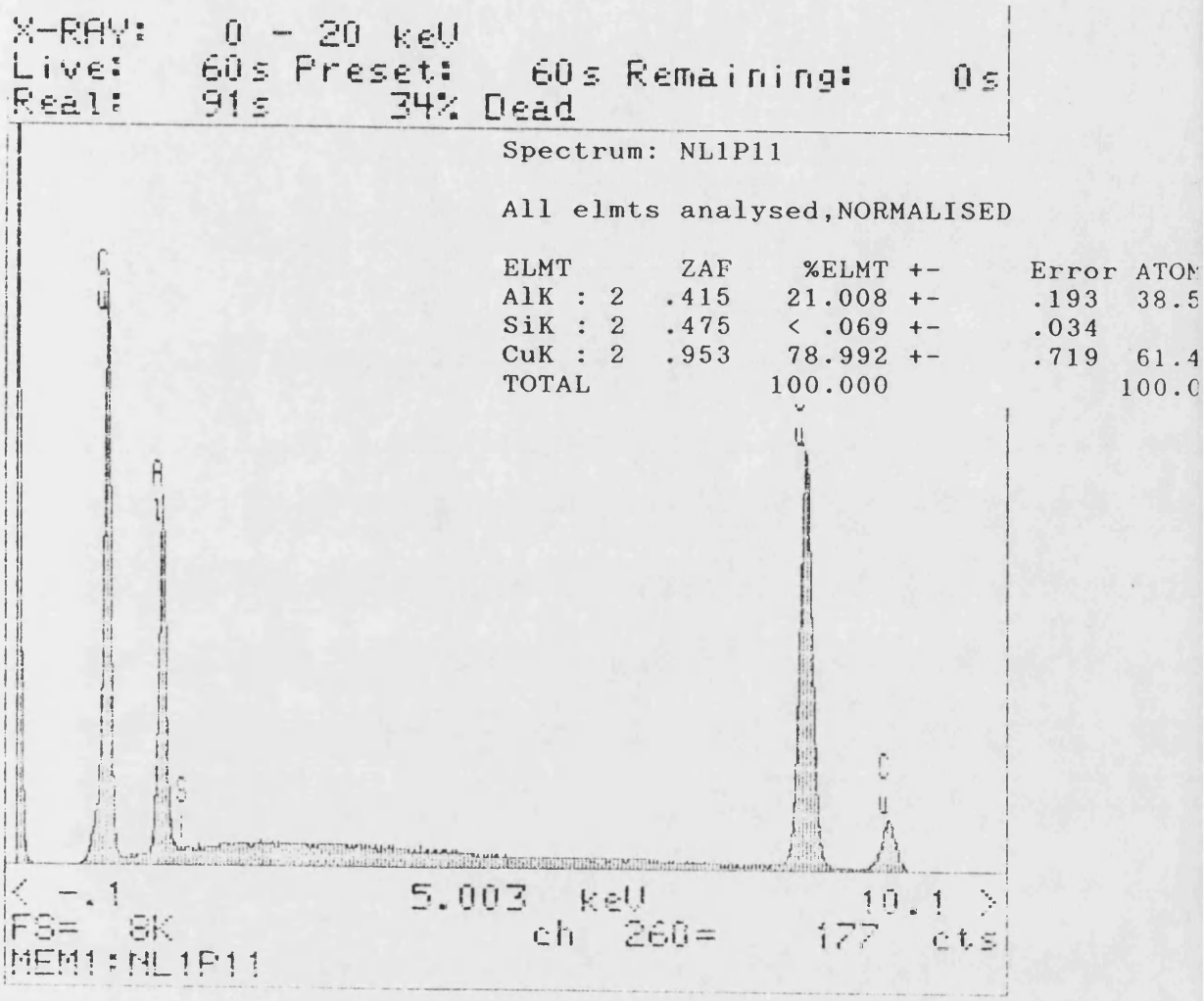

Figure 58: Energy dispersive spectrum for position A in figure 57, indicating formation of δ phase.

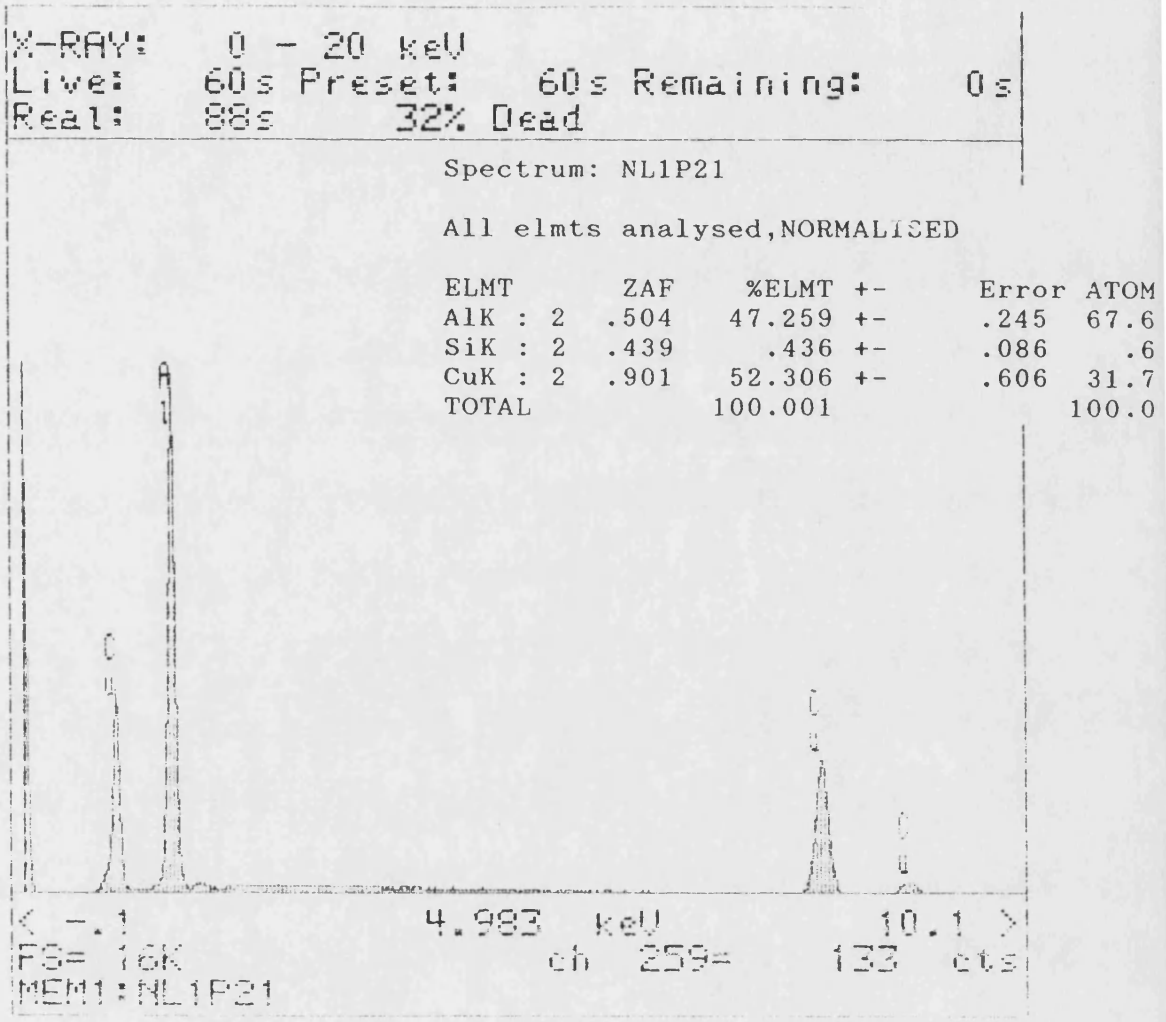

Figure 59: Energy dispersive spectrum for position B in figure 57, indicating formation of θ phase ($CuAl_2$).

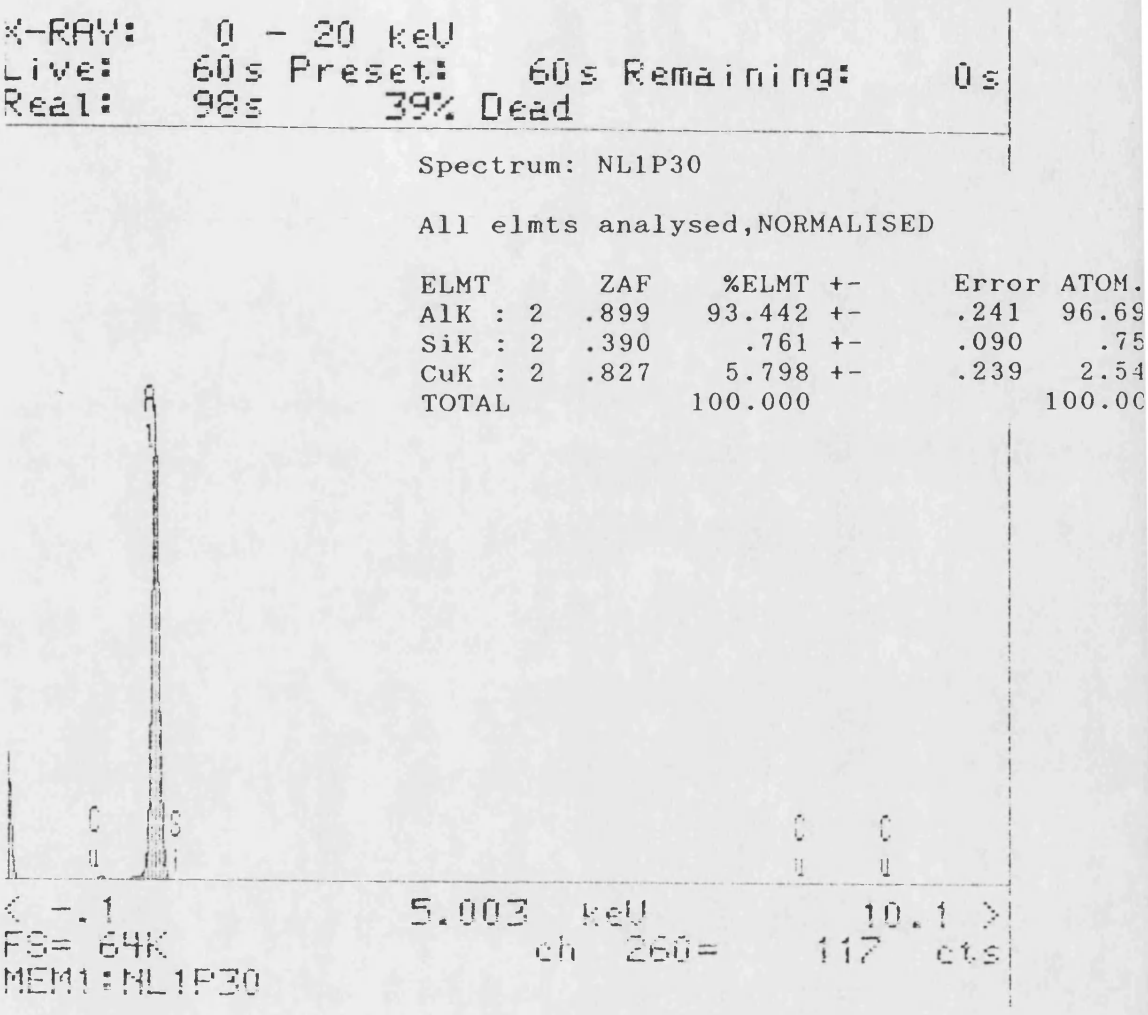

Figure 60: Energy dispersive spectrum from dark areas in figure 57, indicating the presence of aluminium containing some copper and silicon in solution.

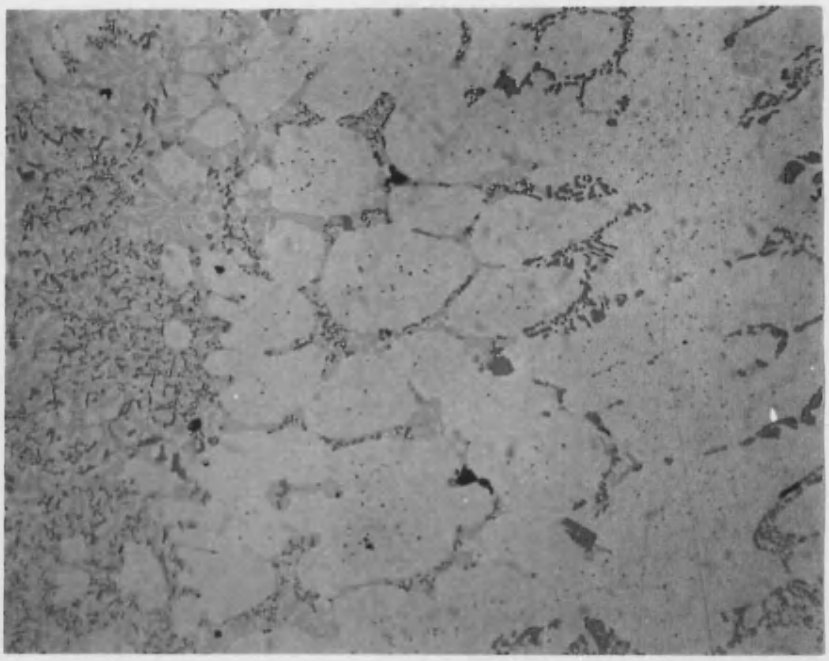

Figure 61a: Optical micrograph of grain boundary reaction forming Al/Si/$CuAl_2$ eutectic mixture. Mag x200

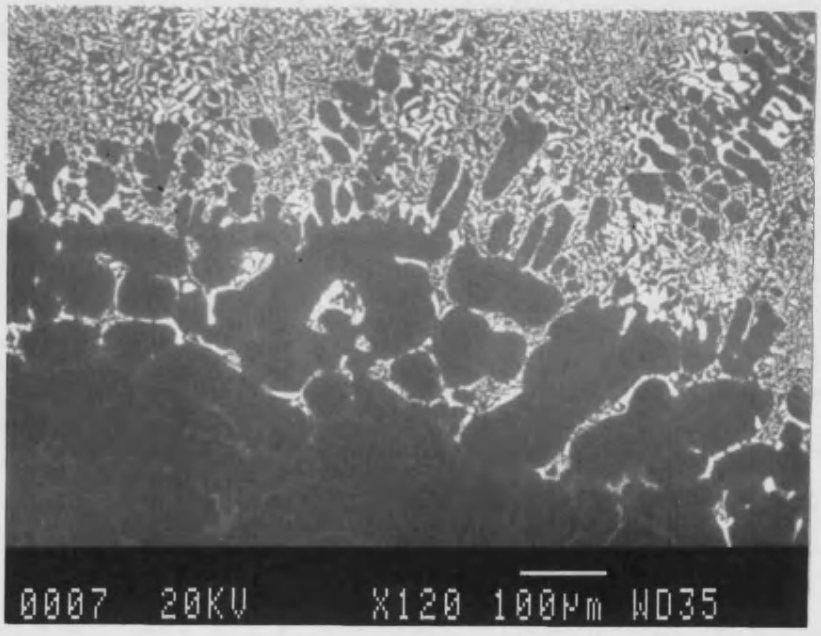

Figure 61b: Backscattered SEM image of grain boundary reaction forming Al/Si/$CuAl_2$ eutectic mixture.

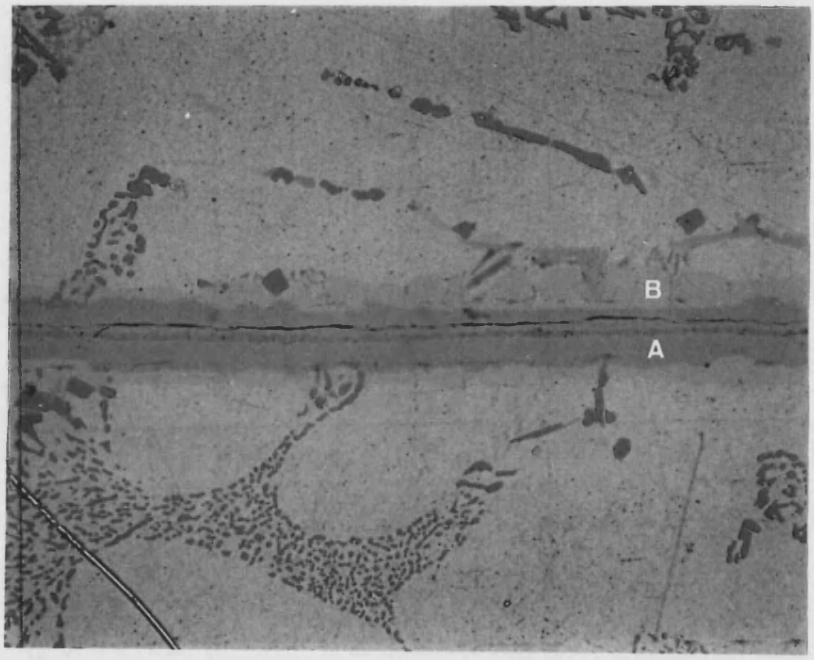

Figure 62: Reaction layers formed during solid state diffusion bonding of A357 alloy with a copper foil insert. Optical micrograph x400.

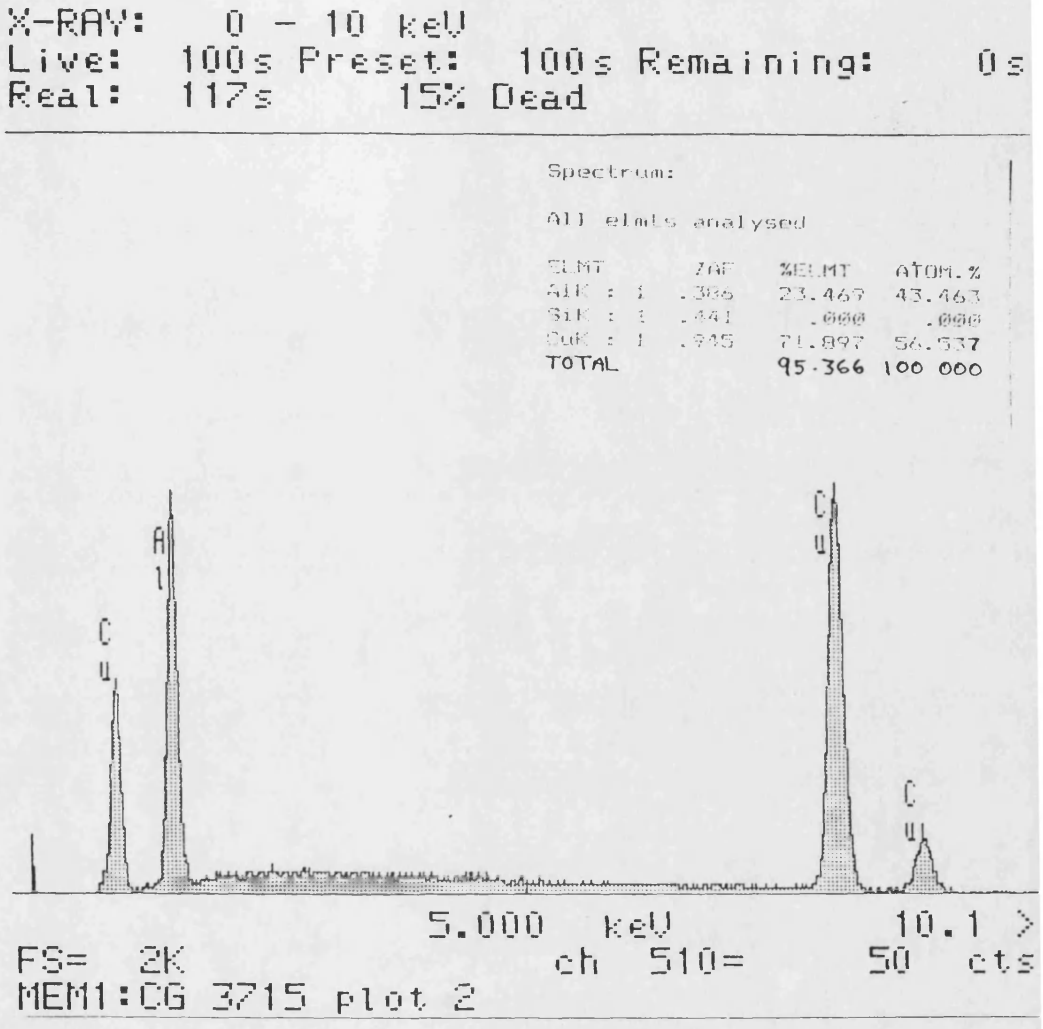

Figure 63: Energy dispersive spectrum for position A in figure 62, indicating formation of ζ_2 phase.

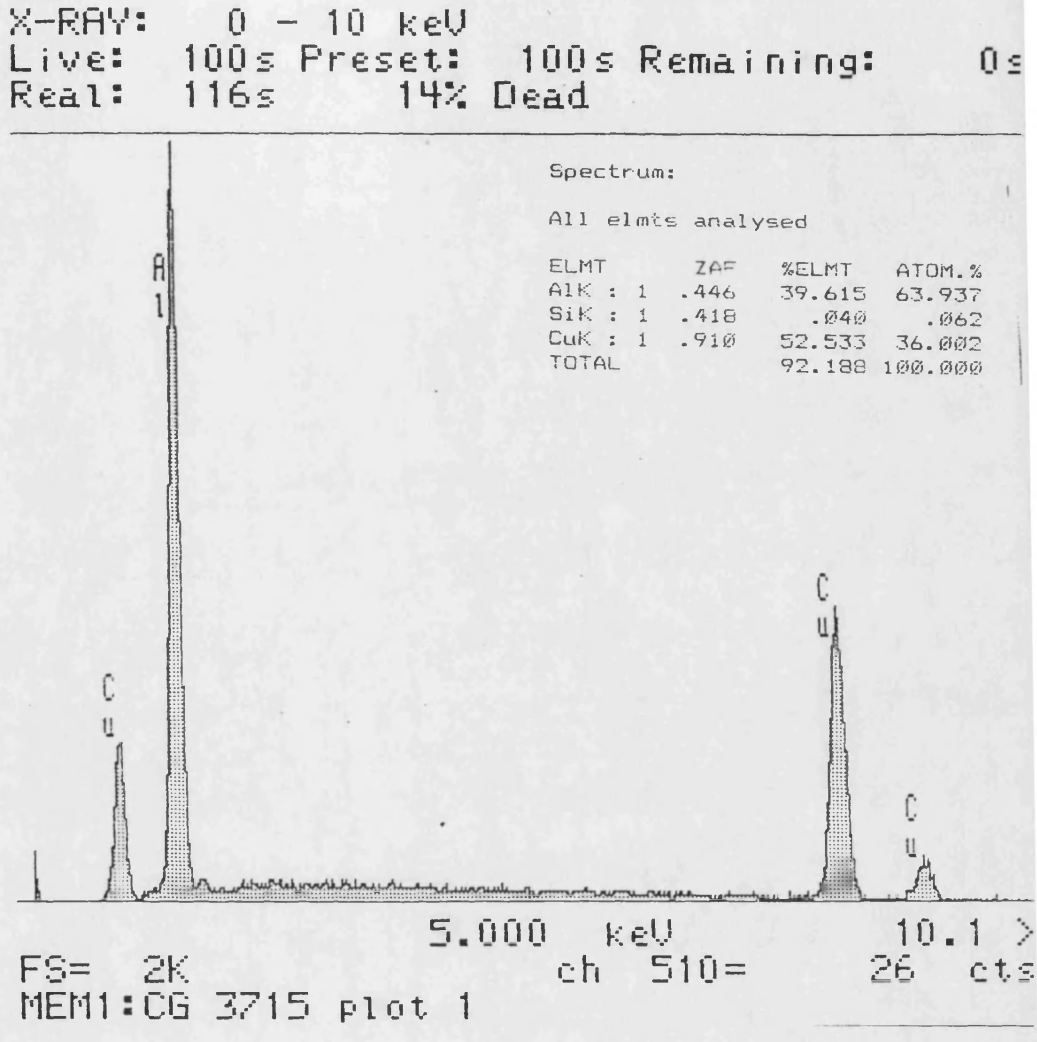

Figure 64: Energy dispersive spectrum for position B in figure 62, indicating formation of θ phase ($CuAl_2$).

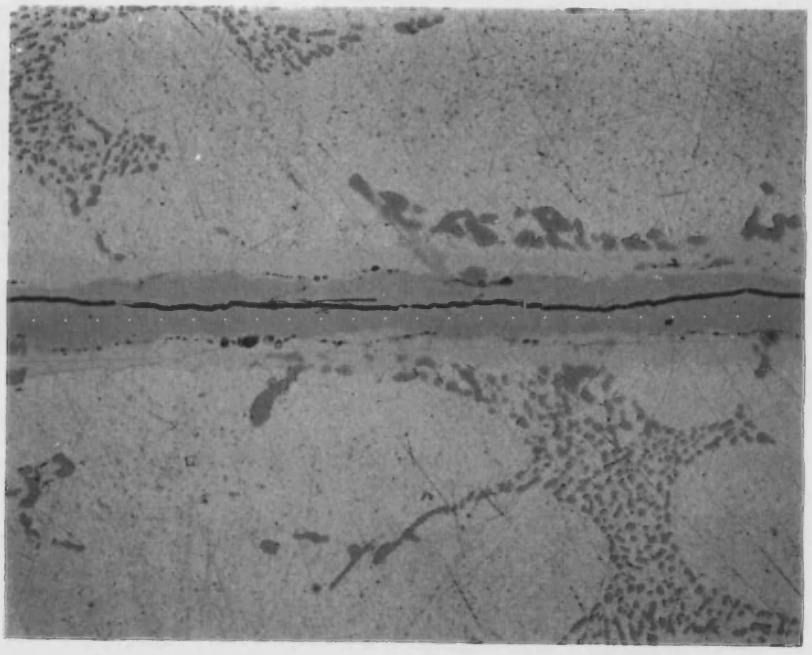

Figure 65: Removal of copper remnant from interface of A357 by prolonged exposure to bonding conditions, thermal cracking evident in intermetallic reaction layer.

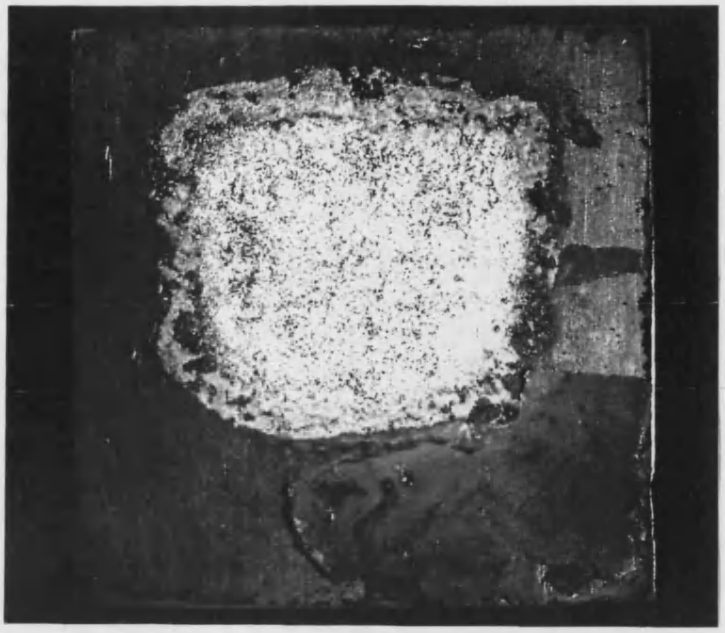

Figure 66a: Fracture surface of diffusion bonded specimen, 5% applied strain. Edges surrounded by unreacted copper foil.

Figure 66b: Fracture surface of diffusion bonded specimen, 10% applied strain. Edges surrounded by unreacted copper foil.

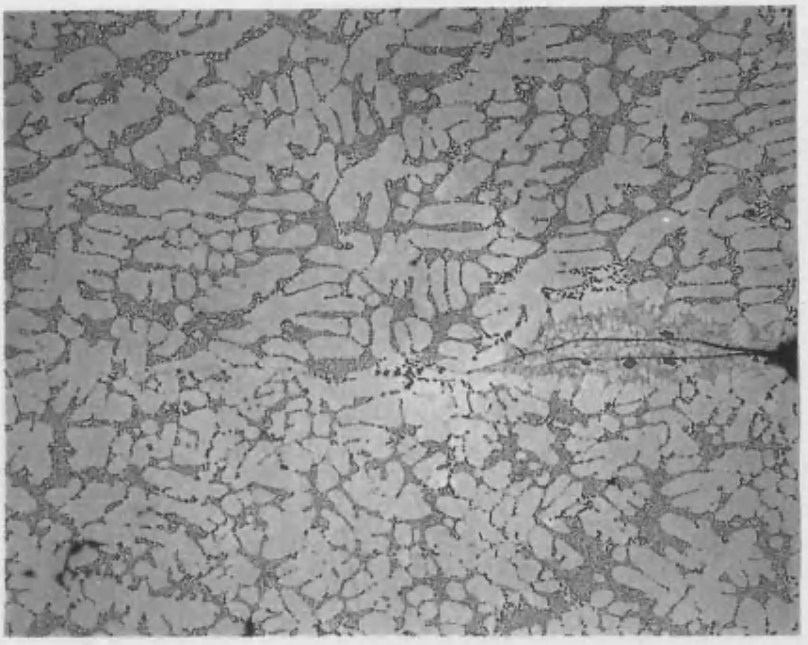

Figure 67a: Bond-line of sample joined with a copper foil forming a transient liquid phase. Optical mag x 50

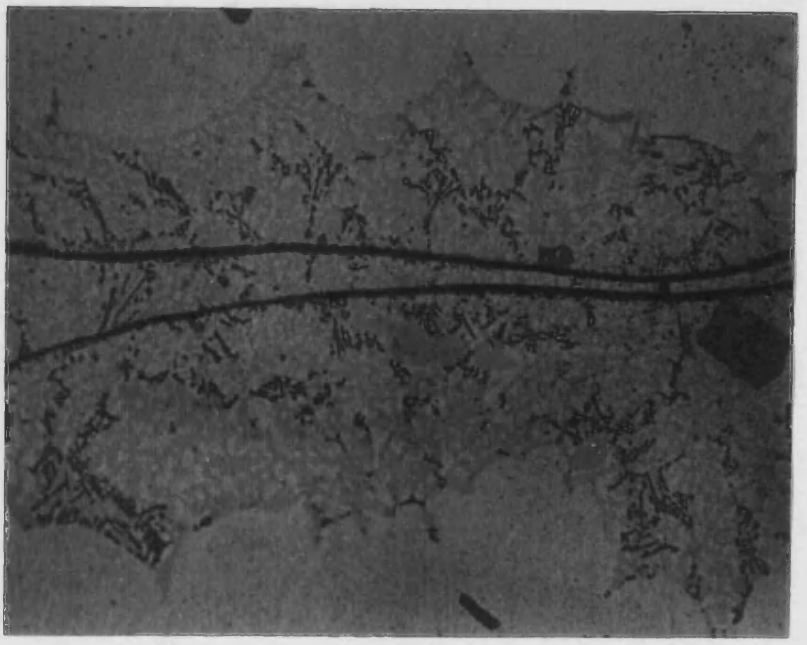

Figure 67b: Edge of sample bonded with a copper foil forming a transient liquid phase. Optical mag x400

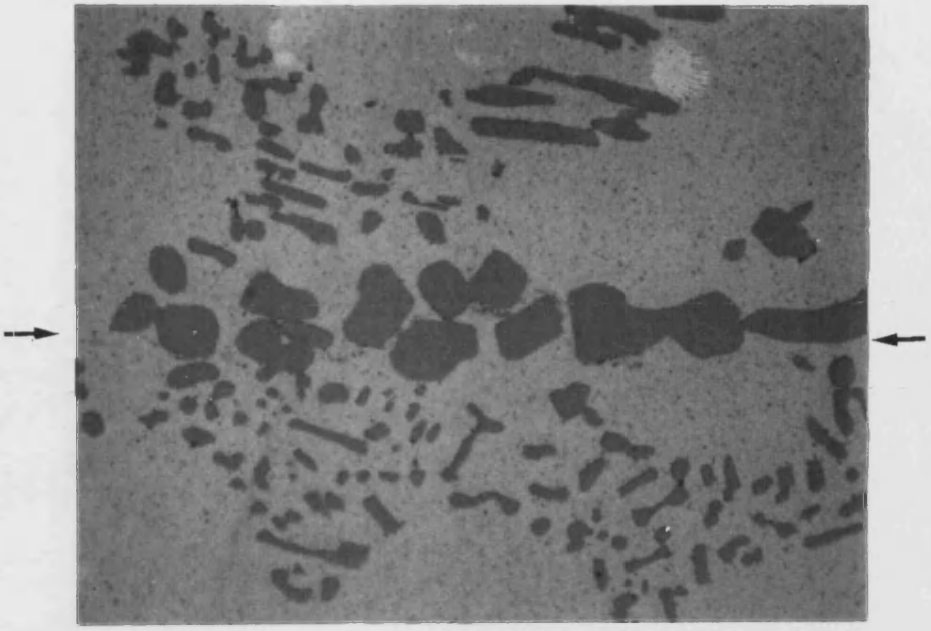

Figure 68a: Silicon morphology at interface of A357 alloy bonded with copper foil to form a transient liquid phase. Optical x1000

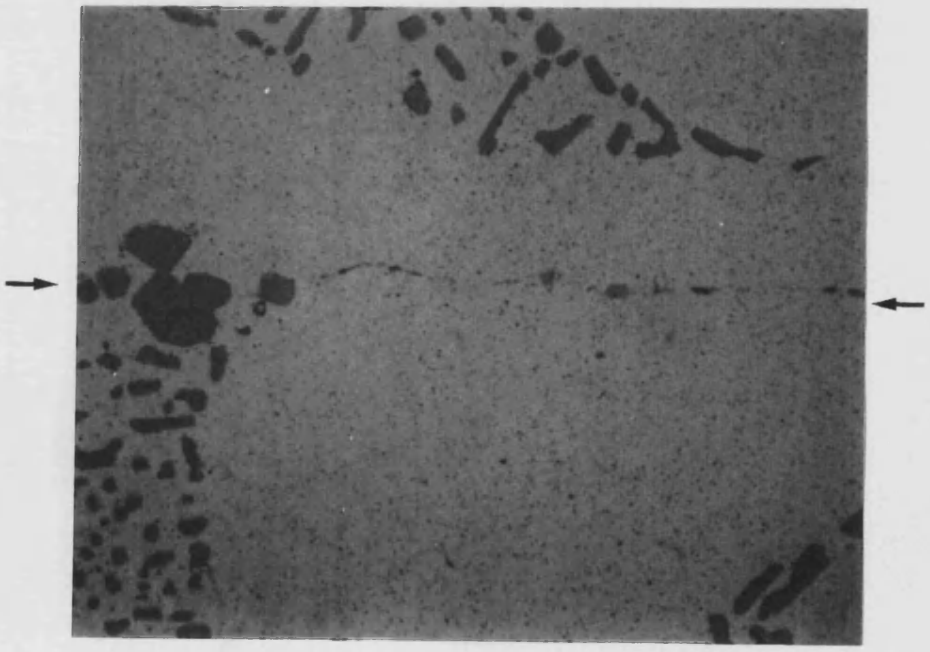

Figure 68b: Silicon-free region of the interface of A357 alloy bonded with a copper foil to from a transient liquid phase. Optical x1000

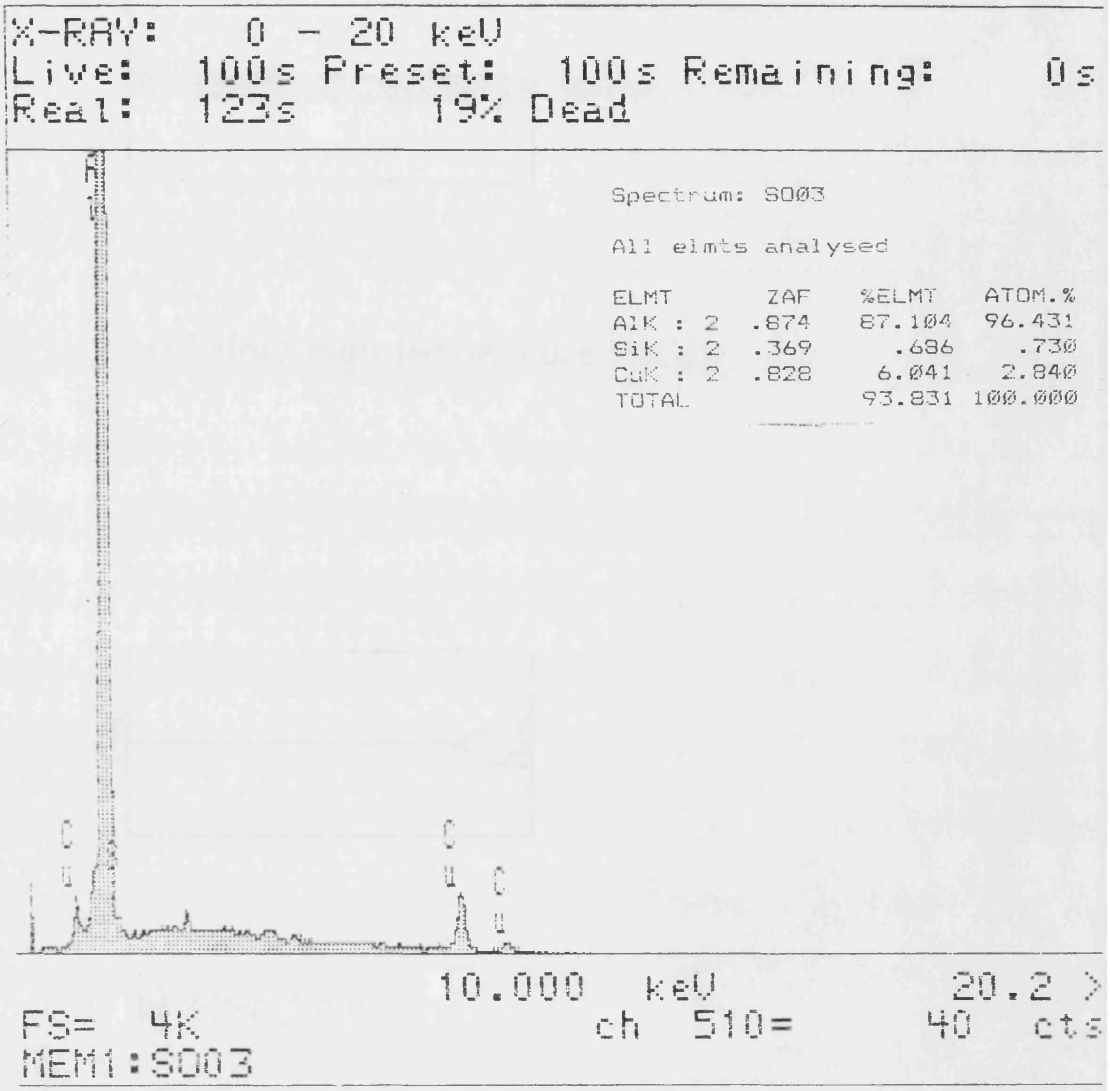

Figure 69: Energy dispersive spectrum taken from bond-line in figure 68 b) showing presence of copper in solution after liquation of Cu foil insert.

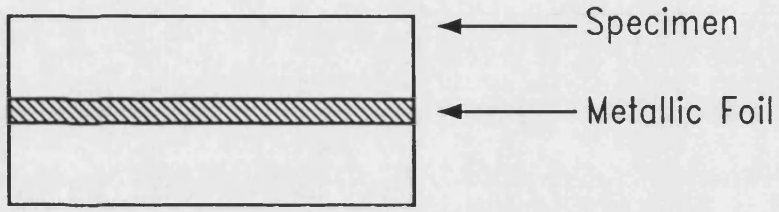

a) Before high temperature joining

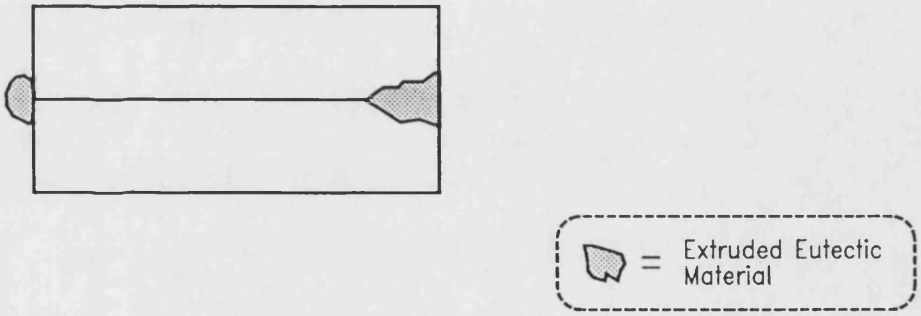

b) After joining

Figure 70: Schematic diagram of the formation and transport of molten eutectic material.

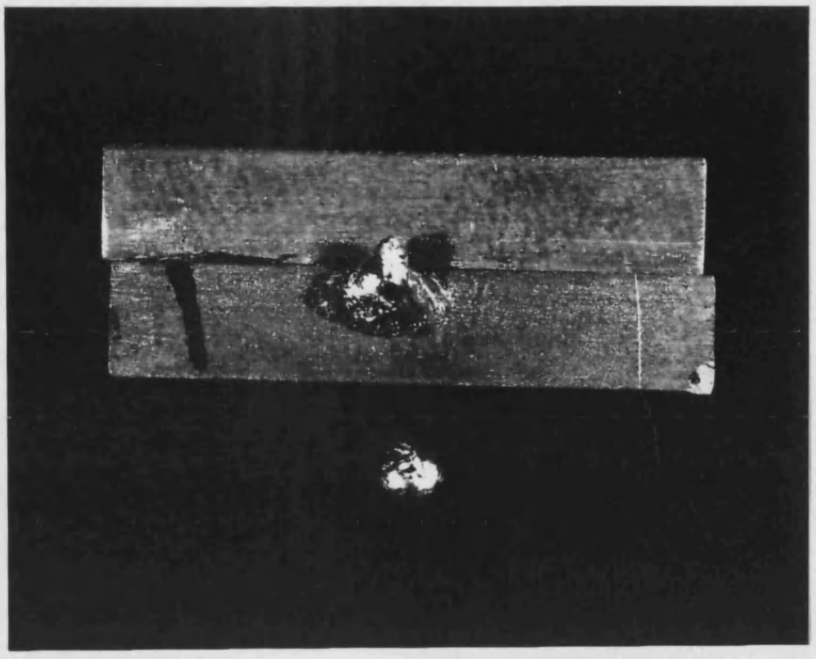

Figure 71a: Macro of A357 alloy bonded with a copper foil showing expelled liquid eutectic material.

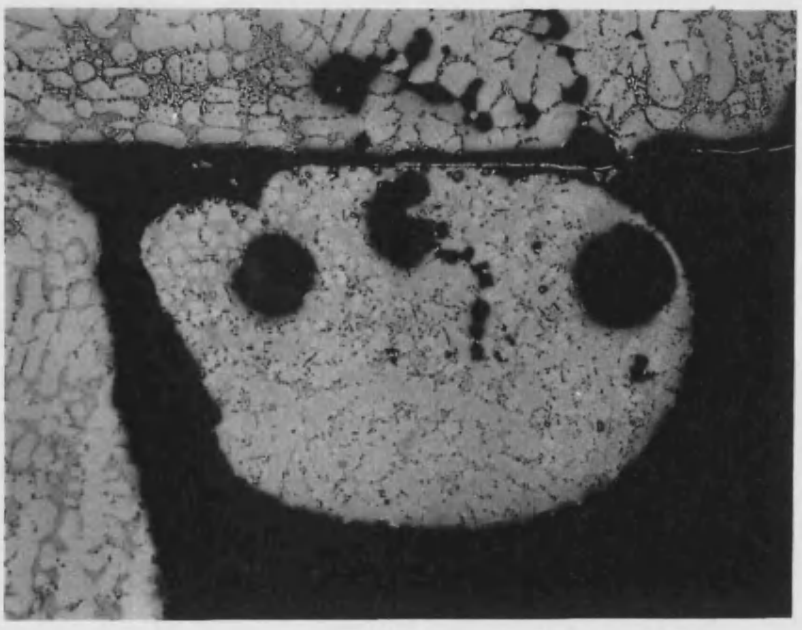

Figure 71b: Optical micrograph of expelled eutectic material formed with a copper foil and A357 alloy. Mag x50

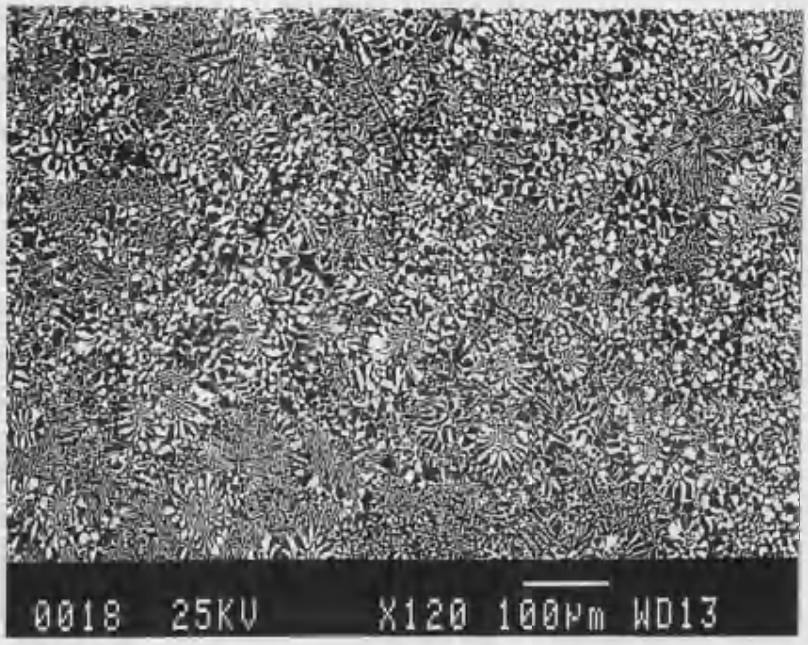

Figure 72a: Backscattered SEM micrograph of expelled eutectic material formed with A357 alloy and copper foil.

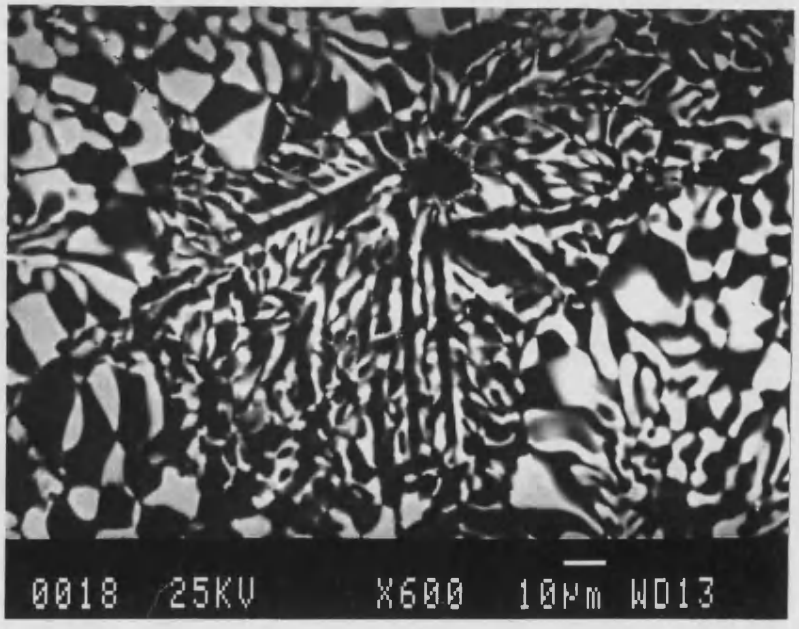

Figure 72b: Backscattered SEM micrograph of expelled eutectic material formed with A357 alloy and copper foil.

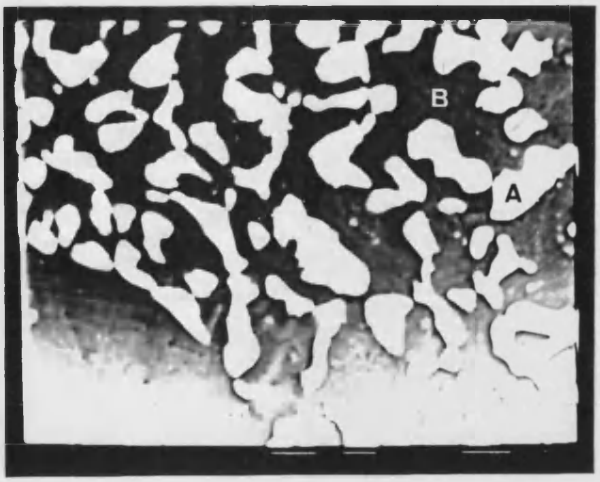

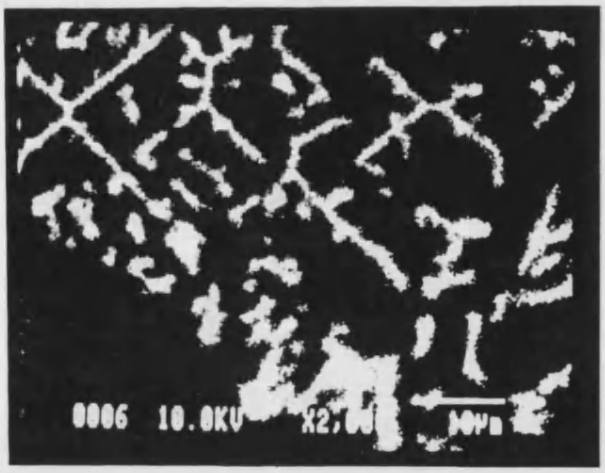

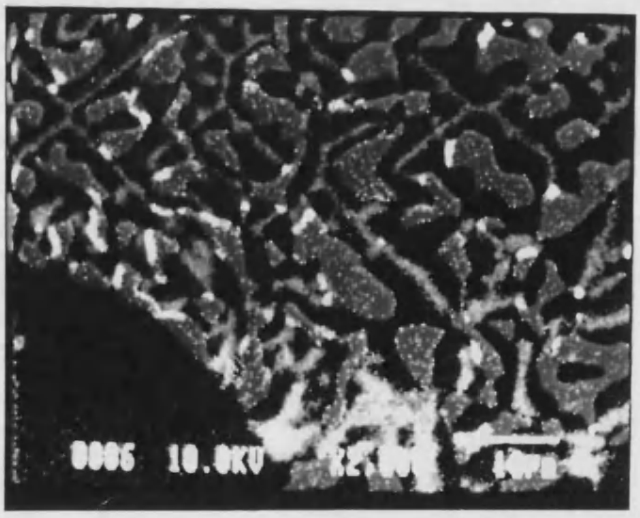

Figure 73: a) backscattered SEM image of expelled liquid eutectic mixture; b) Si x-ray map showing position and distribution of silicon; c) double exposure composite photograph of a) & b) showing exact position of silicon within the eutectic mixture.

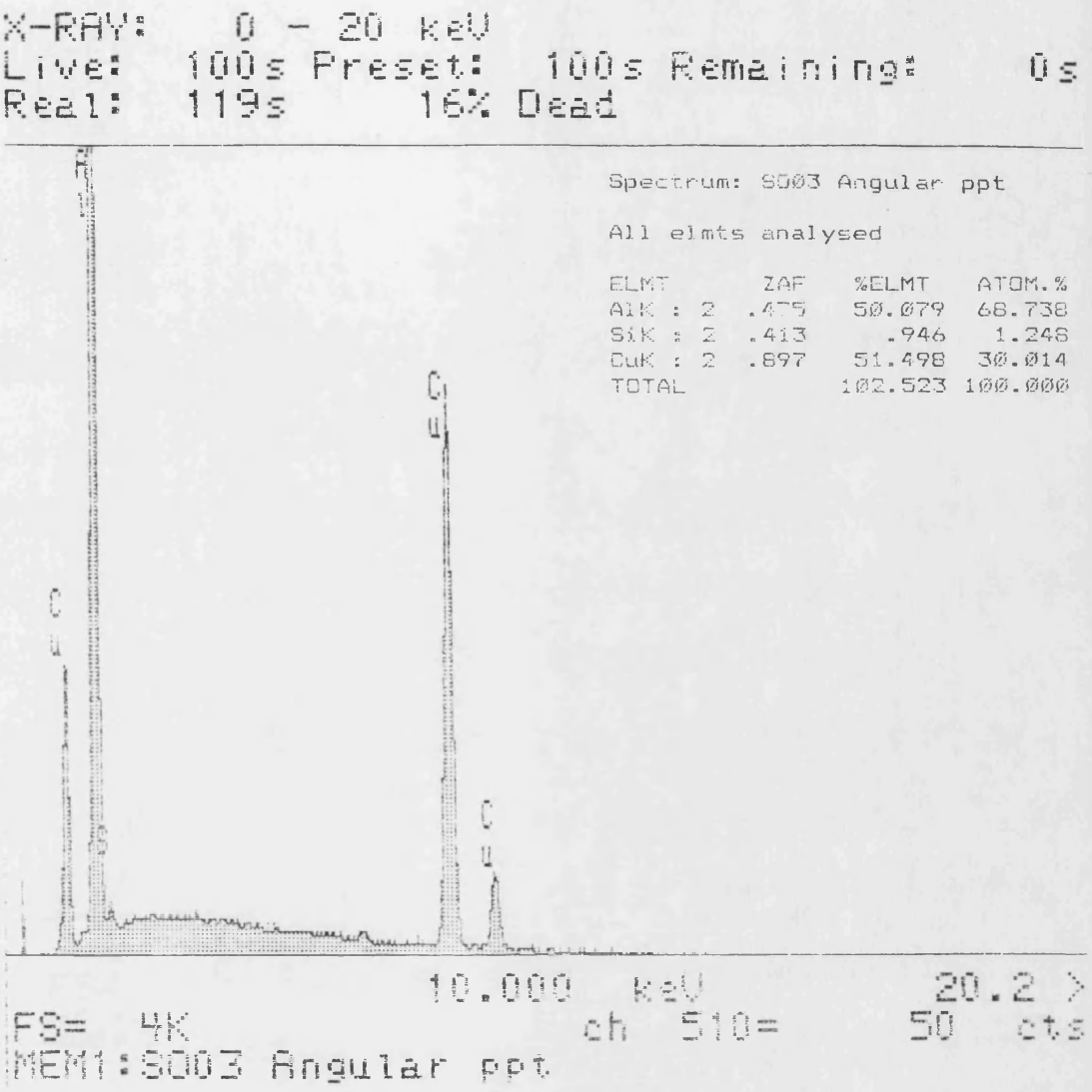

Figure 74: Energy dispersive spectrum of white phase at position A in figure 73a) indicating formation of θ phase ($CuAl_2$).

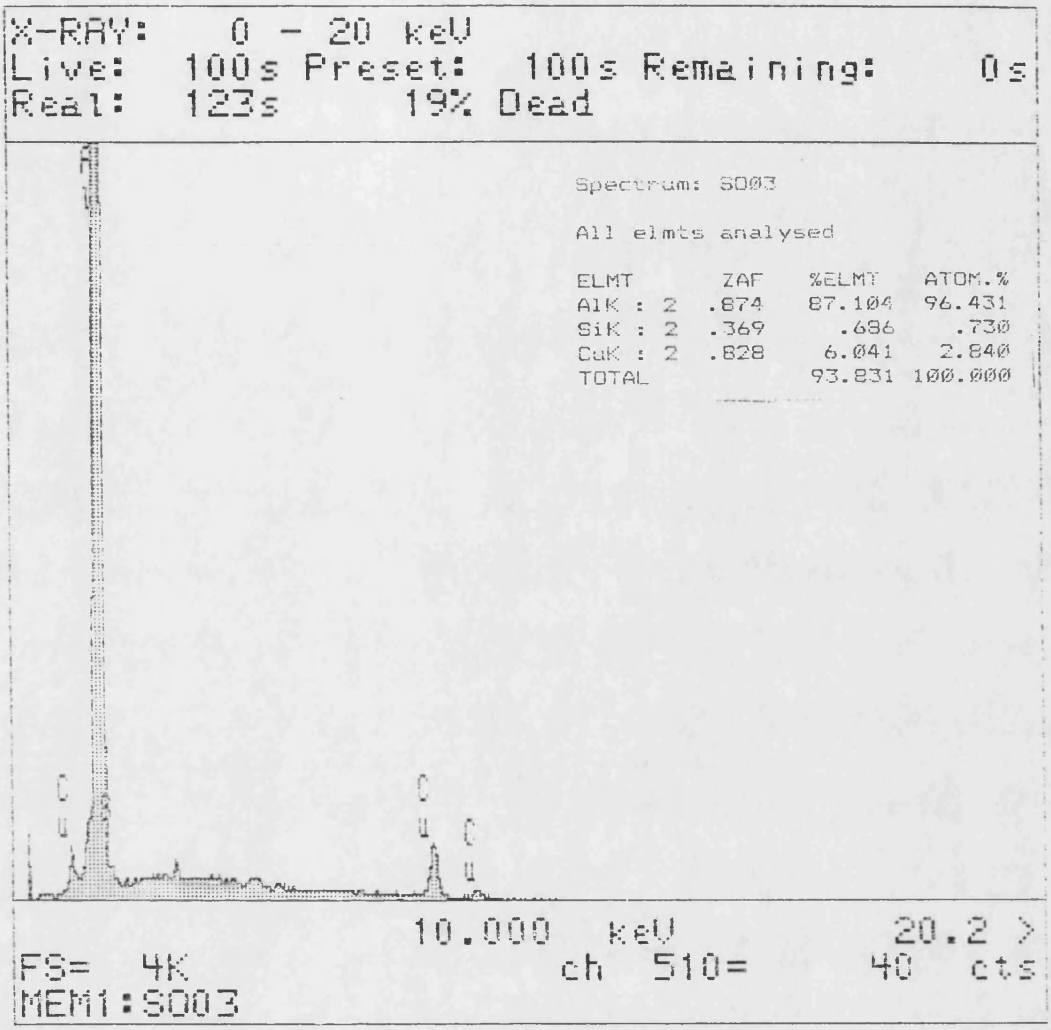

Figure 75: Energy dispersive spectrum of grey phase at position B in figure 73 a), indicating the presence of aluminium containing some copper in solution.

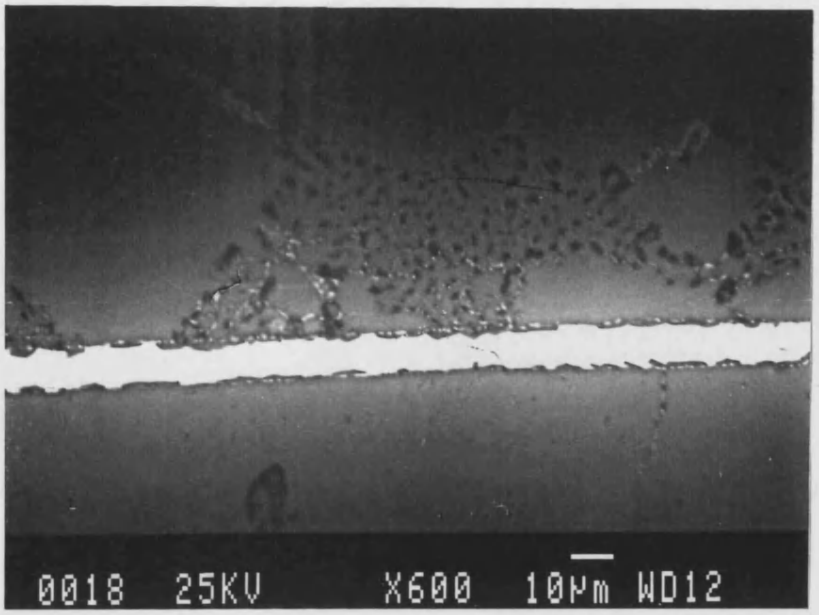

Figure 76a: Interface of A357 bonded in solid state with a silver foil. Backscattered SEM micrograph.

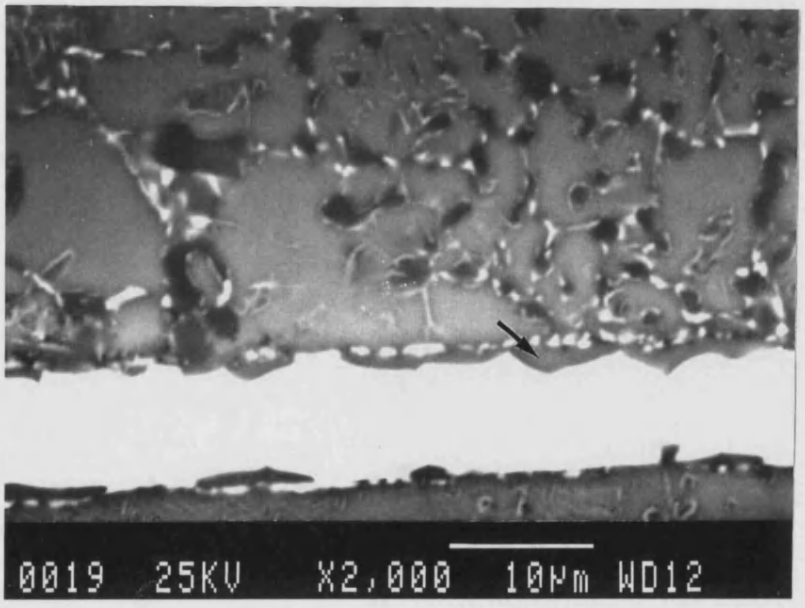

Figure 76b: Interface of A357 bonded in solid state with a silver foil. Visible transport of silver around silicon particles. Backscattered SEM micrograph.

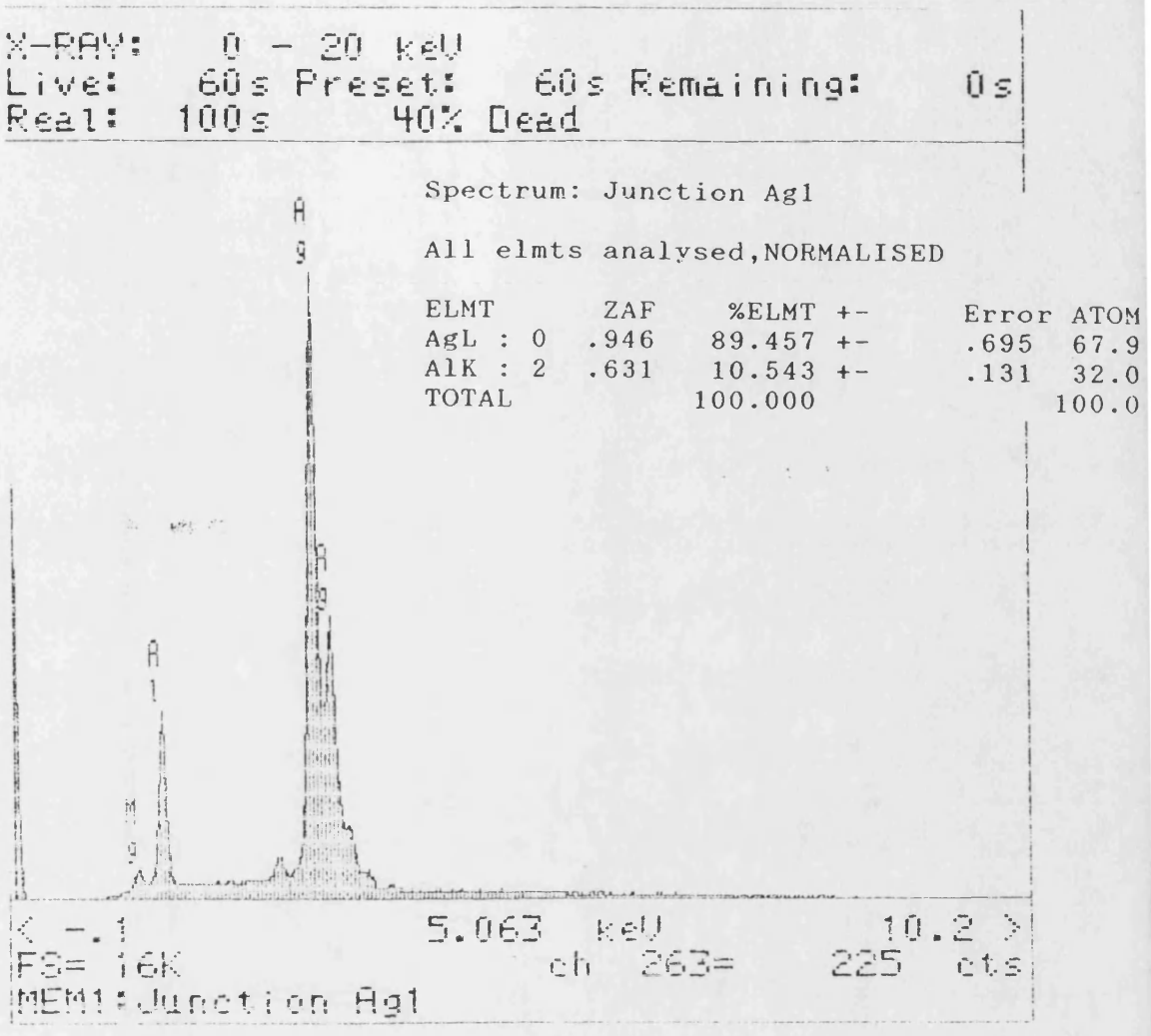

Figure 77: Energy dispersive spectrum of central white phase in figure 76 b) indicating formation of Ag_2Al.

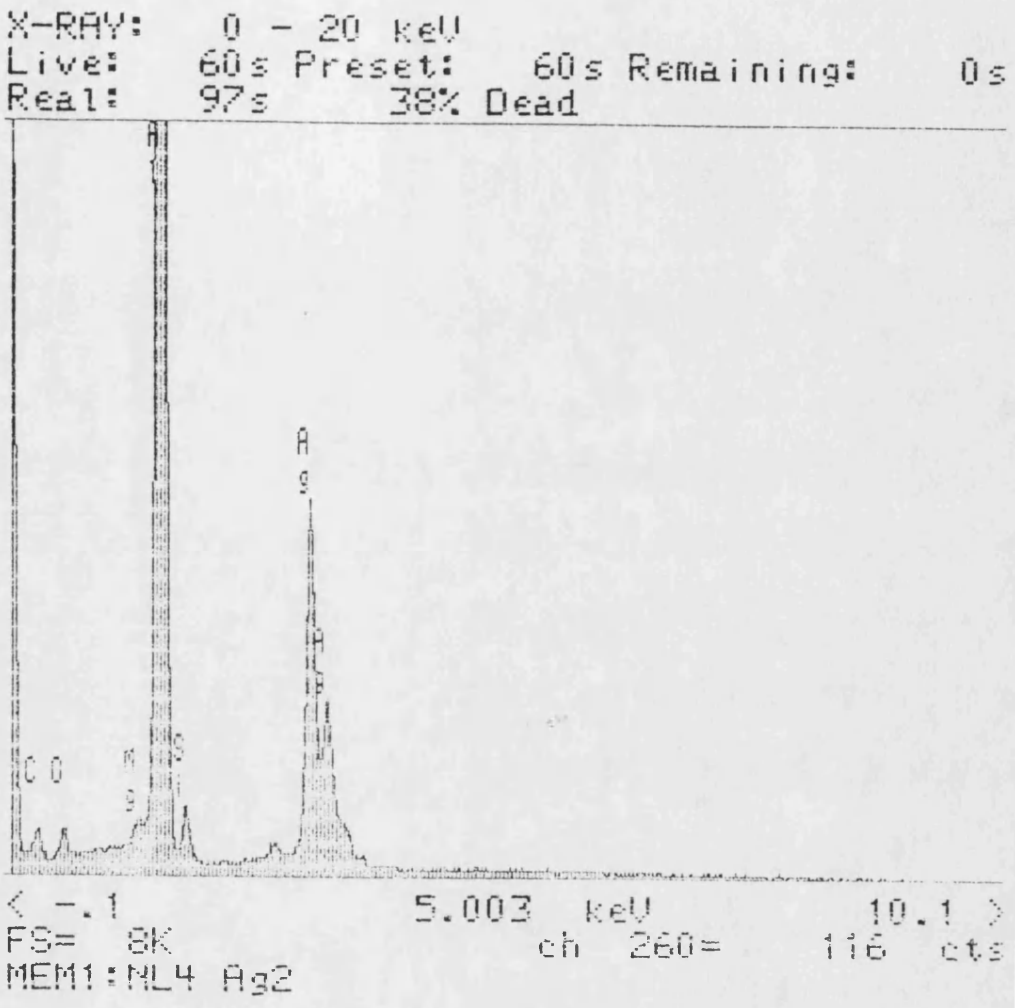

Figure 78: Energy dispersive spectrum of dark precipitate phase arrowed in figure 76 b) showing a complex composition.

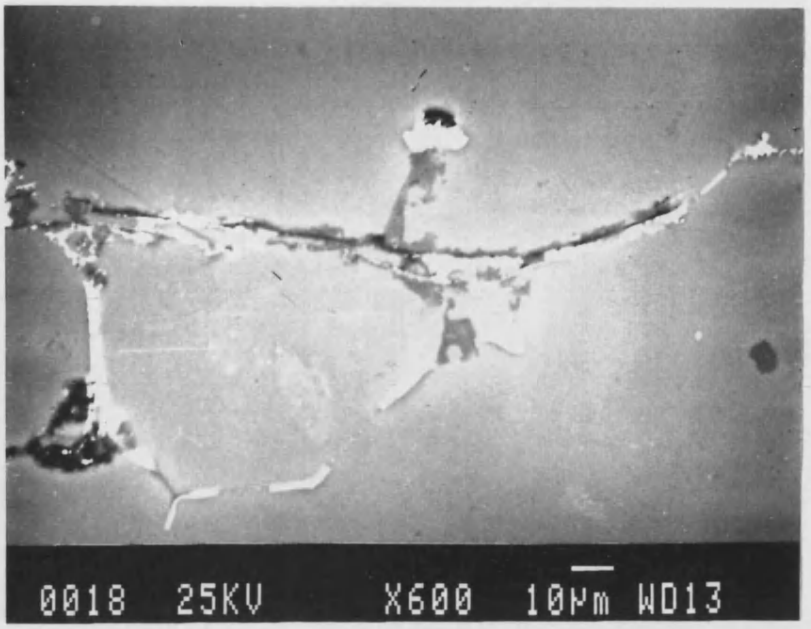

Figure 79a: Interface of A357 alloy joined by the formation of a transient liquid phase with a silver foil.

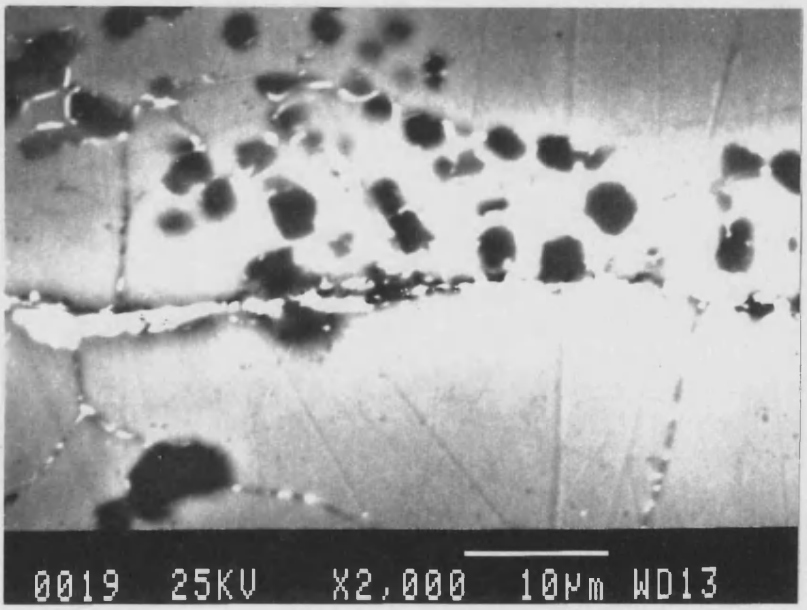

Figure 79b: Detail of interface of A357 alloy joined by the formation of a transient liquid phase with a silver foil.

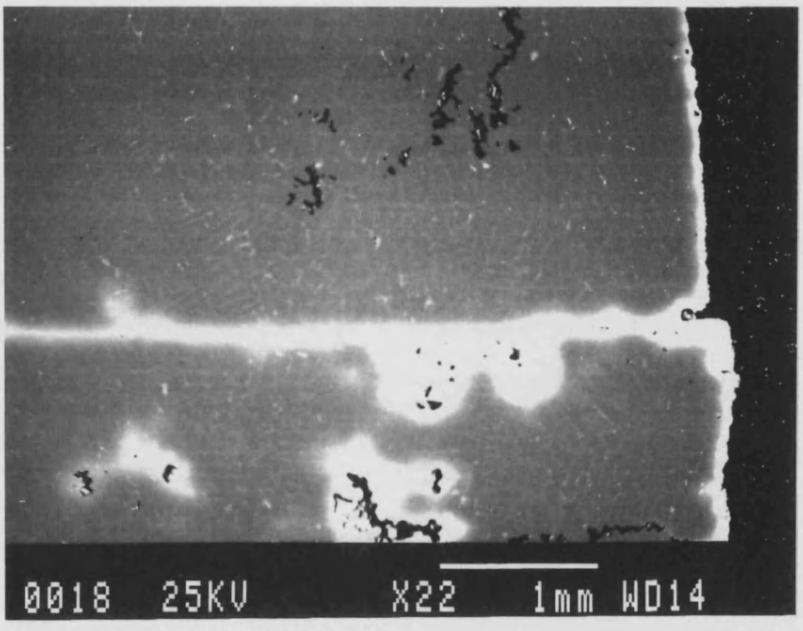

Figure 80: Low magnification backscattered SEM image of A357 alloy bonded in liquid state with silver foil insert. Bright areas indicate the visible extent of transport of liquid eutectic mixture.

Figure 81a: Backscattered SEM micrograph of expelled liquid eutectic material formed by reaction of A357 with silver foil.

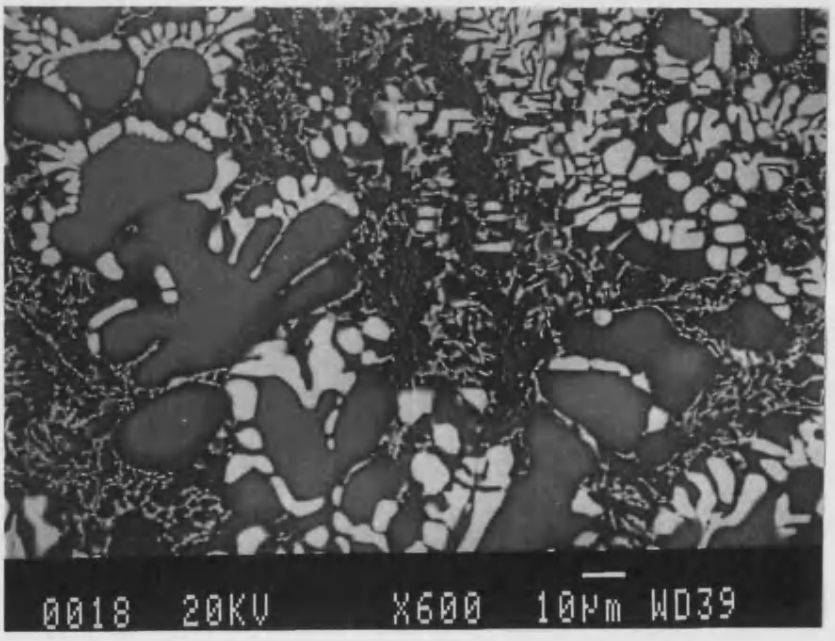

Figure 81b: Detail of backscattered SEM micrograph of expelled liquid eutectic material formed by reaction of A357 with silver foil.

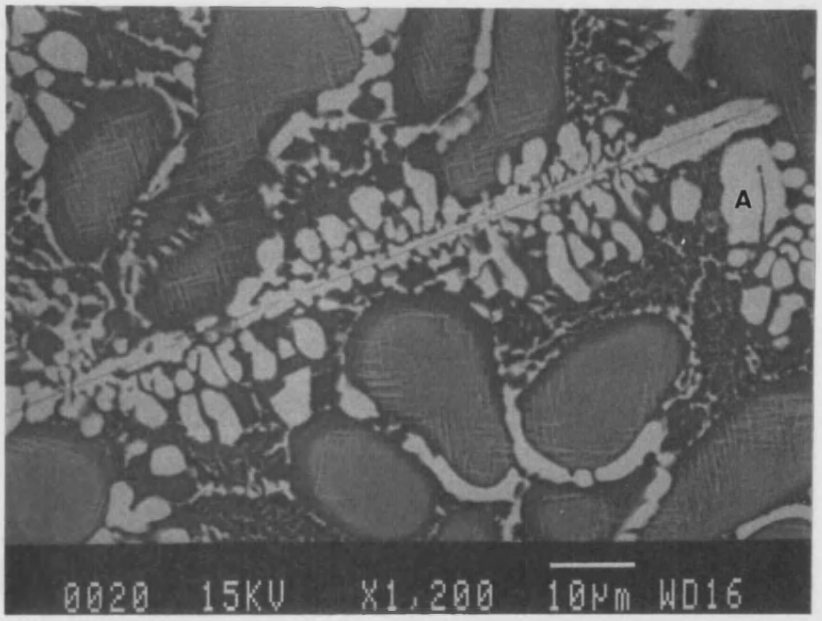

Figure 82: Backscattered SEM image of expelled liquid eutectic material formed by liquation of silver foil during bonding of A357 alloy.

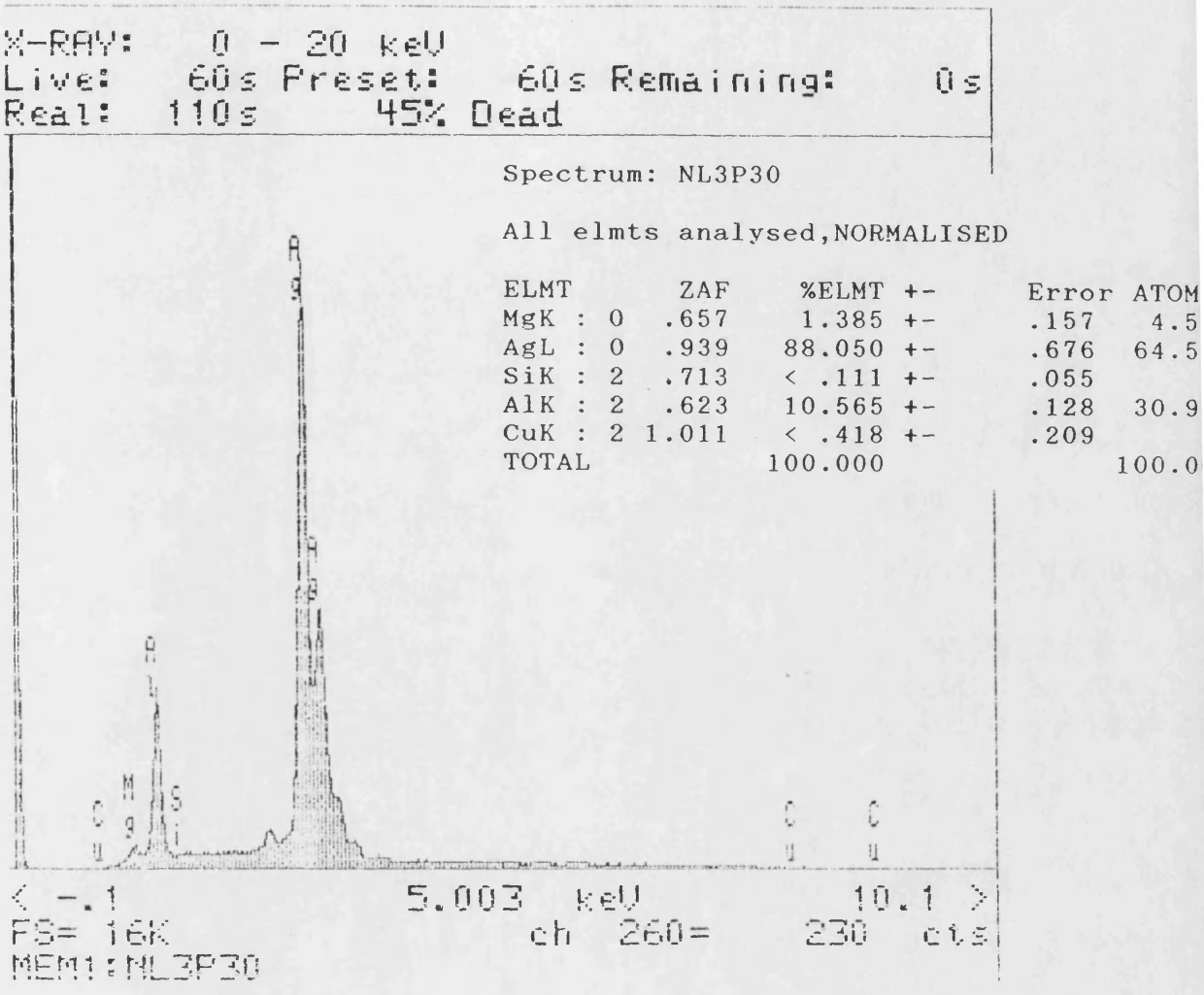

Figure 83: Energy dispersive spectrum of white phase, marked "A" in figure 82 indicating formation of Ag_2Al.

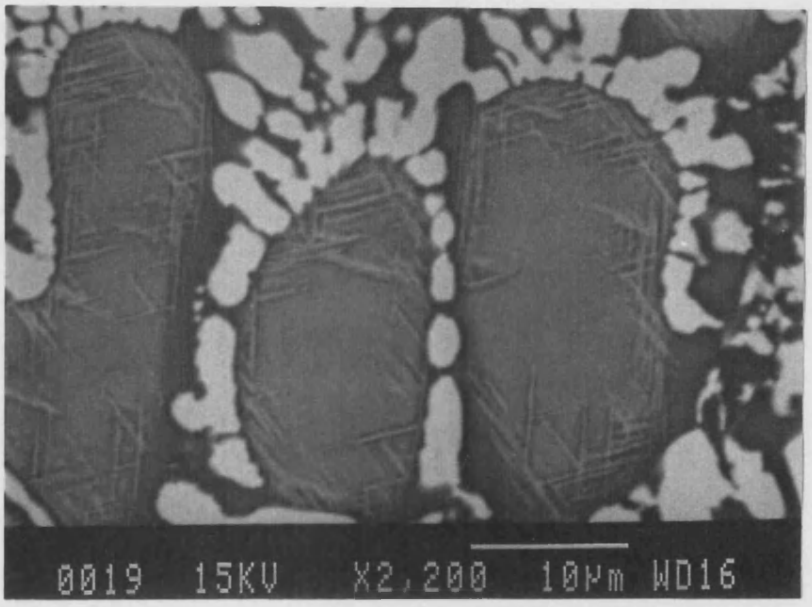

Figure 84: Backscattered SEM image of large grains occurring in liquid eutectic mixture, as in figure 82. Widmanstätten formations clearly evident.

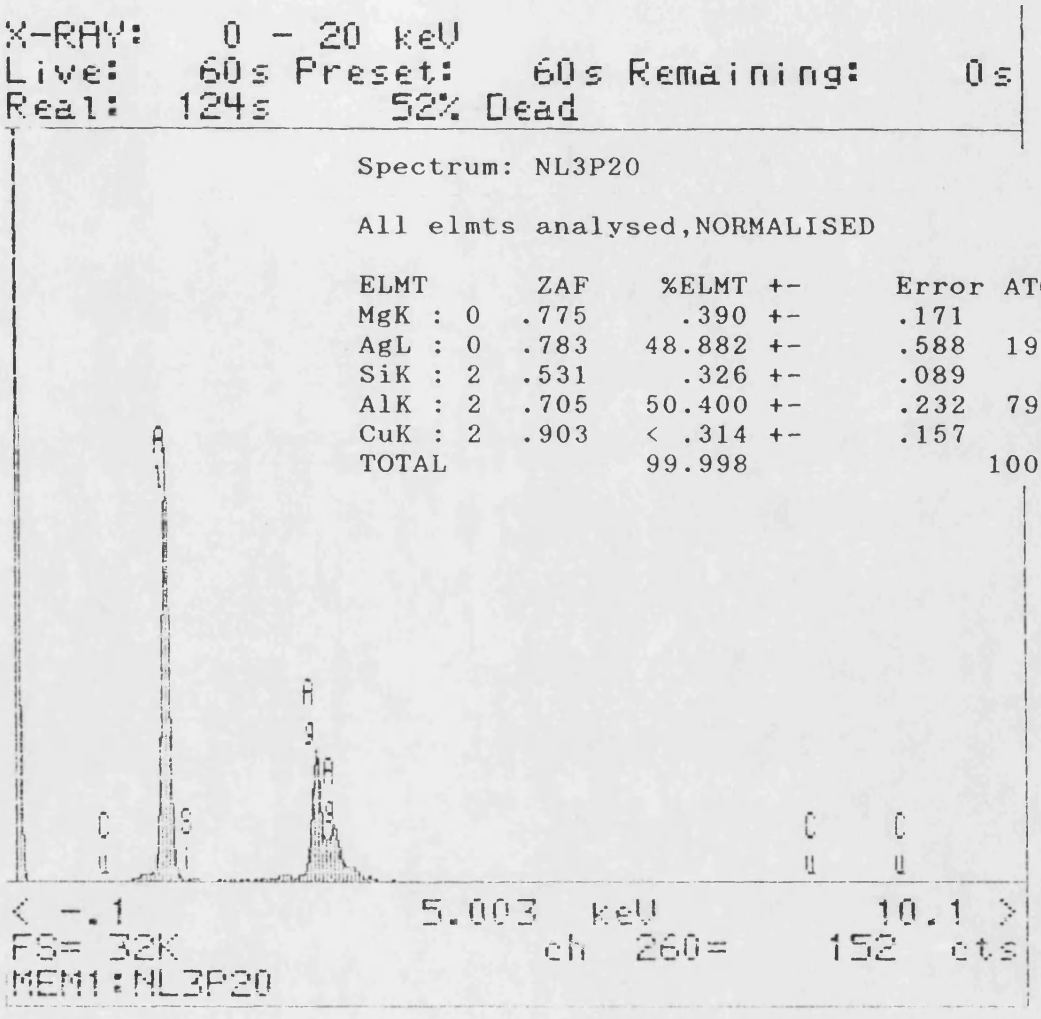

Figure 85: Energy dispersive spectrum taken from the centre of a grain in figure 84 showing high percentage of silver in solution.

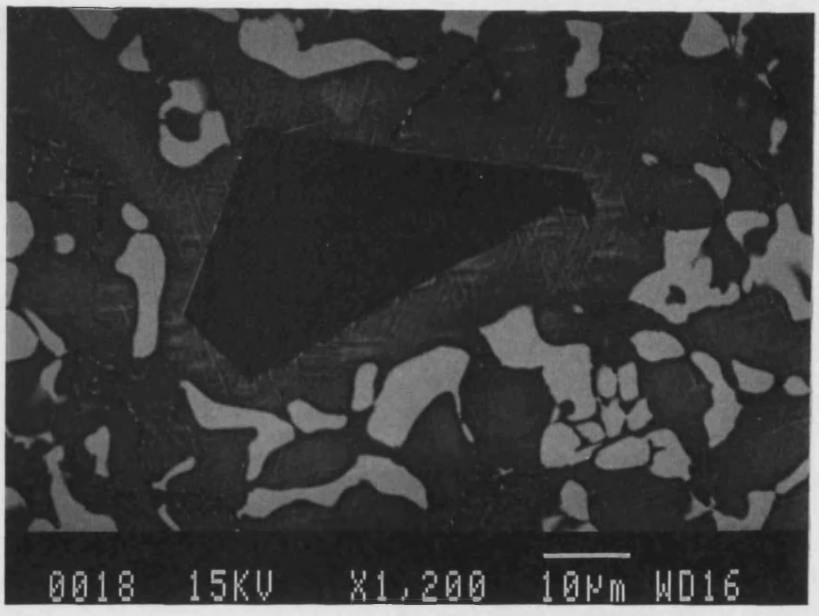

Figure 86: Backscattered SEM image of angular structure found in liquid eutectic mixture, Widmanstätten formations appear to be associated with the sharp corners.

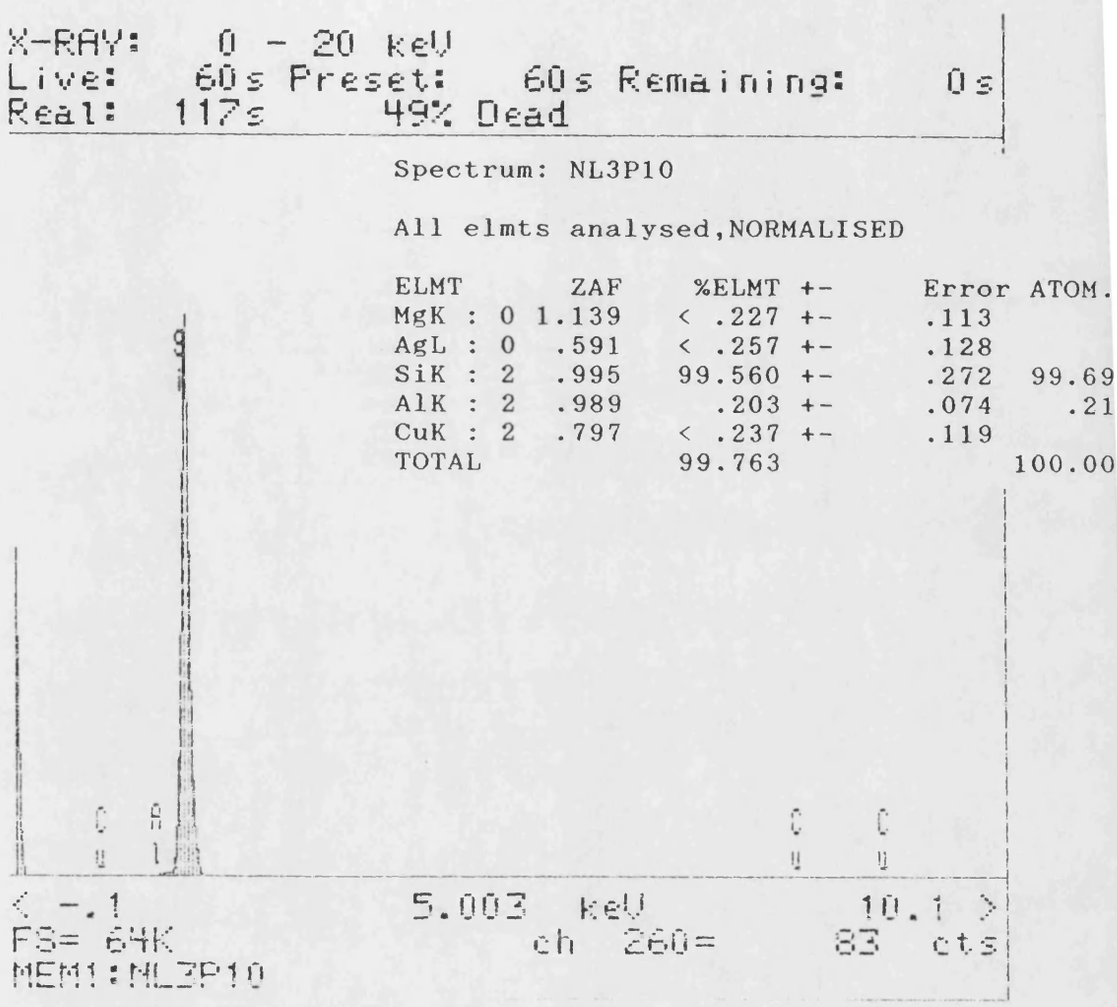

Figure 87: Energy dispersive spectrum of dark phase in figure 86 indicating primary silicon.

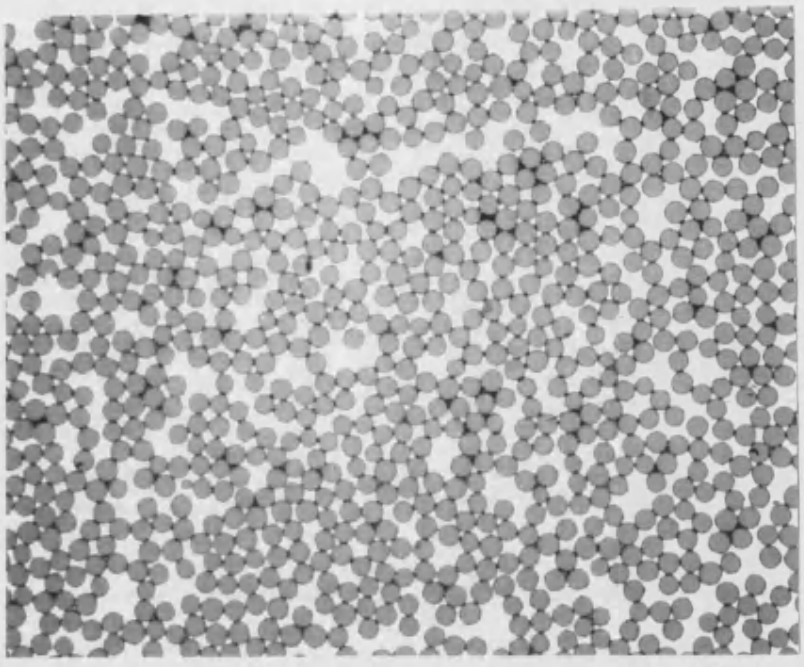

Figure 88a: Transverse section of carbon-reinforced A357 alloy.
Optical micrograph mag x400

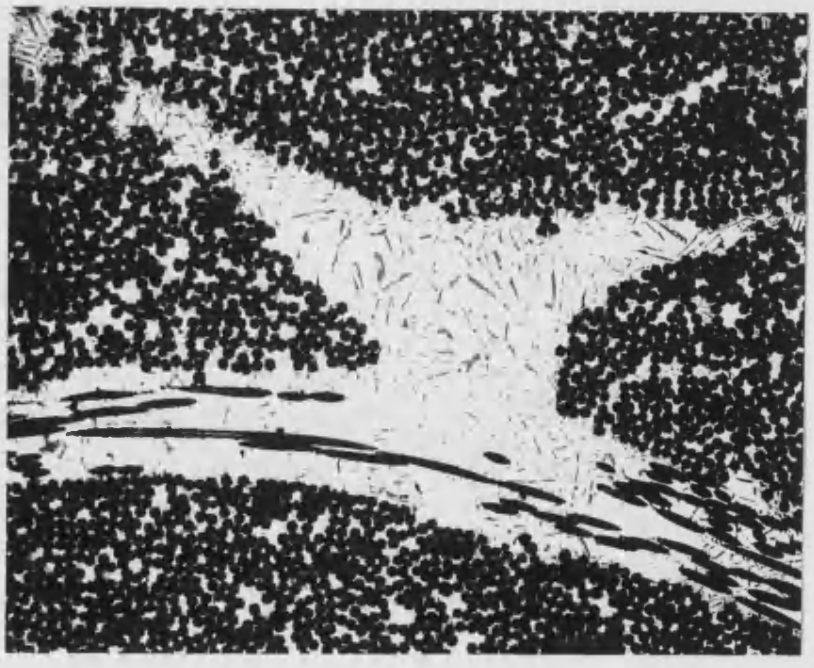

Figure 88b: Transverse section of carbon-reinforced A357 alloy.
Optical micrograph mag x200

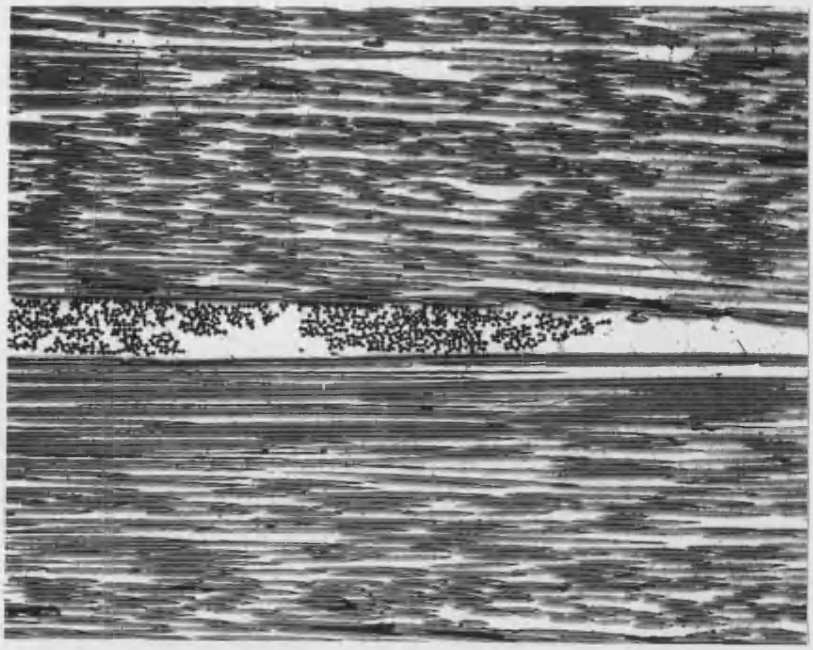

Figure 89a: Longitudinal section of carbon-reinforced A357 alloy.
Optical micrograph mag x100

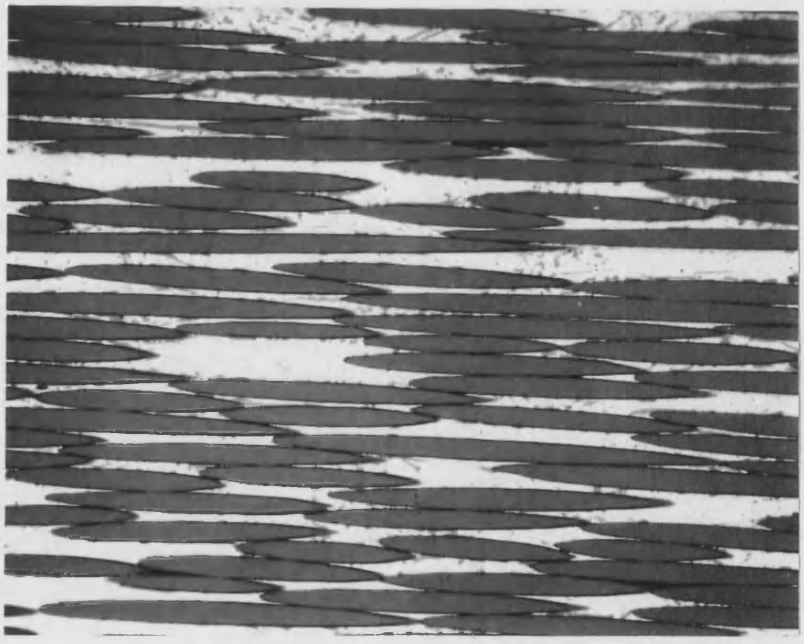

Figure 89b: Longitudinal section of carbon-reinforced A357 alloy.
Optical micrograph mag x400

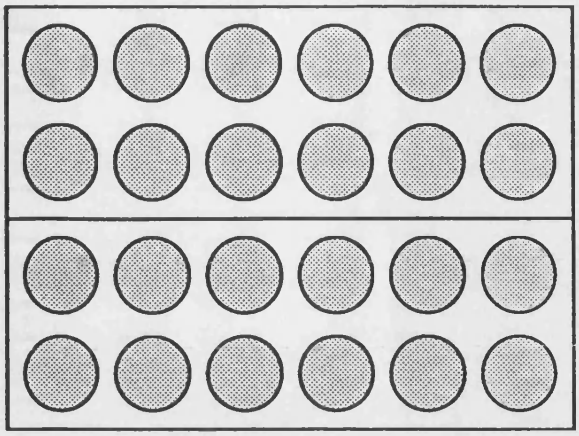

bonding of longitudinal sections

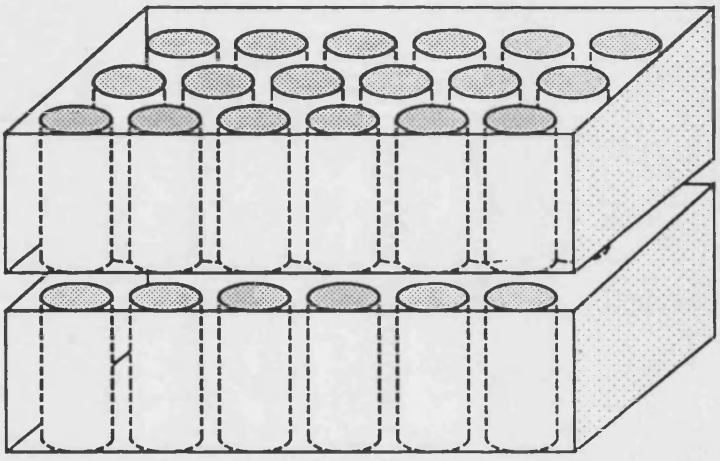

bonding of transverse sections

Figure 90: Configurations for diffusion bonded composite specimens

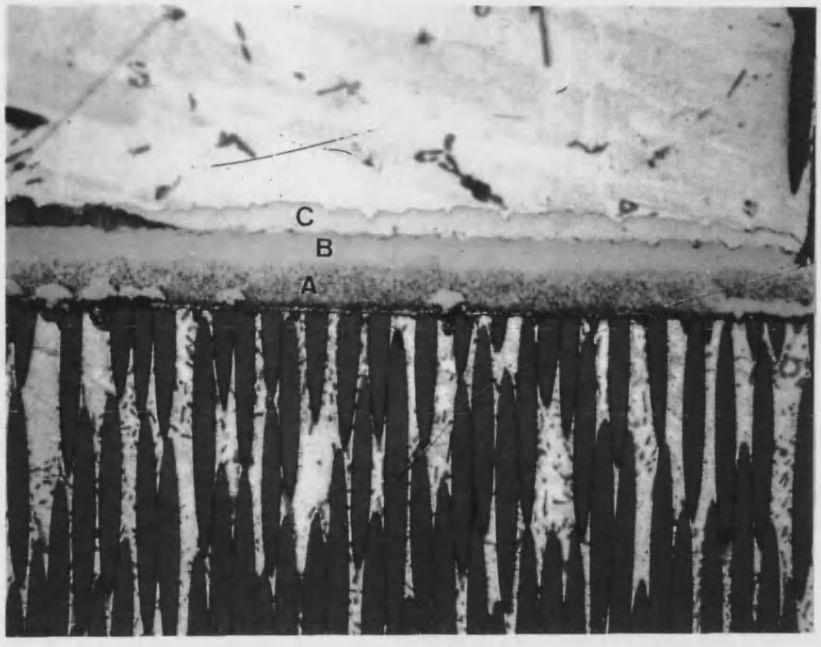

Figure 91a: Cross-section of composite sample bonded with copper foil at 525 C. Optical mag x400

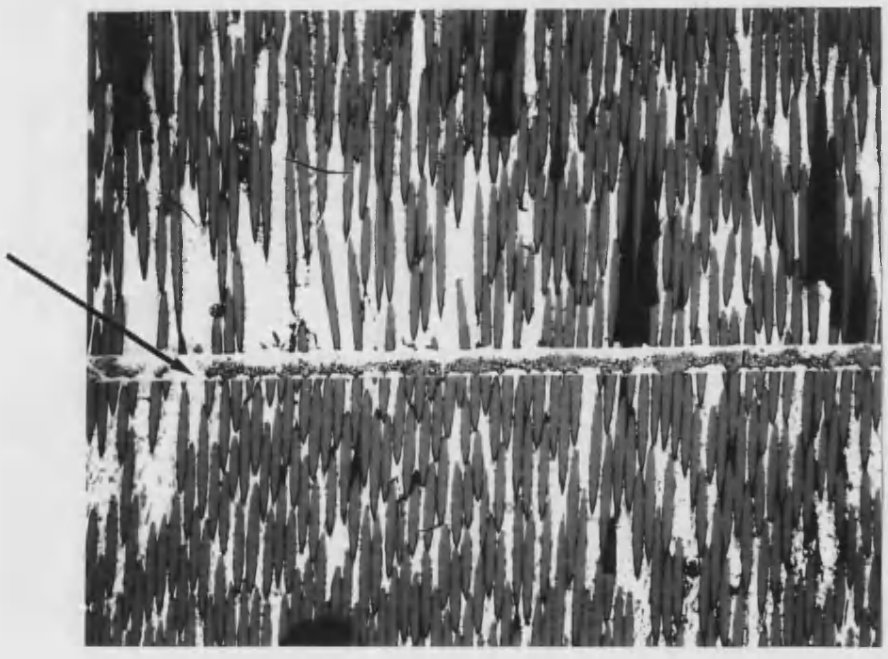

Figure 91b: Cross-section of composite sample bonded with copper foil at 525 C. Optical mag x200

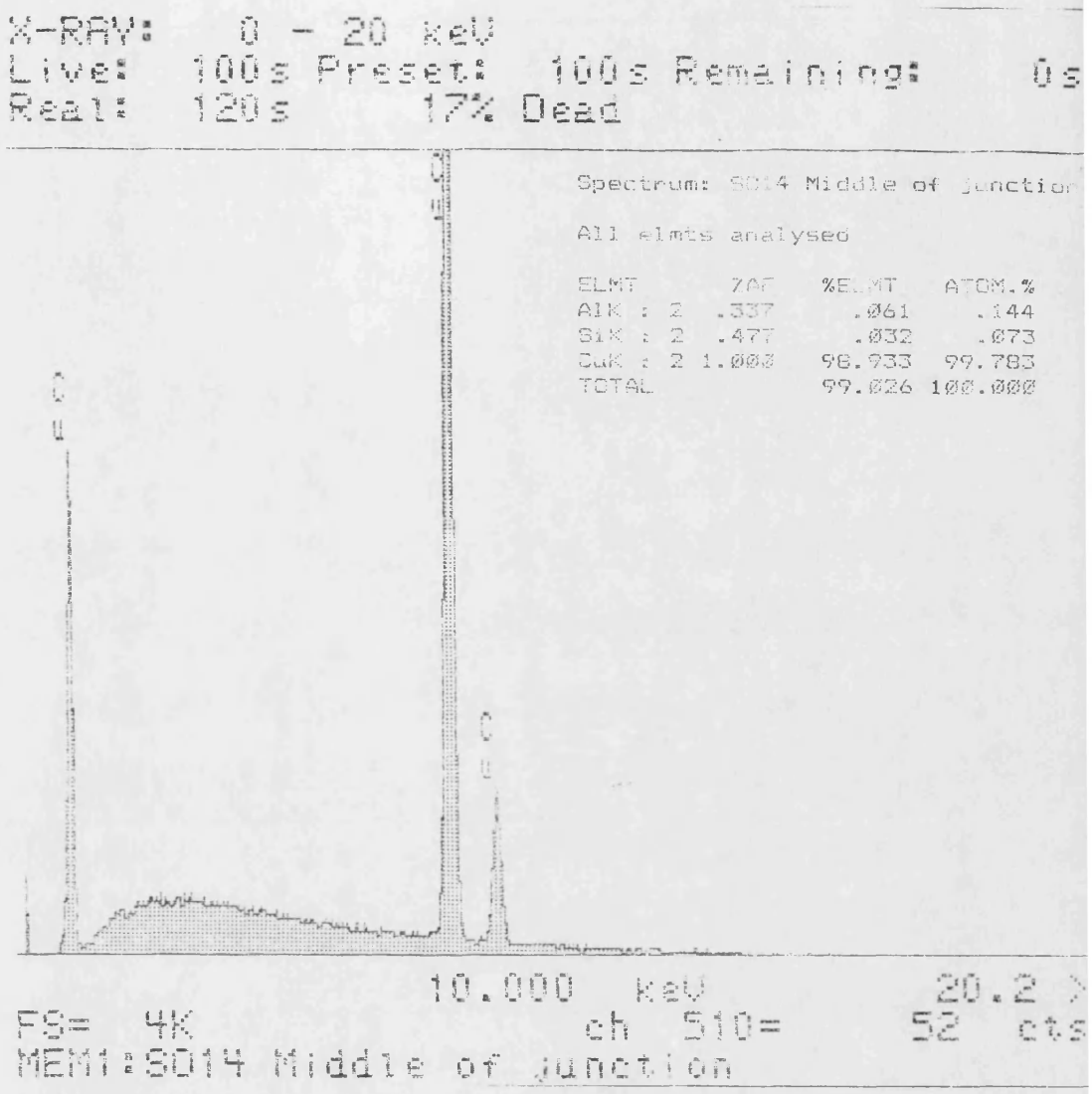

Figure 92: Energy dispersive spectrum taken from layer A in figure 91 indicating unreacted metallic copper.

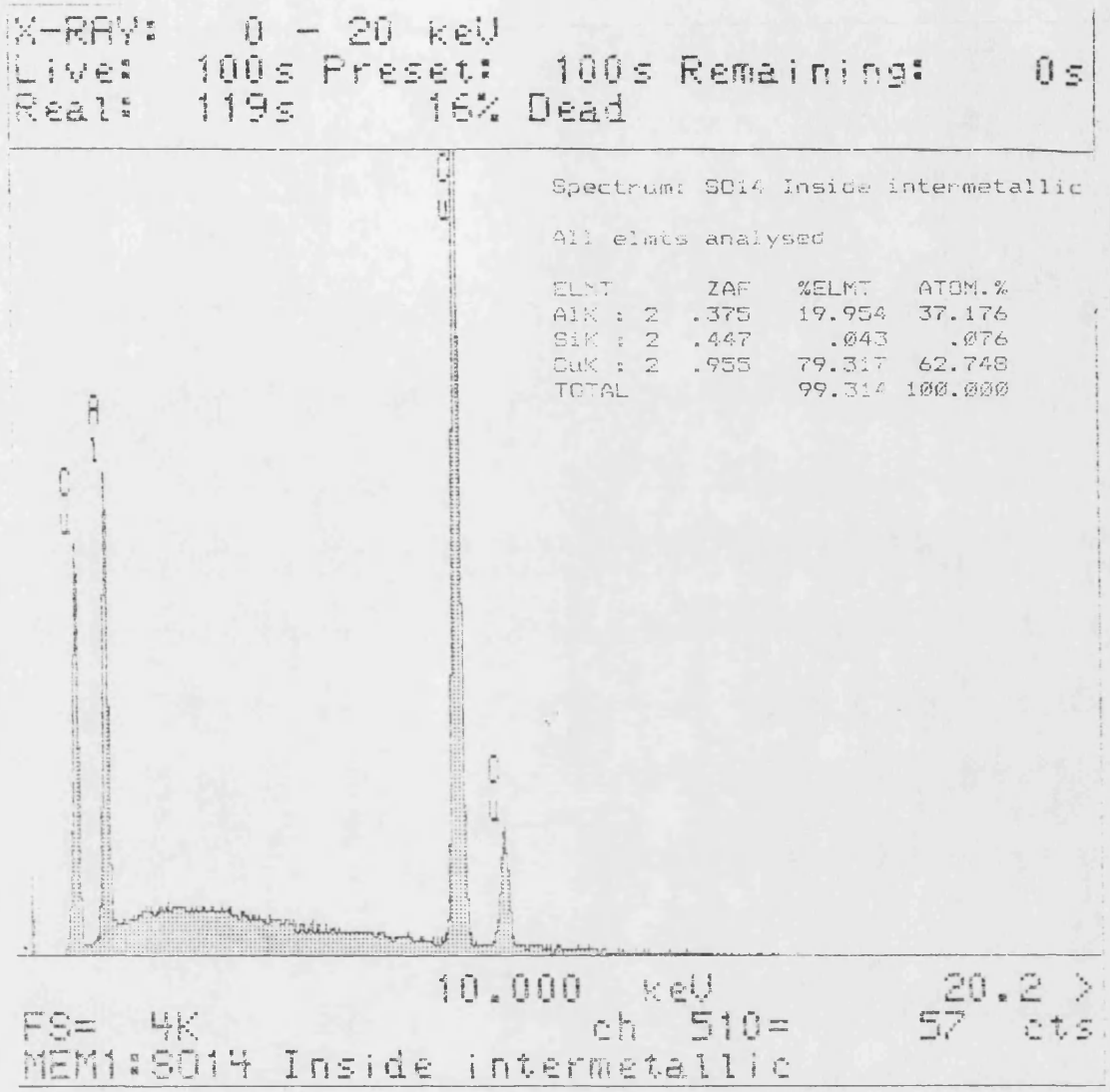

Figure 93: Energy dispersive spectrum taken from layer B in figure 91 indicating presence of δ phase.

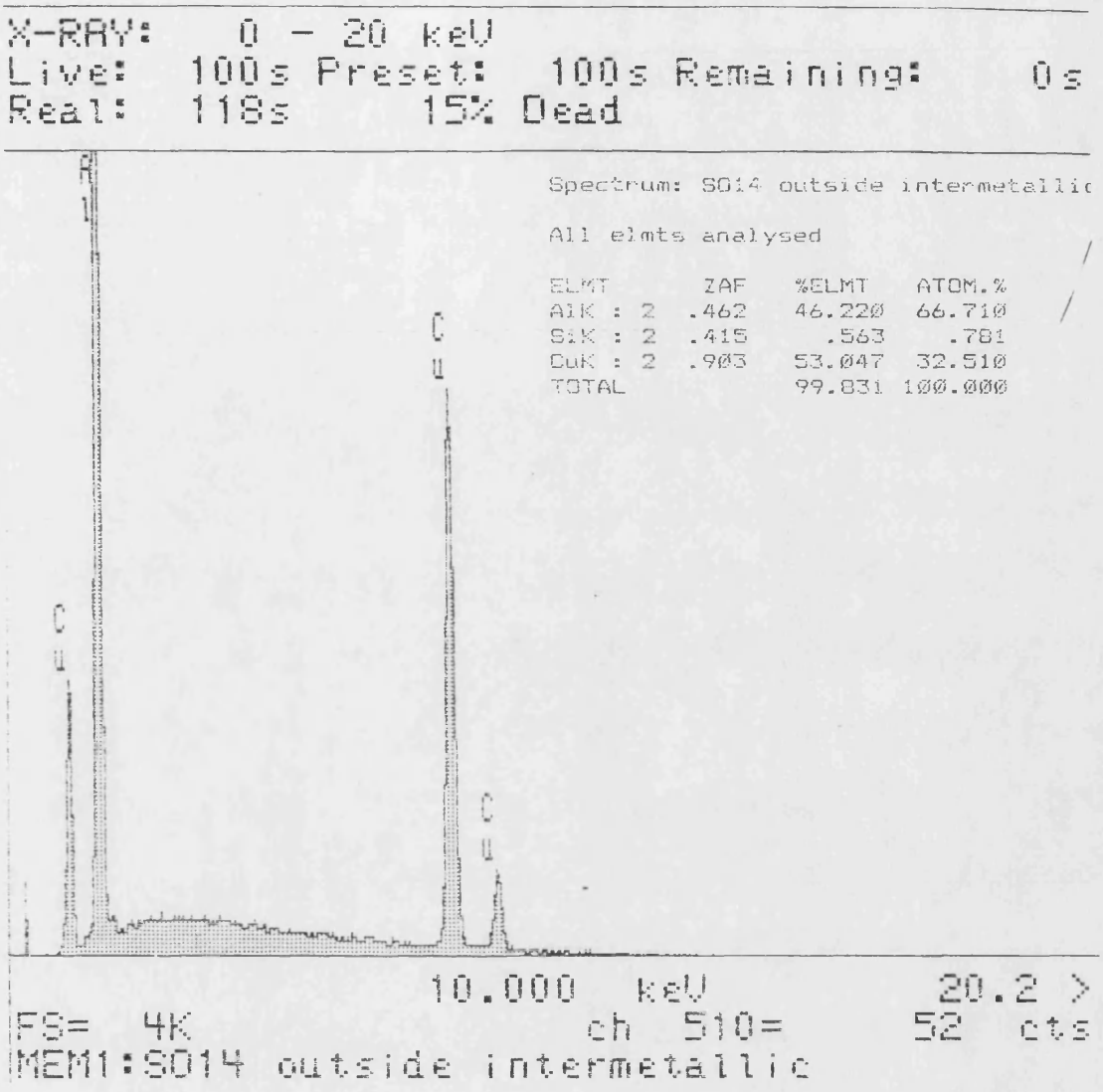

Figure 94: Energy dispersive spectrum taken from layer C in figure 91 indicating the formation of $CuAl_2$ (θ phase).

Figure 95a: Backscattered SEM image of composite specimen bonded at 550 C with copper foil.

Figure 95b: Fibre damage of composite material bonded at 550 C with copper foil. Optical micrograph x50.

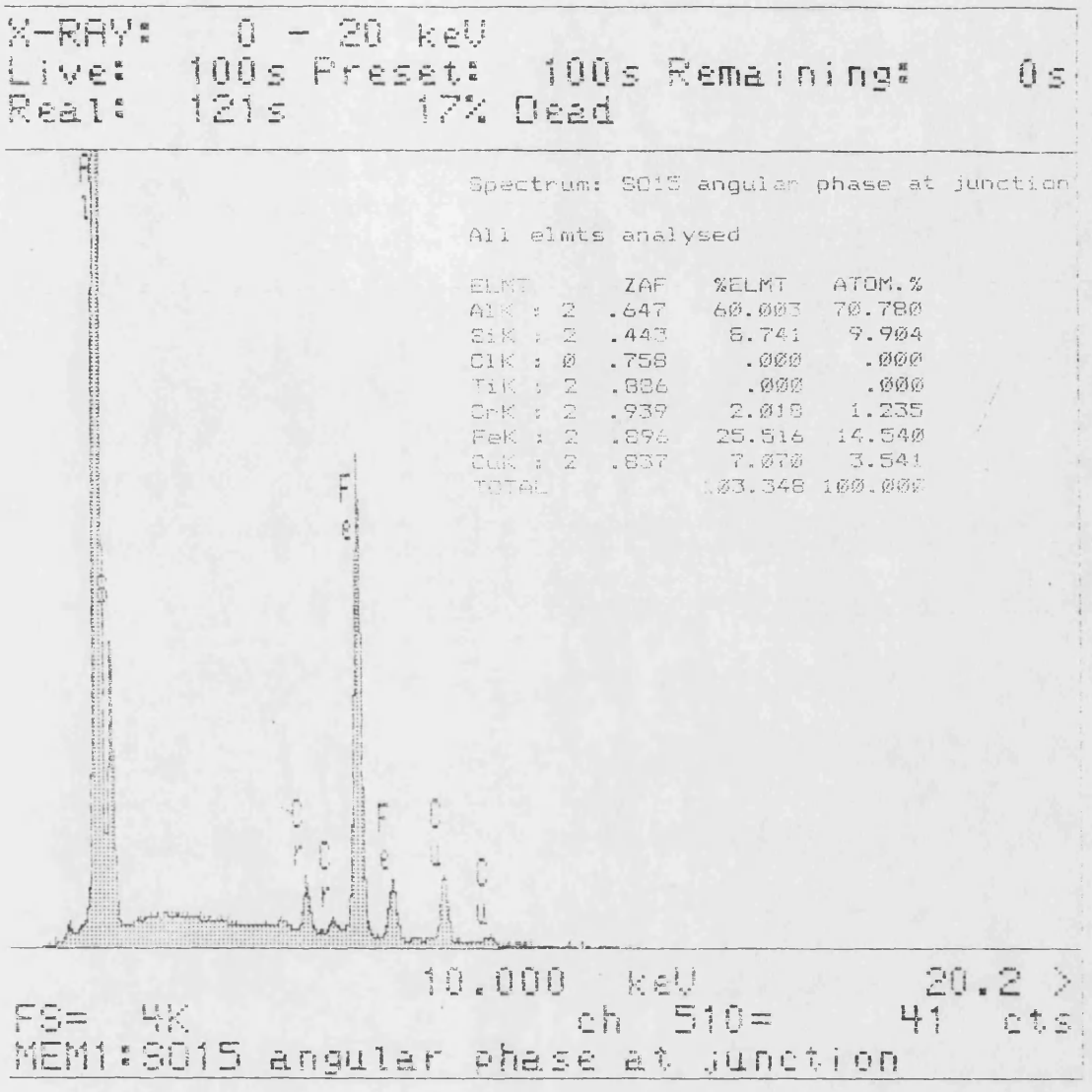

Figure 96: Energy dispersive spectrum taken from angular intermetallic arrowed in figure 95 a) indicating a complex composition.

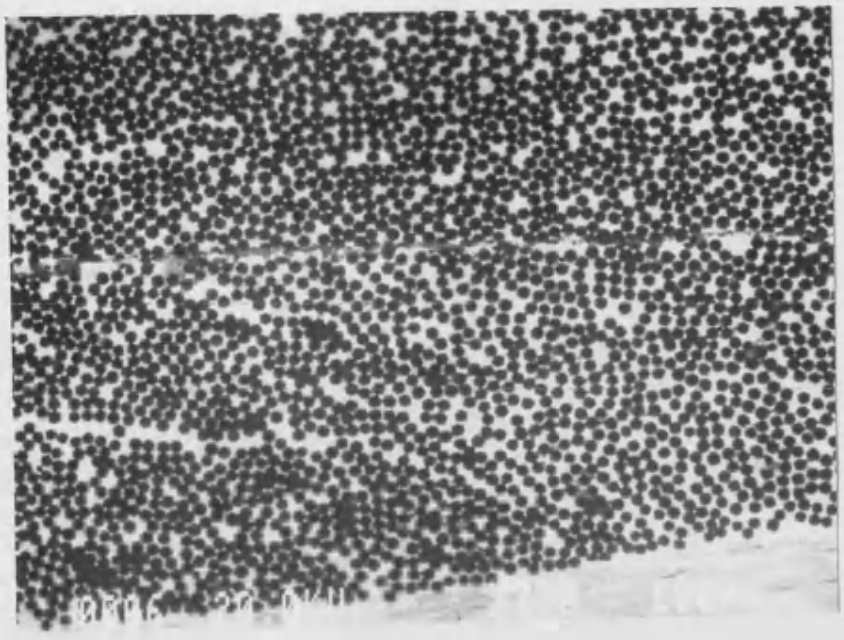

Figure 97a: Backscattered SEM image of longitudinally-bonded composite material. 550 C with copper foil.

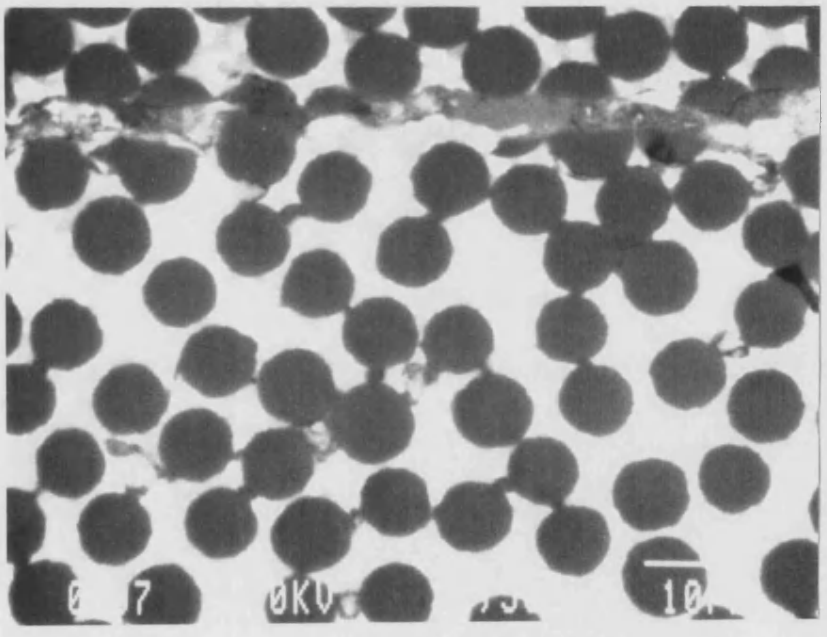

Figure 97b: Detail of backscattered SEM image of longitudinally-bonded composite material. 550 C with copper foil.

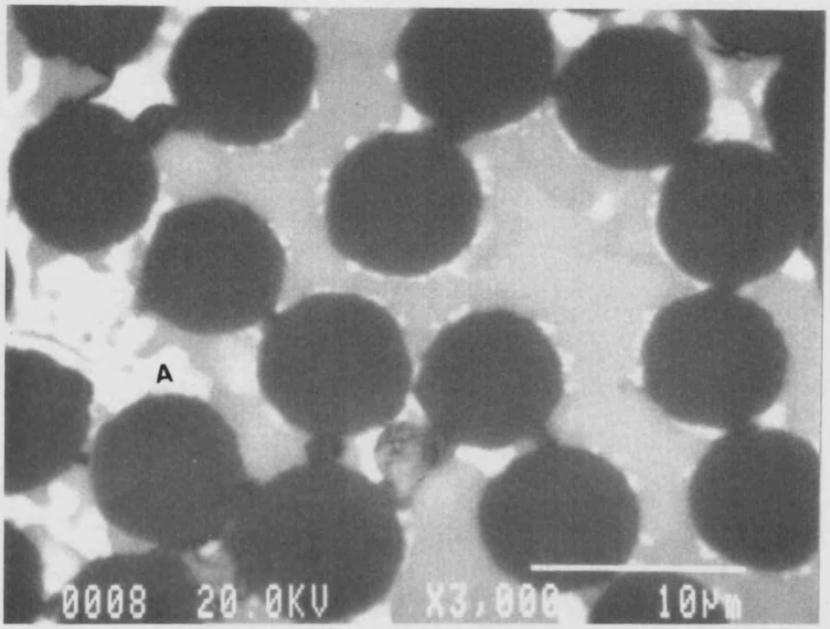

Figure 98: Backscattered SEM image showing distribution of liquid eutectic phase around fibres in composite material.

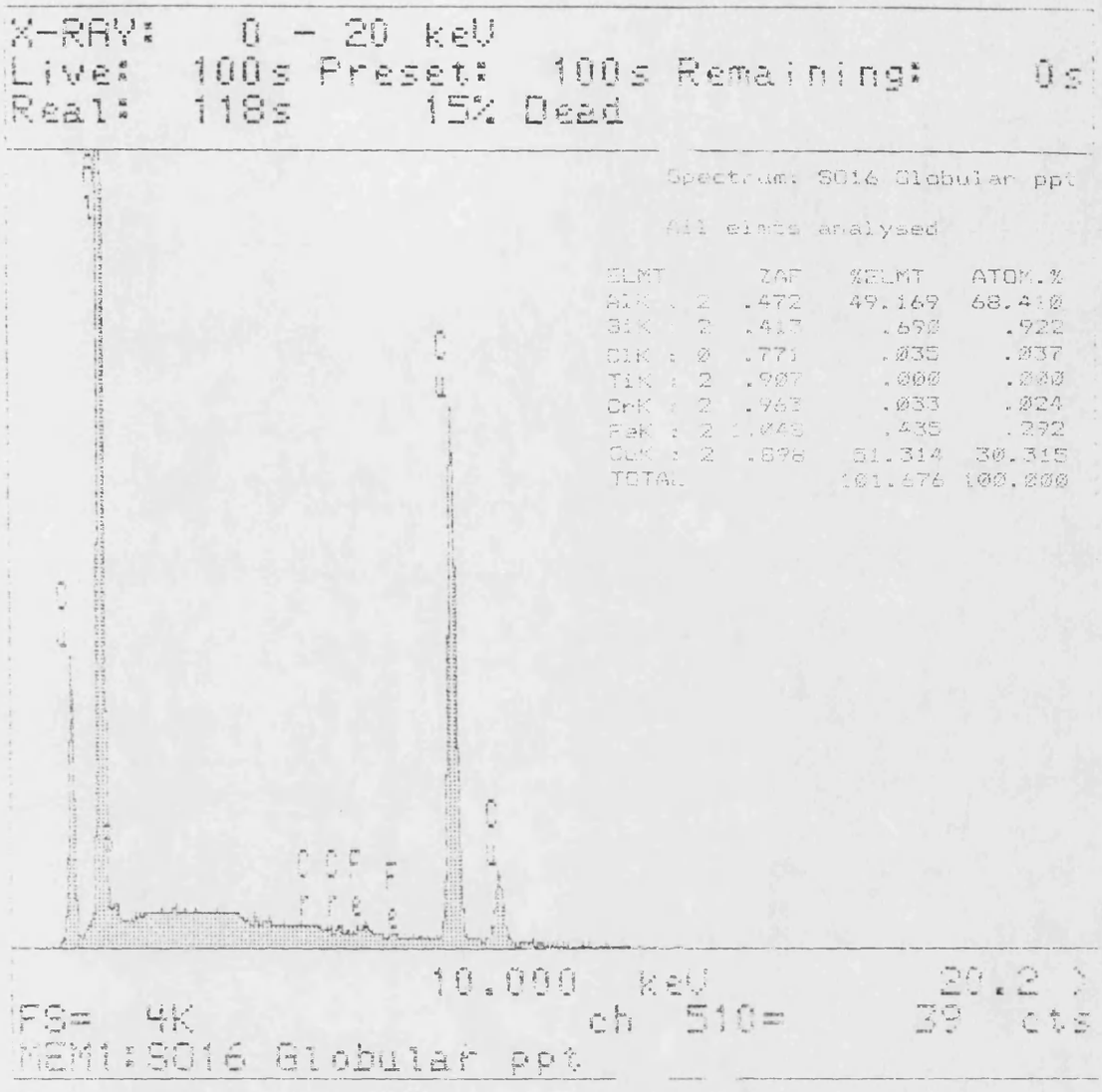

Figure 99: Energy dispersive spectrum taken from white phase in figure 98 indicating $CuAl_2$ (θ phase).

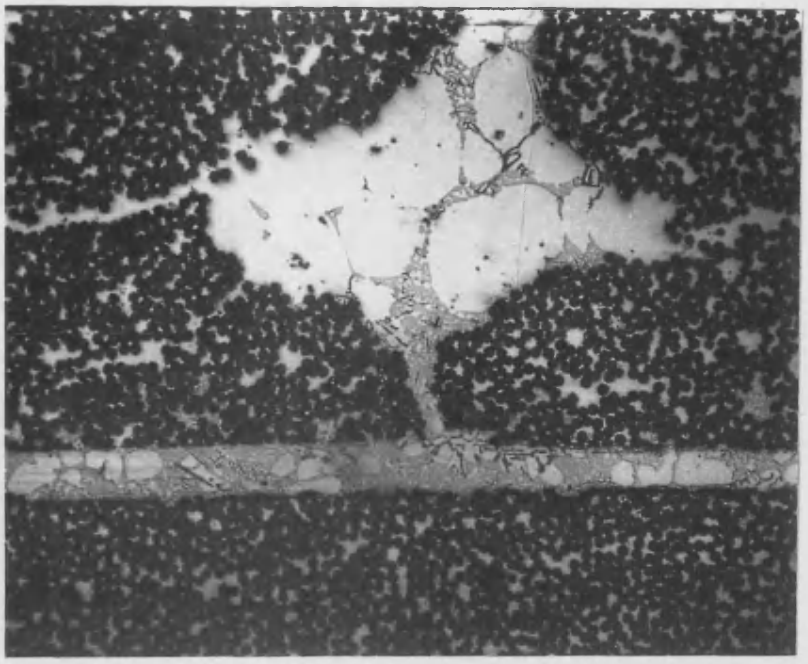

Figure 100a: Liquid reaction at interface of longitudinally-bonded composite, joined at 550 C with copper foil. Optical micrograph x200.

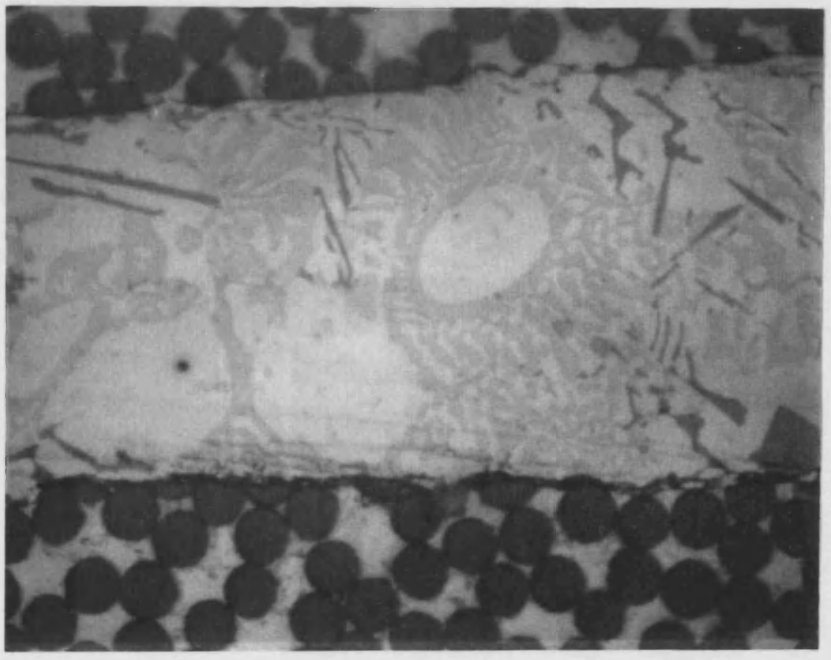

Figure 100b: Detail of liquid reaction at interface of longitudinally-bonded composite, joined at 550 C with copper foil. Optical micrograph x1000.

Figure 101a: Macro photograph of fracture surface of diffusion bonded composite.

Figure 101b: Macro photograph of fracture surface of diffusion bonded composite.

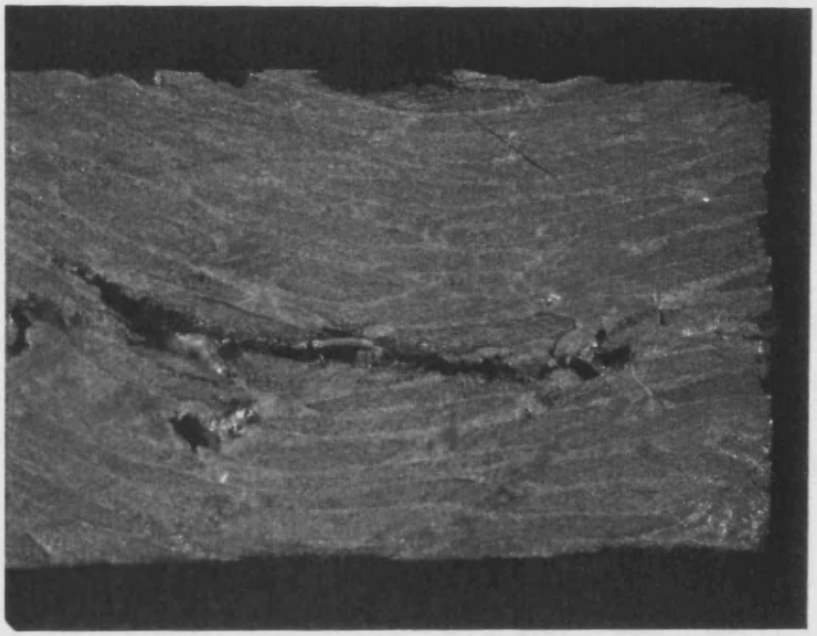

Figure 102: Macro photograph showing damage to composite induced by application of load during bonding.

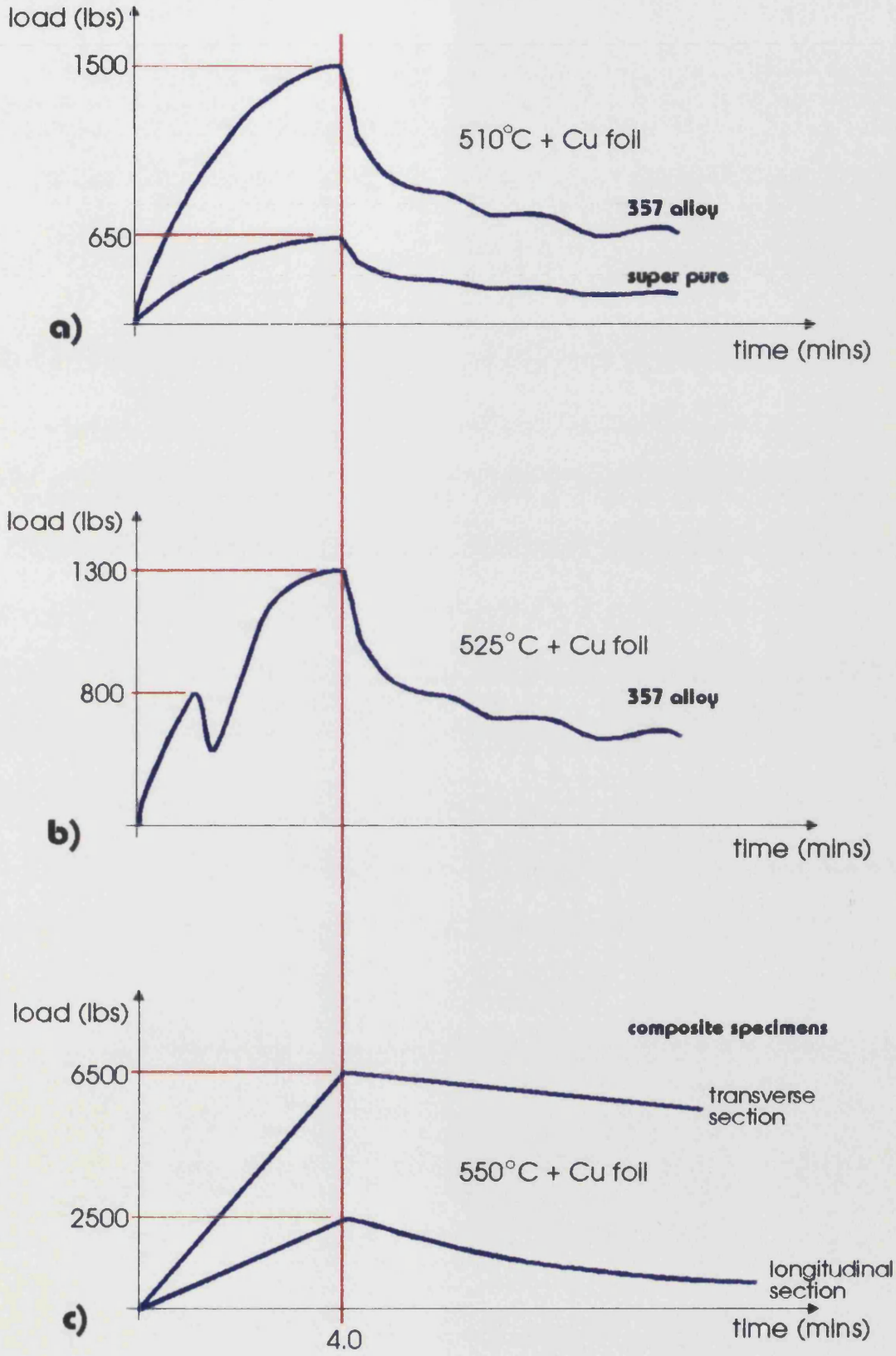

Figure 103: Load vs. Time profiles obtained during diffusion bonding

Al / Si Alloy
20 m Cu foil Load at failure (N)

	525-530°C		510-515°C	
	2875		1650	*
	2560	*	2010	
	2200		1400	*
	2855		1330	
	1650		1910	
	2100		1050	
Average	2373	N	1558	N
	47	MPa	31	MPa

Al / Si Alloy
10 m Cu foil Load at failure (N)

	525-530°C		510-515°C	
	800		1000	
	970		450	
	850		750	
	1400	*	940	
Average	1005	N	785	N
	20	MPa	16	MPa

Pure aluminium
10 m Cu foil Load at failure (N)

	560°C	
	180	
	860	
	650	
Average	563	N
	11	MPa

Figure 104: Single lap shear data for diffusion bonded alloy samples

a) t-Test: Two-Sample Assuming Equal Variances

20 μm Cu	*525 °C*	*510 °C*
Mean	2373.33	1558.33
Observations	6.00	6.00
df	10.00	
t	3.31	
P(T<=t) two-tail	0.01	
t Critical two-tail	2.23	

b) t-Test: Two-Sample Assuming Equal Variances

10 μm Cu	*525 °C*	*510 °C*
Mean	1005.00	785.00
Observations	4.00	4.00
df	6.00	
t	1.19	
P(T<=t) two-tail	0.28	
t Critical two-tail	2.45	

c) t-Test: Two-Sample Assuming Equal Variances

525 °C	*20 μm Cu*	*10 μm Cu*
Mean	2373.33	1005.00
Observations	6.00	4.00
df	8.00	
t	5.12	
P(T<=t) two-tail	0.00	
t Critical two-tail	2.31	

d) t-Test: Two-Sample Assuming Equal Variances

510 °C	*20 μm Cu*	*10 μm Cu*
Mean	1558.33	785.00
Observations	6.00	4.00
df	8.00	
t	3.66	
P(T<=t) two-tail	0.01	
t Critical two-tail	2.31	

Figure 105 t tests for diffusion bonded samples (Cu foils)

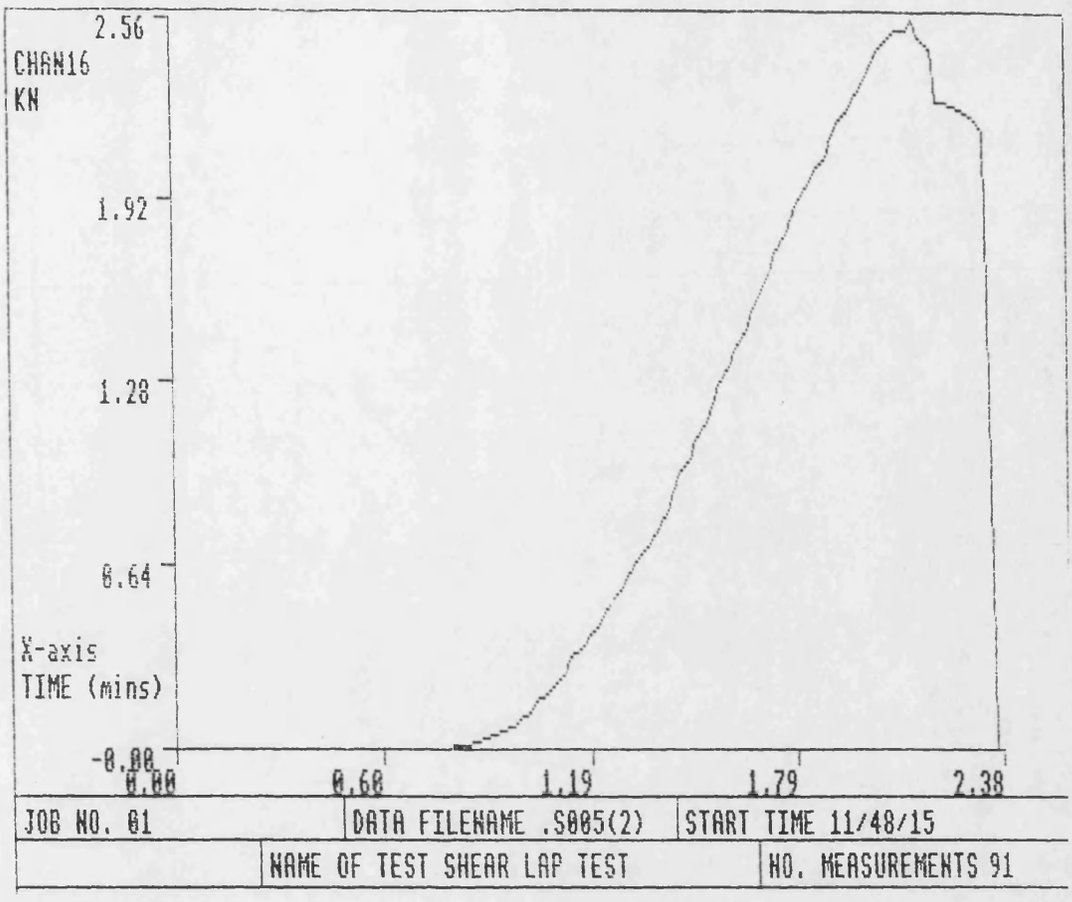

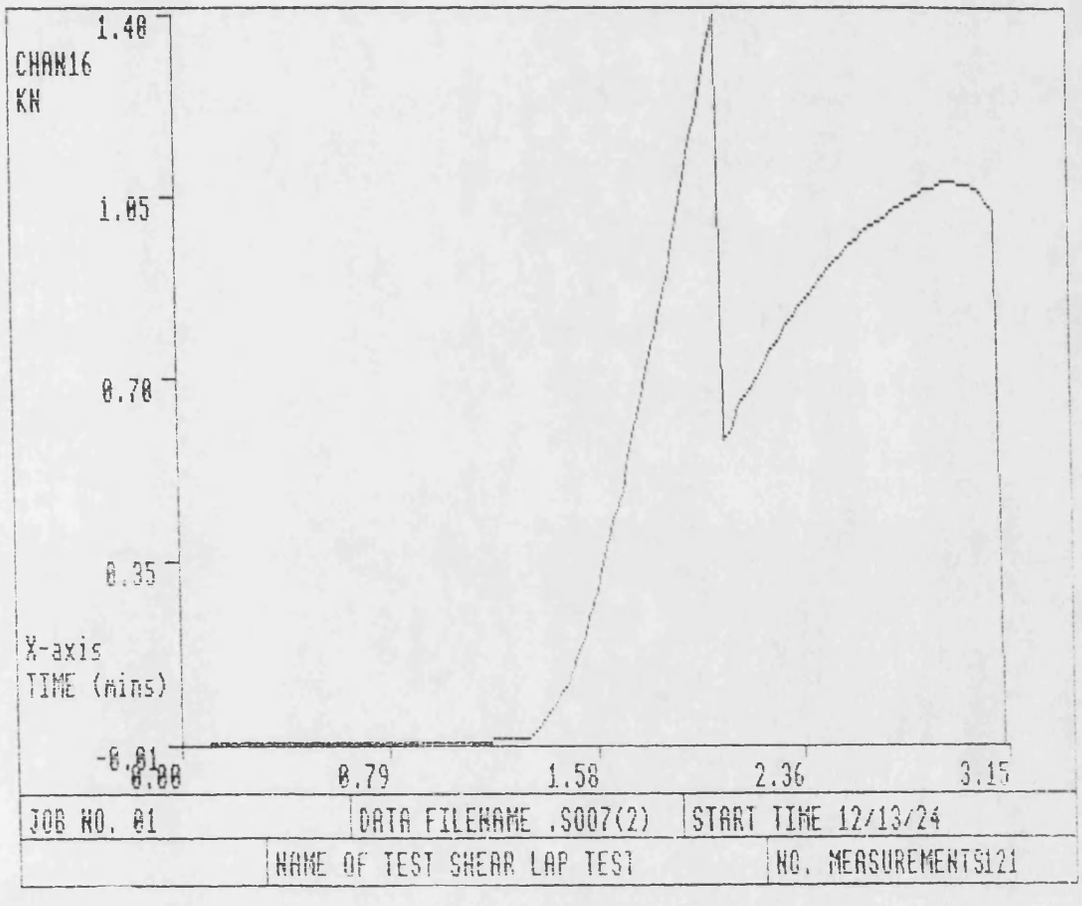

Figure 106: Examples of Load vs Time profiles for two diffusion bonded specimens

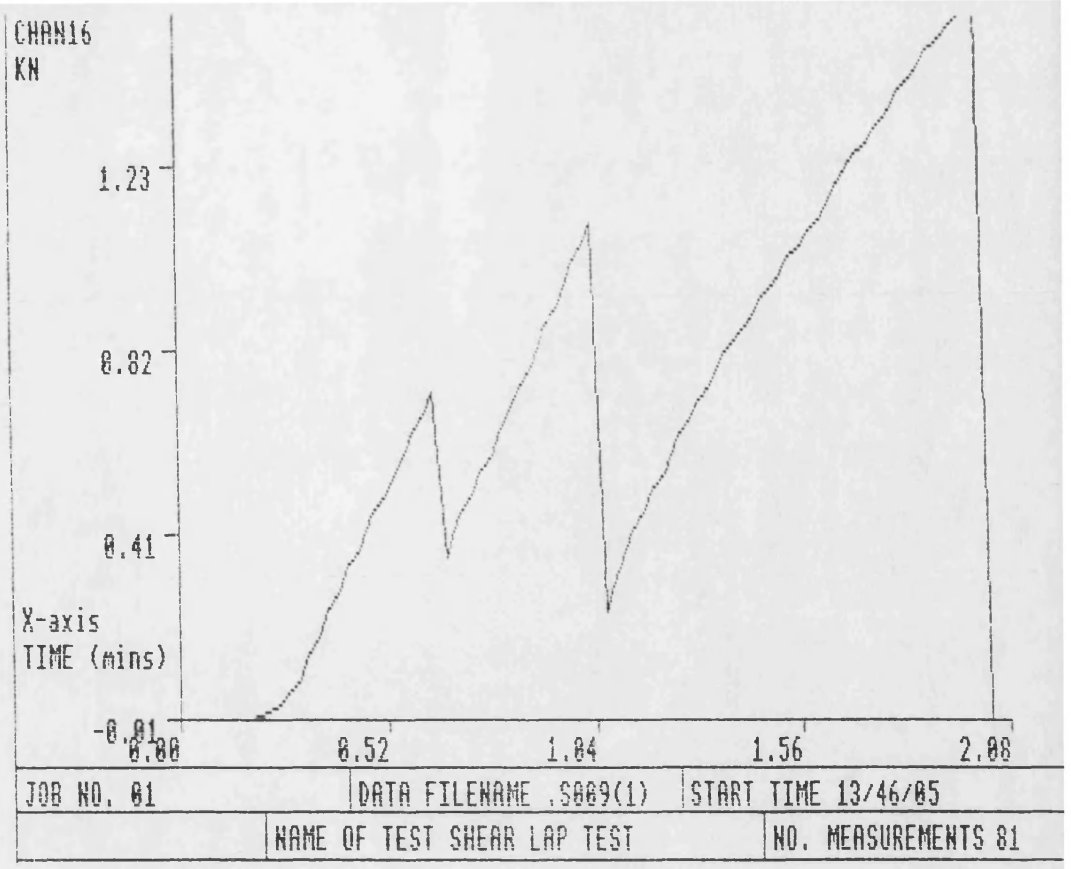

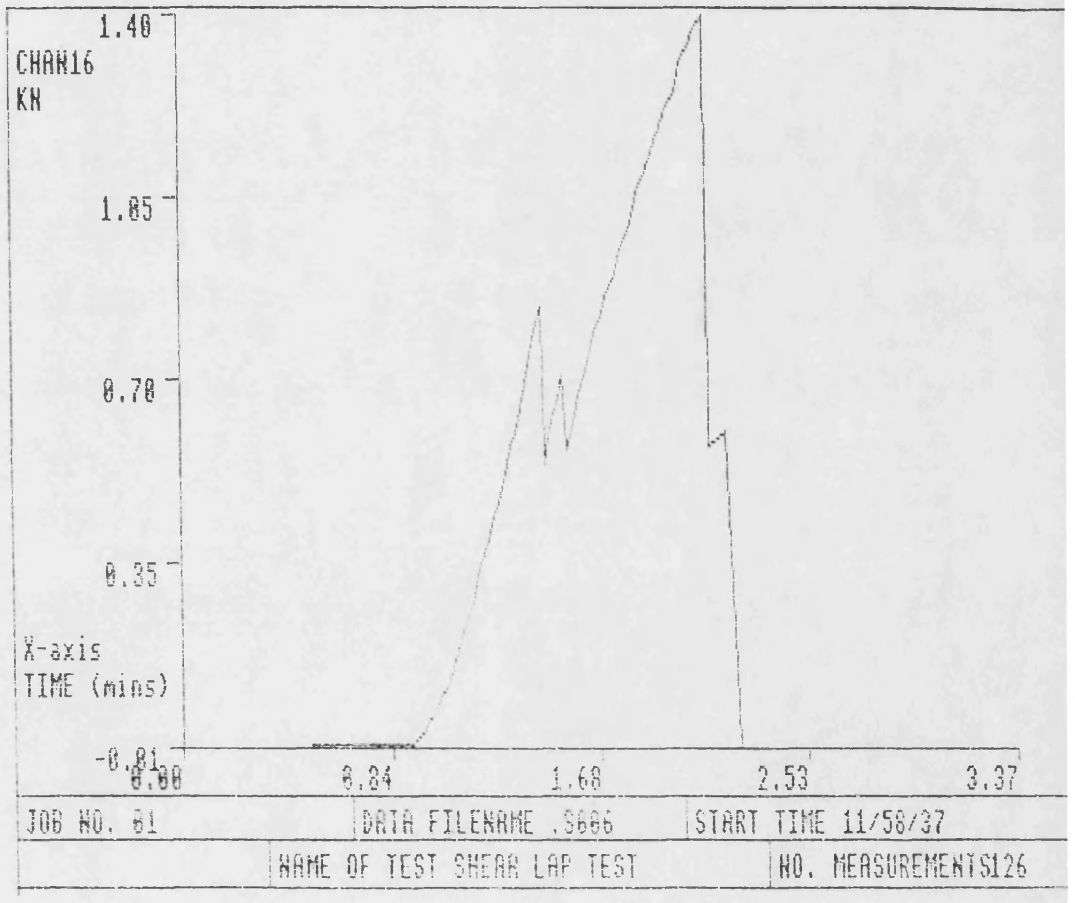

Figure 107: Examples of Load vs Time profiles for two diffusion bonded specimens

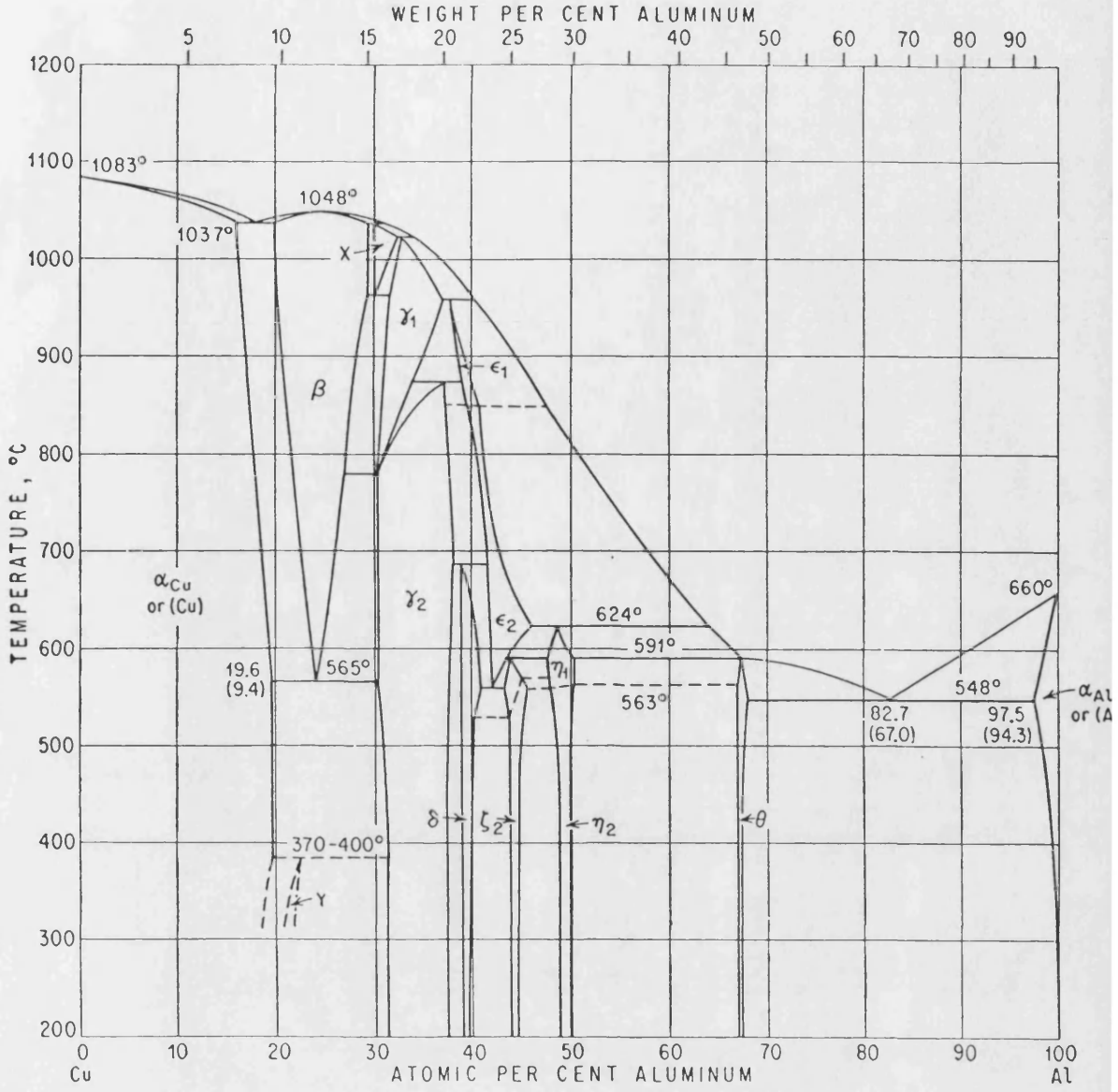

Figure 108: Aluminium / Copper equilibrium phase diagram.

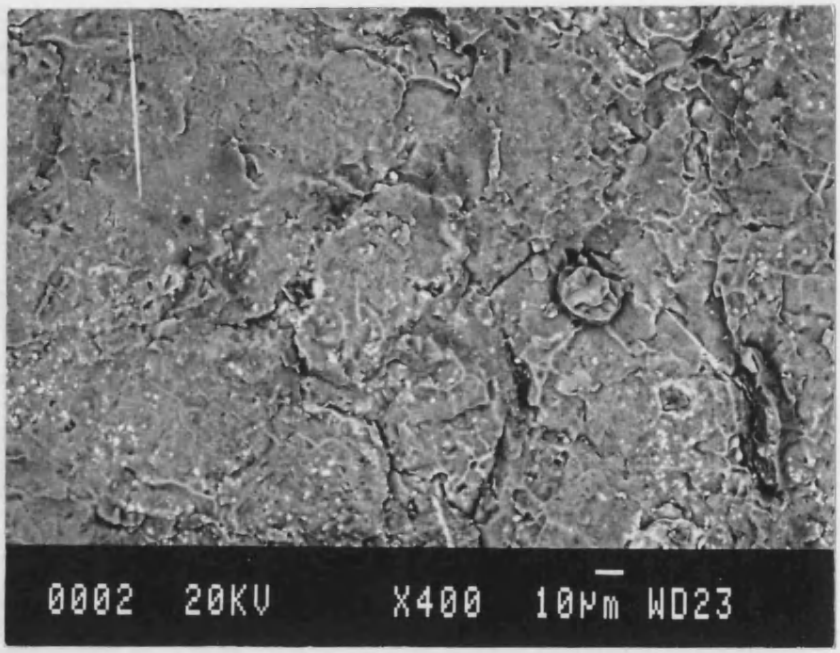

Figure 109: Fracture surface of A357 bonded by formation of liquid eutectic with copper foil insert.

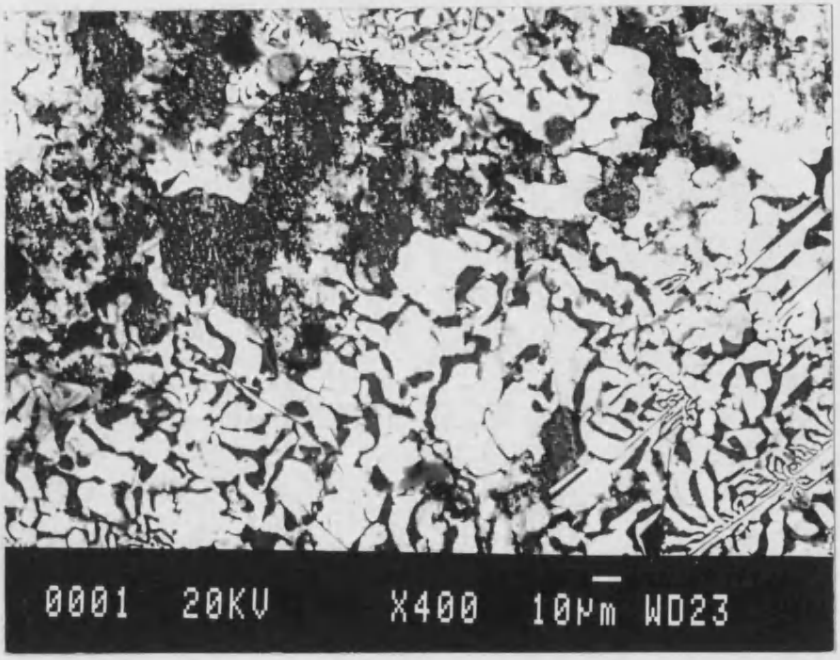

Figure 110: Fracture surface of A357 bonded by formation of reaction layer with a silver foil insert.

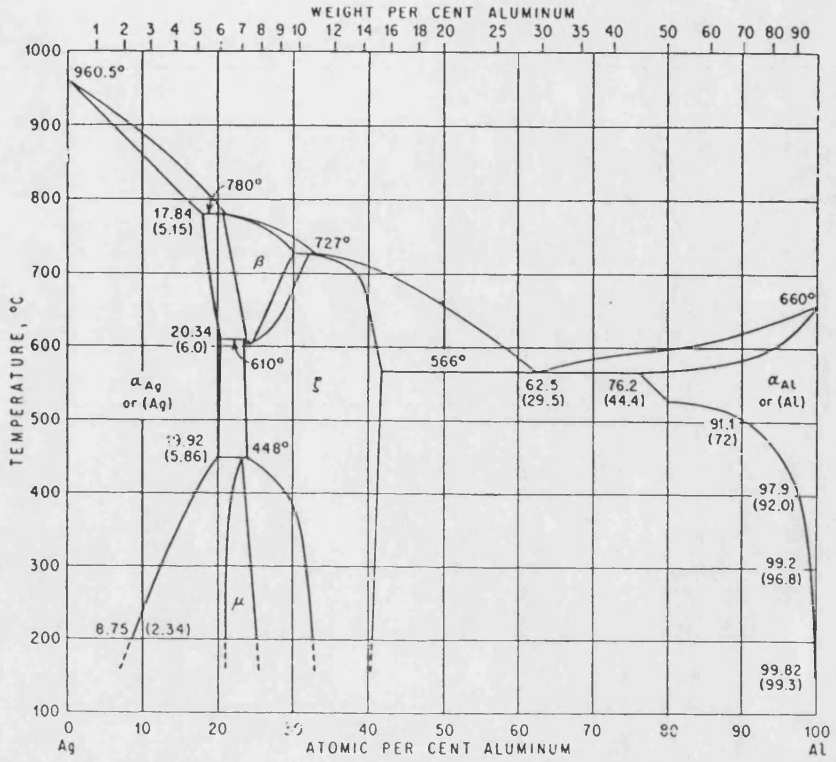

Figure 111: Aluminium / Silver equilibrium phase diagram.